Université de Lille

THÈSE

PC2A

Présentée à l'Université de Lille Sciences et Technologies

Laboratoire de Physicochimie des Processus de Combustion et de l'Atmosphère

En vue de l'obtention du grade de

Docteur de l'Université de Lille Sciences et Technologies

École Doctorale des Sciences de la Matière, du Rayonnement et de l'Environnement

Optique, Lasers, Physico-Chimie, Atmosphère

Caractérisation et déploiement d'un instrument FAGE pour l'étude des processus d'oxydation atmosphériques

Présentée Par

Mohamad AL AJAMI

Thèse soutenue le 26 Octobre 2018

Rapporteur :	M. Yoshizumi KAJII	Professor,Kyoto université,Japon
Rapporteur :	M. Valérie GROS	Directrice de Recherche, LCSE,Paris
Examinateur:	M. AlexandreKUKUI	Chargée de Recherche, LPC2E, Orléans
Examinateur :	M. Sébastien DUSANTER	Maître Assistant, IMT Douai
Directrice de thèse :	Mme. Christa FITTSCHEN	Directrice de Recherche, PC2A Lille
Co-Encadrant de thèse :	Mme. Coralie SCHOEMAECKER	Chargée de Recherche, PC2A Lille

cnrs

Labex CaPPA

To my beloved parents

for their everlasting love and support…

Acknowledgments

My thanks are first addressed to my PhD supervisors, Christa Fittschen and CoralieSchoemaecker for their guidance, advices, encouragements, and patience throughout my PhD, and for providing me the opportunity to be involved in exciting science in different places.I am extremely grateful for all you have taught me, it has been a pleasure working with you.I apologize if I have done anything that you did not like. I would also like to thank Laurefor her great sympathy, all her advice and encouragements.

My sincere thanks to the various members of the jury for agreeing to evaluate this thesis work. Thank you, Valérie Gros, and Yoshizumi Kajii for invaluable time spent in reading my thesis and writing the report. Their remarks and comments added value to my manuscript. Thanks to the examinersSébastien Dusanter, and AlexandreKukuifor the exchanges we had during our meetings for different field campaigns and at the defense.

I would like to sincerely acknowledge Pr. Yoshizumi Kajii from the Atmospheric Chemistry, Department of Natural Resources, in Kyoto University for his great hospitality during my visit to his laboratory in Japan and for the good times that we spent together.

I thank Laurent Gasnot, laboratory director of PC2A, for his hospitality as well as all the administrative and technical staff who allowed me to work in very good conditions. In particular, I would like to thank Sébastienand Christophe for their technical help, availability, advice and numerous interventions, and without which the manipulation would not have worked as well.

Many thanks to the scientists and engineersthat I met in different field campaigns where I was participated, I lookforward to meeting them again in the future.

I owe my sincere thanks to Marion Blocquet and Emmanuel Assaf for their everlasting help and support throughout my stay.

I would like to thank all the people who have made this thesis successful and have made it possible for me to evolve in a very healthy and friendly working atmosphere.

Many thanks my office mates, past and present, for their friendship, advice, andfor providing welcome distractions. My thoughts go first to Emmanuel, Florent, Elaine, Sonia, Dorra, Nicolas, and Patrice. Thank you for all our good times together in the laboratory and outside in different activities. I would continue with all the other people of the laboratory, Jinan, Nabil, Lucia, Ahmad, Lisa, Junteng.To all those I forget, the following white page is dedicated to you.

Thanks to all my friends, Elias, Salim, Mario, Grace, Mohamad nour, Ahmad, Sandy and Jalal for their support and encouragement.

On a more personal level, I obviously owe this success to my parents who have dedicated their whole lives to the education and well-being of their sons.I am very grateful to my family for their constant encouragement and support.

Finally, my father's dream comes true.

Thank you again…

Abstract

The hydroxyl radical, OH, the hydroperoxyl radical HO_2 (known collectively as HO_x) and peroxy radicals RO_2, play a key role in the tropospheric chemistry and are intricately related to the chemical cycles that control the concentration of greenhouse gases such as methane and have important implications for air quality through VOC oxidation and ozone formation. Accurate quantification of these three important radicals and investigations on the chemical mechanisms that control their formation and removal through comparisons between measured and modeled concentrationsare needed to develop a better understanding of the atmospheric chemistry mechanisms.

Different types of instruments have been developed and deployed to quantify HO_x radicals in the field. One has been developed over the last few years in our group based on the most deployed technique: the FAGE (Fluorescence Assay by Gas Expansion). This technique represents direct measurement of OH and indirect measurement of HO_2 radicals by chemical conversion to OH after addition of NO. However, some RO_2 radicals can also be converted to OH by a similar radical reaction sequence as HO_2, so that they are potential interferences for HO_2 measurements. For UL-FAGE, the conversion efficiency of various RO_2 species to HO_2 has been investigated and it has been shown that variation of NO allows to selectively detect HO_2 and double bound RO_2.With similar FAGE instruments, field campaigns have been carried out in remote biogenic environments (dominated by isoprene emission) in the last decade. They have highlighted unidentified interferences in these measurements. In our laboratory, we used our FAGE instrument in controlled conditions to investigate the origin of the interference and we have shown that ROOOH (trioxides), product of radical-radical reactions in the atmosphere may be responsible.

PC2A calibration cell was intercompared to other calibrators (IMT-Douai and LPC2E) of similar design over wide range of conditions. One goal of the intercomparison was to evaluate each other's calibration and to make sure that they had no significant biases. The results showed a good agreement between the three calibration cells for HO_x and RO_2 radicals. Finally, the UL-FAGE in both configurations (quantification and reactivity) was deployed to a field measurement (LANDEX) in forest environment. Part of the campaign was conducted to an intercomparison between LP-FAGE and LSCE-CRM instruments. Measured reactivity showed very good agreement between both techniques.

Keywords: Atmospheric chemistry, HO_x radicals, Peroxy radicals, FAGE instrument, Laser Induced Fluorescence, Field campaigns, interference, calibration

Table of contents

Context and objectives of the thesis

The study of the atmosphericcomposition and its evolution is crucial as it has a direct impact on our health(particles and dangerous gaseous species with potential cancerogenic effect, respiratory diseases) and the climate (greenhouse gases). The atmospheric composition is driven by biogenic and anthropogenic emissions and their transformation due to physical and chemical processes.

Within the major species involved in oxidation processes in the atmosphere are the hydroxyl radical, OH, and the hydroperoxyl radical, HO_2 (known collectively as HO_x). They play a key role in tropospheric chemistry and are intricately related to chemical cycles that control the concentration of greenhouse gases and the formation of tropospheric ozone, and acid rainwith important implications for air quality and ecosystems. Hydroxyl radicals initiate the hydrocarbons degradation and are linked to the hydroperoxyl radical, HO_2, through a series of oxidation steps leading to the formation of different peroxy radicals (RO_2, R being a hydrocarbon group) as a function of the hydrocarbons present in the local air mass.As the composition of different air masses can vary a lot from one environment to another one (forest, urban, marine,…) and because of the multiplicity of species present, accurate measurements of these radicals are needed forinvestigating the oxidationmechanisms that control their formation and removal. Comparison between measured and modeled profilesallow to develop more representative atmospheric chemistry mechanisms and a better understanding of atmosphere.

Different types of instruments have been developed and deployed to measure these radicals in the field. Although $HO_x$and RO_2quantification provides important information about theatmospheric chemistry, to access to a better description of the radical balance, another parameter is particularly interesting to measure: the reactivity of the OH radical. OH reactivity is defined as the first order loss rate of the hydroxyl radical and provides information about the budget of all species reacting with OH present in the atmosphere. Recent instruments have been developed to measure OH reactivitywhich can then be compared to a calculated reactivity obtained from the concentrations of species reacting with OH,simultaneously measured at the same location. Any discrepancy between measured and calculated OH reactivity (called missing reactivity) represents OH sinks that have not been characterized by trace gas measurements and indicates that important unmeasured reactive species are present.

The development of the different instruments used to quantify the radicals or the OH reactivity is very challenging due to the low concentration of the species and to the complex composition of the

atmosphere. This is why it is necessary to check that the measurements are not subjected to potential interferences due to the presence of other species in the atmosphere and if present a particular attention should be taken to characterize well these interferences and to reduce them. In the last few years, interferences have been identified on OH and HO_2 measurements.

In this context, this thesis concentrates on the continued development of a dedicated HO_x radical detection instrument, based on laser induced fluorescence spectroscopy at low pressure (fluorescence assay by gas expansion (FAGEinstrument of the PC2A called the UL-FAGE)).

The aims of my thesis were focused on the improvement of the reliability of the measurements with the UL-FAGE instrument and on its deployment for a better understanding of biogenic environments.It includes:

- a better characterization of the origin of interferences in ambient measurements of OH and HO_2, and the identification of the interference on the OH measurement,
- the improvement of the instrument to limit the interferences,
- the study of the possibility of measuring RO_2 radicals
- a better characterization of the calibration of the FAGE instrument which can be source of error in measurementsother than interferences,
- the deployment of UL-FAGE in the field forradical quantification and OH reactivity measurement in order to better characterize the oxidation processes in a forest where nocturnal particle formation has been observed.

The present thesis consists of six chapters.The first chapter describes the atmosphere and in particular the region of interest for my work:the troposphere, the atmospheric chemistry of the troposphere involving HO_x radicals and the instruments available for the characterization of these key radicals as well as their potential interferences.
The second chapter provides a detailed description of the instruments used in this thesis:

- the FAGE instrument in the quantification mode measuring OH and HO_2radicals, the improved calibration cell and the preinjector system installed to allow a selective measurement of OH,
- the FAGE in the OH reactivity mode also called pump - probe FAGE.

The third chapter presents the kinetic studies of RO_2 + OH to highlight the interference of products formed by these reactions on the OH measurement in the FAGE. These findings could explain the discrepancies between measured and calculated OH concentrations that have been seen in different field campaignsin biogenic environment with low NO concentrations.

The first part of chapter four presents the characterization of the FAGE cells concerning the wall loses, the humidity,the interferences of different peroxy radicals (RO_2) on the HO_2 measurement in the UL-FAGE instrument. Conversion efficiencies of different peroxy radicals are presented.The second part of chapter IV presents the results of an intercomparison between different calibration cells for different instruments measuring HO_x and/or RO_2radicals (FAGE forPC2A, PERCA for IMT-Lille Douai, and CIMS for LPC2E). Results show the reliability of UL-calibration system with Mines Douai and LPC2E calibration systems.

Finally, chapter five presents the results of the deployment of the UL-FAGE during the LANDEX field campaign that was conducted in July 2017 in a pinus forest near Bordeaux in the south of France, where HO_xconcentrations and OH reactivity were measured. This campaign involved different groups to characterize the environmental conditions (wind, temperature, solar radiation), the plant emissions, the ambient gas phase (VOCs, ozone, NO_x, NO_3, HO_x, OH reactivity)and the particles (granulometry, composition) and to better understand the formation of particles in such environment. As two instruments to measure the OH reactivity were presents, this chapter presents results of the intercomparison that have been done between the pump-probe UL-FAGE and the CRM instrument of LSCE.

Chapter I: The tropospheric chemistry of OH and HO_2 radicals

I.1 Introduction

I.1.1 The Atmosphere

The Planet Earth is surrounded by a layer of solid, liquid and mainly gas constituents called the atmosphere. This layer of gas, known as air, is retained by Earth gravity. The word atmosphere was introduced into the western languages in the 17th century and comes from the Greek ‘’atmos’’ meaning vapor and ‘’sphaira’’ meaning ball.The atmosphere plays an essential role in the protection of the life on the Earth.It absorbs short ultraviolet (UV) radiation which alters the DNA and the Infrared (IR) radiation reemitted by the Earth surface,and thus maintains temperatures favorable to life(greenhouse effect) and reducestemperature variationbetween day and night.It is considered that the atmosphere extends up to an altitude of more than 800 km (Seinfeld and Pandis, 2016). The atmosphere is generally described in layers as a function of different parameters such as the pressure, chemical composition, andtemperature or the electromagnetic properties.

I.1.2 Regions and characteristics of the atmosphere

The atmosphere is generally divided into several regions depending on the chemical composition, pressure, and mainly on the vertical temperature profile.Based on the evolution of the vertical temperature, the atmospheric regions, as shown inFigure I- 1, are namely the troposphere, stratosphere, mesosphere, thermosphere and a further region at about 500 km above the Earth'ssurface, called the exosphere(Finlayson-Pitts and Pitts Jr, 1999). Temperature shows a complex dependence on altitude linked to the chemical composition of the atmosphere and the capacity of the different molecules to absorb sunlight.The inversionpoints of the temperature gradient mark the boundaries between regions of the atmosphere (Finlayson-Pitts and Pitts Jr, 1999; Seinfeld and Pandis, 2016).

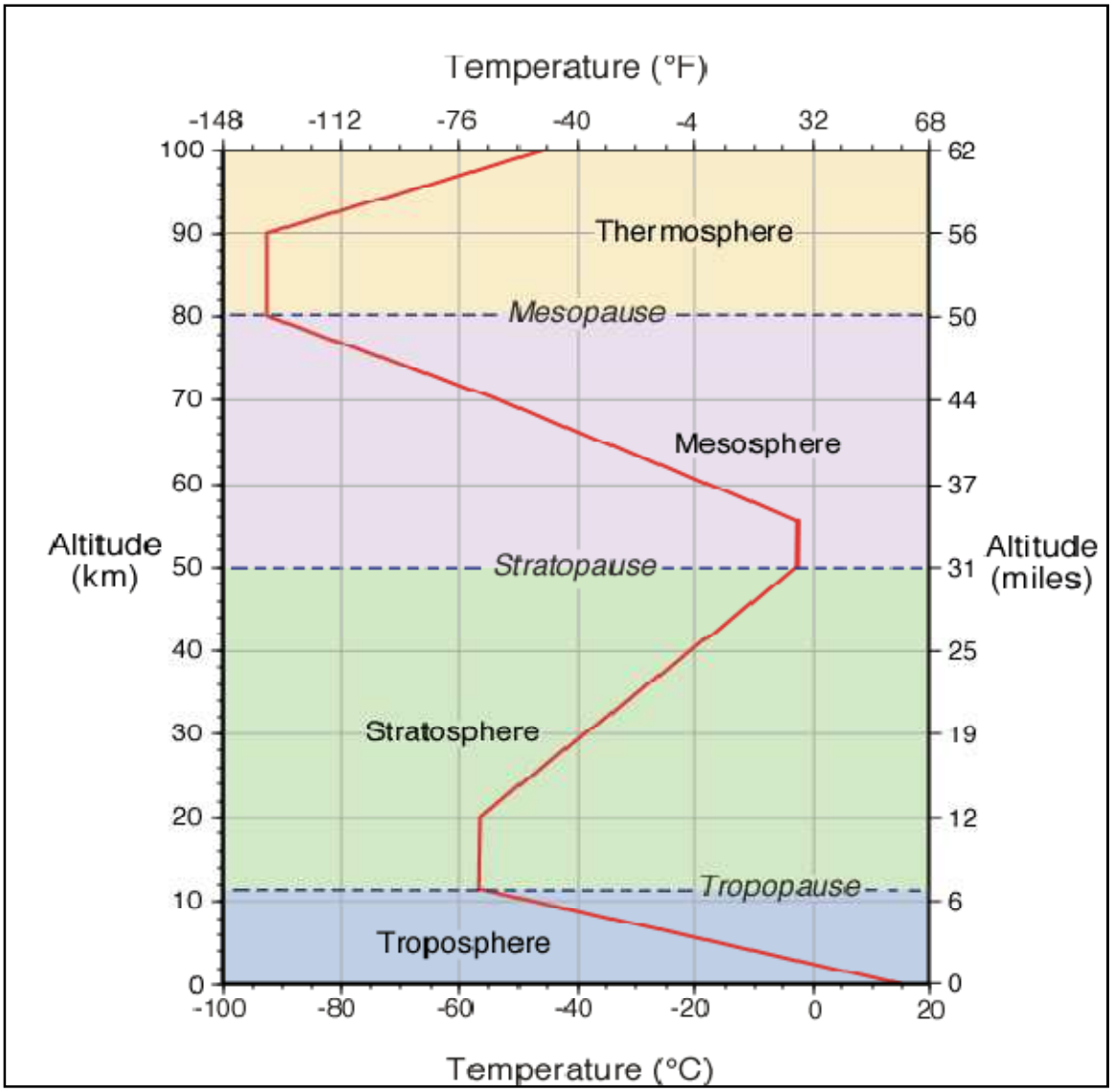

Figure I- 1: the temperature profile and layers of the atmosphere(Barker, 1995)

The different layers of the atmosphere are described in more details in the followings paragraphs.

I.1.2.1 The Troposphere

This is the lowest part of the atmosphere. It is the region where we live and the day to day phenomena associated with the weather take place (clouds, rain, snow...). The word troposphere originates from 2 Greece words (tropos) which means turning or mixing and (sphaira) meaningball.

The troposphere ranges from 0 to 15 km and is divided into two parts depending on the latitude (Finlayson-Pitts and Pitts Jr, 1999; Wayne, 2000): a small layer above the surface which is called the planetary boundary layer (PBL) and the free troposphere (FT). PBLis the air layer near theground affected by diurnal heat, moisture etc. The depth of the boundary layer varies depending on the location. Approximately it was found that the boundary-layer depth is between 0.5 and 2 km(Vogelezang and Holtslag, 1996). This is the region of the atmosphere which is directly affected by

the earth surface emissions and surface temperature. PBL hasan essential influence on the chemical composition of the atmosphere as the majority of the trace gases are emitted from the earth surface(Finlayson-Pitts and Pitts Jr, 1999).

In the troposphere, the temperature gets colder as the distance above the earth increases, by about 6.5°C per kilometer which is termed as environmental lapse rate (ELR). This temperature profile in the troposphere arises from the heating of the surface by the solar radiation. The absorbed radiation is re-emitted to the atmosphere, warming it close to the surface. As a result, the heated air masses above the earth's surface arise vertically due to convection. Cooling and adiabatic expansion of the air takes place as it is going up resulting in a vertical mixing. This mixing allows the transportation of the species from the surface to the free troposphere in several days depending on the weather conditions in the troposphere and the chemical stability of the species.The troposphere is a region of continuous turbulence and mixing, and it is where most of the chemical and physical processes take place (Finlayson-Pitts and Pitts Jr, 1999).The boundary layer between the troposphere and the stratosphere where the temperature profile changes from a decreasingtrendto an increasingone is called the tropopause.

I.1.2.2 The Stratosphere

The stratosphere extends upwards from the tropopause to about 50 km. It fulfills the conditions (composition, pressure, sunlight wavelengths) for the formation of the ozone layer. It contains much of the ozone present inthe atmosphere. The increase in temperature with height occurs because of absorption of ultraviolet (UV) radiation in a series of exothermic reactions involved in the formation cycle of the stratospheric ozone. Temperatures in the stratosphere are highest over the summer pole, and lowest over the winter pole. The ozone formation and destruction reactions are known under the "Chapman cycle"(Barker, 1995).

$$O_2 + h\vartheta(< 240\ nm) \rightarrow 2O^{\cdot} \qquad \text{R I- 1}$$

$$O^{\cdot} + O_2 \rightarrow O_3 \qquad \text{R I- 2}$$

$$O^{\cdot} + O_3 \rightarrow 2O_2 \qquad \text{R I- 3}$$

$$O_3 + h\vartheta\ (< 320\ nm) \rightarrow O^{\cdot} + O_2 \qquad \text{R I- 4}$$

As a result, less and less UV radiation passes through the stratosphere creating different temperature layers. This brings the name stratosphere because a stratification of the temperature occurs. In the stratosphere, the vertical mixing is weak compared to the horizontal mixing because of the lack of convection (Finlayson-Pitts and Jr, 1999; Finlayson-Pitts and Pitts Jr, 1999; Seinfeld and Pandis,

2016).Since ozone absorbs most of the solar light with wavelengths lower than 320 nm, it makes the stratospheric ozone an indispensable factor for the life on earth (Finlayson-Pitts and Pitts, 2000) by absorbing dangerous UV radiation (range 200-300 nm) destructing the DNA. However, chemicals (called CFCs or freons, and halons) which were used until the 90's for example in refrigerators, spray cans andfire extinguishershave reduced the amount of ozone in the stratosphere, leading to the so-called "Antarctic ozone hole".The stop of their use has ledalready to the gradual recovering of the ozone.

At the top of the stratosphere, a boundary layer called stratopause separates the stratosphere from the mesosphere. The temperature atthis level is about 270 K at a height of about 50 to 55 Km above the surface.

I.1.2.3 The Mesosphere

The region above the stratosphere is called the mesosphere (middle of the atmosphere), it extends from the stratopause up to 80-85 Km. In this region, the temperature again decreases with increasing altitude, reaching a minimum of about -90°C at the mesopause.

In the mesosphere, heating due to light absorption is less important than in the stratosphere due to the decrease in the concentration of oxygen and thus ozone. Subsequently, the temperature falls again with altitude and the vertical mixing within this region occurs. The mesopause is the layer which separates the mesosphere from the thermosphere, and it is the coldest region in the atmosphere.

I.1.2.4 The Thermosphere

The thermosphere lies above the mesopause, at an altitude of approximately 80 Km. The thermosphere is a region in which temperature again increases with altitude. Even if the density is less than in the mesosphere, in the thermosphere the molecules receive high amounts of energy from the Sun, at short wavelengths. This leads to a temperature increase, caused by the absorption of energetic ultraviolet and X-Ray radiation ($\lambda < 200$) from the Sun (Finlayson-Pitts and Jr, 1999; Finlayson-Pitts and Pitts Jr, 1999) by O,$^{\cdot}$ O_2 and N_2, filtering the atmosphere of these wavelengths.

I.1.2.5 The Exosphere

Itis the upper part of the atmosphere, based on electromagnetic properties. It extends from about 550 Km tothousands of kilometers. It contains mainly oxygen and hydrogen atoms, but there are so few of them that they rarely collide - they follow "ballistic" trajectories under the influence of gravity,

and some of them escape right out into space. This is the area where satellites orbit the earth.My PhD thesis work is focused on the chemistry of the troposphere and its chemical composition is described in more detail in the next paragraph.

I.1.3 Chemical composition of the troposphere

The troposphere is the layer where most of the air is concentrated, in particular in the planetary boundary layer (PBL)and where most of the chemical transformations take place. The air consists of 2major constituents which are nitrogen N_2(78% by volume), andoxygenO_2(21% by volume) molecules. The remaining 1% of theatmospheric gasesis known as trace gases because they are present in small concentrations. The concentration of these gases is generally expressed in mixing ratio (ratio of the number of molecules of the trace gas to the total number of molecule in the same volume) in part per million (10^{-6}) by volume (ppmv), per billion (ppbv, 10^{-9}) or per trillion (pptv , 10^{-12}). The most abundant of the trace gases is the noble gas argon (approximately 1% by volume). Noble gases, which also include neon, helium, krypton and xenon, are inert and do not take part inany chemical transformation within the atmosphere. In addition, other trace gasesas CO, CO_2, CH_4 and volatile organic compounds (VOC), nitrogen species as NO, NO_2, N_2O, $NH_3$and peroxyacylnitrates (PANs), sulphur containing species as SO_2, dimethylsulphine (DMS) and H_2S, ozone, and halogenated compounds as hydrochlorofluorocarbons(HFCs), hydrochlorofluorocarbons(HCFCs), HCl, HF, CH_3Cl, CH_3Br and CH_3I are present(Seinfeld and Pandis, 2016).In addition, there is a variable concentration of water vapor ranging from less than 1% to 4% (Wayne, 2000). Water vapor concentration can be represented by therelative humidity(abbreviated RH) which is the ratio of thepartial pressureof water vapor (P_{water}) to theequilibrium vapor pressureof water at the given temperature (P_s). The equilibrium vapor pressure decreases with decreasing temperature and depends only on the temperature.RH will change in the atmosphere as a function of the local composition of the air mass (varying P_{water}) and the temperature (varying P_S).

Natural processes which produce trace gases include emissions from trees and plants, volcanic eruptions, natural fires, thunderstorms and biological processes.Anthropogenic origin related to the human activities such as agriculture, transport, industries and household activities are also a source of trace species.Despite their relative scarcity, the role of trace species is crucial in the atmosphere. Carbon dioxide, methane, nitrous oxide,water vaporand ozone are called greenhouse gases. Their name comes from their capacity to warm the atmosphere. Apart from water vapor, the most abundant greenhouse gas (by volume) is carbon dioxide.

Organic compounds are another type of trace species emitted in the atmosphere through natural and anthropogenic activities. In this way, VOCs are regarded as biogenic VOCs (BVOCs) and anthropogenic VOCs (AVOCs). There is also another important class of VOCs, called oxygenated VOCs (OVOCs), which includes compounds having at least an oxygen atom in their structure, both from natural and anthropogenic origin, or generated from oxidation reactions occurring in the atmosphere, hence secondary products. Natural activities are responsible of the emission of the largest majority of VOCs (90%). However, even if minor, anthropogenic emissions increase drastically since the 1900's with an impact on radiative processes and air quality by controlling the formation of tropospheric ozone and secondary organic aerosols in different environments.

Unstable reactive species like ions, atoms and radicals are also present in very small concentrations (ppt level or below).Some of these radicals have an essential effect on the chemical composition and the chemistry of the atmosphere like hydroxyl radicals (OH), hydroperoxyl radicals (HO_2)and peroxy radicals (RO_2, R being an hydrocarbon group) (Finlayson-Pitts and Jr, 1999).They are involved in most of the gas phase oxidation processes during the day, whereas NO_3 radicalsplay a similar role than OH during the night.The concentrationranges of several species present in the atmosphere are listed inTable I- 1.These are typical ranges of atmospheric mixing ratios but they are not representative for every place in the world (for example, remote environments have often NMHC below 5 ppbv).

Table I- 1:Fraction of volume of air occupied by different species at 1 atm in the troposphere (Wallace and Hobbs, 2006)

Gas	Chemical formula	Fraction of volume of air occupied by the species
Nitrogen	N_2	78.084%
Oxygen	O_2	20.946%
Argon	Ar	0.934%
Carbon dioxide	CO_2	379 ppmv
Neon	Ne	18.18 ppmv
Helium	He	5.24 ppmv
Methane	CH_4	1.7 ppmv
Hydrogen	H_2	0.56 ppmv
Nitrous oxide	N_2O	0.31 ppmv
Carbon monoxide	CO	40-200 ppbv
Ozone	O_3	10-100 ppbv
Nonmethane hydrocarbons	-	5-20 ppbv
Halocarbons	-	3.8 ppbv
Hydrogen peroxide	H_2O_2	0.1-10 ppbv
Formaldehyde	HCHO	0.1-1 ppbv
Nitrogen species	NO_X , N_2O_5 , HNO_3	10 pptv - 1 ppmv
Ammonia	NH_3	10 pptv - 1 ppbv
Sulfur dioxide	SO_2	10 pptv - 1 ppbv
Dimethyl sulfide (DMS)	CH_3SCH_3	10-100 pptv
Hydrogen sulfide	H_2S	5-500 pptv
Carbon disulfide	CS_2	1-300 pptv

Hydroxyl radicals	HO	0 – 0.4 pptv
Hydroperoxy radicals	HO_2	0 – 5 pptv

Smallsolid and/or liquid particles are present in suspension in the atmosphere and are called atmospheric aerosols (excluding cloud particles). These particles range in size from a few nanometers to millimeters (Finlayson-Pitts and Pitts Jr, 1999).

Atmospheric aerosols can be either primarily emitted to the atmosphere or secondarily formed during the transformation of chemical species in the atmosphere. Typically, primary aerosols are dust, sea salt, volcanic ashes or soot. Sulphuric acid, sulphates, nitrates, organic matter and biogenic VOCs are the typical precursors for secondary aerosols (Finlayson-Pitts and Pitts Jr, 1999; Wayne, 2000).

The different species present in the troposphere can interact through physical and chemical processes which influence its composition, with impact on air quality, health and climate change. The main motivations and strategies to study the chemical transformations in the troposphere are described in the following paragraph.

I.2 Interest of the atmospheric measurements and motivations

Due to direct impact of the atmosphere composition on our healthand onthe climate,pressure is being put on governments to act and control the rise in greenhouse gases and pollutants. They determine policy changes to limitthe climate change and improve the air quality based on the results ofcomplex models that aim to predict pollutant levels and the future of our climate. These models are based on the description of the physical and chemical processes taking place in our atmosphere.In order to develop, test and improve these models, observations of atmospheric constituents and laboratory studies,investigatingthe understanding of the chemical processes, are needed. For example, the atmospheric lifetimes of certain greenhouse gases, particularly methane, are controlled by the chemical oxidation. Oxidationprocesses can enhance the production of much more toxic gases and particulate matter than the primary emitted species, and participate to the chemical aging of particles, modifying their properties. All these processes impact the atmospheric composition and the change in our climate with consequences for natural resource sectors, such as agriculture, forestry, ecosystems, water resources, and fisheries and on other human activities. It is why it is essential to have a good understanding ofthe reactions and processes that take place in the atmosphere in order to be able to predict the pollution events at shorter scale,the evolution of the atmosphere on long term scale, and their impact on the climate change.

One of the most important oxidants in the atmosphere is the OH radical.It'scalled the detergent of the atmosphere. OH reactions are the primary removal processes for many trace gases, such as carbon monoxide, methane andorganic compounds (VOCs). The degradation of these trace gases leads to the formation of secondary gaseous species and organic aerosols (SOA). Hydroxyl radicals are linked to the hydroperoxyl radical, HO_2, through a series of oxidation steps involving VOCs, NO and leading to the formation of different peroxy radicals (RO_2) as a function of the hydrocarbons present in the local air mass.These highly reactive radicals, known collectively as HO_x for the sum of OH and HO_2, have short tropospheric lifetimes (<1 s and ~100 s for OH and HO_2 respectively) and their concentrations are therefore uninfluenced by transport processes.Close monitoring of $HO_x$and RO_2concentrations can therefore provide useful information on the chemical reactions taking placeand the oxidative capacity of a specific environment.

I.2.1 Chemistry of HO_x radicals in the atmosphere

The OHradical plays a very important role in the chemistry of the atmosphere oxidizing both anthropogenic and natural trace species. It controls the rates of removal of most of these trace gases during the day. These chemicaltransformations involve rapid interconversion between OH and HO_2,initiatethe hydrocarbons degradation,the formation of tropospheric ozone, the photochemical smog and influencethe global warming and acid rain. The reactions producing or consuming OH, HO_2 and RO_2 radicals are listed in the coming sections.

I.2.1.1 OH radical

OH is highly reactive; its concentration ranges between 10^5-10^7 molecule cm^{-3} and its lifetime from ms in polluted areas to 1 second in clean environments. Its processes of formation and consumption are multiple and briefly described here.

The main source of OH in the troposphere is *via* the ozone photolysis (λ <310 nm) to form an electronically excited oxygen atom O (^1D)that reacts with water vapor to form OH.

$$O_3 + h\nu_{< 310\ nm} \rightarrow O(^1D) + O_2 \qquad \text{R I- 5}$$

$$O(^1D) + H_2O \rightarrow 2\ OH \qquad \text{R I- 6}$$

Reaction R I- 6is, however, a minor consumption pathway of the O (^1D) since the water vapor concentration in the troposphere is low (~1%) compared with the $N_2$and O_2 concentration (~99%) with whichexcited oxygen atom O (^1D) can also relax by collision (calledquenching,R I- 7) to decay to the ground state O(^3P), whichreact with O_2 to reform O_3 according to the following reactions:

$$O(^1D) + M\ (N_2, O_2 \text{ or } H_2O) \rightarrow O(^3P) + M \qquad \text{R I- 7}$$

$$O_2 + O(^3P) + (M) \rightarrow O_3 \qquad \text{R I- 8}$$

The production rate of OH by ozone photolysis is determined by the relative rates of reactionsR I-5andR I- 7and the concentration of H_2O.

OH production can also be done in the troposphereby photolysis of other species such as nitrous acid (HONO),or hydrogen peroxide (H_2O_2). These photolysis sources typically constitute a minor route to OH formation.

$$HONO + h\nu_{< 400\ nm} \rightarrow OH + NO \qquad \text{R I- 9}$$

$$H_2O_2 + h\nu >_{300\ nm} \rightarrow 2\ OH \qquad \text{R I- 10}$$

In addition, other reactions such as the reactions of O_3 with alkenes including isoprene andmonoterpenes lead to the formation of OH (Chew and Atkinson, 1996).

$$O_3 + \text{alkenes} \rightarrow OH + \text{products} \qquad \text{R I- 11}$$

OH can also be formed through the reactions of HO_2 with O_3.

OH can be consumed by reaction with NO_2 or hydrocarbon species (called RH in the following) but in that case, it initiates a cycle which forms HO_2andthe reactions involving the conversion of HO_2 into OH can be seen as OH reservoir reactions.These reactions are summarized below.

$$OH + RH \rightarrow R + H_2O \qquad \text{R I- 12}$$

$$R + O_2 + M\ (\text{third collision partner}) \rightarrow RO_2 + M \qquad \text{R I- 13}$$

$$RO_2 + NO \rightarrow RO + NO_2 \qquad \text{R I- 14}$$

$$RO + O_2 \rightarrow HO_2 + R'CHO \qquad \text{R I- 15}$$

$$HO_2 + NO \rightarrow OH + NO_2 \qquad \text{R I- 16}$$

The sum of $RO_2 + RO + HO_2 + OH$ is called RO_xradicals.

Sources and consumption paths of HO_2 are described in the next paragraph.

I.2.1.2 HO_2 radical

HO_2 is less reactive than OH,its lifetime varies between 10 s in polluted areas and 1 min in clean environmentsand its concentration is in the rangeof 10^7-10^8molecule cm^{-3}. In the presence of NO_X and RO_2, HO_2 radicals are productsof reactionsR I- 12to R I- 15. In the case of methylperoxyl (R = CH_3), it also leads to the formation of formaldehyde:

$$CH_3O_2 + NO \rightarrow CH_3O + NO_2 \qquad \text{R I- 17}$$

$$CH_3O + O_2 \rightarrow CH_2O + HO_2 \qquad \text{R I- 18}$$

The reaction between CO and OH is also producing HO_2:

$$OH + CO + O_2 \rightarrow \quad HO_2 + CO_2 \qquad \text{R I- 19}$$

In areas with lowNO_X, HO_2 radicals can be consumed and producedby reaction involving ozone:

$$HO_2 + O_3 \rightarrow OH + 2O_2 \qquad \text{R I- 20}$$

$$OH + O_3 \rightarrow HO_2 + O_2 \qquad \text{R I- 21}$$

or from reactions of recombinationofRO_2illustrated here forCH_3O_2:

$$CH_3O_2 + CH_3O_2 \rightarrow \quad 2\ CH_3O + O_2 \qquad \text{R I- 22}$$

$$CH_3O + O_2 \rightarrow CH_2O + HO_2 \qquad \text{R I- 18}$$

or from reaction between OH and RO_2, here for example for CH_3O_2 (Assaf et al., 2017a):

$$CH_3O_2 + OH \rightarrow CH_3O + HO_2 \qquad \text{R I- 23}$$

HO_2 canalso be produced by photolysis of aldehydes such as formaldehyde:

$$CH_2O + h\nu \rightarrow H + HCO \qquad \text{R I- 24}$$

$$H + O_2 + M \rightarrow HO_2 + M \qquad \text{R I- 25}$$

It is consumed by reacting with NO (R I- 16) or ozone (R I- 20) or halogen compounds, X representing a halogen such as Cl, Br, I (R I- 26 and R I- 27) to form OH:

$$HO_2 + XO \rightarrow \quad HOX + O_2 \qquad \text{R I- 26}$$

$$HOX + h\nu \rightarrow OH + X \qquad \text{R I- 27}$$

It can also react with itself to form H_2O_2 or with RO_2:

$$HO_2 + HO_2 \rightarrow H_2O_2 \qquad \text{R I- 28}$$

$$RO_2 + HO_2 \rightarrow ROOH + O_2 \qquad \text{R I- 29}$$

$$\rightarrow ROH + O_3 \qquad \text{R I- 29a}$$

$$\rightarrow RO + OH + O_2 \qquad \text{R I- 29b}$$

$$\rightarrow R'CHO + H_2O + O_2 \qquad \text{R I- 29c}$$

The yield of the different reaction pathways varies according to the RO_2 and little is known about these reactions (Dillon and Crowley, 2008), especially for larger peroxy radicals.At night, the production of HO_X is from the reaction of NO_3 with VOCsleading to peroxyl radicals (RO_2) (Bey et al., 2001) or by reactions between ozone and alkenes.

I.2.1.3 RO_2 radicals

Peroxy radicals,RO_2, are producedby the reactions of OH, during the day, and NO_3 with anthropogenic andbiogenic organic gaseous species in the atmosphere such as CH_4(Parker et al., 2009) or VOCs. OH, HO_2 and RO_2 radicals form a catalytic reaction cycle in which RO_2has an essential effect on OH and HO_2 removal and production in the atmosphere as described in the reactionsR I- 12 to R I- 29.This cycle is connected to the photochemically driven equilibrium between NO_2 and NO. Both together are responsible for the production of ozone in the atmosphere(Fuchs et al., 2008)(Monks, 2005). Peroxy radicals are present in the atmosphere at similar concentrations than HO_2.When producedby R I- 12andR I- 13, peroxyradicals undergo reaction with NO (R I- 14) or HO_2 (R I- 29). Reaction with NO is dominated by the production of NO_2 and an alkoxy radical, RO, (R I- 15) and further reaction with O_2 produces HO_2 (Figure I- 2).

This is summarized in the following reactions (R I- 30 being the result of R I- 10 to R I- 13andR I- 32being the result of R I- 30toR I- 31)

$$RH + 2\,O_2 + 2\,NO \rightarrow R'CHO + H_2O + 2\,NO_2 \qquad \text{R I- 30}$$

$$2(NO_2 + h\nu < 420\ nm \rightarrow NO + O(^3P)) \qquad \text{R I- 31}$$

$$2\,(O(^3P) + O_2 + M \rightarrow O_3 + M) \qquad \text{R I- 32}$$

$$RH + 4\,O_2 + h\nu \rightarrow R'CHO + H_2O + 2\,O_3 \qquad \text{R I- 33}$$

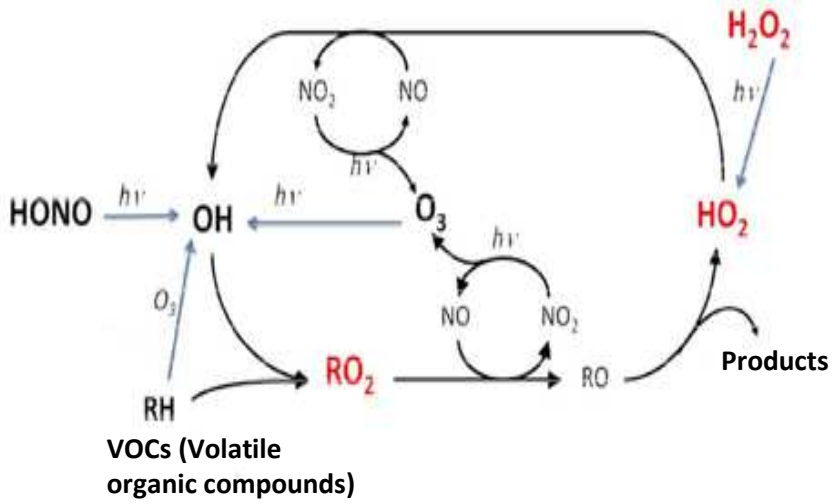

Figure I- 2: simplified schematic of the radical photochemistry in the troposphere.

RO_2 can also react with HO_2(R I- 29)or other RO_2 or with NO or $NO_2$to produce organic nitrates or peroxynitrates (R I- 34,R I- 35) which are stable during night time.

$$RO + NO + M \rightarrow RONO + M \qquad \text{R I- 34}$$

$$RO_2 + NO + M \rightarrow RO_2NO + M \qquad \text{R I- 35}$$

Recently, the reactions of the smallest RO_2(C1 to C4) with OH have been measured and found to be fast(Assaf et al., 2016, 2017b). Depending on the yield of the different paths, these reactions can have important effect on the atmospheric composition.

$$RO_2 + OH \rightarrow ROOOH + O_2 \qquad \text{R I- 36}$$

$$\rightarrow ROH + O_2 \qquad \text{R I- 37}$$

$$\rightarrow RO + HO_2 \qquad \text{R I- 38}$$

I.2.2 Determinants of HO_x radicals concentration in the atmosphere

OH and HO_2concentrations depend on the chemical composition of the atmosphere and the photolysis processes, and will vary depending on the location as well as the meteorological conditions. The concentration of OH is governed by the balance between the processes of formation and consumption.

$$\frac{d([OH])}{dt} = P(OH) - L(OH) \qquad \text{Eq I- 1}$$

where P represents the OH production rate and can be expressed as:

$$P(OH) = k_{HO2+O3}[HO_2][O_3] + k_{NO+HO2}[NO][HO_2] + \sum \Phi_{OH} k_{O3+alkenes}[alkenes][O_3] + \sum v_i J_i[i] \quad \text{Eq I- 2}$$

including the production of OH by HO_2 (with ozone or NO), by ozonolysis of alkenes (Φ_{OH} is the OH yield of the reaction), by photolytic sources using O_3 or other sources such as HONO, H_2O_2 (where v_i is the OH yield and J is the frequency of photolysis of species i in s^{-1}).

The photolysis frequencies are calculated as follows:

$$J(T) = \int \sigma(\lambda,T).\varphi(\lambda,T).F(\lambda).d\lambda \quad \text{Eq I- 3}$$

where F (λ) is the actinic flux(in photons cm^{-2} s^{-1} nm^{-1}), σ (λ, T) and ϕ (λ, T) are respectively the absorption cross sections (in cm^2 $molecule^{-1}$) and the quantum efficiency of the molecule, that represents the probability that the molecule dissociates after absorption of a photon.

L(OH) represents all the losses of OH such as the consumption by NO, NO_2, CH_4, CO and with all the reactive species (X) such as volatile organic compounds (VOCs).

$$L(OH) = k_{OH+NO}[NO][OH] + k_{OH+NO2}[NO_2][OH] + k_{OH+CH4}[CH_4][OH] + k_{OH+CO}[CO][OH] + \sum k_{OH+X}[X][OH] \quad \text{Eq I- 4}$$

The consumption and formation pathways of OH in the atmosphere are so fastthat,in a firstapproximation, the steady state can be assumed for the OH concentration in the atmosphere. d[OH]/dt= 0 can be considered, andan estimation of the OH concentration is given as the ratio between its production sources and its consumption pathways.

$$[OH] = \frac{k_{Ho2+O3}[HO_2][O_3] + k_{NO+HO2}[NO][HO_2] + \sum \Phi_{OH} k_{O3+alkenes}[alkenes][O_3] + \sum_i v_i J_i[i]}{k_{OH+NO}[NO] + k_{OH+NO2}[NO_2] + k_{OH+CH4}[CH_4] + k_{OH+CO}[CO] + \sum_n k_{OH+X}[X]_n} \quad \text{Eq I- 5}$$

However, this approximation provides only a rough estimation of the OH concentration and measurements are needed to determine the real concentration of OH in different environments in order to understand its chemistry. Different types of instruments have been developed and deployedduring intensive field campaigns(Di Carlo et al., 2004; Fuchs et al., 2017a; Griffith et al., 2016; Hansen et al., 2015; Stone et al., 2012; Tan et al., 2016; Whalley et al., 2016)at ground or

inairplanes to study the OH and HO_2 sources and sinks. These ambient measurements arecompared to modeled concentrationsobtained using atmospheric models. These models reflect the chemical reactions taking place in the atmosphere and simulate the concentration level of the different species depending on conditions. We can mention, for example, the MCM (Master Chemical Mechanism) with more than 12,700 reactionsand 4,400 species (Jenkin et al., 2003). Summary of the main results can be found in paragraph I.3.3.

Good agreement between ambient measurements of [OH] and [HO_2] under a variety of atmospheric conditions and the results of chemical models constrained to the concentrations of long-lived species such as VOCs, NO_x, and O_3, is a good indicationthat our understanding of the oxidation chemistry in these regions of the troposphere is robust.Though it should be noted that agreement can also be achieved even if sinks and sources of similar magnitude are missing inthe model. Poor agreement indicates that chemical or physical processes are missing inthe model, and usually prompts further atmospheric measurements or laboratory experiments to discover the missing part of the mechanism.

Recent studies in environments rich in biogenic VOCs such as isoprene and low in nitrogen monoxide (<100 ppt) often exhibit significant differences between measurement and modeling (Kubistin et al., 2010; Lelieveld et al., 2008; Pugh et al., 2010; Tan et al., 2001; Whalley et al., 2011). These discrepancies suggest either measurement artifacts for OH, HO_2 potentially, or an incomplete understanding of reaction mechanisms involving HO_x radicals (more details in paragraph I.3.3).

It can be mentioned that studies in laboratories (Winiberg et al., 2015) or in simulation chambers (Fuchs et al., 2017b), using similar instruments can also help in determining more accurate chemical mechanisms.This combination of laboratory and field measurements coupled to modeling studies is the key to the study of atmospheric chemistry.

I.2.3 OH reactivity in the atmosphere

Although HO_x quantification providesimportant information about radicalchemistry, to access to a better description of the radicals balance, another parameter is particularly interesting to measure: the reactivity of the OH radical. OH reactivity is defined as the first order loss rate of the hydroxyl radical with ambient air and represents the inverse of its lifetime.

OH reactivity provides a globalinformation about the budget of the species reacting with OHpresent in the atmosphere. In general, the higher the reactivity is,the more polluted is the area, butthe OH reactivity directly depends on the species concentrations in the air weighted by their respective rate constant. OH reactivity is expressed in s^{-1} and is defined by:

$$k_{air} = \sum_i k_{Xi+OH}[Xi] \qquad \text{Eq I- 6}$$

with X_i being a reactive chemical species, $k_{Xi}$the rateconstant of OH with X_i and, $[X_i]$ the concentration of the species X_i. OH reactivity (R_{air}) can be calculated by summing the individual reactivity of the different species (Eq I- 6).

Recent instruments have been developed to measure OH reactivity which can be compared to acalculated reactivity from the concentrations of species reacting with OH simultaneously measured at the same place(Nölscher et al., 2012a). Any discrepancy between measured and calculated OH reactivity represent OH sinks that have not been characterized by trace gas measurements and indicates that important unmeasured reactive species are present. The difference between the measured and calculated reactivity is called missing reactivity.

$$k_{missing} = k_{air} - k_{calculated} = \sum k_{OH+Xi\ un}\ [Xi_{un}] \qquad \text{Eq I- 7}$$

with $[Xi_{un}]$ the concentration of unmeasured species Xi_{un}.

The missing reactivity provides an important parameter for the study of chemical processes in the atmosphere even if it does not provide direct information on the nature of the species involved(Zannoni, 2015). Several ambient measurements were done in different sites and different techniques in an attempt to understand the hidden chemistry of the OH reactivity(Yang et al., 2016).

A large number, probably more than 10^5, of different VOCs exists in the atmosphere (Goldstein and Galbally, 2007), but less than one hundred are commonly measured in field campaigns.Different field experiments showed that there is in many environments a missing OH reactivity, which could be due to a fraction of organic compounds missed by the instrument dedicated to VOCs and deployed simultaneously with OH reactivity instruments(Mao et al., 2009; Sadanaga et al., 2005). Thus, incomplete VOCs measurement and/or not suitable techniques used can explain at least a part ofthe missing OH reactivity.TheOH reactivitymeasurement is useful in urban environments where the amount of VOCs is often very high, above the canopy to study the highly reactive biogenic species or in remote environmentswhere oxidized or "aged" air masses can be studied.

Heterogeneous losses of radicals on the surface of aerosol particles could be one of the possible processes to explain the difference, however, the consumption of OH being fast by reactions in the gas phase, this contribution should be minor. Indeed, correlations between measured and missing reactivities showed that the missing reactivity could not be explained by loss of OH on the surface of particles(Mogensen et al., 2011). Until now, from the different fields campaigns, the missing reactivity seems rather due to VOC oxidation products that form more oxidized, semi-volatile compounds reacting with OH, but that are not detected(Mogensen et al., 2011; Sinha et al., 2010; Whalley et al., 2016).Another use of the OH reactivity measurements is to estimate the rate of ozone production. Indeed, the instantaneous production rate of ozone can be linked to the reactivity of OH when combined with measurements of NO_X, OH and peroxy radicals. This approach was used to analyze the impact of point sources of ozone during a campaign in a coastal site in Spain (Sinha et al., 2010). It showed that ozone production was higher when the site was influenced by continental air masses. This studydemonstrated that monitoring the air quality could be improved by measures of the reactivity of OH, NO_X and O_3.The different techniques used to characterize the HO_x and RO_x radicals and the OH reactivity are described in the following paragraph.

I.3 Review of the techniques for the quantification of $HO_x$and RO_xradicalsin the atmosphere

The important role of HO_x radicals in atmospheric chemistry has motivated the development of measurement techniques for atmospheric OH, HO_2 and RO_2 radicalsand the OH reactivity.Instruments developed for field measurements are described briefly below. These measurements are essential to understand the atmospheric chemistry and toimprovemodels. The high reactivity of HO_x radicals results in low ambient steady state concentrations (~10^6 and ~10^8 molecule cm^{-3} for OH and HO_2 respectively) and hence detection techniques need to be highly sensitive.

I.3.1 Techniques for $HO_x$and RO_xquantification

Different techniques are used to measure the concentration of OH, or OH and HO_2or the sum of RO_2 or RO_X (RO_2 + RO + HO_2 + OH). The most common instruments used to make these measurements in the field are describedin the following sections which summarize various techniques used by different groups in the world with their principles of operation, the advantages and disadvantages. More information can be found for OH and HO_2in the dedicated review article from Heard and Pilling(Heard and Pilling, 2003)and in the articles related to an inter-comparison campaigns (Fuchs et al., 2010a; Schlosser et al., 2009).

I.3.1.1 OH detection

Experimental devices for quantifying OH radicals in the atmosphere are few due to the many constraints related to this species suchas the low concentration and high temporalvariability. They are either based on spectroscopic techniques: Fluorescence Assay by Gas Expansion (FAGE, temporal resolution of 1-10 min), Differential Optical Absorption Spectroscopy (DOAS, temporal resolution of 200 s to 10 min), or chemical techniques: Chemical Ionization Mass Spectrometry (CIMS temporal resolution of 30 s 1 min), oxidation by detecting ^{14}CO (time resolution of 5 minutes), by chemical trapping using the salicylic acid (temporal resolution of 30 to 90 min) or trapping on cold matrix (temporal resolution of 20 to 30 minutes (Heard and Pilling, 2003). It may be noted that among the chemical techniques, only the method by CIMS enables temporal resolution measurements high enough for a detailed analysis of the atmospheric chemistry. Indeed, to identify phenomena involving OH, it is necessary to be able to achieve god time resolution since fast variation of the environmental conditions (sun, pollutants) will impact rapidly the OH concentration.Among FAGE, it was therefore chosen to focus on the description of the methods CIMS and DOAS with similar performances in terms of detection limit and temporal resolution compared to those of FAGE, used during this work.

I.3.1.1.1 FAGE (Fluorescence Assay by Gas Expansion)

Following the discovery of the importance of OH radicals in the atmospheric oxidation chemistry (Levy, 1971; Weinstock, 1969), it was suggested in 1972 (Baardsen and Terhune, 1972) that the laser induced fluorescence (LIF) technique can be suitable for OH measurement in the atmosphere.It was applied to make the first quantification of OH and HO_2in the atmosphereby Hard et al. (Hard et al., 1979).

However due to constraints linked to the atmospheric environment (as the presence of ozone and the low concentration of OH), the first instruments developed suffered from interferencesdue to the photolysis of ozone and low sensitivity due to high background signal. Following this, theFAGE (Fluorescence Assay by Gas Expansion) techniquehas been developed, still basedon the detection of OH by LIF but at a longer excitation wavelength and at low pressure.

Nowadays, about ten groups in the world are using this type of instrument.Laser Induced Fluorescence (LIF) involves the excitation of a molecule or radical in a rovibronic transition from its ground state to an electronically excited state using laser light. The subsequent relaxation of the species from the excited state can be accompanied by spontaneous emission of light (fluorescence), the intensity of which is directly proportional to the concentration of the species probed. The speciescan also relax *via* nonradiative processes such as collisional quenching, in which the excess energy is transferred to another molecule (O_2 or N_2).For the first atmospheric OH measurement, laser light at λ=282 nm was used to excite the OH radical in order to spectrally separate the fluorescence light from the OH relaxation from the scattered laser light (Baardsen and Terhune, 1972). However, at that excitation wavelength, the photolysis of ozone causes asignificant interference by the OH production (R I- 5,R I- 6). For this reason, all LIF instruments now are using laser light atλ=308 nmto excite one line of the OH radical in the A (v′=0) -X (v′′=0) transition, and detect the fluorescenceover the fluorescence band in the same wavelength range(Figure I- 3).This reduces the photolysis of ozone by about a factor of 30. The use of high repetition rate lasers with low pulse energies allows increasing the sensitivity and the time resolution. The main drawback of this excitation/collection scheme is that the fluorescence cannot be separated spectrally from the excitation and a temporally delayed detection is needed.

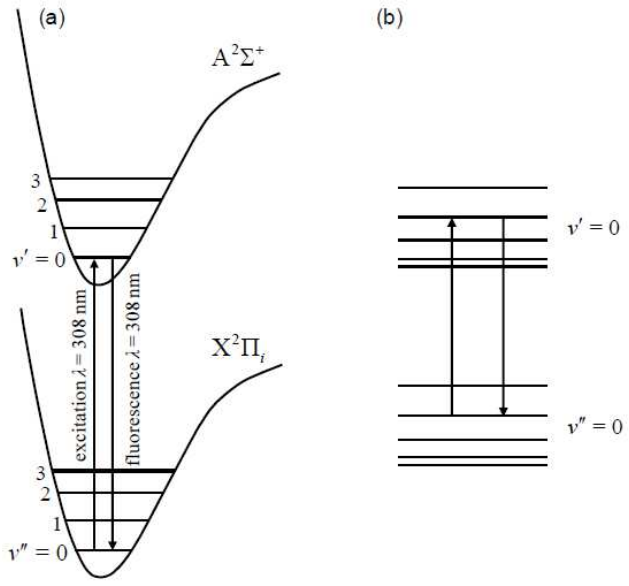

Figure I- 3: Excitation and fluorescence scheme of $A^2\sum^+$ (V′=0)← $X^2\prod_i$ (V́′′=0) OH transition at λ=308 nm(Heard, 2006).

In the conditions of the UL (University of Lille)-FAGE instrument,the OH fluorescence lifetime is about 800 ns, which is longer than the laser pulse (τ_{laser} =20 ns). Then the laser scattered light can be

temporally discriminated from the fluorescence signal by using a gated detector (see chapter IIfor more details).The FAGE instruments are generally calibrated with a source based on water vapor photolysis by a mercury lamp but other calibration sources have also been tested(Dusanter et al., 2008).

I.3.1.1.2 CIMS (Chemical Ionization Mass Spectrometry)

The CIMS technique is a technique were OH is chemically converted in a reactor at atmospheric pressure into a molecule that can be ionized and then detected using a mass spectrometer (Berresheim et al., 2000; Eisele and Tanner, 1991).The CIMS technique is based on a rapid titration of the OH radicals by $^{34}SO_2$after sampling to produceand detect $H_2{}^{34}SO_4$without interference with the ambient $H_2{}^{32}SO_4$:

$$OH + {}^{34}SO_2 + M \rightarrow H{}^{34}SO_3 \qquad \text{R I- 39}$$

$$H{}^{34}SO_3 + O_2 \rightarrow {}^{34}SO_3 + HO_2 \qquad \text{R I- 40}$$

$$^{34}SO_3 + 2\ H_2O \rightarrow {}^{34}SO_4\ H_2 + H_2O \qquad \text{R I- 41}$$

$H_2{}^{34}SO_4$ is then ionized into $H{}^{34}SO_4^-$ in an ionization chamber by reaction with NO_3^-produced separately in the ion source by a corona discharge. The $H{}^{34}SO_4^-$ ions are then pumped and selectively detected by a quadrupole mass spectrometer.

$$H_2{}^{34}SO_4 + NO_3^- \rightarrow H{}^{34}SO_4^- + HNO_3 \qquad \text{R I- 42}$$

The CIMS instruments are calibrated using a H_2O photolysis calibration system similar to those used for FAGE instruments. The limit of detection of this technique is below 10^5 cm^{-3} for 5 min average (Eisele et al., 1996). The main limitation of the CIMS is the conversion of HO_2(from R I- 41) into OH at high NO concentrations which then causes an artificial signal. Care was taken in order to reduce this effect by minimizing the reaction time between OH and SO_2(Tanner and Eisele, 1995). Propane is also regularly added in order to quantify other interferences.

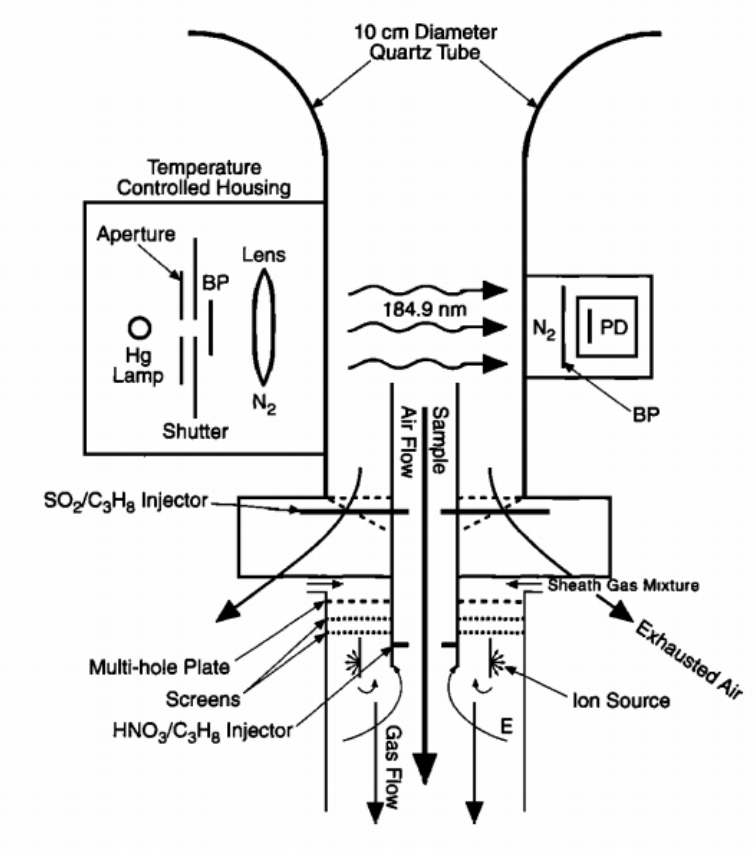

Figure I- 4:schematic of CIMS instrument employed by Eisele (Tanner and Eisele, 1995). The gas flow enters the detection chamber coming from a calibration cell at the top of the CIMS.The resultant ions from chemical titration of tropospheric OH are detected by mass spectrometry. In the calibration cell, BP:is a bandpass filter which filter only the 185 nm wavelength and reject the others and PD: is a photodiode for measuring the wavelength magnitude passed through the filter.

I.3.1.1.3 DOAS (Differential Optical Absorption Spectroscopy)

The DOAS technique is a spectroscopic technique. It is based on the extinction of UV light passing through the atmospheric sample by absorption of OH over a long path according to the Beer Lambert law:

$$ln\left({}^{I_0}/_{I}\right) = \sigma_{OH\,(\lambda)} \times [OH] \times l \qquad \text{Eq I- 8}$$

with I_0 and I the light intensities before and after travelling through the air sample and $\sigma_{OH}(\lambda)$ the absorption cross section of OH (cm^2)atthe wavelength λ, [OH] the concentration of OH (molecule cm^{-3}) and lthe absorption length (cm).The basic drawing of the technique is shown inFigure I- 5.

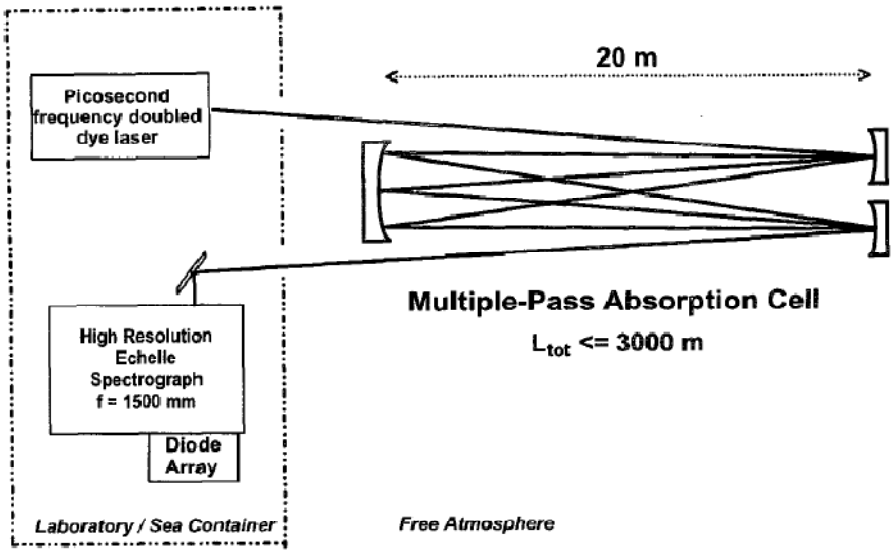

Figure I- 5:schematic of Differential Optical Absorption Spectroscopy instrument(Dorn et al., 1995).

The instrument consists of 4 elements:

1) A laser source. The light intensity should have a high luminance because of the long path length and a homogeneous spectral profile for each laser pulse is necessary in order to be selective.

2) An open cell with multi-path reflection to improve the spatial resolution with a distance of several meters between the input mirror and the back mirrors depending on the instrument and its deployment (the beam makes typically hundred pathsto give an absorption path length of several km in order to obtain a good detection limit).

3) A high resolution spectrometer for detecting OH absorption lines.

4) A cooled photodiode for improved signal detection.

Hence DOAS is an absolute *in-situ* measurement technique that requires no calibration.The absorption cross sections are available in the literature and if the absorption path length is known, the OH concentration is obtained by deconvoluting the spectrum by the laser profile and the absorption spectrum of OH. On the other hand, it requires a long absorption path to achieve a detection limit of about 10^6 molecules.cm^{-3}, which makes it much less spatially resolved that the FAGE. This should be taken into account when analyzing the data based on DOASmeasurement with a lower spatial resolution thanother instruments. For example, the DOAS of Jülich,in conditionsof field measurement at ground reached a limit of detection (LOD) of 1.5×10^6 molecules cm^{-3} for 200 s (Hausmann et al., 1997)measurement averaged over 200 m. In addition, the only operational instrument is now permanently installed in theSAPHIR chamber(Simulation of Atmospheric PHotochemistry In a large Reaction chamber)in Jülich (current LOD = 7.3×10^5 molecules.cm^{-3} for a measurement distance of 20 m) (Fuchs et al., 2012).

I.3.1.2 HO_2 and RO_2detection

Several techniques for measuring HO_2 exist, and some of them, also allow the measurement of RO_2 radicals. The MIESR technique (Matrix Insulation Electron Spin Resonance) can simultaneously measure selectively different types of radicals such as HO_2, the sum of RO_2, $CH_3C(O)O_2$, NO_2 and NO_3 using the method of Electron Spin Resonance (ESR) after collection of radicals on a cold matrix. But only three techniques: FAGE, CIMS and PERCA (Peroxy Radical Chemical Amplification) are currently deployed in the field and will be described below. It is interesting to note thatmost of the studies concern HO_x (OH and HO_2), rare are the measurements of RO_2 radicals.However, their monitoring enables more precise characterization of OH / HO_2 / RO_2 system, and therefore a better identification of potential gaps in atmospheric chemistry mechanisms.

I.3.1.2.1 FAGE (Fluorescence Assay by Gas Expansion)

The HO_2 radicals cannot be detected by fluorescence because theydo notfluoresce but dissociate after electronic excitation. In order to be able to detect and measure HO_2 concentrations, they are converted into OH by addition of NO according to reaction (R I- 16) and the OH radicals produced are detected by LIF.

As described in the section I.3.1.1.1, the FAGE technique is based on the laser-induced fluorescence (LIF) detection of the hydroxyl radical (OH) at low pressure.
Detection of HO_2 was pioneered by Hard et al. (Hard et al., 1984) and described by Faloona et al.(Faloona et al., 2004) and used by several groups ((Heard and Pilling, 2003), (Dusanter et al., 2009)). HO_2 is measured by adding NO above the HO_2detection part of the instrument. Both the OH radicals present in the sampled air and the OH which results from the conversion of HO_2 radicals contribute to the fluorescence signal. This means the sum of ambient OH and HO_2 concentrations is measured. Measurements with a time resolution of 150 second are possible(Fuchs, 2006), with typical detection limits of ~10^5 molecule/cm^3 of both OH and HO_2(Dusanter et al., 2009).This technique is adapted to the selective quantification of HO_2 only with low NO concentration injected in the FAGE. Indeed, it has been shown that for some RO_2 (with double bonds), conversion into HO_2 and subsequently HO_2 in OH is effective for high NO level in the FAGE(Fuchs et al., 2011). The potential use of this interference and the precautions to measure selectively HO_2 will be discussed in theChapter IV.

In order to distinguish between OH, $HO_2$and RO_2 radical concentrations, the development of RO_x-LIF was done at Forschungszentrum Jülich(Fuchs et al., 2008). The setup involves one measurement channel for the specific detection of OH, one for HO_2while another measurement channel (RO_x-LIF) is used for detection of RO_x. The RO_x-LIF concept involves a two-stage chemical conversion of RO_x into OH. The conversion of RO_x in HO_2 takes place in the first cell at about 30 Torr (NO and CO addition) and of HO_2 in OH in the FAGE cell (NO addition), in which the OH is then detected by laser induced fluorescence. To calibrate the instrument, a calibration cell similar to those used for the generation of HO_x based on photolysis of $H_2O$is used with addition of hydrocarbons reacting with OH to produce RO_2 radicals.

I.3.1.2.2 PERCA (Peroxy Radical Chemical Amplification)

The peroxy radical chemical amplification technique is a method to measurethe total concentration of peroxy radicals, which is the sum of HO_2 and RO_2(Cantrell and Stedman, 1982). The air is supplied into a reaction chamber in which CO and NO are added to the ambient air to produce a high concentration of NO_2 (up to 100 times the initial concentration of RO_2 radicals) *via* chain reactions. The chain reactions are based on the conversion of RO_2 into $HO_2$and HO_2 into OH due to the presence of NO,producing NO_2. The amplification chain is based on the cycling conversion of HO_2 into OH due to the presence of NO and OH into HO_2 due to the presence of CO. The chain length (number of conversion HO_2/OH before termination) depends on the ratio between termination reactions (R I-34,R I- 35) and amplification reactions (R I- 12to R I- 16) shown inFigure I- 6.

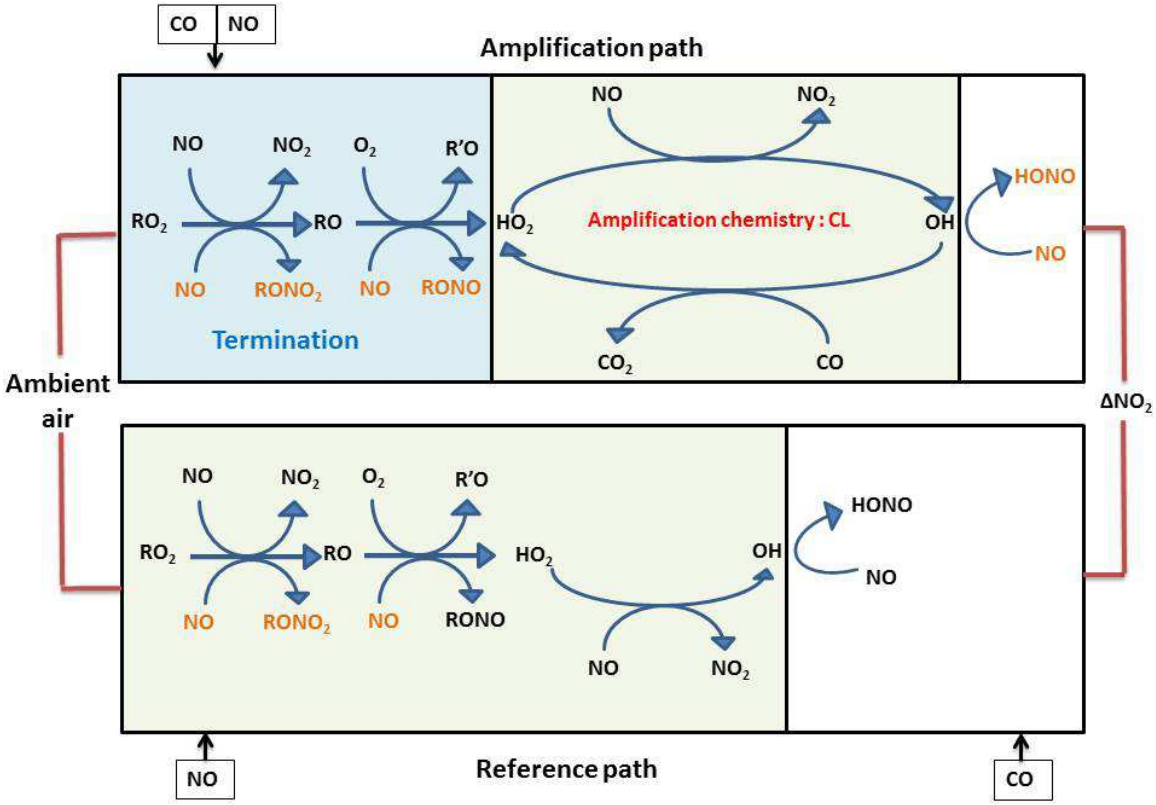

Figure I- 6: Reaction pathways in a 2 reactor PERCA system (from Dusanter, CLIMIBIO presentation)

NO_2 is finally detected with a NO_2 sensor(based on Chemiluminescence of luminol (Parker et al., 2009), LIF (Miyazaki et al., 2010; Sadanaga et al., 2004a), CRDS (Liu et al., 2009), or CAPS instrument (Wood and Charest, 2014)).The instrument can have one reactor and 2 modes (ON with CO injection at the entrance of the reactor of NO and CO for the conversion and OFF with only the injection of NO to quantify the ambient NO_2 and NO_2produced by other reactions like O_3 with NO) or 2 reactors (with and without co-injection of CO). The peroxy radical concentration is determined knowingthe chain reaction length and the difference of the NO_2 concentration ΔNO_2between the OFF and ON mode (Sadanaga et al., 2004a).The chain length (CL) of the chain reaction defines the number of NO_2 produced by one initial HO_2radical. The CL has a limited number because the reaction cycle ends due to a series of loss reactions in the reactor.

$$[HO_2 + RO_2] = \frac{\Delta NO_2}{(chain\ length)} \qquad \text{Eq I- 9}$$

To characterize the chain length and calibrate the instrument, a calibration cell similar to those used for the generation of HO_x based on photolysis of $H_2O$is used with addition of hydrocarbons reacting with OH to produce RO_2 radicals.

I.3.1.2.3 PeRCIMS (Peroxy Radical Chemical Ionization Mass Spectrometry)

As for measuring OH, the CIMS technique can be used for the measurements of HO_2 and peroxy radicals (Σ HO_2 + RO_2) using the conversion of peroxy radicals into HO_2 and HO_2 intoOH in presence of NO (R I- 13, R I- 14, andR I- 16)and the detection of OH after reaction with $SO_2$by quantifying H_2SO_4.

As mentioned before, H_2SO_4 is then ionized into HSO_4^- and detected by a CIMS. It is possible to have a speciation between HO_2 and RO_2 using the dependence of the conversion efficiency of RO_2 depending on the ratio of concentrations of O_2 and NO (Hornbrook et al., 2011). Thereforedepending on the variation of these concentrations, itcan be used alternatively in a "HO_2 + RO_2 mode" at low [NO]/[O_2] more favorable to the conversion of RO in HO_2(R I- 14) or a "HO_2 mode" at higher ratio more favorable to the conversion of RO in RONO (R I- 34). Table I- 2summarize all the techniques and their features dedicated to HO_x measurement instruments.

Table I- 2: List of techniques and features of HO_x measuring instruments(Heard and Pilling, 2003)[a]

Methods	Principals	Species measured	advantages	drawbacks	groups	Limit of detection (molecule.cm^{-3})	Time resolution (min)[a]	Uncertainty[a]
FAGE (Fluorescence Assay by Gas Expansion)	LIF detection of OH at low pressure, conversion of HO_2 into OH by NO addition	OH HO_2	Rapid, Sensitive, Selective, Able to measure other species (RO_2)	Calibration needed	PC2A Lille, France (Amedro et al., 2012)	OH: 3×10^5 SNR=1, 1 min HO_2: 1×10^6 SNR=1, 1 min	0.5	15 %
					Leeds Univ., England (Creasey et al., 1997)	OH: 1.4×10^5 SNR=1, 2.5 min HO_2: 5.4×10^5 SNR=1, 2.5 min	0.5	31-35 %
					Forschungszentrum Jülich, Germany (Holland et al., 1999)	OH: 1.75×10^5 80 s HO_2: 9×10^5 SNR=2, 80 s	0.67	10 %
					Pennsylvania State Univ., United States (Faloona et al., 2001)	OH: 1.4×10^5 SNR=2, 30 s HO_2: 1.4×10^5 SNR=2, 30 s	0.5	16 %
					Portland State Univ., United States (George et al., 1999)	OH: 1×10^6 6 min HO_2: 1×10^6 6 min	6	$\pm10^6$ cm-3
					Tokyo Univ., Japan (Kanaya et al., 2001)	OH: 3.3×10 SNR=2, 1 min HO_2: 3.6×10^6 SNR=2, 1 min	1	23-24 %
					Nagoya Univ., Japan (Matsumi et al., 2002)	OH: 7×10^5 SNR=2, 1 min	-	-
DOAS (Differential Optical Absorption Spectroscopy)	absorption	OH	Auto calibration	Long optical path, interferences	Johann Goethe Univ., (Armerding et al., 1994)	OH: 4×10^5 SNR=1, 1 min	4.5	$\pm10^6$ cm-3
					Forschungszentrum Jülich, Germany (Dorn et al., 1995)	OH: 1.5×10^6	200 s	7 %
					NOAA, Fritz Peak, Unites States (Mount and Eisele, 1992)	OH: 5×10^5 1 min	10	30 %
					MPI Mainz, Germany (Perner et al., 1987)	OH: 2×10^6 SNR=2, 15 min	-	-

CIMS (Chemical Ionization Mass Spectrometry)	Conversion of OH to H_2SO_4 then detection by ionization mass spectrometry	OH HO_2 RO_2	Very sensitive	Calibration needed, Possible interferences	NCAR Boulder, United States (Mauldin et al., 1998)	OH: <1×10^5 SNR=2, 5 min HO_2 : 0.5-1 pptv	0.5 1	16 %
					DWD, Hohenpeissenberg, Germany (Berresheim et al., 2003)	OH : 1.2×10^5 5 min	0.5	20 %
					LPC2E Orleans, France (Kukui et al., 2008)	OH : 2 à 5×10^5 10 min HO_2 : 1×10^5 10 min	1	25 – 30 %
					MPI Heidelberg, Germany (Hanke et al., 2002)	HO_2 : 0.5 pptv	1	18 %
PERCA/LIF(Peroxy Radical Chemical Amplifier)	Conversion into NO_2 and detection by LIF	HO_2 RO_2	-	Calibration needed	Tokyo Univ., Japan (Watanabe et al., 1982)	HO_2 : $1\times10^7$1 min	1	-
MIESR (Matrix Isolation Electron Spin Resonance)	HO_2 trapped in a matrix at 77 K, ESR	OH, HO_2, NO_2, NO_3, RO_2	Direct measurement of HO_2	Calibration needed, long, laboratory analysis	Forschungszentrum Jülich, Germany (Mihelcic et al., 1999)	HO_2 : 2.5×10 30 min	30	2.5×10^7 cm^{-3}
CO radiocarbon	Addition of ^{14}CO to the air $^{14}CO+OH$ to $^{14}CO_2+H$	OH	absolute	long	Washinton State Univ., United States (Felton et al., 1988)	OH : 2×10^5 2 min	5	16 %
Spin trapping	OH trap sheet	OH	-	Long, not used anymore since 1982	Tokyo Univ., Japan (Watanabe et al., 1982)	OH : 5×10^5 20 min	20-30	< 30 %

I.3.2 Potential interferences with HO_x measurements

OH and HO_2 concentration measurements involve complex instruments that may be subjected to different types of interference. In this section, potential interferences, in particular for FAGE instruments as the one used in this thesis, are described.

I.3.2.1 Interferences on OH measurement

The OH measurement can be biased by two types of interference: chemical and spectral interferences in the case of spectroscopic techniques.

Chemical interference is related to the presence of species other than OH that would lead to a signal identical to OH in the instrument. As an example, the CIMS technique can be affected by the formation of H_2SO_4 through oxidation of SO_2byspecies other than OH. However, the systematic measurement of H_2SO_4 signal in the presence of a species that reacts rapidly with OH, called trap or scavenger species (for example propane)(Petäjä et al., 2009) is commonly used when deploying these instruments in the field. Conversion can be also influenced by levels of NO_x and must be considered (Kukui et al., 2008). For instruments using laser sources, chemical interferences can also occurs due to photolysis.

Spectral interference occurs when other species absorb (as measured by DOAS) or fluoresce (as measured by FAGE) at the same wavelength as OH. However, the DOAS technique is only slightly subjected to these spectral interferences because the absorption spectrum is measured over a large spectral range, which makes it possible to precisely and selectively extract the contribution of OH (Dorn et al., 1995)from the contributions of the other absorbing species in this range. There may also be OH production in the probe beam, by photolysis phenomena, resulting in interference on the measurement by FAGE instrument.

I.3.2.1.1 Spectral interference in the FAGE

Spectral interference in FAGE instruments can occur if species present in the air can be excited at the same wavelength as the one used for OH and fluoresces in the same wavelengthrange than collected in the FAGE. Naphthalene, sulfur dioxide and formaldehyde may cause this type of interference. A study was carried out to test the effect of a large number of chemical species on the OH signal measured with the FAGE instrument of Pennstate University (Ren et al., 2004). Only naphthalene has an excitation spectrum with define lines close to the OH lines. However, since the structure of the OH spectrum is fine and well known, this type of interference can be eliminated by well selecting the

laser wavelength and by alternating the measurement at a wavelength corresponding to a OH line (on resonance) and out of a OH line (off-resonance) and subtract the signal off resonance to the on resonance, which is done systematically in the FAGE instruments.

I.3.2.1.2 Photochemical interference in the FAGE

This interference can be due to the excitation laser and is called then photochemical interference. It can be observed when the mixture is excited several times by the laser (linked to the high repetition rate of the laser) and species are present that can be photolyzedto form OH at the wavelength used to excite OH.If the refreshing time of the gas mixture in the detection volume is longer than the time between two laser pulses, a first pulse could allow the generation of OH and the following its excitation. Consequently, this type of OH interference signal has a quadratic dependence on the laser power. These interferences can be reduced if the volume probed by the excitation laser is renewed more rapidly or if the repetition rateis reduced. The atmospheric species whose photolysis at 308 nm is known to lead to OH formation, have also been tested with the Penn State FAGE instrument (Ren et al., 2004), in different concentration ranges: ozone (up to 4 ppm), hydrogen peroxide (up to 120 ppb), nitrous acid (up to 5 ppb), formaldehyde (up to 250 ppb), nitric acid (up to 50 ppb),acetone (up to 200 ppm). Ozone (formation of OH originates from the photolysis of ozone which produces an excited oxygen atom that reacts with water vapor to form OH, (R I- 5 and R I- 6)) and acetone photolytic interferences have been identified with a quadratic dependence of the interference signal with the laser power confirming the two-photon process in this instrument but represent very low levels under atmospheric conditions in this device.

Unlike the results of Penn State University, other studies showed that the ozone interference is not a photolytic process but is due to possibly heterogeneous reactions within the FAGE cell.

I.3.2.1.3 Chemical interferences in the FAGE

(Holland et al., 1995) showed ozone interference with a linear dependence with laser power of the OH artificial signal for a given concentration of O_3. This interference was attributed to an unknown reaction within the FAGE cells in the gaseous mixture or on the walls of the cell. Tests with different kinds of materials (black paint, teflon, black anodized aluminum) were made and it was observed that the interference was weaker using black anodized aluminum to cover the walls of the cells and also by changing the sampling conditions.

Lu et al. (Lu et al., 2012) have reported that ozone interference is only dependent on the ozone concentration entering the cell. Ozone interference on OH measurements of $(6 \pm 2) \times 10^3$ molecule

cm^{-3} per ppb of ozone was observed in their instrument (Lu et al., 2012). On the other hand,Kanaya et al. (Kanaya et al., 2007)have reported interferences in measurements of OH and HO_2 that scale linearly with [O_3] and laser power, suggesting that the ozone interference is instrument-specific.Other studies with theoretical (Zeng et al., 1998) and experimental (Schlosser et al., 2009)approaches have also reported that the OH production via this route is negligible in atmospheric conditions but some groups still correct for the ozone as Jülich group.

Ozone interference was tested by our group (Amédro, 2012a) by varying O_3 concentration up to 1 ppm and laser power from 0.3 to 3 mW. The experiment was done by generating O_3 through photolysis of O_2 by an Hg lamp, O_3 was diluted by a humid zero air in a photolysis cell which was used for the kinetic measurements. O_3 and H_2O concentrations were measured in the cell using standard analyzers. Ozone was varied with constant laser power and repetition rate. Other measurements varying the laser power has shown a linear dependence(Amédro, 2012a).

The O_3 interference have been well characterized by several groups and found to be minor and can be negligible (Schlosser et al., 2009). On the other hand, and during ambient measurements, the interference by O_3 can be corrected knowing the laser power, the repetition rate, the ozone concentration and H_2O concentration.

The chemical interference can also involve species otherthat ozone which would decompose in the FAGE to produce OH radicals in the FAGE measurement cell. The hypothesis of this type of interference for species was made following the large differences between the modeled OH concentration profilesand the measurements in tropical forests (Edwards et al., 2013; Mao et al., 2012; Whalley et al., 2011),still unexplained despite improvements in chemical mechanisms such as the isoprene one.

Several sources of interference are suspected, such as that of peroxy radicals (Fuchs et al., 2011) or the Criegee biradicals (Novelli and Harder, 2012; Novelli et al., 2014a) formed during the reaction between isoprene orother alkenes and O_3 which would dissociate during gas expansion and produce OH detected by FAGE. Another assumption linked to the specific chemistry of tropical forests, characterized by a low level of NOx, which favors RO_2 reactions (from biogenic VOCs such as isoprene) with other radicals whose products could be photolyzed or dissociated in the FAGE cell.

In order to estimate the non-photolytic interference level in real environments, experiments were carried out in different campaigns using a pre-injector to trap ambientOH upstream of the FAGE by periodic injection of a scavenger, allowing quantifying the OH signal produced within the FAGE cell. The first results published using a pre-injector are those obtained with the instrument of Penn State

University during the BEARPEX09 campaign(Mao et al., 2012)(California). They used C_3F_6as OH scavengerand they showed an interference of up to 50%.

Other ambient measurements carried out with the FAGE of the MPI (HORUS instrument: Hydroxyl Radical measurement Unit based on Spectroscopy fluorescence)equipped with an injector above the sampling (Novelli et al., 2014b).Theyshowed that OH is generated within the instrument in a non-negligible proportion of up to 30 to 80% of the total signal during the day and 60 to 100% overnight depending on the forest environment were type and concentration of VOCs varied. This study gathers data collected over three measurement campaigns. On HUMPPA COPEC 2010 and 2012 (boreal forest in Finland) and DOMINO HO_X (Atlantic coast in Spain), propene was used as a scavenger with an efficiency> 95% and on HOPE 2012 propane and propene were injected with consumption efficiency of the OH of 60 to 95%. The best results for OH scavenger in the air mixture in this study were obtained with propane as a scavenger at a concentration of 2.5×10^{15} molecule cm^{-3}. Interferences on the OH measurement of 5×10^5 to 1×10^7 cm^{-3} were observed in HOPE 2012 campaign. However, these results depend on the instrument used and at a workshop on HO_x measurements in Jülich in March 2015 it was recommended that each group using a FAGE instrument should at least periodically measure with a system of injection of an OH scavenger upstream of the sampling. Preliminary studies with C_3F_6 were carried out at PC2A and a first deployment during the LANDEX campaign has been done and is discussed in Chapter V.

I.3.2.2 Interference on the quantification of HO_2

In order to be able to be detected by LIF, the HO_2 radical is converted to OH by the rapid reaction with NO. It has long been considered that peroxyl radicals RO_2, which are also present in the atmosphere, do not react fast enough with NO within the FAGE, at low pressure, to produce HO_2 and subsequently OH radicals. However, it was based on interference tests performed only on simple species (peroxyl C1-C4) which have shown no interference (Ren et al., 2004; Stevens et al., 1994) andthe same assumptionwas made for all types of RO_2.However, a more recent study (Fuchs et al., 2011) showed that RO_2 radicals derived from atmospheric compounds having double bonds such as alkenes, aromatics and dienes can react quite rapidly with NO to give HO_2 radicals under the low pressure conditions present in the FAGE (up to more than 90% conversion to HO_2 under certain conditions). These interferences can be reduced by reducing the reaction time and/or NO concentration in the detection cell, but this also causes a decrease in sensitivity to HO_2(see chapter IV). However, this is not critical given the high concentrations of HO_2 in the atmosphere relative to OH.

The level of interference may vary depending on the species and the apparatus used (expansion conditions, reaction time, pressure, NO concentration) and must be characterized in each instrument (see Chapter IV for the UL-FAGE).

I.3.3 HO_x measurements in field campaigns

A comparison between measurements in a specific environment (marine, forest, urban) and modeled results allowshighlighting gaps between the chemical model considered and the chemistry, which really takes place in this environment. Detailed atmospheric models exist and are used to analyze the results of field campaigns such as the Regional Atmospheric Chemistry Model (RACM) that modeled the PROPHET campaign (Tan et al., 2001) or the Master Chemical Mechanism (MCM) used for the EASE96 campaign (Carslaw et al., 1999) for example.

It was observed during the analysis of the results of many field campaigns(Stone et al., 2012) that the modeled profiles did not reproduce the experiment. These differences depend on the conditions and experimental environments and may arise from lack of reactions involving OH in models.

In urban environments, for example, during the PMTACS-NY2001 campaign conducted in New York, the modeled data correctly reproduce the production of HO_X during the day: with OH coming from about 56% of the photolysis of ozone and HONO, and reproduce the production of HO_2 at night with a model / experiment ratio of around 1. On the other hand, the model overestimates by an average factor 6 the production of OH at night when this is produced by the ozonolysis of alkenes, which means that this production path is poorly represented in the models used(Ren et al., 2003).

In biogenic environments, comparisons between model and measurements show higher measured concentration levels than predicted by models(Lu et al., 2012; Tan et al., 2001). During the 1998 PROPHET campaign in a deciduous forest in northern Michigan, OH measurements are 2.7 times larger than the model on average, while the model is in good agreement with the measured HO_2.By adding an additional source of OH from the ozonolysis of unmeasured terpenes, the measurement of OH remains 1.5 times higher than the model and the HO_2 modeled with this added source is 15% to 30% higher than the measurement. In addition, modeled HO_2 / OH ratios are 2.5 to 4 times higher than those measured, indicating that the cycle between OH and HO_2 is poorly described by the model (Tan et al., 2001)

During the CABINEX campaign, which was conducted at the canopy level of a Michigan forest in the United States in 2009, the prediction of OH concentrations by the model was in good agreement with those measured, with measured/modeled ratio of (0.70 ± 0.31) for isoprene levels of 1 to 2 ppb on

average (Griffith et al., 2013; Hansen et al., 2014). However, differences were observed when isoprene concentrations were higher. Measurement campaigns in biogenic environments with low NO_x levels revealed significant overestimates of OH concentration relative to the model(Kubistin et al., 2010; Whalley et al., 2011). The hypotheses raised up to explain these differences in concentration were that sources of OH were missing in the models. Sources from RO_2 recycled to HO_2 and then to OH via reactions with unidentified species(Fuchs et al., 2013; Hofzumahaus et al., 2009) have been proposed. Another study (Pugh et al., 2010) suggested that this underestimation of OH sources may be partially offset by OH production via the OH + isoprene reaction or its products such as methacrolein and methyl-vinyl ketone. Numerous investigations have focused on the understanding and improvement of the isoprene oxidation mechanism(Peeters and Müller, 2010; Peeters et al., 2009; Stavrakou et al., 2010), the most abundant biogenic VOC in the atmosphere and main biogenic species emitted in these environments).

The mechanism of oxidation of isoprene involves many intermediate species, and the work carried out by the different groups, highlight new ways of formation of OH. The first step is the addition of OH on the double bond followed by the reaction between the hydroxyl radical and O_2.

However, work (Lu et al., 2012)indicates that the addition of these sources is not enough to fill the observed differences. A recent study(Fuchs et al., 2013) carried out in the SAPHIR simulation chamber, confirms these conclusions. They highlight the significant recycling of OH during the oxidation of isoprene, with more than half of the OH consumed being recycled. However, levels lower than those measured in the outdoor environment were observed. The interference hypothesis on measurements was also mentioned and highlighted during a campaign in a Californian forest(Mao et al., 2012). This subject will be developed in chapter III.

The results obtained in urban areas or biogenic show that the chemical processes related to HO_X radicals are not yet well understood in these different environments and that it remains important both to perform measurements in the field but also to improve the atmospheric models.

I.4 Techniques for OH reactivity measurement

The reactivity of OH is a parameter more recently measured than the concentration of HO_X or RO_X radicals and threetechniques have been developed: twobased on OH detection techniques already used for the atmospheric measurement of OH coupled to different type of reactors: by FAGE (flow tube-LIF or laser photolysis LIF) or CIMS (flow tube-CIMS), the other based on a completely new approach tracking a tracer reacting with OH (Comparative Reactivity Method, CRM)(Sinha et al.,

2008; Yang et al., 2016). The principle of these various instruments as well as their deployment on the ground is presented in the following paragraph. The characteristics of the various instruments described in the literature are given in Table I- 3.

I.4.1 Flow tube-LIF (FT-LIF)

The flow tube technique coupled to a FAGE detection, also called TOHLM technique (Total OH Loss rate Method),is based on the continuous generation of OH radicals in a flow tube (Kovacs and Brune, 2001) by photolysis of H_2O by a mercury lamp placed in a moving injector and detection of OH by FAGE coupled to the flow tube for different positions of the injector (corresponding to different reaction times). The air to be analyzed is pumped at high speed (residence time from 0.4 to 11.25 s depending on the tube used, requiring an enormous pumping rate up to 70 L min^{-1}) into the reactor and is mixed with the OH generated in the injector (OH residence time <1 s). The species present in the pumped air react with the OH produced. Analysis of the concentration of OH as a function of the position of the injector gives access to the decay constant. It should be noted that this technique can be disturbed by the presence of high levels of NOx because the generation of OH by photolysis of water results in the production of an equivalent amount of HO_2 which can react with NO to reform OH. This recycling add an extra signal of OH which affect the decay. Corrections are therefore made after measurement of ambient NO and HO_2 in thereactor (Ren et al., 2003; Shirley et al., 2006).

I.4.2 Laser photolysis –LIF (LP-LIF)

This technique,also called pump-probe technique, is based on detection of OH by FAGE, similarly to the FT-LIF but OH generation is made in a reactor (photolysis cell) bypulsedphotolysis of ozone at 266 nm in presence of water vapor(Sadanaga et al., 2004b). It has the advantage of forming only OH which limits the phenomena of recycling of HO_2 to OH under high NOambient conditions. This technique, used in this thesis, is described in detail in chapter II. To summarize, ambient air is pumped into the photolysis reactor where the speciesreact with the OH produced by laser photolysis.The gas mixture is then pumpedinto the FAGE cell coupled to the photolysis cell and OH is detected with a temporal resolution corresponding to the repetition rate of the OH excitation laser (few kHz). The exponential decay of the fluorescence signal is then observed. The reactivity of OH is obtained by an exponential fitof the decay obtained from the sum of several photolysis shots.

I.4.3 Flow tube – CIMS (FT-CIMS)

This technique is similar to the FT-LIF for the OH generationby a mercury lamp but the measurement is made at one reaction time by alternatively injecting sulfur dioxide in the reactor at the entrance or at a position corresponding to a detection time of about 75 ms. OH detection is made by CIMS. Like for the FT-LIF, corrections are needed due to the recycling of HO_2 in OH with ambient NO.

I.4.4 CRM (Comparative Reactivity Method)

The CRM technique is the only technique which does not measure OH but a tracer of the reactivity. The CRM technique is based on the competition of the reactions of OH with the species present in the mixture to be analyzed and with a tracer molecule quantifiedby a suitable detectorat the output of the reactor where OH is produced. The tracer chosen in the various instruments developed is pyrrole (C_4H_5N). Theadvantage of this molecule is that it is not present in the atmosphere except in the case of biomass fires. Moreover, its reactivity with OH is very high ($k_{pyrrole+\ OH} = 1.28 \times 10^{-10}$ cm^3 $molecule^{-1}$ s^{-1}(Dillon et al., 2012)and is therefore rapidly consumed in the atmosphere, making its presence negligible even near forest fires. In addition, it can be detected by various field instruments (PTR-MS or GC-PID).

The CRM device is composed of two parts: the first one is a reactor in which OH is mixed with the tracer and alternately withzero air (without reactive species) or the ambient air and the second is a detector allowing the measurement of the concentration of the tracer. This is generally a Proton Transfer Reaction-Mass Spectrometer (PTR-MS), or a GC-PID-type gas chromatograph (Nölscher et al., 2012b). Reactivity is measured by monitoring the pyrrole concentration (Figure I- 7) in different conditions.

The first step is to introduce only pyrrole and dry zero air to measure C1 corresponding to pyrrole concentration in absence of OH.Then humid zero air is added to produce OH by photolysis of water vapor through a light source emitting at 185 nm (eg a mercury vapor lamp), the pyrrole concentration C2 is then measured. C2 is less than C1 because pyrrole reacts with OH. In the last step, zero air is replaced by ambient air, there is then competition between the reactions of OH with pyrrole and OHwithreactive species present in the ambient air and C3, higher than C2, is measured.

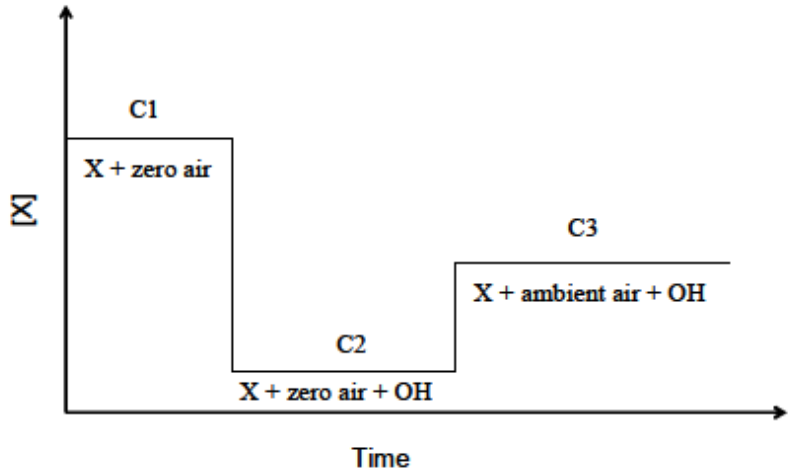

Figure I- 7: Schematic representation of the CRM measurement pattern (where X is pyrrole)(Sinha et al., 2008)

The value of the reactivity of OH is obtained by the following equation:

$$R_{air} = \frac{C3 - C2}{C1 - C3} . K_{pyrrole+OH} . C1 \qquad \text{Eq I- 10}$$

However, this calculation is subject to different types of corrections depending on the operating conditions of the instrument (dilution and pseudo first order corrections) and the environmental conditions (notably the NO_x level (Michoud et al., 2015)).When the concentration of ambient NO is high, the HO_2 radicals produced by the water photolysis can be rapidly converted into OH radicals within the reactor. These additional OH can react with pyrrole and thus modify the level of pyrrole concentration and thus induce an error in the calculation of the value of the reactivity that have to be corrected.

There are several CRM devices in the world: one at the Max Planck Institute (MPI) in Mainz (Sinha et al., 2008), one at the LSCE(Dolgorouky et al., 2012), one in the US at NCAR (Kim et al., 2011), three very recent ones: one at the Indian Institute of Science Education and Research (IISER, Mohali, India (Kumar et al., 2013)), one at IMT-Lille-Douai (MD) and one at the Finnish Meteorological Institute (IMMI, Helsinki, Finland).

The characteristics of the various instruments are summarized inTable I- 3.

Table I- 3: Techniques for measuring the reactivity of OH and the characteristics of the various instruments in the world (Fuchs et al., 2017b; Hansen et al., 2015).

Technique	Reference	LOD(s^{-1})[a]	Laboratories	comments
FT-CIMS	(Berresheim et al., 2000)	0.5	German Meteorological Service (DWD), Germany	-
FT-LIF	(Kovacs and Brune, 2001)	2.4/4	Penn state University (USA)	Laminar flow reactor
	(Ingham et al., 2009)	2.0/5	Leeds University (UK)	Turbulent flow reactor
	(Hansen et al., 2014)	2.1/2.5	Indiana University (USA)	Turbulent flow reactor
PL-LIF	(Sadanaga et al., 2004b)	-[b]/3[c]	Tokyo Metropolitan University (Japan)	-
	(Lou et al., 2010)	0.9d/1-3	Forschungszentrum Julich (Germany)	-
	(Parker et al., 2011)	3.6-0.9/1-3	Lille 1 University-PC2A (France)	-
	(Whalley et al., 2016)	1-1.5/1-3	Leeds University (UK)	-
Comparative Reactivity Method (CRM)	(Sinha et al., 2008)	3.5-6[e]/15	Max Planck Institute Mainz (Germany)	PTR-QMS[f] for pyrrole measurement
	(Kim et al., 2011)	15/-[b]	NCAR (USA)	PTR-QMS
	(Nölscher et al., 2012b)	3-6[h]/1	Max Planck Institute Mainz (Germany)	GC-PID for pyrrole measurement
	(Dolgorouky et al., 2012)	3.0/2[i]	LSCE (France)	PTR-QMS
	(Kumar and Sinha, 2014)	-	IISER Mohali (India)	PTR-QMS
	(Hansen et al., 2015)	3.4/5	Mines Douai (France)	PTR-ToF-MS

a: Limit of detection: 3σ unless otherwise stated; [b]Value not reported, c: Value reported by (Yoshino et al., 2006); d:LOD 3σ determined by decay in zero air reported by (Lou et al., 2010); e: LOD of 6 s^{-1} reported by (Sinha et al., 2008), LOD of 3.5 s^{-1} reported by (Sinha et al., 2010) ; f: Proton Transfer Reaction-Quadrupole Mass Spectometry; g: Reported from (Nölscher et al., 2012b) ; h: Value reported at 2σ, relative to C2; i: Based on the measurement frequency reported in (Dolgorouky et al., 2012).

These techniques have been deployed in different environments in addition to other measurements (VOC, ozone, NO_X and sometimes HO_X).

I.4.5 OH reactivity measurements in field campaigns and modeling

More than twenty campaigns involving OH reactivity instruments have been carried out in recent years (Table I- 4: OH Reactivity Measurement Campaigns (Hansen et al., 2014 updated)). They took place in various environments: urban (in cities of varying sizes, therefore more or less rich in NO_X), rural and forestry with predominance of different species with consequently very different chemical compositions (rich in isoprene, pinenes, terpenes ...) or coastal. The measurement campaigns are used to establish the global losses of OH. The measured OH reactivitycan be comparedto a calculated reactivity from the concentrations of all the species measured in order to identify the part of reactivity identified and the "missing" part, that is to say unexplained by the calculation and coming from species not measured for reasons of technical limitations, for example (case of oxygenated VOCs, radical species). The missing reactivity characterizes the level of representativeness of the composition of the air measured by the instruments present in these environments in term of OH sink.The evolution of the missing OH reactivity as a function of the conditions (period of the day, temperature, …) allows to make assumptions concerning the unmeasured but important species in the budget of OH. It is also possible to compare the measured reactivity with that obtained by modeling. The comparison can show the part of the pathways of consumption not represented in the chemical mechanism used (Dusanter et al., 2009). It is also possible to force the models with the measured reactivity in order to correctly represent the consumption of OH (Whalley et al., 2011).

Table I- 4: OH Reactivity Measurement Campaigns (Hansen et al., 2014 updated) and more recent campaigns

Campaign	Site	Dates	Environment	Technique	Other measurements[a]	RM[b]	Reference
SOS	Nashaville,TN, USA	June-July 1999	Urban	TOHLM	HICOF	1.4	(Kovacs et al., 2003)
PROPHET 2000	Michigan, USA	July-august 2000	Forest (mix)	TOHLM	HIC[c]	~1.5	(Di Carlo et al., 2004)
TexAQS 2000	Houston, TX, USA	August-Septemper 2000	Urban	TOHLM	HICOFB[d]	~1	(Mao et al., 2010)
PMTACS-NY	New York City, USA	June-August 2001	Urban	TOHLM	HICOF	~1	(Ren et al., 2003)
-	Pennsylvanie, USA	May-June 2002	Rural	TOHLM	HI[e]	-	(Ren et al., 2005)

PMTACS	Whiteface Mountain, NY, USA	July-August 2002	Forest (mix)	TOHLM	HICOF	~1	(Ren et al., 2006)
MCMA 2003/MILAGRO	Mexico City, Mexico	April 2003	Urban	TOHLM	HICF[e]	-	(Shirley et al., 2006)
-	Tokyo, Japan	July-August 2003	Urban	Pump-probe	ICOFB	1.4-1.5	(Sadanaga et al., 2004b)
PMTACS	New York City, USA	Jan-Feb 2004	Urban	TOHLM	HICF	<1.5	)(Ren et al., 2006)
TORCH-2	Weybourne, Norfolk, UK	May 2004	Sea coast	TOHLM	HICOF	1.7	(Lee et al., 2009)
-	Tokyo, Japan	Nov 2004	Urban	Pump-probe	ICOFB	1.3	(Yoshino et al., 2006)
-	Mainz, Germany	August 2005	Urban	CRM	-	-	(Sinha et al., 2008)
-	Brownsberg, Suriname	Oct 2005	Forest (tropical)	CRM	CO	~3.5	(Sinha et al., 2008)
INTEX-B	Pacific Ocean	April-May 2006	Marine	TOHLM	HICOF	2.5	)(Mao et al., 2009)
PRIDE-PRD 2006	Pearl River Delta, China	July 2006	Rural	Pump-probe	HIC	~2	(Lou et al., 2010)
TRAMP2006	Houston, TX, USA	August-Sep 2006	Urban	TOHLM	HICOFB	~1	(Mao et al., 2010)
-	Tokyo, Japan	August 2007	Urban	Pump-probe	ICOFB	~1.4	(Chatani et al., 2009)
OP-3	Borneo, Malaysia	April-May 2008	Forest (tropical)	TOHLM	HICOFB[f]	3	(Edwards et al., 2013)
SMEAR-BFORM	Hyytiala, Finland	August 2008	Forest	CRM	ICOB	~3-4	(Sinha et al., 2010)
BEACHON-SRM08	Colarado, USA	August 2008	Forest (Coniferous)	Pump-probe	ICOB	1.4	(Nakashima et al., 2014)
DOMINO	El Arenosillo, Spain	Nov-Dec 2008	Sea coast	CRM	HIF[e]	-	(Adame et al., 2014)
BEARPEX09	California, USA	June-July 2009	Forest (Coniferous)	TOHLM	HICOFB	~1.5	(Mao et al., 2012)

CABINEX[g]	Michigan, USA	July-August 2009	Forest (mix)	CRM	COB	~1	(Kim et al., 2011)
CABINEX[h]	Michigan, USA	July-August 2009	Forest (mix)	TOHLM	HICOFB	~2	(Hansen et al., 2014)
MEGAPOLI	Paris, France	Jan-Feb 2010	Urban	CRM	ICO	~2	(Dolgorouky et al., 2012)
CalNex-SJV	California, USA	May-June 2010	Rural	TOHLM	HICO	-	(Pusede et al., 2014)
HUMPPA-COPEC	Hyytiala, Finland	July-August 2010	Forest	CRM	ICOFB	5.2	(Nölscher et al., 2012b)
-	Lille, France	October 2012	Urban	CRM, FAGE (Pump-probe)	ICOF[i]	-	(Hansen et al., 2015)
-	Wangdu, China	June -July 2014	Rural	Pump-probe	HICOFB	-	(Fuchs et al., 2017a)
ClerfLo	London, UK	July-August 2012	Urban	Pump-probe	ICOFB	6.7	(Whalley et al., 2016)
SMA	Seoul, South Korea	May-June 2015	Urban	CRM-CIMS	-	-	(Kim et al., 2016)
Intercomparisom campaign	Julich, Germany	October 2017	Simulation chamber	CRM, FAGE (Pump-probe)	-	-	(Fuchs et al., 2017b)
LANDEX campaign	Salles, France	July-August 2017	Forest	CRM, FAGE (Pump-probe)	HICOFB	-	-This work, see chapter VI
-	Beijing, China	August 2013 and October -November 2014	Urban	CRM	HICOFB	-	(Yang et al., 2017)
CARBOSOR	Ersa, Corsica	16 July -5 August	remote	CRM	ICOFB	2.8	(Zannoni et al., 2017)
ATTO	Amazon, Brazil	October 2012 – September 2013	Remote	CRM	HICOFB	4.1	(Nölscher et al., 2016)
CANOPEE	Haute	Spring 2014	Remote	CRM	HICOFB	2	(Zannoni et

	Provence, France						al., 2016)
SOAS	Alabama, USA	June-July 2013	Remote	CRM	ICOFB	-	(Kaiser et al., 2016)

a: Measurements carried out in the same place. H = HO_x, I = Inorganic (including CO), C = Anthropogenic NMHCs (including isoprene), O = COVOs (formaldehyde excluded), F = formaldehyde, B = Biogenic COVs (BCOVs); b: Missing OH reactivity fraction, expressed as the ratio of OH reactivity measured over OH calculated (Lou et al., 2010); C: COVOs, Formaldehyde, and BCOVs estimated in the PROPHET campaign in 1998 for the calculation of OH reactivity; d: according to(Mao et al., 2010)**; e: Measurements not used for the calculation of reactivity; f: Measurements of isoprene oxidation products not used for the calculation of reactivity; g: Branch enclosure OH reactivity measurements; h: Ambient measurements; i: no CO measurements, limited measurements of COVOs, formaldehyde.**

Field measurements have shown that in urban areas the reactivity is higher than in rural areas due to a large number of anthropogenicspecies such as NO_2, alkenes and aromatics, present in high concentrations. For example, reactivities up to 100 s^{-1} were measured in Tokyo (Yoshino et al., 2006, 2012) with a missing reactivity on the order of 30%, similar reactivities were measured in India in an environment dominated by urban and agricultural emissions (Kumar and Sinha, 2014), the highestreactivity of approximately 200 $s^{-1}$was measured in Mexico City (Shirley et al., 2006).

Forest environments, on the other hand, are dominated by biogenic VOCs. In forests, in temperate climates or in rural areas, reactivitieson the order of ten s^{-1}wereobserved with biogenic VOC levels measured. During the PROPHET campaign, carried out in this forest, the missing reactivity increased significantly with temperature but also with the emission rates of terpenes and other biogenic VOCs. These observations seem to show that unknown reactive biogenic VOCs are responsible for a large part of the missing reactivity of OH (Di Carlo et al., 2004).

Reactivities in tropical forests (under low NO_X conditions) may exceed 100 s^{-1} (Figure I- 8). During a campaign in the Borneo forest, overestimations of both the concentration of OH compared to the model but also a measured reactivity much higher than that expected especially in the middle of the day (Whalley et al., 2011)have been demonstrated, probably in connection with photochemical processes (ex: photolysis of peroxides). In the Suriname forest, reactivities of about 50 s^{-1} were measured with a peak of up to 72 ± 18 s^{-1}(Sinha et al., 2008) and 35% of total reactivity was attributed to isoprene (Kubistin et al., 2010).

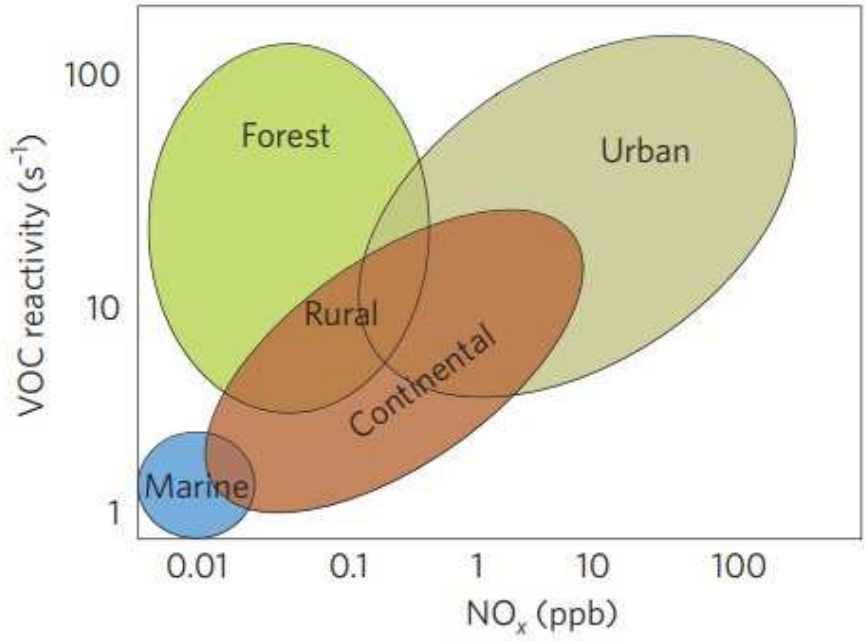

Figure I- 8: OH reactivity levels as a function of environment (Rohrer et al., 2014)

Recent campaigns have shown an important missing reactivity, from 58 to 89% in the boreal forest. Missing reactivity is largely attributed to unmeasured primary species and to oxygenated volatile organic compounds (OVOCs), secondary products derived from the oxidation of VOCs(Nölscher et al., 2012b).

These different campaigns have demonstrated a lack of chemistry understanding. Some assumptions are made but it is not yet possible to clearly identify the species responsible for this reactivity. It is therefore necessary to continue the field measurements to identify gaps in measurements and models and to understand the chemical phenomena taking place in these different environments.

However, considering that different instruments were used during these different campaigns it is also necessary to check the reliability of the different instruments under the different conditions. Indeed, differences between field measurements and models may also be related to biases in measurements.

I.4.6 Intercomparison campaigns for reactivity measurements

In order to compare the behaviors of different types of instruments, two campaigns have been carried:

- one comparing the UL-FAGE instrument and the CRM-Mines Douai on the campus of the university of Lille, in an urban environment, with a globally good agreement between the

two instrument even if the CRM data were about 20% lower than the FAGE data due to photolysis processes identified and reduced later in the CRM instrument. The discrepancy was higher for high NO_x levels (Hansen et al., 2015) due to the HO_2 recycling affecting the CRM measurements.

- a more extended campaign took place in the SAPHIR chamber and highlighted higher scattering for CRM instruments and lower reactivity in monoterpenes environments (Fuchs et al., 2017b) compared to the LIF based techniques. Measurements in rich NO_x environments have also been shown to be biased, in particular due to recycling processes in the instruments.

Reactivity measurements using the pump-probe technique are probably the least sensitive to interference phenomena related to the recycling. Indeed, the source of OH is the pulsed photolysis of ozone which does not produce HO_2 in contrast to the continuous photolysis of the water vapor used as source of OH in TOHLM or CRM techniques (Michoud et al., 2015).

However, in the pump-probe technique, even though HO_2 is not a co-product of the OH generation source, HO_2 formation can occur in the photolysis cell by chemical reactions during VOC oxidation in the pollutedenvironments, rich in NO_x and VOC.The OH decay can then be modified. This has been observed only in extreme conditions of pollution where an analysis with a bi-exponential decay allows to limit its impact (Fuchs et al., 2017b).

I.5 Conclusion

This chapter has highlighted the complexity of the atmosphere and the importance of field measurements and modelling to study the atmospheric chemistry. The OH radical is the most important oxidizing species in the troposphere, involved in greenhouse gases such as methane lifetime, oxidation of VOCs, and ozone formation. Comprehensive knowledge of its distribution and its sources and sinks throughout the atmosphere is necessary as well as those of linked radicals HO_2 and RO_2 in the boundary layer and measurements in real environments are needed.

HO_x and RO_xradicals exist in very low concentrations and highly variable with time and location. For this reason, different types of instruments have been developed and deployed to measure these radicals in the field.The Fluorescence Assay by Gas Expansion (FAGE) technique used at the University of Lille is presented in Chapter II. As previous campaigns highlighted disagreement between measurements and modelled profiles in different environments, more studies are needed to better understand the chemistry of these radicals in our atmosphere or to highlight interferences

in the measurements. In chapter III, one origin of the OH interference in UL-FAGE instrument in biogenic environments is identified. This interference was tested by UL-FAGE instrument using a pre-injector, the results are presented in Chapter V.

AlthoughHO_x and RO_xquantification provides important information about the atmospheric chemistry, instruments to measure another parameter: the reactivity of the OH radical, instruments have been recently developed.It allows, when compared to a calculated reactivity to identify missing OH losses. Chapter II contains a section concerning the technique used in Lilleto measure OH reactivity (LP-FAGE).The UL-FAGE instrument has been deployed in the field during the LANDEX campaign (see Chapter V).

Chapter II: Materials and Methods

II.1 Introduction

The UL-FAGE is one of the most recent FAGE instruments. It has been developed to characterize with a high sensitivity and selectivity OH and HO_2 radicals for atmospheric conditions and different applications: atmospheric, smog chamber, indoor measurements and combustion applications (Blocquet et al., 2016). During my thesis,UL-FAGE instrument has been characterized and improved to quantify the interferences of different peroxy radicals (RO_2) on the HO_2 measurement as well as the interference on the OH measurement.

The UL-FAGE instrument was also coupled to a photolysis cell to allow the measurement of the OH reactivity and to do kinetic analysis (Amédro, 2012a; Blocquet et al., 2013). This coupling was better characterized during my thesis and used for both; kinetic analysis (see Chapter III) and deployment in the field (see Chapter V).

The UL-FAGE enables four different types of measurements: OH and HO_2 quantification, HO_2* (sum of HO_2 + double bond RO_2) quantification, RO_x quantification when coupled to a conversion tube (under development) and OH reactivity measurement when coupled to a photolysis cell. In this Chapter, the UL-FAGE in its quantification configuration is described as well as the calibration cell used to get the absolute concentration of OH and HO_2 radicals. The improvements of the calibration cell are also described. Then, the UL-FAGE in its reactivity configuration detailed in the following paragraphs.

II.2 Experimental description of the UL-FAGE (University of Lille - Fluorescence Assay by Gas Expansion) for HOx quantification

The FAGE instrument is based on the LIF technique applied to OH at low pressure. It consists of 5 main elements (Figure II- 1): the excitation laser, the measurement cells, the probing system, the LIF collection, and the reference cell used to control that the laser is always centered in wavelength on the OH excitation line used.

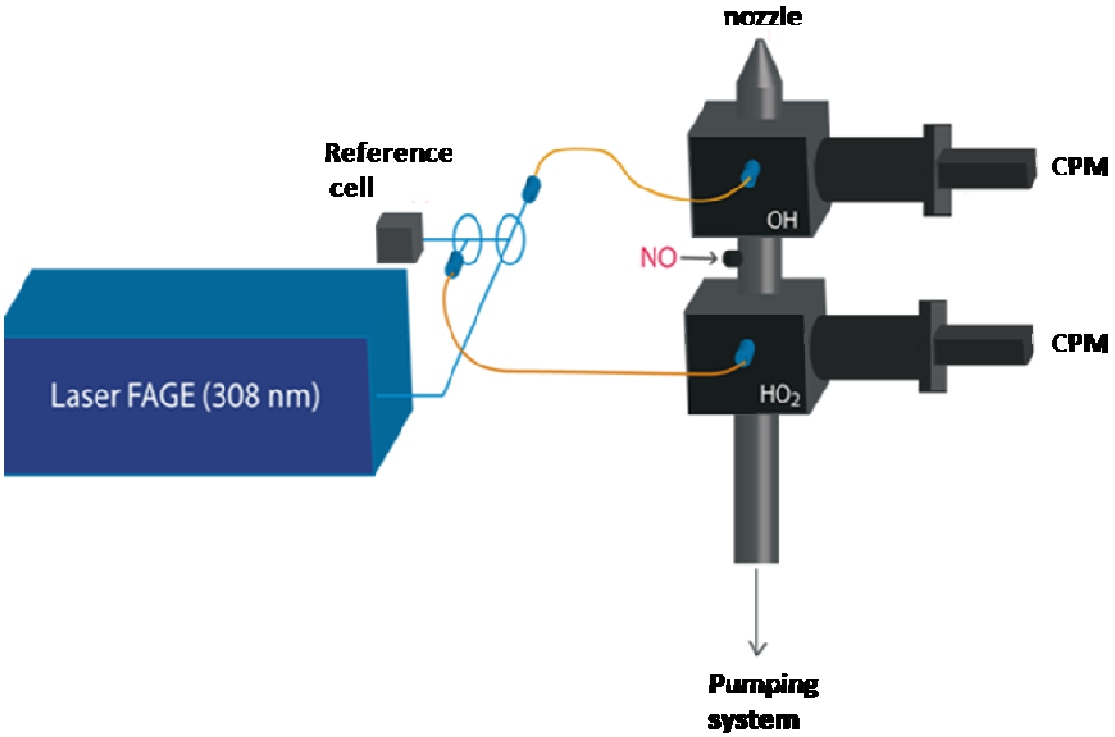

Figure II- 1: Representative diagram of the UL-FAGE device in the quantification mode. CPM: channel photomultiplier

II.2.1 The laser system

The FAGE technique requires a high repetition rate UV light source for the excitation of OH in order to average fluorescence signal while keeping a high time resolution. The method to generate this radiation is a frequency doubled dye laser (Sirah Laser PrecisionScan PRSC-24-HPR) pumped by the output of a frequency doubled Nd: YVO_4 laser (Spectra Physics Navigator II YHP40-532QW). The diode pumped Nd: YVO_4 laser produces a laser beam at a wavelength of 1064 nm which is converted to green light at 532 nm through a doubling crystal. The 532 nm light is used to pump a tunable single stage dye laser using a mixture of Rhodamine 610 (B) and Rhodamine 640 diluted in ethanol. The maximum of the red shifted output is centered at 616 nm, which is frequency-doubled using a

BBO doubling crystal to produce the 308 nm emission. The UV light is then separated from the fundamental (red) light using four Pellin-Borca prisms. The diagram of the laser system is shown in Figure II- 2. The output power at 308 nm is of about 30-40 mW with a repetition rate of 5 kHz and a pulse width of 20 ns.

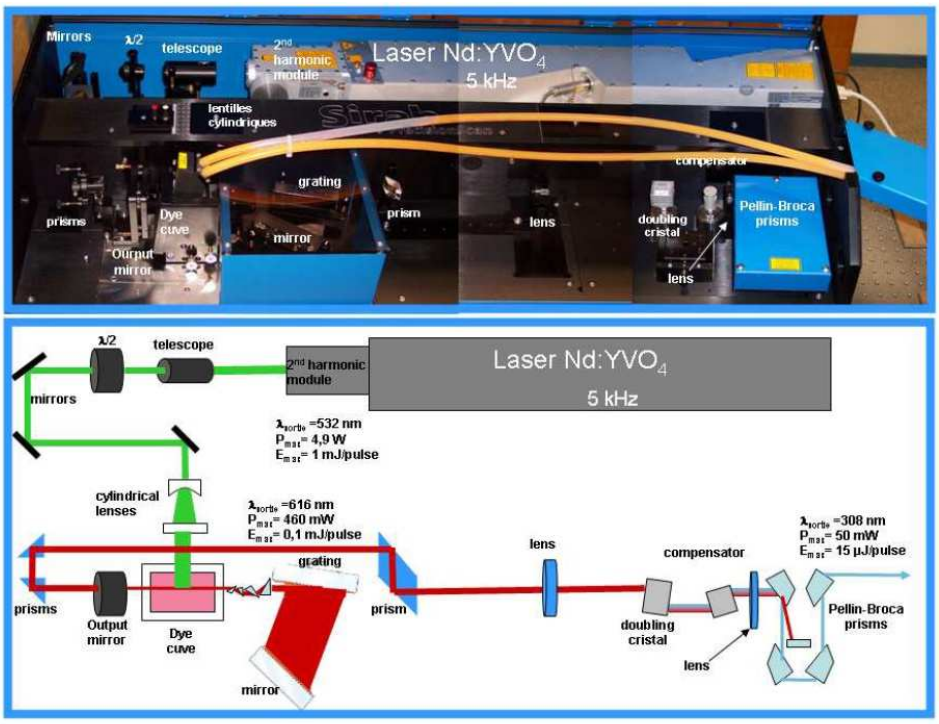

Figure II- 2: schematic of the laser system used for the UL-FAGE

The output light is transferred to the fluorescence cells to excite one line of the OH A-X (0, 0) band, using a set of optics (Figure II- 3).

The laser beam at the output of the laser is shaped to optimize its injection into the fibers by 2 cylindrical lenses (Melles Griot LQC, f = 75 mm and f = 50 mm) and separated in different beams by beam splitters. Depending on the configuration of the UL-FAGE instrument used (HO_x quantification, with or without OH reactivity, with or without RO_x measurement), the beam has to be split in 3, 4 or 5. During this work, at the maximum 4 beams were used (HO_x quantification with OH reactivity).

Here is described the configuration used for the HO_x/HO_2* quantification with the OH reactivity measurement as deployed during the LANDEX field campaign (see chapter VI). For this, 4 beams are needed: 1 for the OH cell, 1 for the HO_2/ HO_2* cell, 1 for the reactivity cell and one for the reference cell. The output beam is split by a first beam splitter (Melles Griot 16BSQ035 / Reflexion R =80% / Transmission T= 20%) which sends 20% of the laser power to a collimator (Melles Griot 13 FOA 101) that focuses the beam on the entrance of the optical fiber to inject it into the fiber leading to the

FAGE cell used for reactivity (principle of the measurement explained later). The remaining power (80 %) arrives on a mirror that reflects all the incoming radiation to a second beam splitter (Melles Griot 16BSQ035/R50/T50). The second beam splitter transfers 50% of the beam to the OH cell (through a collimator and a fiber) and 50% is transmitted to a third splitter (50/50). The latter sends 50% of the beam power to the HO_2 cell (through a collimator and a fiber). The remaining 50% of the beam power is transmitted to the reference cell after passing through a prism (Melles Griot, AR308, 01PQB001/072), and a window which reflects a part of the beam on a photodiode (Hamamatsu, S1722) to continuously measure the laser power (Figure II- 3). The detection cell fibers are about 10 m long and have transmission efficiency of 50-75 %.

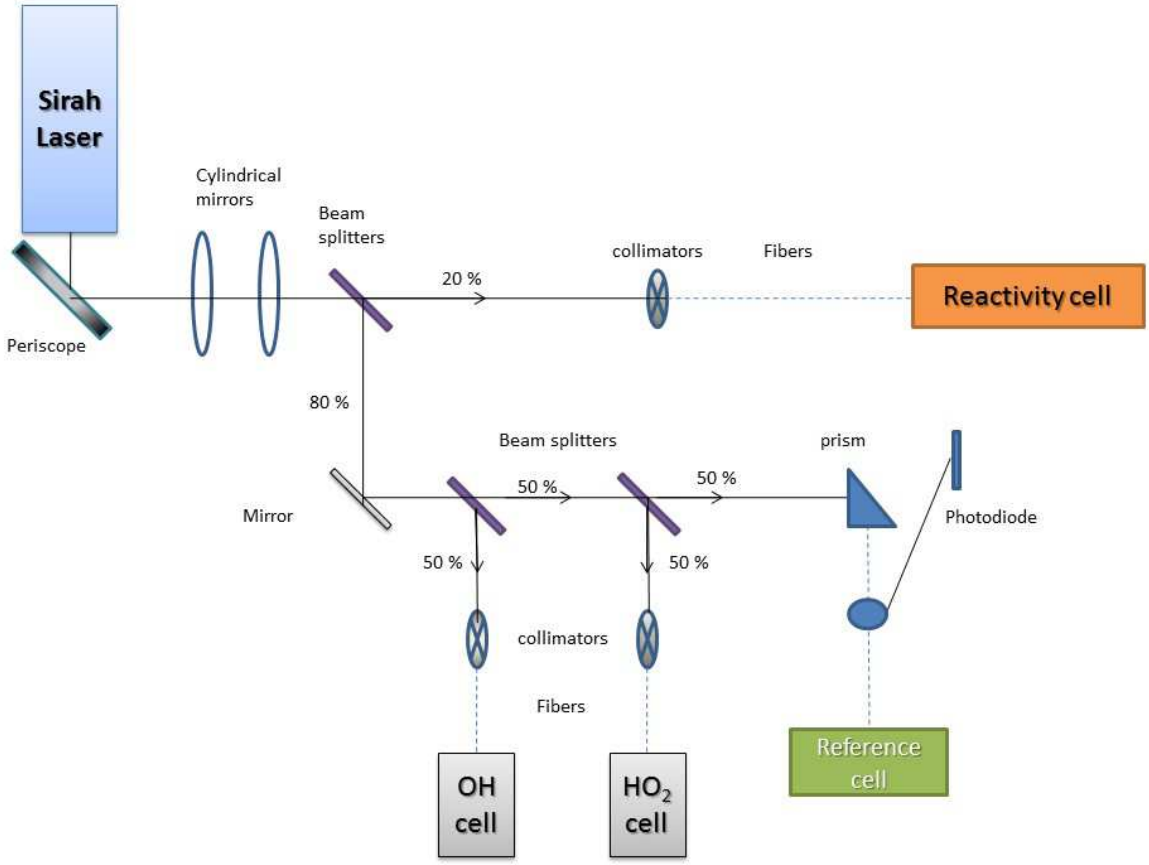

Figure II- 3: schematic diagram of the optics set in front of the excitation laser

II.2.2 Probing system

In order to probe ambient air to quantify HO_x radicals by OH LIF in low pressure cells (see next paragraph), a nozzle is used as well as a pumping system. To quantify the potential interferences on

OH measurements, a preinjector has been implemented above the nozzle and has been characterized. The different parts of the probing system are described here.

II.2.2.1 Sampling

The air is sampled into the FAGE fluorescence cells through a small orifice (1 mm for atmospheric measurements). The gas expansion allows the measurement of the OH fluorescence at low pressure. After the expansion, the molecular beam consists of a first supersonic jet and then a subsonic jet. The gas expansion leads to a sudden drop in temperature and pressure, which «freezes» the reactions between the sampling and the measurement. This leads to reduced losses of OH. The low pressure (1.5-2 Torr) in the FAGE cells allows also to extend the lifetime of the fluorescence by limiting the collisions between the molecules (see paragraph II.2.3.2). In the UL-FAGE, the air is continuously pumped through a 1mm pinhole with a pumping rate of 9.2 l min^{-1} using an Edwards Vacuum pump (iXL 1000) to the two low-pressure cells for OH and HO_2 measurement (Figure II- 4).

Figure II- 4: Lille 1mm orifice size adjusted to the top of the detection cells

II.2.2.2 Preinjector

As significant interferences have been observed with other FAGE instruments during campaigns (see chapter 1, paragraph 3.2.1), and given that the OH interference is probably instrument-specific, it was very important to test this interference on the UL-FAGE. To do so, it is necessary to use a preinjector on top of the sampling nozzle to remove periodically the atmospheric OH using an OH

scavenger before it is sampled by the nozzle. It allows to quantify the OH signal generated within the instrument. A preinjector system above a nozzle, both provided by the University of Bloomington (USA), were installed on the UL-FAGE instrument (Figure II- 5) to replace our sampling system.

Figure II- 5: Preinjector with 1 mm nozzle that was applied on UL-FAGE instrument above the nozzle (borrowed from Indiana University)

The scavenger consists of a circular aluminum frame of 3.5 cm internal diameter and 1 cm thickness. The scavenging gas is injected via 0.5 mm diameter holes from the internal side of the frame into the center of the flow of the air sampled by the FAGE instrument. The scavenging gas was injected with a carrier flow of nitrogen in order to achieve a good penetration of the scavenger into the sampled flow as well as to improve the mixing between the sampled air and the scavenger gas.

The flow reaching the preinjector is controlled by 2 mass flow controllers (MFCs), one controls the carrier gas (nitrogen) and the second one controls the scavenger gas (propane or C_3F_6). In function of the position of the two 3 way electric valves, the scavenging gas reaches or not the preinjector or the line is flushed (scavenger modes ON, OFF, flush). The scavenger is mixed with the carrier gas before it is injected into the sampled atmospheric air. In the mode OFF, the nitrogen flow is increased to keep the same flow (40 sccm) as shown in Figure II- 6.

In the mode scavenger OFF, no scavenging gas is injected to the carrier gas (the measured signal corresponds to the ambient OH + interference signal). In the second mode: scavenger ON, C_3F_6 or propane gas is injected to the scavenger replacing a small portion (0.02 L/min) of the carrier gas flow (measured signal corresponds to the interference signal). The third mode called flush mode the lines

are purged with nitrogen at a flow of approximately 500 sccm for 20 s. This mode takes place in between the ON and the OFF mode to remove rapidly residual scavenging gas from scavenger lines. The duration of the three modes can be adjusted by a LabView program. The real OH signal is the difference between the signal measured in scavenger OFF mode and scavenger ON mode.

	3 way valve (1)	second 3 way valve (2)
scavenger ON	b	a
scavenger OFF	b	b
Flush	a	b

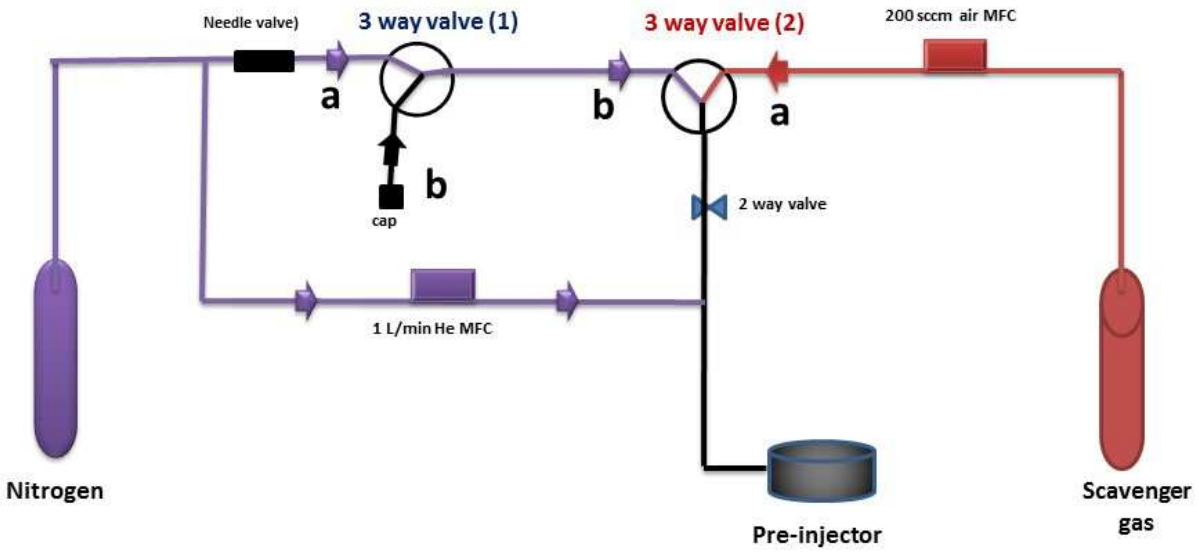

Figure II- 6: schematic of the scavenger system connected to the UL-FAGE. 3-way valve 1: valve status a: high nitrogen flow, valve status b: cap (no flow). 3-way valve 2: valve status a: scavenger gas flow, valve status b: flow coming from the first 3-way valve.

The UL-FAGE instrument samples around 9.2 L min^{-1} of air directly from the center of the scavenger. The residence time between the injection of the scavenger and the instrument inlet was ~ 2 ms. Conditions of operation of the preinjector determining the efficiency of OH removal (scavenger used, concentration of the scavenger, the flow of the carrier gas) were characterized on the UL-FAGE with the calibration cell generating constant concentrations of OH radicals at the top of the preinjector and measure the OH signal with and without the scavenger gas. The gas flow passing through the calibration cell was 40 $L.min^{-1}$ which may not be representative in term of flow conditions of the ambient conditions and can affect the removal efficiency of OH. Therefore, laboratory experiments were conducted with the calibration cell placed at different positions on top of the preinjector to measure the fraction of OH that was removed by the scavenger at each position as function of the scavenger used and its flow.

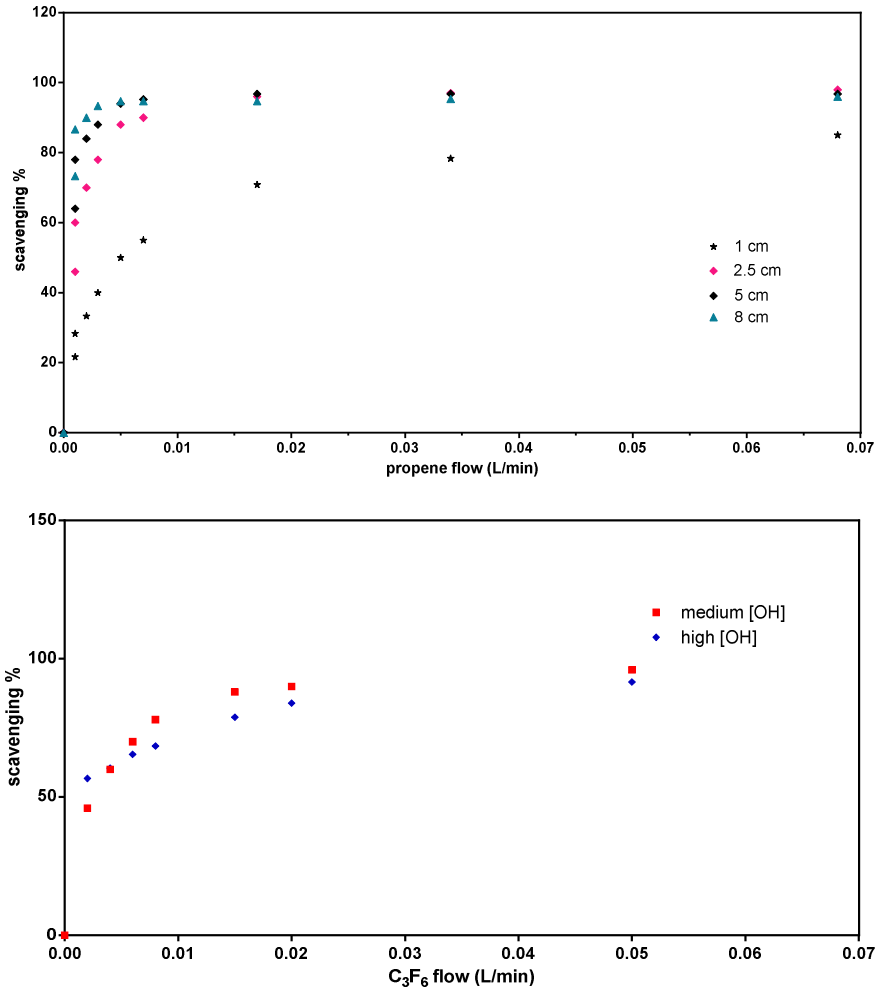

Figure II- 7: upper graph represents the scavenging efficiency as function of the propane flow used as scavenger for different distance between the exit of the calibration cell and the nozzle of the FAGE. Lower graph represents the scavenging efficiency of OH as function of the hexafluoropropylene (C_3F_6) flow used as scavenger at the optimized distance (2 cm). For both scavengers, the carrier gas flow was 0.02 L/min)

The upper graph in Figure II- 7 shows the results of the scavenging efficiency with respect to the distance between the exit of the calibration cell and the scavenger as function of the propene flow. The results showed that with a distance of 2 to 8 cm from the preinjector, the scavenging efficiency reached 95-97 % with at least 0.02 L/min of propene flow. At 1 cm, the high flow provided by the calibration cell probably generates turbulences and limited the mixing of the flow with the scavenger. A similar experiment was done with C_3F_6 as scavenger gas with distance of 2 cm between the OH source and the scavenger using 2 different OH concentrations (low and medium).For low concentrations, [OH] was in the range of $2.5 \times 10^8 cm^{-3}$, while for medium concentrations, [OH] was in the range of $1 \times 10^9 cm^{-3}$. Same results were seen in the lower graph of Figure II- 7, where the scavenging efficiency reached 95 % with 0.02 L/min of C_3F_6.

The carrier flow rate did not impact the scavenging efficiency and did not have a significant impact on the dilution of the scavenger as it represents a minor percentage of the total flow sampled by FAGE. This type of chemical method was used in LANDEX campaign for 2 days where an interference was clearly seen (see more in Chapter V).

II.2.3 The detection cells

As mentioned above, the UL-FAGE instrument dedicated to the HO_x quantification is composed of two multi-pass cells:

1) The first one allows the measurement of OH radical directly by laser induced fluorescence,

2) The second one allows the HO_2 measurement indirectly after its conversion to OH by the addition of NO (NO concentration are calculated assuming perfect mixing in the cell), OH is then detected by LIF similarly to the first cell (Figure II- 8).

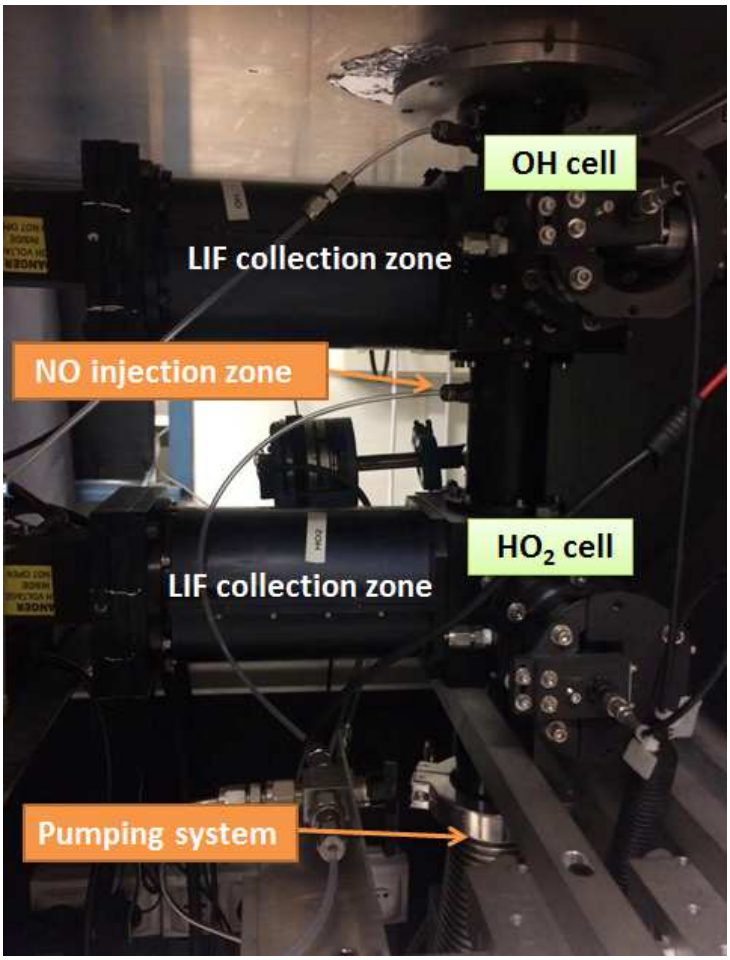

Figure II- 8: Picture of the measuring cells of the UL-FAGE instrument (The upper cell used to detect OH, the second for HO_2, where NO is injected in between).

II.2.3.1 OH and HO_2 cells

The OH and HO_2 detection cells that are shown in Figure II- 8 are White cells composed of 3 concave mirrors (Figure II- 9): one at the front, cutout, allowing the beam to enter and exit, and two at the back aligned. The advantage of White cells compared to single pass cells is to increase the total path length of the laser beam travelling through the cell (about 40 multi-passes in our case) and therefore an increase in sensitivity.

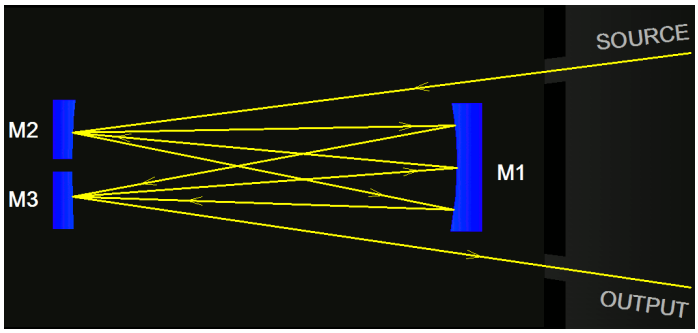

Figure II- 9: representative scheme of the detection cell

Their disadvantages concern interference due to photolysis which may be higher compared to single path configurations, depending on the laser power used. Also, the background signal due to scattered laser light may be higher compared to the single pass cells, reducing the gained increase in sensitivity to a certain extend.

II.2.3.2 The OH fluorescence collection system

As mentioned previously, the OH fluorescence lifetime is extended to several hundreds of nanoseconds through the reduced pressure, significantly longer than the laser pulse. So, for the discrimination between the OH fluorescence and the scattered laser light, gated detectors are used.

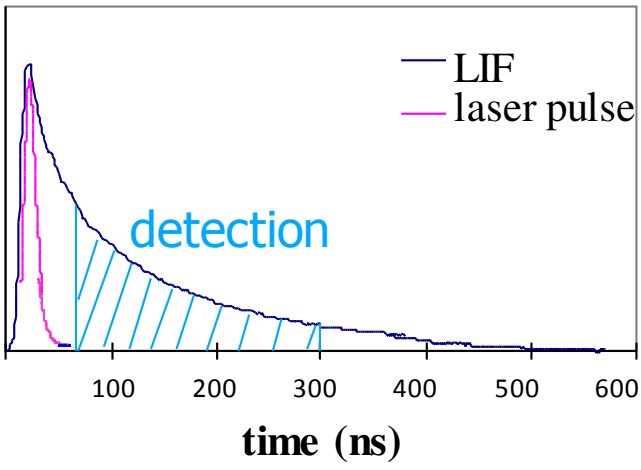

Figure II- 10: OH fluorescence using gated detectorsCPM (Channel Photon Multiplier)

This detection is ensured by CPM (Channel Photon Multiplier, Perkin Elmer MP-1982-RS232) which are switched off during the laser pulse (they do not measure any signal) and rapidly switched on after the laser pulse to collect the OH fluorescence signal (Figure II- 10).

The LIF signal is collected perpendicularly to the excitation beam. The optical system is optimized in order to collect the maximum of the OH fluorescence signal and to minimize the light scattered from the laser beam. A set of two lenses is used to focus the fluorescence signal on the detector. A narrow band interference filter at 308 nm is installed between the two lenses to limit the noise due to ambient light (λ ≈ 310 nm, bandwidth ≈ 5 nm).

CPM detectors are composed of 3 elements: a photocathode, an electron multiplier and an anode. The photocathode converts the photons into electrons, which are then multiplied on the walls of the semiconductor tube of the detector, and are then collected at the anode. To gate the CPMs, the voltage applied at the cathode is modulated by home build switches controlled by a delay generator. Each switch is a power supply generating variable voltages applied to the cathode. A voltage higher than the input voltage of the CPM tube (Channel entrance) is applied to the cathode to close the detector. A lower voltage is applied to the cathode to turn on the CPM and to collect the fluorescence signal. Two types of CPMs are used in the UL-FAGE instrument, positive or negative ones (Figure II- 11).

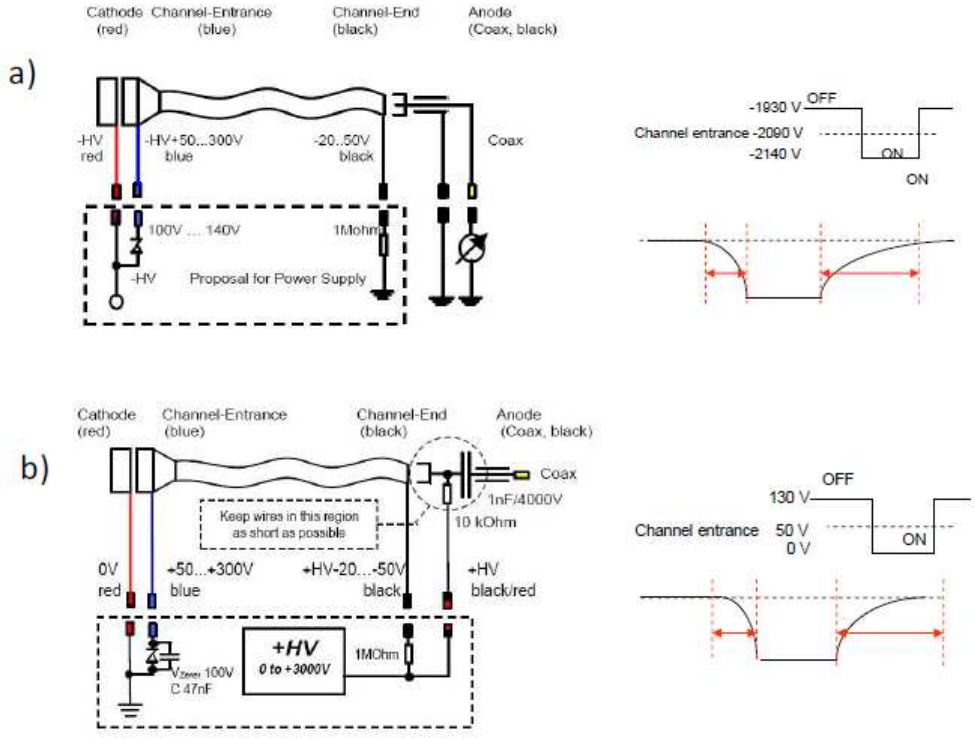

Figure II- 11: Channel Photon Multiplier (CPM): a) Negative mode and b) positive mode.

(a) On the OH cell, a CPM in a negative mode (specific request from manufacturer Perkin Elmer), is used. The CPM is closed (OFF) when the higher voltage applied to the cathode is above -2090 V (voltage of the channel entrance) and is activated (ON) after the laser pulse by applying a voltage lower than -2090 V to the cathode,

(b) positive (standard) CPM is used on the HO_2 cell (also in the cell used for reactivity). In this type of CPM, the voltage of the entrance channel is approximately 50V. The CPM is closed when a voltage above 50 V is applied to the cathode and open when the voltage applied is zero.

Tests have been done to optimize the OFF and ON voltage to ensure that the CPM is completely closed or open when applying the corresponding voltage on the cathode.

These two configurations are used because the response to opening is faster, in principle, in the negative mode (Kanaya et al., 2001), but the comparisons between the two modes did not highlight significant differences (Amédro, 2012a).

A photon counting module is used at the output of the CPM, which means that the anode is connected to an electronic card allowing the individual detection of each photon in the form of a voltage peak with a width on the order of 25 ns. These peaks are then collected and counted with a National Instruments counting card (National Instruments PCI-6602) equipped with fast counters and analyzed by a Labview program on the computer.

II.2.4 The reference cell

The OH excitation peak has a very narrow linewidth (about 0.005 nm) and the laser wavelength can drift with time and due to changing ambient conditions (variation of the temperature). Therefore, it is necessary to check continuously the stability of the laser wavelength in order to be on the peak of the selected OH excitation line (Q_1 (3) in our case). For that, a reference cell, in which a high concentration of OH is produced, is used. It enables precise tuning of the laser wavelength to keep the laser on the peak of the absorption of the OH Q_1 (3) rotational line.

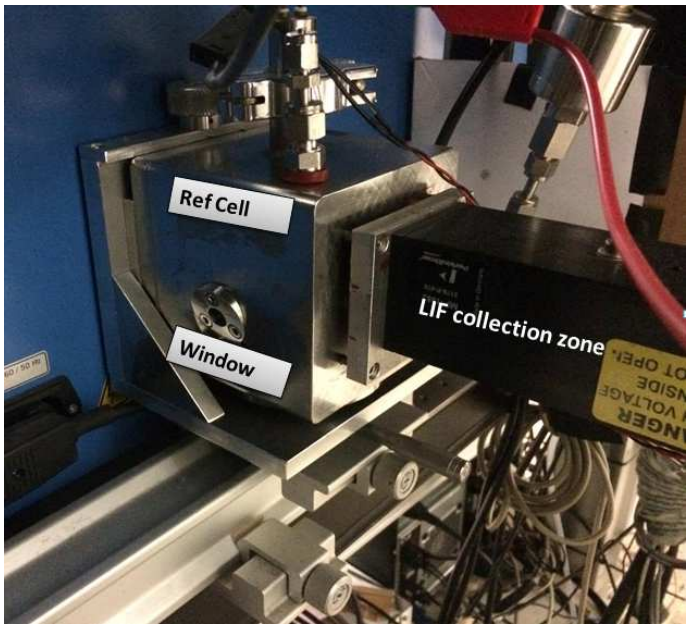

Figure II- 12: UL-reference cell coupled to the FAGE instrument

The reference cell is a stainless-steel cube, through which a small flow of ambient air is passed (Figure II- 12). The pressure inside the cell is maintained at ~ 2 Torr by a small vacuum pump. A heated coiled filament (Thermocoax filament, supplied with 3.27 A at 11.5 V) inside the cell causes thermolysis of water vapour, which produces high concentrations of OH. Laser light from the excitation laser is delivered to the cell by the reflection from the prism (see Figure II- 3). The OH fluorescence is detected by a channel photomultiplier tube (CPM, Perkin Elmer) perpendicular to the laser beam. The concentration of OH in the reference cell is sufficiently high so that the fluorescence signal can be observed above the signal due to scattered laser light, so no temporal gating of the CPM is required. The signal from the CPM coupled to a photon counting module is collected by an acquisition card and monitored by the acquisition software (Labview program) in the computer.

Prior to the start of each OH and HO_2 measurement cycle, the laser wavelength is scanned over a wavelength range including a triplet of peaks easily identifiable: from the P_1 (1) to the Q_1 (3) peaks (308.232 nm to 307.995 nm, relative wavelength, Figure II- 13). The scan on the Q_1 (3) line is then repeated each time the signal from the reference cell is lower than 95 % of the peak signal from the initial scan.

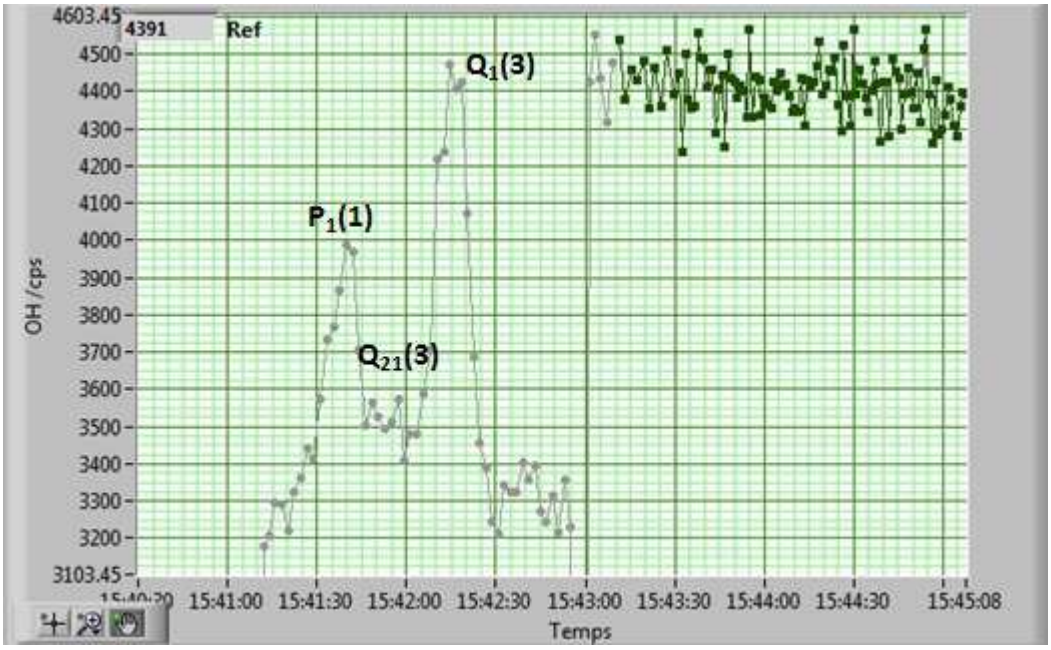

Figure II- 13: reference cell signal for FAGE Measurement sequence, scan to identify the triplet and set to the wavelength corresponding to the OH absorption line Q_1 (3).

II.2.5 Data acquisition

To be able to regularly subtract any signal that is not the fluorescence of OH (residual laser scattering, spectral interference, noise...), the fluorescence signal of OH is collected alternatively changing the wavelength of the excitation laser according to a defined cycle. A Labview acquisition program allows continuous data acquisition and control of the laser. After a wavelength scan and the identification of the laser position corresponding to the peak of the OH excitation line by the signal obtained on the reference cell, the laser returns to the wavelength corresponding to the apex of the line Q_1 (3).

The measurement of the fluorescence signal (in counts per second) is then carried out in the OH and HO_2 cells for 20 seconds giving the "online" signal. Then, the laser shifts in wavelength (of the order of one hundredth of nm) for 20 seconds to obtain the signal "offline", which is the combination of the laser scattering and solar radiation. The potential fluorescence of other chemical species absorbing at 308 nm (naphthalene, SO_2, HCHO, ...) can be avoided by a good selection of the excitation line and the offline wavelength (Ren et al., 2004).

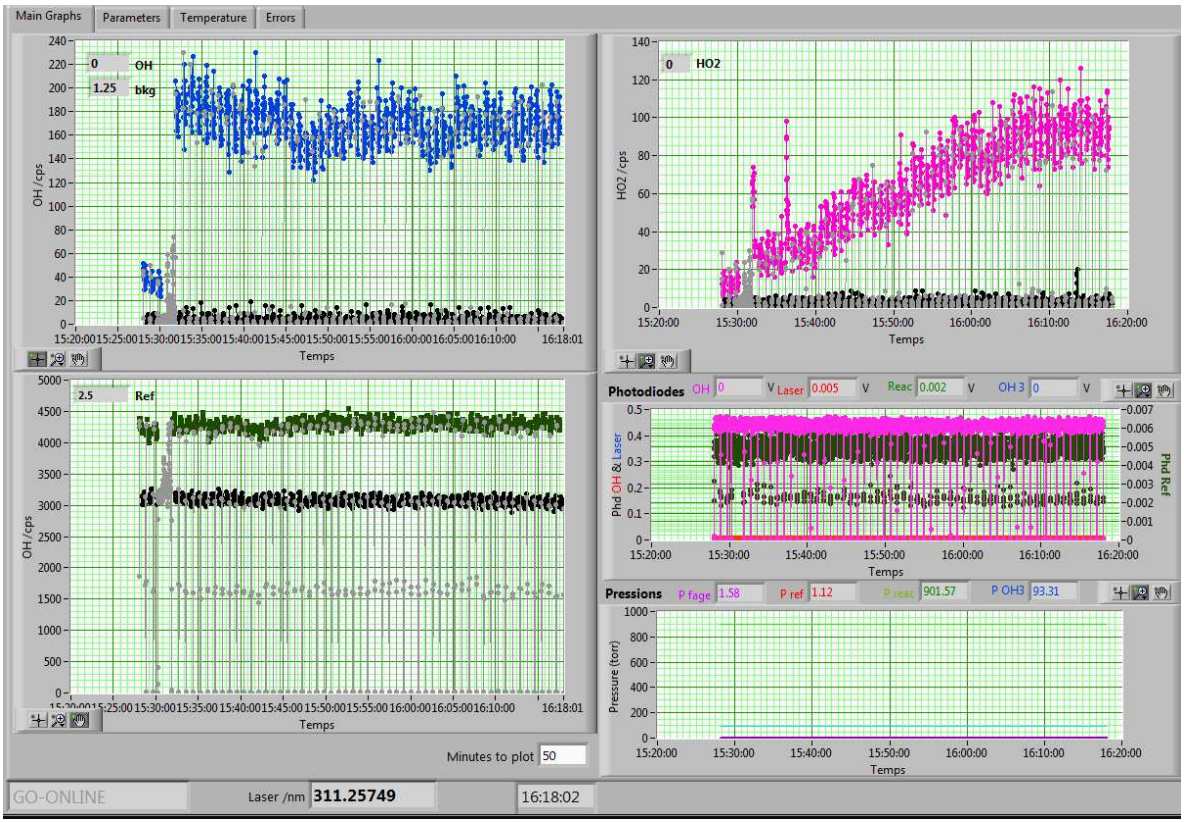

Figure II- 14: Signal for FAGE measurement sequence: scan to identify the triplet (OH peak) and set to the wavelength corresponding to the OH absorption line Q_1 (3) then alternate the OH and HO_2 measurement for 20 s

"online" laser and measure the noise during 20 s "Offline" laser. HO_2 signal in cell 2 increases as NO concentration increases in the presented case.

The Online-Offline cycles are performed alternately on a continuous basis (Figure II- 14). The signal corresponding to the fluorescence of OH is the called $Signal_{online}$ from which the $Signal_{offline}$ is subtracted. In order to subtract the noise (called $Signal_{background}$) associated with the external light which can change fast, it is measured simultaneously to the $Signal_{online}$ and $Signal_{offline}$ by opening the CPMs at a long time after the laser pulse (a few µs). This signal is subtracted during the post-processing to the $Signal_{online}$ and to the signal "Offline".

$$Signal_{online} = Signal_{OH\ fluorescence} + Signal_{scattering} + Signal_{background\text{-}online} \quad \text{Eq II- 1}$$

$$Signal_{offline} = Signal_{scattering} + Signal_{background\text{-}offline} \quad \text{Eq II- 2}$$

$$Signal_{OH\ fluorescence} = (Signal_{online} - Signal_{background\text{-}online}) - (Signal_{offline} - Signal_{background\text{-}offline}) \quad \text{Eq II- 3}$$

However, in order to get the absolute concentration of OH and HO_2, calibration with a well characterized HO_x source is needed. This procedure is described in the next paragraph.

II.2.6 Use of the quantification configuration during the thesis

The UL-FAGE instrument was characterized for the first time for RO_2 interferences on HO_2 measurement. Different peroxy radicals and different conditions of use were tested to quantify the magnitude of signal of different RO_2's in the FAGE cells. The UL-FAGE was used in an intercomparison campaign of different calibration cell systems at Lille University. It has been deployed during the LANDEX campaign to measure OH, HO_2, and RO_2 double-bond radicals in a forest region. The measurement of RO_2 has been done by using different NO concentrations converting differently RO_2 in HO_2 (see chapter IV). Finally, the UL-FAGE is under development to study the RO_2 conversion by RO_x-LIF system and will soon be tested in HELIOS simulation chamber in University of Orleans.

II.3 Calibration of the FAGE Instrument in the quantificationconfiguration

Despite that the laser induced fluorescence technique is highly sensitive, it cannot provide absolute concentration without the determination of numerous parameters difficult to quantify (Holland et al., 1995). Therefore, the FAGE technique requires an accurate calibration system to quantify OH and HO_2.

For that, a known concentration of OH and HO_2 is generated at the entrance of the FAGE by placing a calibration cell above the sampling cone. The relationship that links the fluorescence signal to the OH concentration is given as:

$$S = C \times [OH] \times P \qquad \text{Eq II- 4}$$

where S is the LIF signal (in cts s^{-1}), P the laser power (mW) and C is the calibration factor (in cts s^{-1} $molecule^{-1}$ cm^{-3} mW^{-1}), which defines the relative instrument sensitivity. C depends on several parameters such as the cell alignment, the efficiency of the signal collection, the excitation line probed, etc.

II.3.1 Generation of OH and HO_2 radicals in the calibration cell

The generation of OH in the calibration cell is based on the photolysis of H_2O in controlled conditions. For that, a known concentration of water vapor is introduced with a synthetic zero air flow into the calibration cell (Figure II- 15).The water vapor is photolyzed at 184.9 nm by a low pressure mercury lamp to generate OH radicals and H atoms, with HO_2 being formed in the rapid reaction of H atoms with molecular oxygen present in the synthetic air (80 % N_2, 20 % O_2), according to the following mechanism:

$$H_2O + hv_{(\lambda=184.9\ nm)} \rightarrow OH + H \qquad \text{R II- 1}$$

$$H + O_2 + M \rightarrow HO_2 + M \qquad \text{R II- 2}$$

The quantum yield for OH and HO_2 is equal to 1 (Atkinson et al., 2006).

To determine the OH and HO_2 concentration, it is necessary to know the water vapor concentration and the lamp flux. Indeed, the OH concentration generated can be calculated by the following equation:

$$[OH] = F_{184.9} \times \sigma_{H2O} \times [H_2O] \times \Phi \times \Delta t \times OH_{losses} \qquad \text{Eq II- 5}$$

where σ_{H2O} is the absorption cross-section of H_2O at 184.9 nm (7.14×10^{-20} cm^2,(Cantrell et al., 1997)), Φ the photolysis yield (equal to 1), Δt the exposure time in s, $[H_2O]$ the concentration of water in molecule cm^{-3}, $F_{184.9}$ the photon flux in cm^{-2} s^{-1}, OH_{losses} the losses between the OH generation and the output of the calibration cell.

This flux can be measured directly by a calibrated detector (Faloona et al., 2004) or indirectly by actinometry on O_3 produced simultaneously by the photolysis of O_2 present in the flow or NO produced by the photolysis of known concentrations of added N_2O (Edwards et al., 2003) in a

separate experiment. Actinometry is used by most FAGE groups, including our group, to determine the lamp flux but direct measurement is also possible (Faloona et al., 2004). The principle of chemical actinometry is described in details in Aschmutat et al. (Aschmutat et al., 1994) and briefly summarized here. The ozone actinometry is based on the ozone concentration measurement, generally with a commercial ozone analyser after its production by the photolysis of the dioxygen at 184.9 nm (with a yield $\Phi_2 = 2$, (Atkinson et al., 2006)):

$$O_2 + h\nu_{184.9nm} \rightarrow 2\ O(^3P) \qquad \text{R II-3}$$

$$2\ [O(^3P) + O_2] \rightarrow 2\ O_3 \qquad \text{R II-4}$$

and the lamp flux is obtained as following:

$$F_{184.9} = [O_3] / (2 \times \sigma_{O2} \times [O_2] \times \Delta t) \qquad \text{Eq II- 6}$$

Then by replacing $F_{184.9}$ in Eq II- 5, we get:

$$[OH] = [O_3] \times [H_2O] \times \sigma_{H2O} \times OH_{losses} / (2 \times [O_2] \times \sigma_{O2}) \qquad \text{Eq II- 7}$$

$$[HO_2] = [O_3] \times [H_2O] \times \sigma_{H2O} \times HO_{2losses} / (2 \times [O_2] \times \sigma_{O2}) \qquad \text{Eq II- 8}$$

However, due to the structured absorption spectrum of O_2 in this wavelength region, this coefficient might vary from one lamp to another due to the variation of σ_{O2}. As it has not yet been determined experimentally in our case, its potential variation is included in the uncertainty (see paragraph II.3.3).

II.3.2 Calibration cell configuration and calibration procedure

The calibration cell is a rectangular aluminum tube (1.2 × 1.5 × 50 cm) with 5 rectangular holes in which 6 cm height windows are placed in between rubber seals. Two blocks of aluminum are placed on each side of the tube to maintain the windows (Figure II- 15). The Hg lamp is placed in another aluminum block fixed to the calibration cell. This block can slide along the cell to place the lamp in front of the different windows. A nitrogen flow (50 sccm) goes through the lamp housing mainly to cool the lamp and to avoid absorption by O_2 which could reduce the lamp flux. An interference filter (Melles Griot 185NB20) is placed inside the lamp

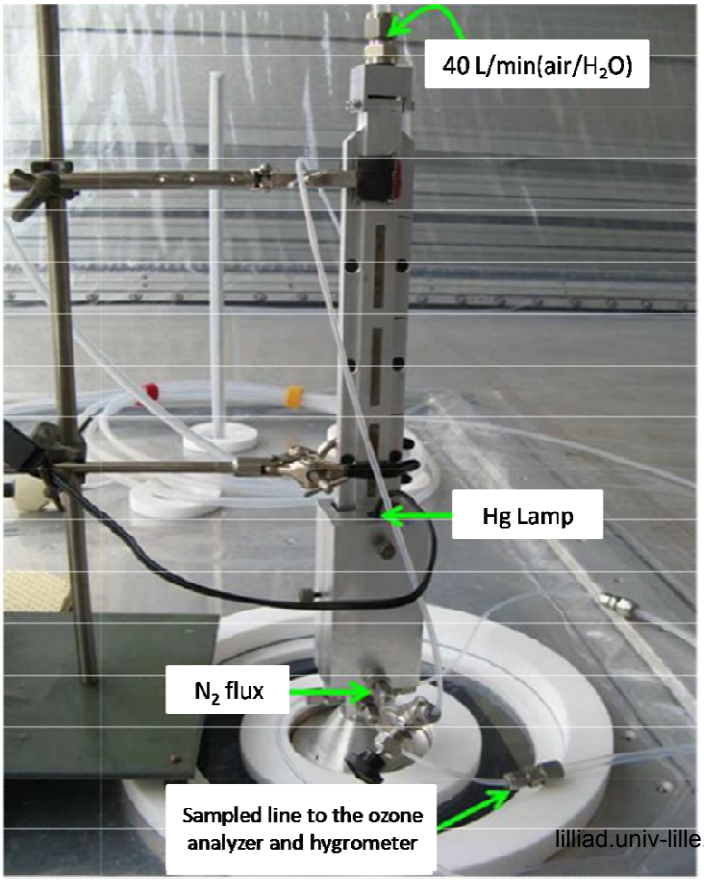

housing to reduce the strong light emissions at λ=254 nm that could photolyse O_3 and generate an additional production of radicals (Figure II- 15).

Figure II- 15 calibration cell for the fluorescence cells (version 1)

Part of the air is sampled at the exit of the calibration cell to measure the ozone and water concentration by gas analyzers (Thermo analyzer TEI 42i for ozone and hygrometer, Michell Instruments, S8000 integral Precision Dewpoint Meter, 95% accuracy for water vapor).

The calibration cell is flushed with a flow of synthetic air passing partly through a bubbler containing distilled water. The total flow is 40 SLPM allowing a turbulent flow in the cell. The flow at the output of the calibration cell is much higher than the pumping flow of the UL-FAGE system (9.2 SLPM) in order to probe air exclusively from the calibration cell by the FAGE. The amount of air passing through the bubbler and the amount of diluting air is controlled by calibrated mass flow controllers (Bronkhorst) as shown in Figure II- 16.

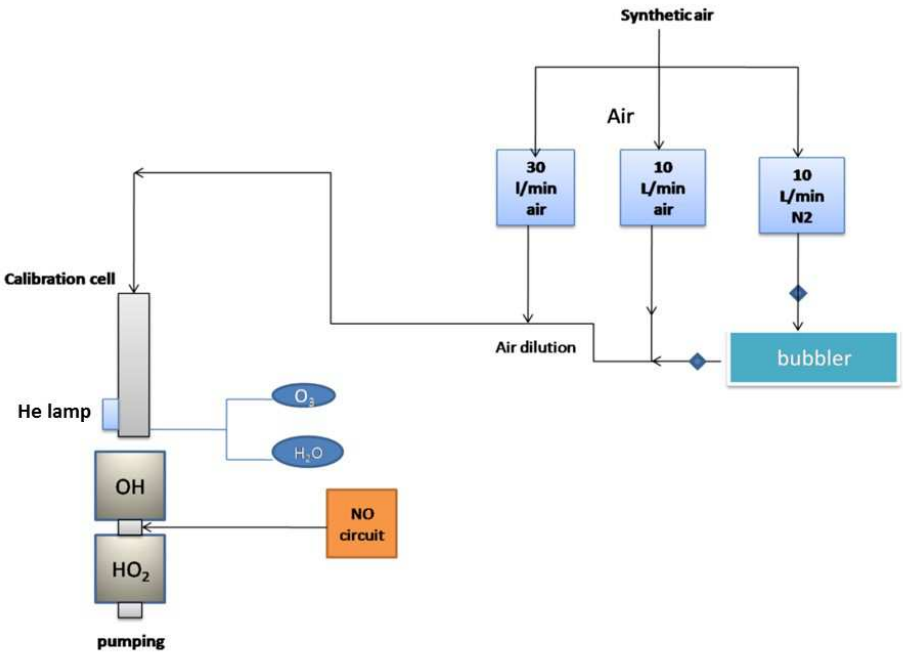

Figure II- 16: Diagram of the gas delivery system for HOx calibrations. O_3: ozone analyzer, H_2O hygrometer, diamonds represent the 2-way valves.

The radical concentrations generated in our system range between 1×10^9 to1×10^{10} molecules.cm^{-3}. To do the calibration, the calibration cell is mounted vertically on the FAGE cell and is held 0.5 -2cm above the nozzle. The calibration is made in 4 different steps:

1) - A stabilization step, lamp OFF during which the water and ozone concentrations stabilize and the background signal is measured (Signal $_{background}$)

2) - A "OH step", lamp ON, without injection of NO in the second cell to get the signal from OH in both cells. After stabilization of the signal and the ozone concentration measured by the analyzer, this step allows the calibration of the first cell and the measurement of the OH contribution in the signal in the second cell, allowing determining the sensitivity to OH of the second cell.

$$C_{\text{cell 2,NO=0}} = \frac{[OH] \times P}{S_{\text{cell}_2,OH}} \qquad \text{Eq II- 9}$$

3) - A "HO_2 step", lamp ON, during which a known flow of NO is injected between the first and the second cell to enable the HO_2 conversion. The signal increases in the cell 2 as it corresponds to the sum of the OH and HO_2 signals. This step allows the calibration of the second cell for HO_2 measurement at this NO flow. For HO_2, the sensitivity depends on the injected NO concentration, modifying the conversion efficiency. The conversion efficiency is determined by the ratio between the HO_2 signal at a given NO concentration and the signal at the maximum of conversion.

$$C_{\text{cell 2,NO}\neq 0} = \frac{[HO_2] \times P}{S_{\text{cell}_2,\text{NO}\neq 0} - S_{\text{cell}_2,\text{NO=0}}} \qquad \text{Eq II- 10}$$

$$\text{Conversion efficiency coefficient } \alpha = \frac{S_{\text{cell}_2,\text{NO}\neq 0} - S_{\text{cell}_2,\text{NO=0}}}{S_{\text{cell}_2,\text{NOmax}} - S_{\text{cell}_2,\text{NO=0}}} \qquad \text{Eq II- 11}$$

The change in the HO_2 conversion and then the HO_2 sensitivity as a function of the NO concentration is shown in Figure II- 17.

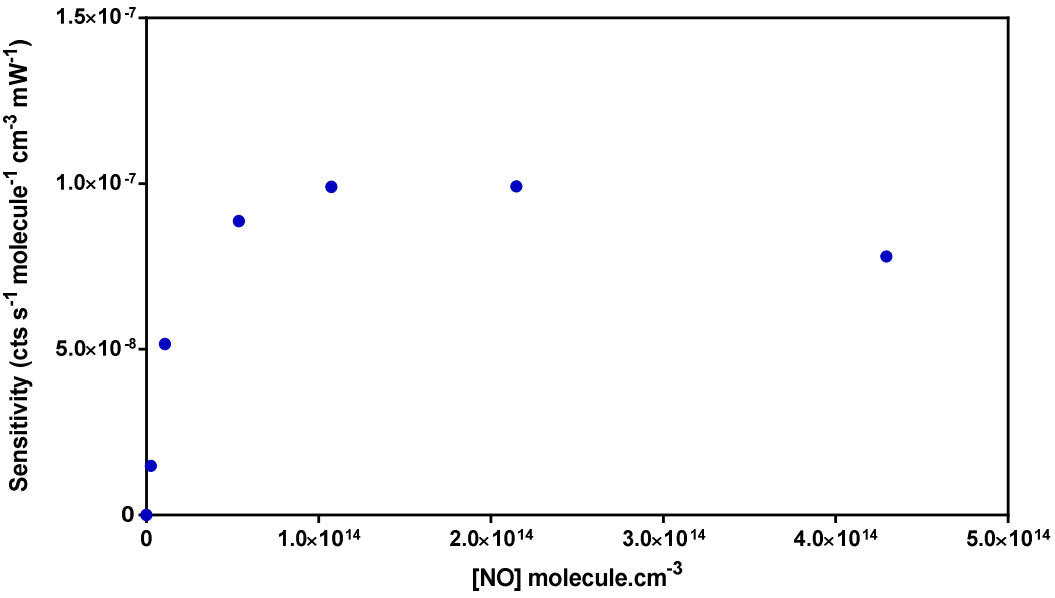

Figure II- 17: Evolution of the sensitivity as function of NO concentration injected in cell 2

The experiment was made by varying the NO concentration from 0 up to 5 × 10^{14} molecules.cm^{-3} (equivalent to NO flow up to 400 sccm) with constant HO_2 concentration. As the NO concentration is increased, thesignal measured in the second cell reached a plateau corresponding to the maximum conversion efficiency. As the NO concentration increased above 3 × 10^{14} molecules.cm^{-3} the conversion efficiency decreases slightly. This can be explained by the loss of OH by its reaction with NO:

$$OH + NO + M \rightarrow HONO + M \qquad \text{R II- 5}$$

4) - A control step, with the Hg lamp turned off to control the O_3 background signal on the ozone analyzer and the $Signal_{background}$.

The losses between the radical generation in the calibration cell and the exit of the calibration cell have to be taken into account for the calibration. A correction factor is determined by moving the lamp at different heights on the calibration cell (see chapter IV). The losses of the radicals in the FAGE cells are taken into account in the sensitivity calculation as the concentration at the exit of the calibration is used to determine this sensitivity. In our case there is heterogeneous radical loss on the walls of the calibration cell and between the two cells. The OH and HO_2 wall loses were characterized during this work.

II.3.3 Calibration uncertainty

The calibration uncertainty is coming from the uncertainty on fluorescence signal to noise ratio, laser power fluctuations and OH and HO_2 concentrations as shown in Eq II- 12.

$$Signal\ error = calibration factor\ (C) \times \sqrt{\left(\frac{SD\ s-b}{signal}\right)^2 + \left(\frac{power\ fiber}{laser\ power}\right)^2 + \left(\frac{OH\ error}{[OH]\ and\ [HO_2]}\right)^2} \qquad \text{Eq II- 12}$$

Where (SD s – b) is the standard deviation of the signal minus the background. The uncertainty coming from the OH and HO_2 concentration calculation is related to the uncertainty on absorption cross section of O_2 and H_2O, the concentration of water and ozone.

$$\left(\frac{\delta[OH]}{[OH]}\right)^2 = \left(\frac{\delta[O_3]}{[O_3]}\right)^2 + \left(\frac{\delta[H_2O]}{[H_2O]}\right)^2 + \left(\frac{\delta\,\sigma H_2O}{\sigma H_2O}\right)^2 + \left(\frac{\delta\sigma O_2}{\sigma O_2}\right)^2 \qquad \text{Eq II- 13}$$

The O_2 absorption coefficient with the mercury lamp used was not measured during the thesis but may vary as a function of the overlap between the oxygen absorption lines and the lamp spectrum, a difference of 20% has been observed in the literature from 1.1 to 1.4 × 10^{-20} cm^2 (Hofzumahaus et al., 1997). This difference has been used as the uncertainty on σ_{O2}. The O_2 absorption coefficient was assumed to be 1.2 × 10^{-20} cm^2(Amédro, 2012a) with an uncertainty of 20%. The uncertainty for each parameter is listed in Table II- 1.

Table II- 1: uncertainty on the parameters used to determine the sensitivity of the UL-FAGE

Parameters	Range	Percentages
$[O_3]$	3-10 ppb	10-33 %
$[H_2O]$	150 -4000 ppm	5 %
σH_2O (Cantrell et al., 1997)	7.14 × 10^{-20} cm^2	3 %
σO_2	1.2 × 10^{-20} cm^2	20 %
Total		23-40%

All error bars in the graphs are calculated depending on Eq II- 13, where we consider all the possible uncertainties coming from the different parameters, while less than 10 % of uncertainties derived from the signal and laser fluctuations.

II.3.4 Improvement of the calibration cell during the thesis

The calibration cell was improved during my thesis:

- To be able to reduce the lamp flux and then to generate lower OH levels even when working at higher humidity levels
- To determine the lamp flux without the use of ozone analyzer (long to stabilize, limited to high lamp fluxes corresponding to measurable ozone levels).

II.3.4.1 Lamp flux reduction

The intensity of the radiation can be reduced by different methods:

I. By adjusting the power of the Hg lamp by a Variac (mainly 3 Variac voltages where used: 220, 170, 110 v) but this can involve variation in the lamp spectrum (see Chapter V).
II. By using a mask in front of the lamp, an aluminum handmade mask was used to hide a part of the lamp. The masked was marked to be reproducibly placed to hide a specific part of the lamp flux (1/2 and ¾ of the lamp the lamp flux).
III. Another way under development is the reduction of the lamp radiation by a N_2O filter, where N_2O absorbs light at 184 nm. This filter will be placed between the lamp and the photolysis region.

II.3.4.2 Use of a photodiode

This method enables to determine the lamp flux even for conditions leading to ozone concentration too low to be measurable. A photodiode (Hamamatsu - S1336-8BQ) was installed on the calibration cell and positioned in a housing system in front of the mercury lamp but on the other side. This addition has implied the modification of the calibration cell to open it on the opposite side of the lamp. The photodiode measures the temporal change in the flux of the lamp. The corresponding voltage is recorded by an acquisition card and a Labview program.

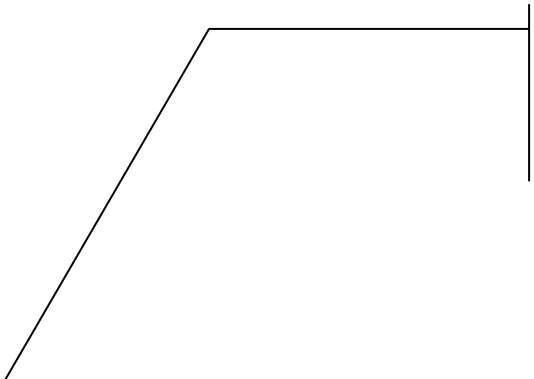

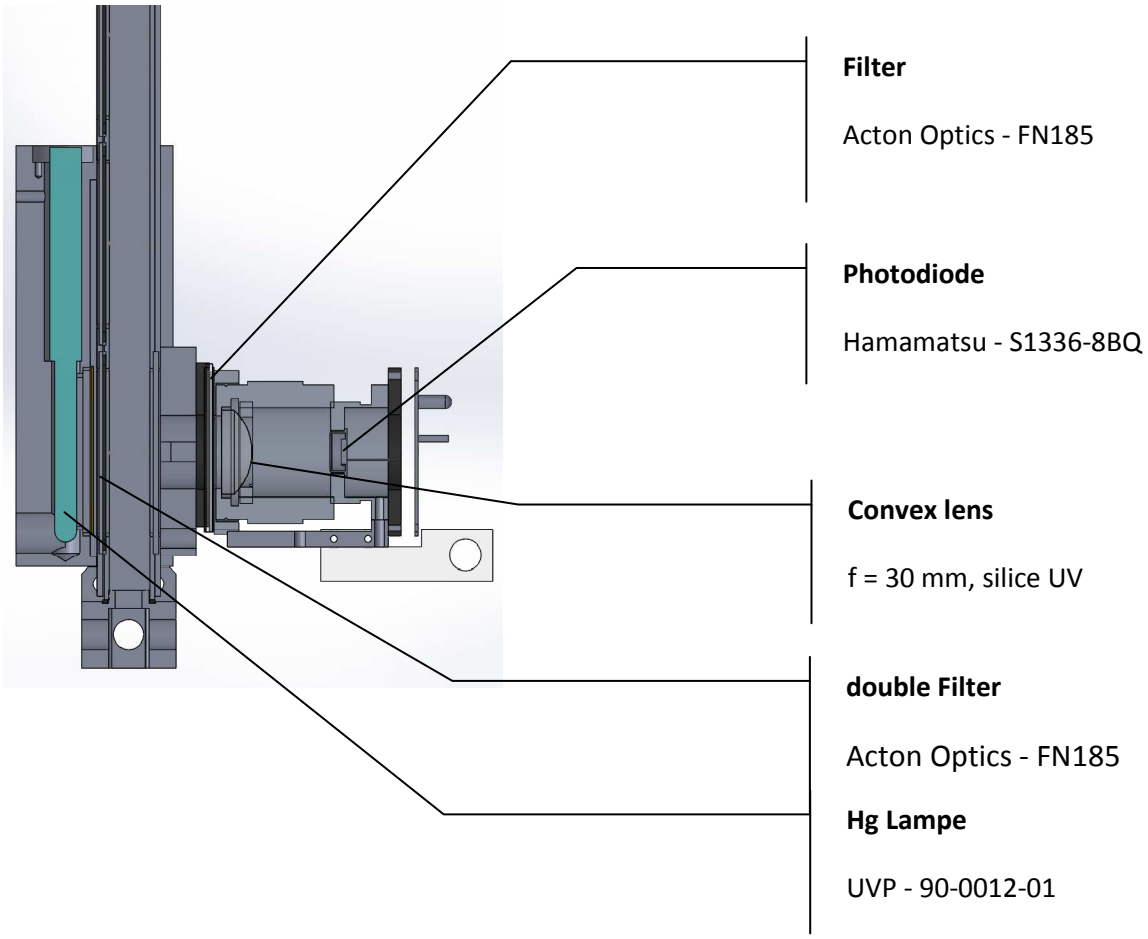

Figure II- 18: Zoomed scheme of the newly developed system (the photodiode adjusted to the calibration cell in front of the first window)

The photodiode housing consists in 3 elements as shown inFigure II- 18: an optical filter centered at λ = 185 nm in order to select the radiation of 185 nm from the lamp, a convex lens to focus the light coming from the lamp to the photodiode which is the third element. The produced ozone at low radical concentration (0.5 -1 ppb) is below the detection limit of a standard ozone analyzer. Thus, the ozone concentration is determined indirectly from the intensity of the mercury lamp radiation which is monitored by the photodiode.

As the photodiode does not provide an absolute value of the lamp flux, a calibration is necessary (Fuchs, 2006). The photodiode is calibrated relative to the ozone concentration for high fluxes. An aluminium mask was used between the window and the lamp to eliminate part of the radiation in order to decrease the flux reaching the photolysis region. The variac voltage was adjusted to 220 v during the photodiode calibration.

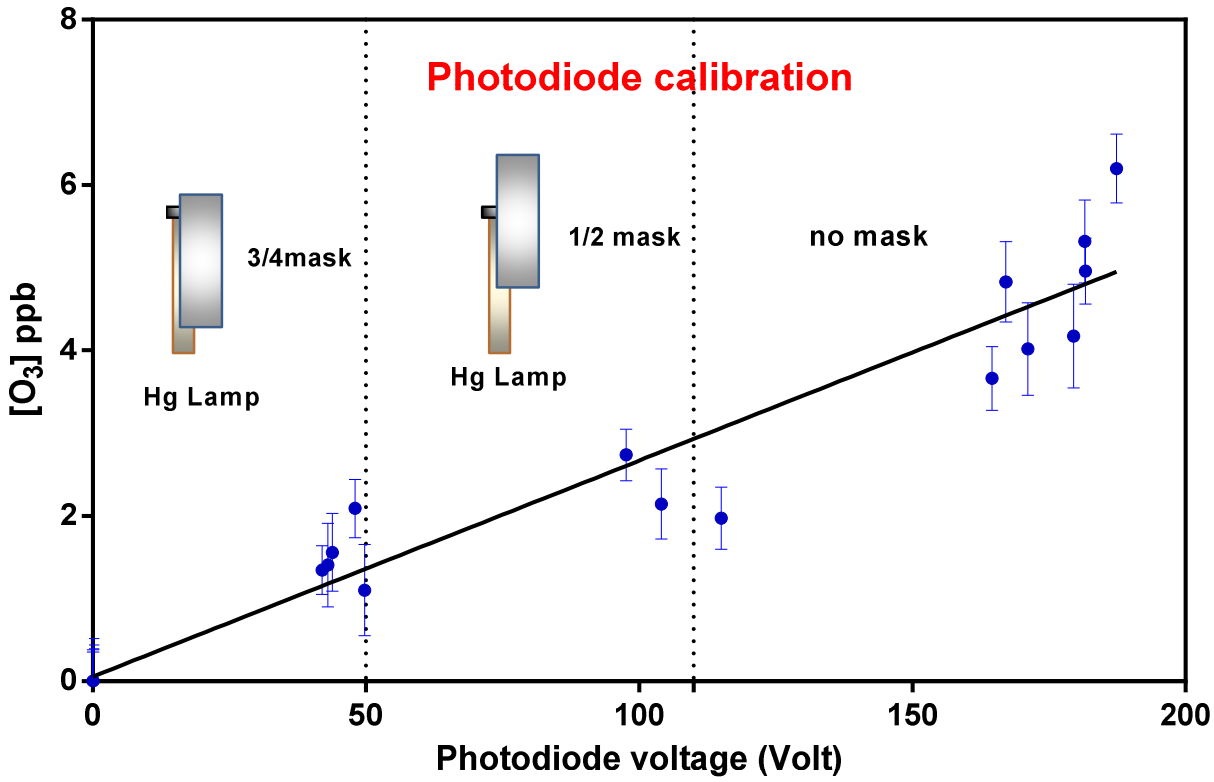

Figure II- 19: Relationship between the produced ozone in the calibration cell and the photodiode signal. The variac

A linear relationship between the ozone production and the photodiode signal is demonstrated by the calibration of the photodiode as a function of the ozone produced (Figure II- 19). Then the ozone concentration produced in the calibration cell can be calculated from the signal measured by the photodiode. The points in the middle range of the signal correspond to the use of the mask cutting half of the radiation. Due to the inaccuracy of putting the mask in front of the lamp to eliminate half of the flux, this zone is less accurate. Another calibration with the N_2O filter will allow providing a more accurate calibration of the photodiode.

II.3.4.3 Use of the calibration cell for the RO_2 generation

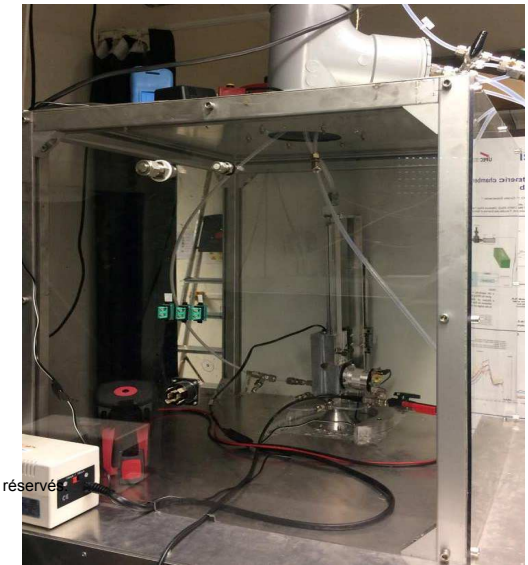

The calibration cell for the HO_x measurements can also be used for the RO_2 generation, needed to characterize the contribution of RO_2 to the HO_2 signal (see Chapter IV) adding VOCs in the mixture injected in the calibration cell. For that, a ventilation box has been built to allow

the extraction of the mixture containing VOCs that is not pumped by the FAGE (Figure II- 20).

Figure II- 20: The calibration cell version 2 inside aventilation box to extract the excess air.

II.4 OH reactivity configuration

The measurement of the reactivity of OH consists in measuring the lifetime of this radical, which varies according to the concentration of reactive species present in the atmosphere. This measurement can be done by FAGE when a photolysis cell, in which OH is artificially generated, is connected to it (Figure II- 21). In our case, OH radicals are generated at an initial time by a pulsed laser photolysis of ozone in the presence of water vapor and the temporal evolution of the concentration of OH is followed by its time-resolved measurement in FAGE cell (Sadanaga et al., 2004b). With our excitation laser for the OH fluorescence, we reach a temporal resolution of 200 µs.

II.4.1 Experimental setup

After the instantaneous generation of OH by the photolysis laser, the decay of OH can be expressed by the following equation:

$$r = -d[OH]/dt = k_{obs}\,[OH] = (\sum_i k_i \times [\text{reactive species}]_i + k_{zero}) \times [OH] \qquad \text{Eq II- 14}$$

where k_{zero} represents the losses of the OH radicals by diffusion or by heterogeneous reactions on the walls in absence of reactive species, i.e. in clean air (zero air). Depending on the quality of the zero air used, the k_{zero} can be influenced by the reaction with impurities (up to about 2-3 s^{-1}).

The integration of the Eq II- 14 leads to:

$$[OH] = [OH]_0 \times e^{-k_{obs} \times t} \qquad \text{Eq II- 15}$$

with $[OH]_0$ being the concentration of OH generated at time t_0 by laser photolysis and assuming that no other generation of OH than the instantaneous one, linked to the photolysis of ozone is present. The time resolved detection of OH in the FAGE cell is used to obtain k_{obs} by performing an exponential fit of the decay over an appropriate time range (Figure II- 21).

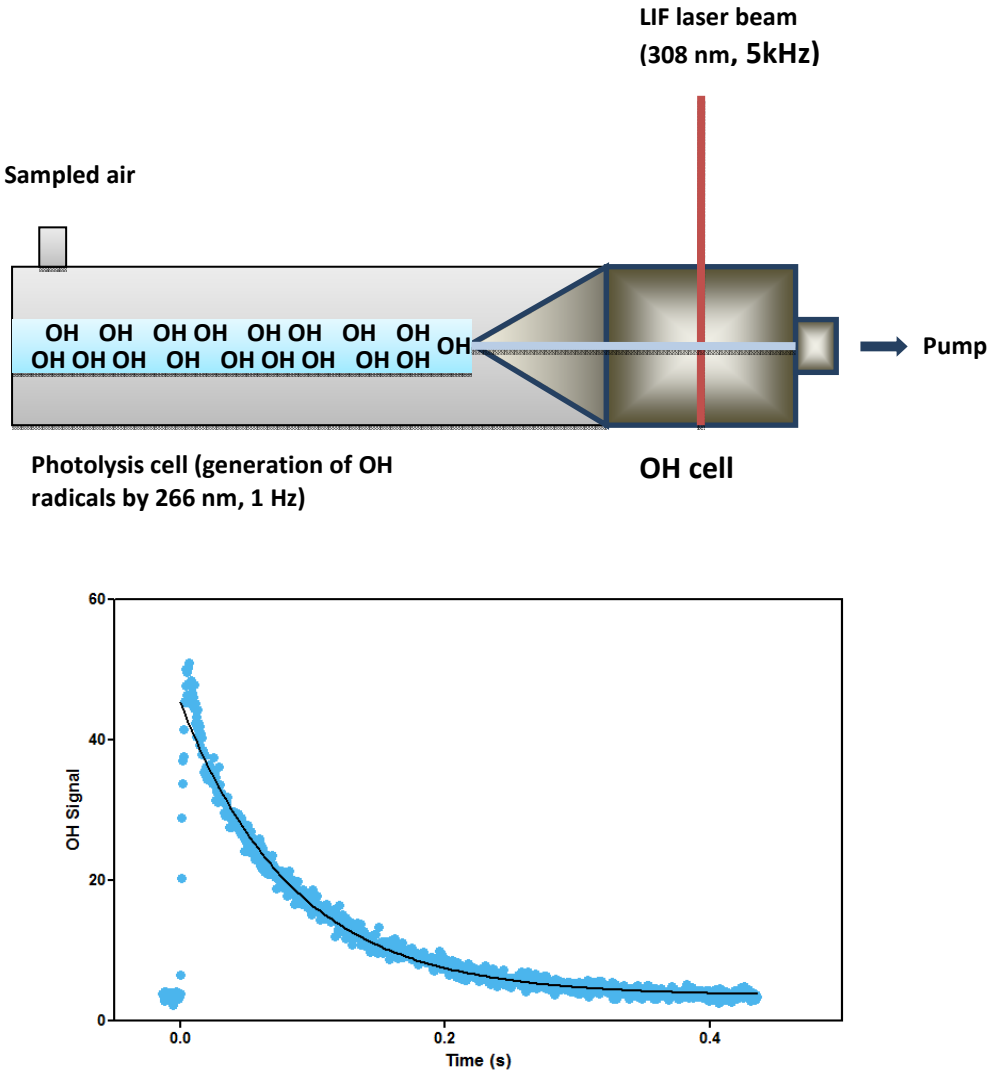

Figure II- 21: Representative diagram of the production of OH radicals in the photolysis cell and detection of OH in the FAGE cell and typical OH decay obtained.

The reactivity instrument thus comprises three parts: the photolysis laser, the photolysis cell and its OH generation system and the FAGE cell. A LabView program for recording and analyzing the decays is used to obtain in real time the OH reactivity.

II.4.2 The photolysis laser

The photolysis laser is used to generate OH radicals within the photolysis cell by the photolysis of O_3 in presence of water vapor. The photolysis laser is a YAG laser (Brilliant EaZy, QUANTEL, 1064nm) with a doubling and a quadrupling stage providing a radiation at 266nm (maximum energy per pulse: 45mJ, pulse duration 4ns, vertical polarization, Figure II- 22).

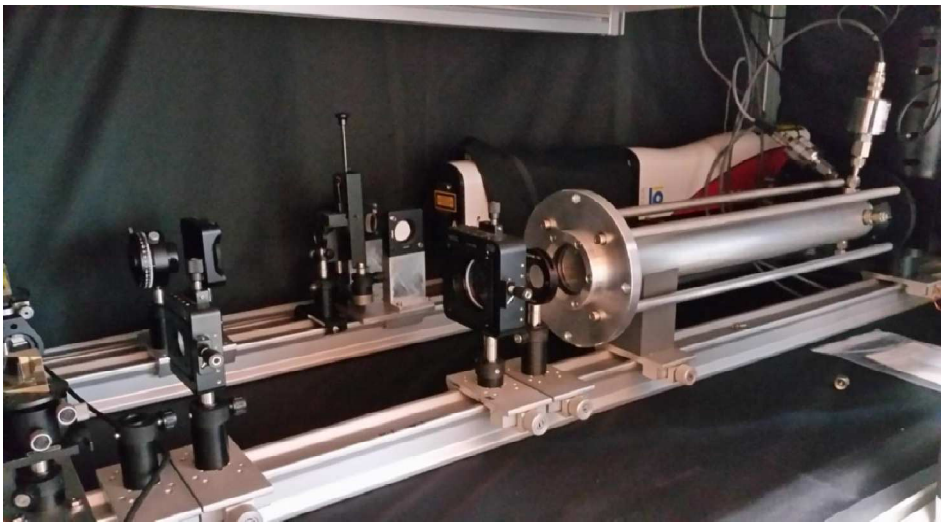

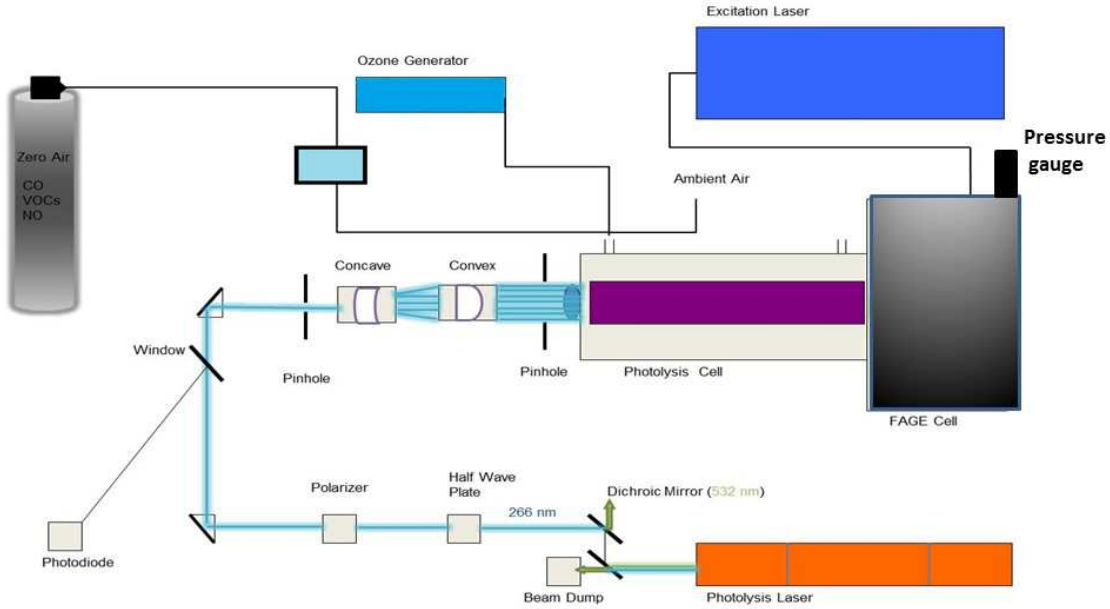

Figure II- 22: Picture and Diagram of optical assembly of the FAGE in reactivity mode

The short pulse duration justifies the instantaneous character of the production of OH radicals by O_3 photolysis. The reaction is very fast because the rate constant of $O(^1D) + H_2O$ reaction is 2.19×10^{-10} $cm^3\ molecule^{-1}\ s^{-1}$(Atkinson et al., 1997) and the water concentration is high which also confirms the instantaneous characteristic of this production . The laser is typically used with a repetition rate of 1 Hz but can be changed when needed (0.5, 2, 3 Hz, etc).

At the output of this laser, a residual 532 nm radiation is present. Consequently, two dichroic mirrors are used to send only the 266 nm radiation to the photolysis cell. Before the cell, the laser beam passes through a half wave plate (CVI Melles Griot) to rotate the laser polarization and a Glan polarizer which transmits only the vertically polarized light, in order to modify if needed the laser

energy without modifying the shape properties of the laser beam. A quartz window allows sending a small part of the beam to a photodiode (Hamamatsu S1722) to follow the stability of the laser power.

The beam is aligned at the center of the photolysis cell by two prisms and is expanded by two lenses (a concave one f=-25mm and a convex with f=150mm) in order to increase the photolysis volume and to limit the diffusion effect in the photolysis cell (Figure II- 22). The result is a laser beam with diameter of 4 cm reaching the entrance of the cell.

II.4.3 Photolysis cell and gas distribution

The cell is a stainless steel cylinder with an internal diameter of 5 cm and a length of 48 cm. It has on the opposite sides two openings, one as an entrance for the air samples and the second opening is connected to a pressure monitor (Keller PAA-41) to check the pressure inside the cell. Ambient or known gaseous mixtures of zero dry and humid air (which is produced by passing a fraction of the dry zero air through a water bubbler) are added through the first opening with a small flow of zero air (about 20 sccm) passing through an ozone generator (Scientech) to get an ozone concentration in the mixture of about 50 ppb in the total flow.

The concentration is chosen to produce enough OH to have a good signal/noise ratio, but kept low to minimize the possibility for reactions involving O_3 to occur. The introduced flow is around 8.2 L/min to maintain an atmospheric pressure in the cell. These gas flows are controlled by a set of Mass Flow Controllers (MFC, Bronkhorst F-201 and brooks 5800s) represented in Figure II- 23.

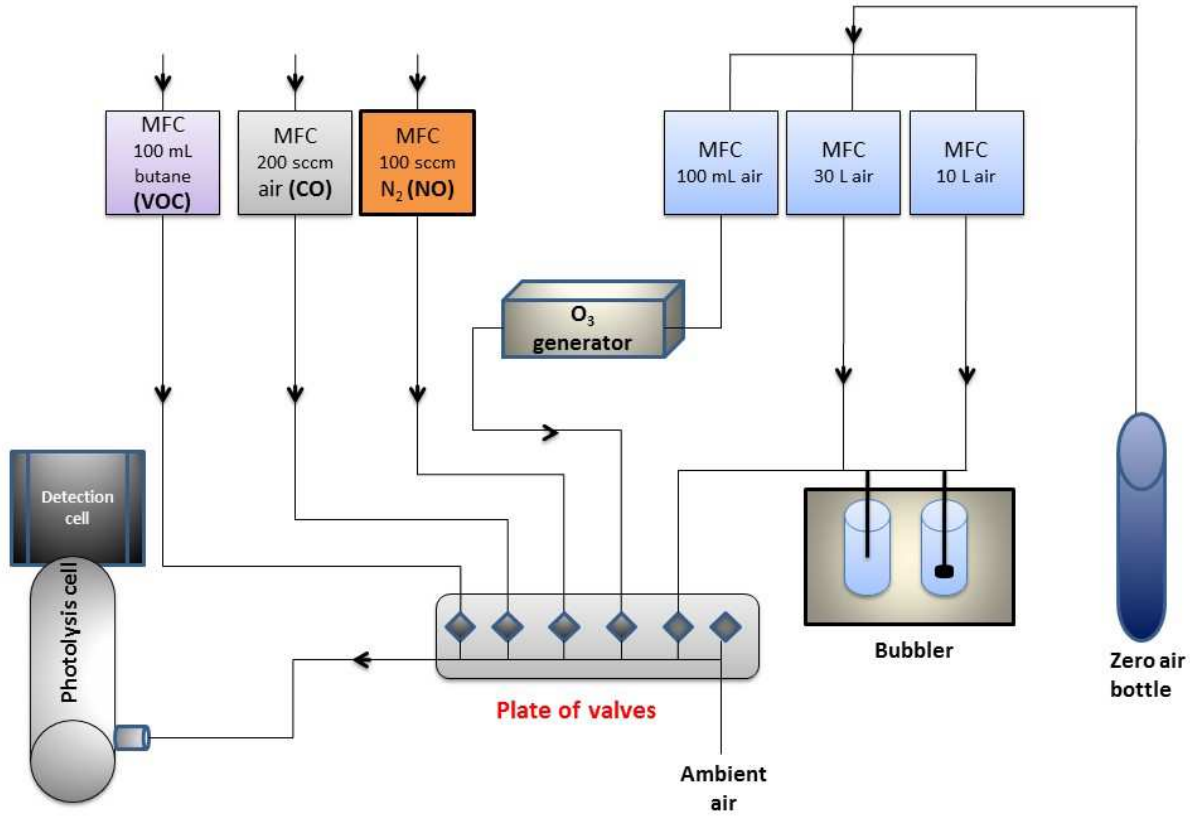

Figure II- 23: **Drawing of the gas flow distribution in the reaction cell, diamonds represents the 2-way valves.**

II.4.4 Decay analysis and validation of the reactivity measurement

The mixture to be analyzed is continuously pumped into the FAGE cell and the LIF signal of the OH radical is collected by a detection system, both similar to the ones used for the quantification, described previously (paragraph II.2.3). In order to obtain the evolution of the concentration of the radicals over time, the detection of the fluorescence is synchronized with the pulse of the photolysis laser by means of delay generators and a LabView program.

The fluorescence signals, having the same delay with respect to the laser pulse, are added for several pulses of the photolysis laser to increase the signal / noise ratio. The number of pulses is set by a selection criterion such as Signal/ noise ratio > 4 in general.Examples of decays measured without and with different concentrations of CO are shown in Figure II- 24.

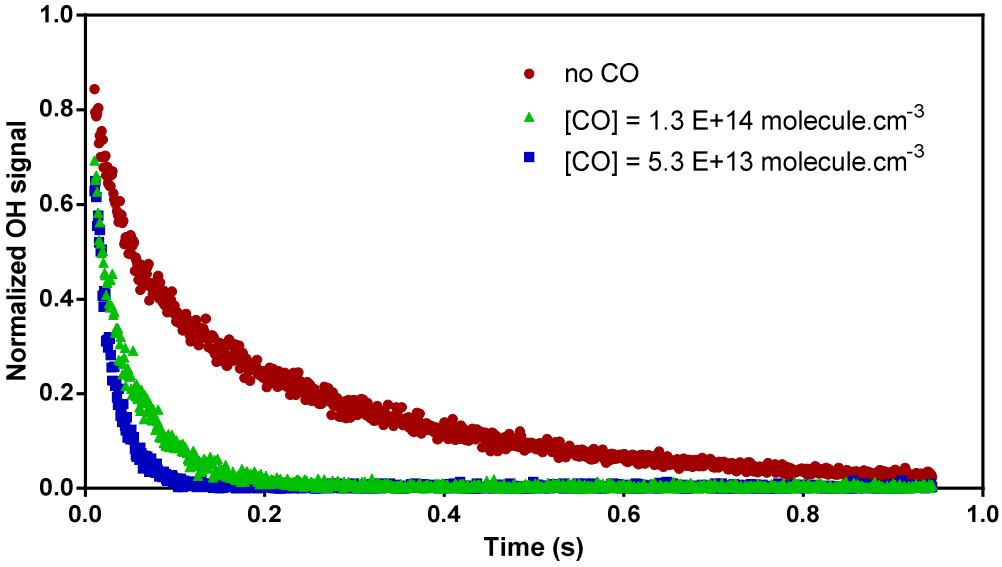

Figure II- 24: OH decays with different CO concentrations

For validating the reactivity setup, this set of data with known concentration of CO in the photolysis cell can be used to measure the rate constant of CO + OH and to compare it with the recommendations.

$$r = -d[OH]/dt = (k_{CO+OH} \times [CO] + k_{zero}) \times [OH] \quad \text{Eq II- 16}$$

For which $$d[OH]/dt = (k' + k_{zero}) \times [OH] = k_{obs} \times [OH] \quad \text{with } [OH] << [CO] \quad \text{Eq II- 17}$$

with $$k' = (k_{CO+OH} \times [CO]) \quad \text{Eq II- 18}$$

The rate constant k_{CO+OH} is determined by plotting k_{obs} for different CO concentrations injected in the system, the slope of the linear regression gives the k_{CO+OH} rate constant, and the intercept is k_{zero}.

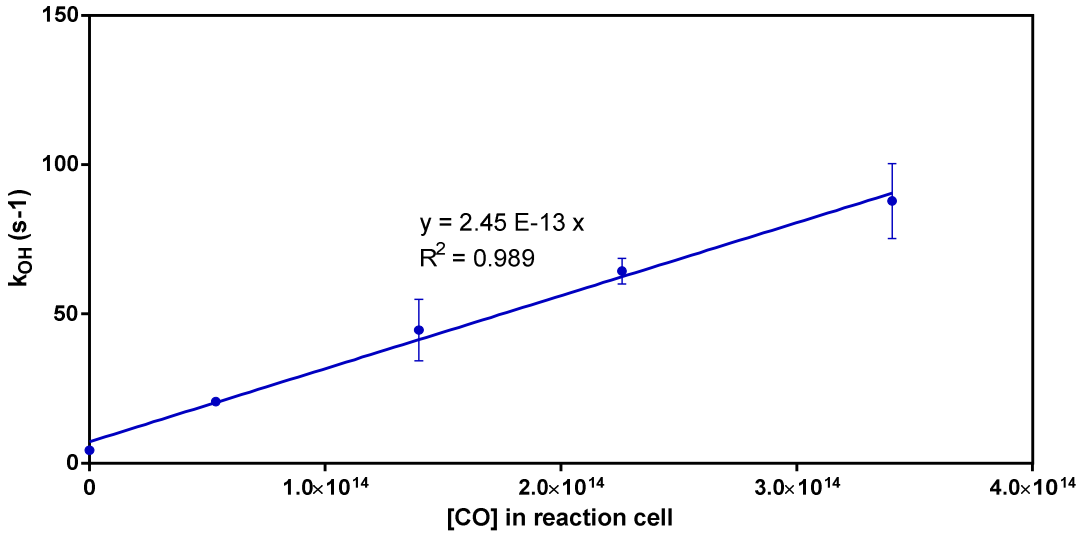

Figure II- 25: Determination of the rate constant of OH + CO reaction by FAGE reactivity system.

This method can be applied for different compounds according to the method described above under atmospheric pressure. The FAGE-reactivity can work for reactivities up to 150 s^{-1} while the decays become too fast at higher chemical reactivities. Dilution can then be used if needed to measure higher reactivities.

II.4.5 Uses of the reactivity configuration during the thesis

As the effect of the beam alignment on the shape of the decay has been highlighted during the intercomparison in the SAPHIR chamber, tests have been performed to optimize and better characterize the effect of this alignment. It has been found that a divergent beam is better suited to get a monoexponential decay.

The instrument in the reactivity configuration has been used for kinetic analysis of RO_2 + OH reactions (see Chapter III) and deployed during the LANDEX campaign (see chapter VI).

II.5 Conclusion

FAGE is the most widely-used technique for detection of OH and HO_2 in the field, having good sensitivity, good spatial and temporal resolution, and sufficiently low detection limits to enable quantification of HO_x radicals. The UL-FAGE allows this quantification as well as the measurement of OH reactivity when coupled to a photolysis cell. During my thesis, the instrument has been better characterized. UL-FAGE has been successfully calibrated for different RO_2 radicals coming from the reaction of OH with methane, butane, isoprene and toluene hydrocarbons.

The calibration cell has been characterised for different parameters (water vapor, wall losses). IN addition, technical changes have been performed to be able to generate lower OH levels even when working at higher humidity levels and to determine the lamp flux without the use of ozone analyzer.

In the following chapters, the results obtained using the FAGE instrument in both configurations (quantification, reactivity) are presented and interpreted in order to fulfill the scientific objective presented in Chapter I.

Chapter III: Kinetic analysis of the role of ROOOH as interference for OH quantification by FAGE

III.1 State of the art concerning OH interferences in FAGE instruments

FAGE instruments have been developed by several groups around the world ((Amédro, 2012b; Brune et al., 1995; Dusanter et al., 2008; Fuchs et al., 2011; Heard and Pilling, 2003)) and deployed in the field (Brune et al., 1995; Creasey et al., 1997; Holland et al., 2003). These FAGE instruments have a high sensitivity but different types of interference were identified. These interferences can be due to photolysis of suitable precursors by the fluorescence excitation laser (chemical interference) or the presence of fluorescing species other than OH (spectral interference). Concerning the first source, extensive interference tests were done in the laboratory (Ren et al., 2004) for different chemical species such as acetone, ozone, nitrous acid, nitric acid, hydrogen peroxide, and formaldehyde (see chapter 1). Except ozone, none of the chemical species tested were affecting the OH measurement under ambient conditions. In addition, this source of interference canbe identified by varying the excitation laser energy: “real” OH only needs one photon to fluoresce, while other species need two (one for generating OH radicals by photolysis, another for their excitation).The second source of interference can be identified by regularly measuring the fluorescence signal with the excitation laser wavelengths slightly tuned off the OH line. This procedure is always adopted during measurements as it enables to account for stray light reaching the detector from the excitation laser or the sun.

Concentrations of OH radicals have been measured for several decades, and comparison of OH concentration profiles with model outputs is taken as a good indicator on the degree of understanding of the chemistry going on.Good agreement is often obtained between measurements and models for environments where levels of nitrogen oxides (NO_x=NO+NO_2) are in excess of 500 pmol/mol, or ppt, however remote and clean environments show much less good agreement(Stone et al., 2012). Several field campaigns in remote environments, dominated by natural biogenic emissions, have been carried out during the last decade(Hofzumahaus et al., 2009; Lelieveld et al., 2008; Whalley et al., 2011), and a very poor agreement has been found, with measured OH concentrations exceeding model predictions by up to a factor of 10.These findings have been interpreted to reflect a lack in our understanding of the oxidation mechanism of biogenic VOCs under low NO_x conditions and have triggered a large number of studies aiming at improving the atmospheric oxidation mechanism of biogenic VOCs(Crounse et al., 2011; Paulot et al., 2009; Peeters et al., 2009). Improvements have been made especially in the oxidation mechanism of isoprene(Wennberg et al., 2018), and new reaction pathways leading to OH recycling have been found. However, none of these new chemical pathways has led to a sufficiently significant increase in modeled OH concentration to bring models into reasonable agreement with measurements(Rohrer et al., 2014). Therefore, the new improved isoprene oxidation mechanism has not been able to

explain the discrepancies between the measured and the modeled OH measurement. Therefore this difference was reported to be a significant interference to the OH radical measurements (Mao et al., 2012).Testsin real environments have been done to identify if this interference could be due to photolysis processes. Even if more difficult to make than in laboratory due to low OH concentrations (and the resulting low S/N ratio) and high temporal variability of OH radical concentration, energy tests during field campaigns seem to show that the high OH concentrations observed, compared to expected concentrations from models,are not from the photolysis of other species(Mao et al., 2012; Novelli et al., 2017).

An alternative explanation for the unexpectedly high OH concentrations measured in biogenic, low NO environments is that the measurements suffer from an unidentified interference which could be related to the decomposition of labile species during the gas expansion into the FAGE cell. Following the large disagreements between measurements and models, the group of W. Brune has conceived a method to quantify such possible interferences(Mao et al., 2012): a device is installed just above the inlet into the FAGE cell, which injects regularly into the airflow a high concentration of a species rapidly reacting with OH radicals. This way all ambient OH radicals are scavenged before entering the FAGE cell, and any remaining signal can be identified as interference.The difference between the signal with and without the scavenger allows the quantification of the real ambient OH.This technique was used for the first time in 2012 in a forest in California(Mao et al., 2012) and led to the identification of a large fluorescence signal following scavenging of all ambient OH radicals. Two methods for determining the background signal were used during the measurement campaign. The first, labelled OH_{wave}, was the traditional method of modulating the laser wavelength to an 'online' and 'offline' position. The second, labelled OH_{chem} (chemical modulation), was by the addition of high-purity gaseous hexafluoropropene (C_3F_6) prior to the detection cell, to scavenge ambient OH and provide a background measurement as shown in Figure III- 1.

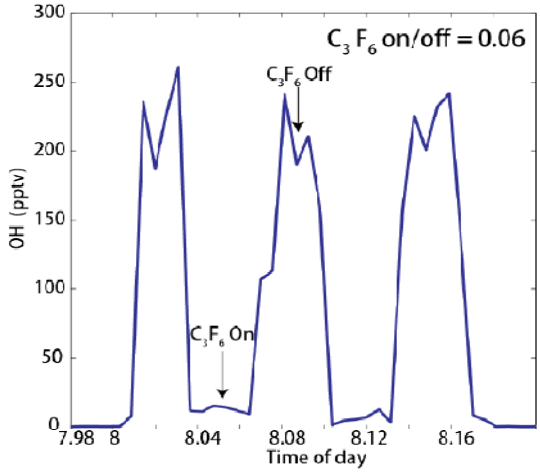

Figure III- 1:Example of OH measurement with external mercury lamp producing OH and periodic C_3F_6 addition. The large OH value is when C_3F_6 is not added and the small value occurs when it is (Mao et al., 2012).

In this campaign, significant differences between OH_{wave} and OH_{chem} were observed, with OH_{chem} signal (representing the real OH) lower than OH_{wave} signal (measured OH). The agreement between modelled OH and $[OH]_{chem}$ was much better than between modelled OH and $[OH]_{wave}$ which exceeded modeled concentrations by up to a factor of 3 (Figure III- 2).

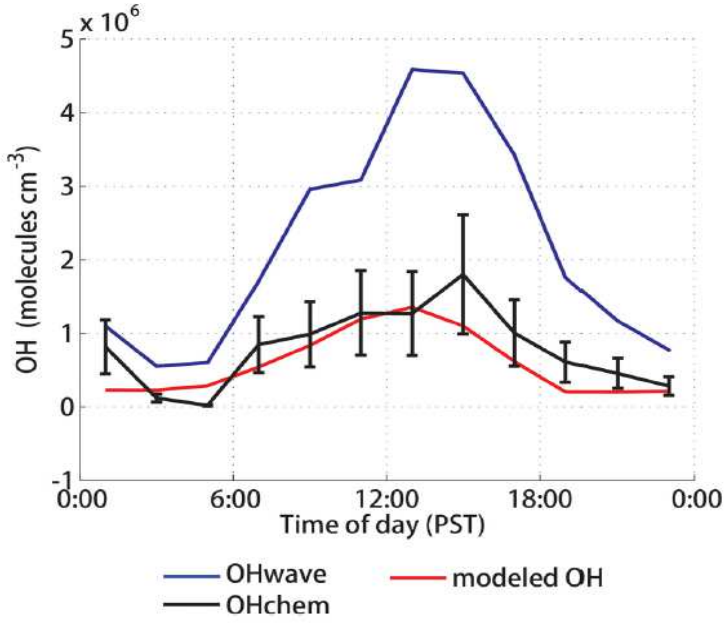

Figure III- 2: Diurnal cycle of measured and modeled OH during California forest. OH_{wave} (blue line) represents the measured OH without using scavenger, OH_{chem} (black line) represents the signal difference with and without the addition of C_3F_6, and modeled OH (red line) is the modeled concentration using photochemical box model(Mao et al., 2012).

It is not known if this interference is common between all LIF-FAGE instruments, and it is more probable that the interference is instrument-specific. Then UL-FAGE was tested for this interference by applying chemical modulation method to the system. This method was used in LANDEX campaign for 2 days where a strong interference was clearly seen (Chapter VI).Two other groups have also developed a pre-injector system in the following years(Griffith et al., 2016; Novelli et al., 2014b).Using this system, Novelli *et al*.(Novelli et al., 2014b) have observed strong interferences in their FAGE system during three field campaigns in remote biogenic environments in Germany, Finland and Spain, while Griffith *et al*.(Griffith et al., 2016) were able to account for the observations through known interferences by O_3 photolysis. Novelli *et al*. proposed that ozonolysis of alkenes, leading to the formation of Criegee intermediates, and the subsequent decomposition of these Criegee intermediates within the FAGE cell, was responsible for the interference(Novelli et al., 2017), while Rickly and Stevens (Rickly and Stevens, 2018) and Fuchs *et al*.(Fuchs et al., 2016) could not confirm this source: even though they detected internally formed OH when mixing O_3 and alkenes in the laboratory, when they extrapolated their results to ambient conditions they found that the

possible interference generated this way would be well below the detection limit of the FAGE. Chamber studies were carried out at the SAPHIR chamber in Jülich(Fuchs et al., 2012), simulating remote forest conditions (*i.e.*, high biogenic VOC and low NO concentrations). OH concentrations were measured simultaneously by FAGE and by absolute DOAS absorption. No sizeable interference was detected in these experiments, even though the same group had previously observed unexpected high OH concentrations in the Pearl River delta in China(Hofzumahaus et al., 2009; Rohrer et al., 2014), exceeding modeled concentrations by up to a factor of 8.

Recent work from W. Brune's group (Feiner et al., 2016a) reported the main trends of the interference as a function of environmental conditions. The Penn state FAGE instrument was deployed for OH and HO_2 measurement during summer 2013 in Alabama forest in USA. The resulting $[OH]_{int}$ (OH interference signal: $[OH]_{chem}$-$[OH]_{wave}$) was up to 3 times higher than the $[OH]_{chem}$ (ambient OH), and there was on average a good agreement between modelled OH using two different models (MCMv3.2, and MCMv3.31) and $[OH]_{chem}$ (Figure III-3). similarly to the first campaign with the preinjector made by this group (Mao et al., 2012). The 2 models correspond to the Master Chemical Mechanism for 2 different versions, MCMv3.2 augmented with explicit isoprene. MCMv3.31 is the updated version of MCMv3.2 that contains an isoprene mechanism and did not need to be augmented. The difference between these 2 isoprene mechanisms appears to be mainly in the isoprene RO_2 isomerization pathways and products, which results in more OH regeneration in MCMv3.31 than in the augmented MCMv3.2 version (Feiner et al., 2016a).

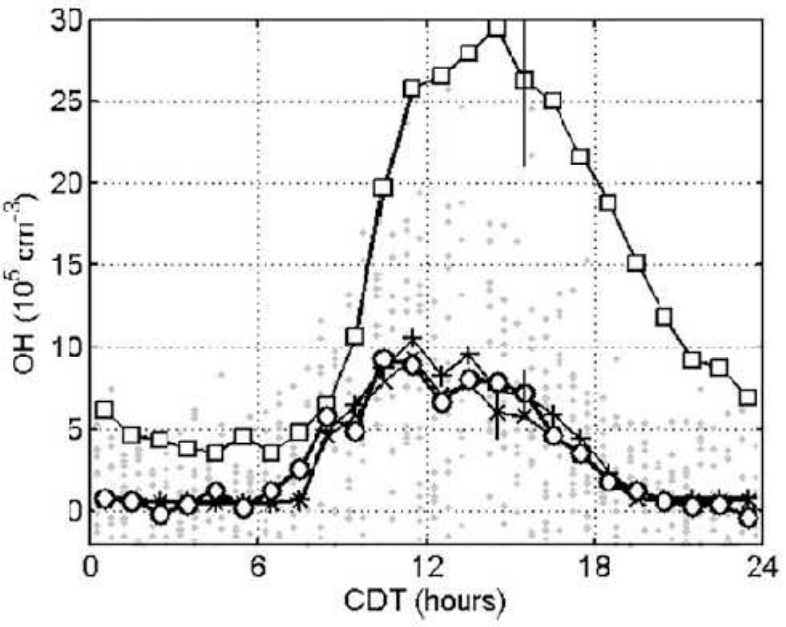

Figure III- 3: Diel variations of OH_{chem} (O), OH_{int} (□), MCMv3.2 OH (×), and MCMv3.31 (+) for 26 Jun-14 Jul. Gray dots are 10 mins measurements. OH is given in units of 10^5 cm^{-3}(Feiner et al., 2016a).

H_{chem}, OH_{int}, and the modeled OH were plotted as a function of O_3, J ($O(^1D)$), NO, and isoprene measured during the campaign to analyse the evolution of the interference signal as function these different parameters (Figure III- 4).

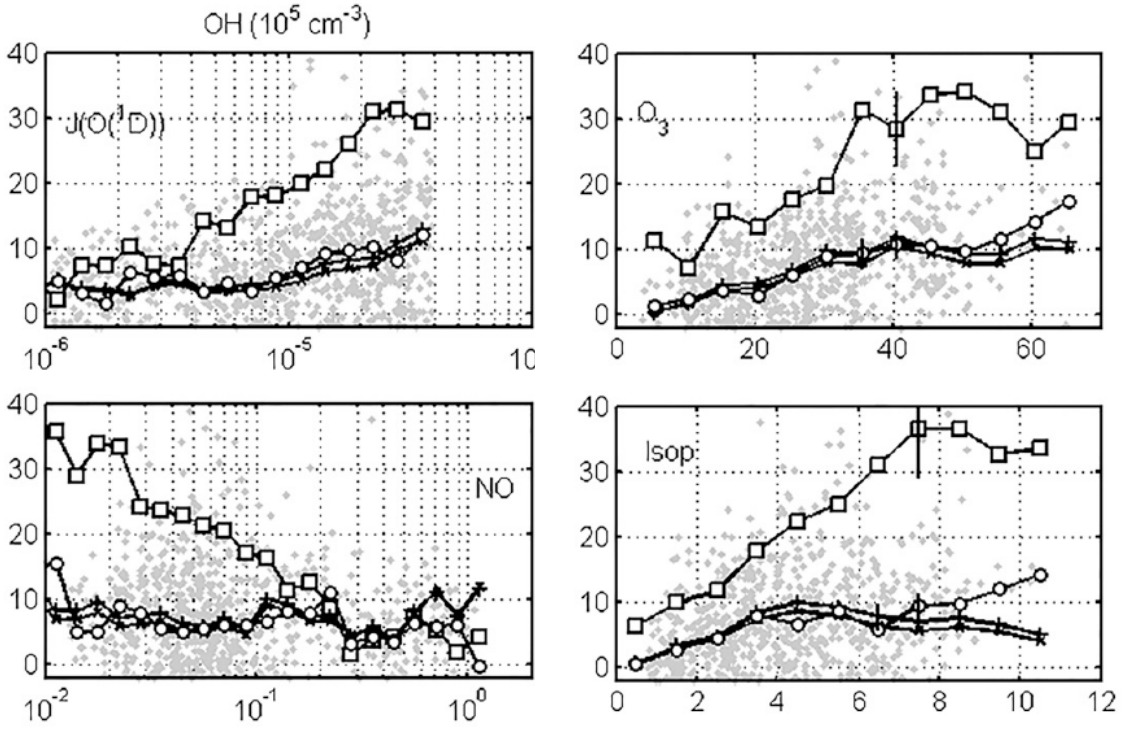

Figure III- 4: OH (10^5 cm^{-3}) as function of JO(^{1}D)(s^{-1}), NO (ppbv), O_3 (ppbv), and isoprene (ppbv). Median OH from measurement (o), augmented MCMv3.2 (×),and MCMv3.3.1(+) and from the interference (□)(Feiner et al., 2016a).

The results showed that OHchem has the same behavior as OH calculated by the models as function of J ($O(^1D)$), NO, and O3 (Figure III- 4). In the case of isoprene, the behavior of measured and modeled OH agreed for concentrations up to 7 ppbv, but as isoprene concentration increases, OHchem split up about twice the modeled OH.

Concerning the interference, it has been shown that it decreases strongly withincreasing NO concentration, and with decreasing J (O^1D), ozone and isoprene concentration. From these observations, they concluded that the interference observed in their FAGE system (a) was due to a rather long-lived species because the interference persists into the evening, (b) it had been observed in different environments dominated by MBO, terpenes or isoprene, hence it must originate from a class of species rather than from only one species such as isoprene, (c) it must somehow be linked to photochemistry and (d) the species responsible for this interference was linked to a low NOx oxidation pathway. Based on these conclusions and previous kinetic studies on RO_2 reactions with OH in our laboratory, products of such type of reaction have been postulated by our group as a good

class of species to explain the interference.It is why laboratory experiments were done with the UL-FAGE in its reactivity configuration (Chapter II) in order to confirm this hypothesis.

We present in this chapter convincing experimental and modelling evidence that this sought-after species is the product of the reaction between RO_2 radicals and OH radicals. Recently, this reaction was explored by modelling and experimentally.It has been shown that this reaction is fast (Assaf et al.,30 2017b;Assaf et al., 2016) and could be competitive to other sinks for RO_2 radicals (Fittschen et al., 2014; Archibald et al.,2009), *i.e.* it becomes increasingly important with decreasing NO concentration. Indeed, in presence of high NO_X (= NO + NO_2) concentrations, RO_2 will rapidly react with NO to form NO_2 and alkoxy radicals RO whereas decreasing NO will be in favor of radical-radical reactions. Ab-initio calculations (Assaf et al., 2018a; Liu et al., 2017; Müller et al., 2016) have shown that the initial reaction product of RO_2+OH is a trioxide (R III- 3), ROOOH, obtained from the recombination of RO_2 and OH. The formation of this adduct is exothermic by around 120 kJ mol^{-1} compared to the initial reaction partners and by around 110 kJ mol^{-1} compared to the major decomposition products (R III- 1), largely independent of the size of the alkyl moiety of the RO_2. Ab initio calculations studies predict the pathway (R III- 2) to be minor reaction for CH_3O_2 and $C_2H_5O_2$.

$$RO_2 + OH \rightarrow ROOOH^* \rightarrow RO\text{-}HO_2 \rightarrow RO + HO_2 \quad \text{R III- 1}$$

$$\rightarrow ROH\text{-}HO_2 \rightarrow ROH + O_2 \quad \text{R III- 2}$$

$$\rightarrow ROOOH \text{ thermalized} \quad \text{R III- 3}$$

For the smallest RO_2 radical, CH_3O_2, stabilization of CH_3OOOH is not the major fate of the initial adduct (Assaf et al., 2017a; Müller et al., 2016) and the major products are CH_3O + HO_2. The HO_2 yield, measured for alkyl peroxy C1-C4, has been found to decrease with increasing size of the alkyl group and it is expected that, already for C_4 peroxy radicals, the stabilization of the initially formed ROOOH is the major product (Table III- 1). The collisional stabilization of the ROOOH of C_3H_7 and C_4H_9 alkyl groups increases in importance compared to CH_3 and C_2H_5. For alkyl-groups larger than C_4H_9, it is expected that the yield of HO_2 becomes very minor (Assaf, 2017). For RO_2 radicals obtained from an initial attack of OH radicals on biogenic VOCs, it can thus be expected that the major reaction product will also be the corresponding trioxides.

Table III- 1: product yields of the RO_2 + OH reactions at 298 K as function of the alkyl group R (Assaf, 2017)

Alkyl group R	Redissociation to $RO_2 + OH$	Fragmentation to $RO + HO_2$	Stabilisation of ROOOH
CH_3	1.2%	91%	8%
C_2H_5	0.5%	11%	89%
n-C_3H_7	0.08%	1.5%	98%
n-C_4H_9	0.01%	0.3%	99.7%

III.2 Experimental setup

To test the hypothesis on the role of ROOOH on the OH interference in the FAGE, we used controlled conditions to produce high concentration of ROOOH and to measure their potential contribution on the FAGE signal. For that, the FAGE has been used with the photolysis cell dedicated to the OH reactivity measurement in order to generate RO_2 and to favor the reaction of RO_2 with OH. To calibrate the signal measured, the calibration cell used for the quantification has been used in front of the FAGE cell in absence of the photolysis cell.

III.2.1 Pump and Probe FAGE (or LP-LIF)

During this work, the UL-FAGE instrument in the reactivity configuration was used. Details of the UL-FAGE pump and probe system have been described in details elsewhere (Chapter II). Briefly, the FAGE instrument is coupled to a photolysis cell, in which a plume of OH is generated by 266 nm photolysis of ozone in presence of water vapor. The pressure in the photolysis cell is around 745 Torr, and pumping from the FAGE cell (3 L min^{-1}, using a smaller pinhole than in the ambient reactivity configuration to increase the residence time)which operates at low pressure (0.3mbar), the O_3 analyzer (0.3 L min^{-1}) and the hygrometer (0.4 L min^{-1}) ensures that the photolysis cell is continuously flushed with gas mixture. The residence time within the photolysis cell is around 20 sec, i.e. at a photolysis repetition rate of 2 Hz, the gas mixture is photolysed around 40 times before it enters the FAGE detection cell. Experiments have been carried out by first covering the photolysis laser in order to start each series with a fresh mixture. An ozone mixing ratio of at least 600 ppbv is maintained inside the photolysis cell by injecting a small flow of 20 cm^3 min^{-1} (negligible compared to the main flow through the reactor) of concentrated ozone using an ozone generator. The water vapor mixing ratio of about 12000 ppmv is injected in the cell by passing a part of the air through a bubbler.

The energy of the photolysis laser was set to 20 mJ $pulse^{-1}$ for a beam diameter of 2.5 cm, which was achieved after expansion through a telescope. This expansion of the beam allows the generation of

OH in a cylindrical volume that is larger than the FAGE nozzle (0.4 mm) in order to probe a more homogeneous volume with respect to the OH concentration, even if the shape of the beam involves a Gaussian distribution. The pulse duration of the photolysis laser is 20 ns (full-width half maximum).

The air from the photolysis cell is pumped through the FAGE nozzle into a FAGE cell where OH is measured by LIF (Laser Induced Fluorescence).The excitation laser operates at 5 kHz, and hence the OH profiles are obtained with a time resolution of 200 µs. The laser power used to probe OH was approximately 2 mW. Hydrocarbons are added to the photolysis cell through calibrated flow meter, either directly from the gas cylinder (CH_4 and n-C_4H_{10} for a few series) or from a canister in which a diluted gas mixture of n-C_4H_{10} or isoprene had been prepared manometrically.

III.2.2 LIF Calibration procedure

In order to access the absolute concentrations of OH radicals, calibrations are made using a calibration cell. For calibration purposes, the photolysis cell is unmounted and the calibration cell is placed in front of the FAGE nozzle. Very high flow of synthetic air (40 l min^{-1}) is flown through the calibrator to assure (a) turbulent flow conditions within the calibration cell and (b) that the entire gas intake by the FAGE consists of calibration gaz. Details on FAGE calibration procedure can be found elsewhere (Chapter II).

III.2.3 Experimental conditions

With the goal of forming sizeable amounts of trioxide (ROOOH), experiments have been carried out in the UL pump-probe FAGE instrumentwhere a gas mixture containing isoprene (or C_4H_{10} or CH_4, see Figure III- 12andFigure III- 13respectively) and O_3/H_2O is photolysed as described above.Experiments start with a fresh mixture (*i.e.*, with the photolysis laser covered) and 40 decays are then registered every 0.5 s for 20 s. 1.4×10^{10} cm^{-3} OH radicals are produced at each pulse. After 40 photolysis pulses, the laser is covered again for 2 minutes to allow the mixture to completely refresh, and (in order to improve S/N ratio) a new series of measurements is started. After 20 series, the signals are averaged so that one OH decay profile is obtained for each sequential photolysis pulse. An example is shown in Figure III- 5 in the case of isoprene used as a RO_2 precursor, where, for clarity, only one every 10^{th} decay profile is plotted.

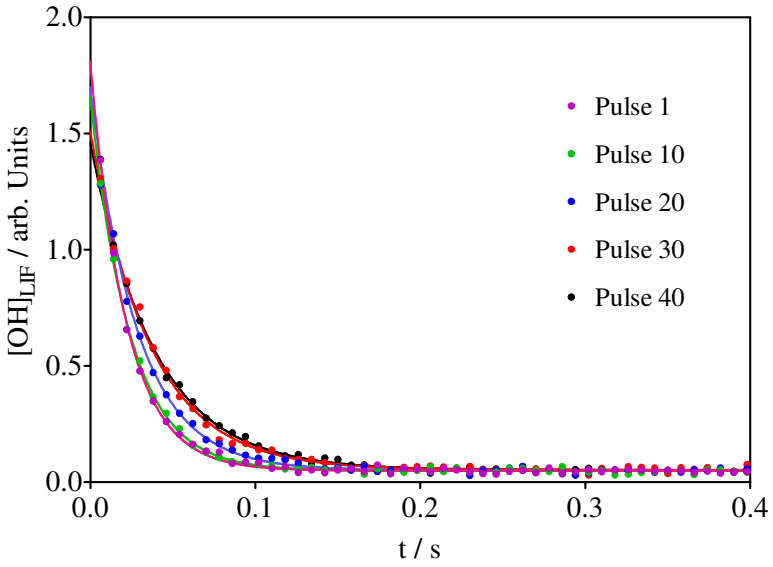

Figure III- 5: OH concentration time profiles following the photolysis of 600 ppb O_3 (leading to initial OH concentrations of around 1×10^{10} cm^{-3}) in the presence of 3×10^{11} cm^{-3} isoprene. For clarity, only every 10^{th} photolysis shot is shown. Time resolution was decreased from 200 µs to 8 ms for increased S/N ratio by averaging 40 data points.

III.3 Results and discussions

In order to quantify the role of ROOOH on the OH interference signal, different reactions of RO_2 with OH, with different expected ROOOH yield have been studied: from isoprene, butane and methane precursors. As isoprene was a major component of environments where interferences have been observed, the behavior of RO_2 from isoprene reacting with OH has been compared with those of methane and butane. Indeed, CH_3O_2+ OH is expected to have low ROOOH yield whereas $C_4H_9O_2$ is expected to have high ROOOH yield. Concentration profiles of the reactants and products have been modelled to determine an upper limit of ROOOH produced in the photolysis cell. Other tests have been done in order to verify if the interference observed was not due to a two-photon process. Finally, global modelling has been used to estimate the ROOOH concentration present in real environments.

III.3.1 Tests with isoprene

III.3.1.1 Modeling the chemistry in the photolysis cell

In order to determine the level of products in our conditions, a very simple model was run to get a rough estimate of the concentration of ROOOH that could be produced and accumulated within the photolysis cell in presence of isoprene at conditions favoring the reaction of RO_2 with OH. The model assumes a yield of 1 for the formation of ROOOH by OH+RO_2 and a rate constant for OH+ROOOH estimated equivalent to the one of OH+CH_3OOH:

Table III- 2: Model used to estimate the accumulation of ROOOH in the photolysis cell before entering the FAGE cell, all rate constants have been taken from the most recent IUPAC evaluations(Atkinson et al., 2005, 2006)

Reaction	k / cm^3 s^{-1}
OH + Isoprene → RO_2	1×10^{-10}
OH + RO_2 → ROOOH	1×10^{-10}
OH + ROOOH → products	$1 \times 10^{-11, a}$
OH + O_3 → HO_2 + O_2	7.3×10^{-14}
OH + HO_2 → H_2O + O_2	1×10^{-10}
RO_2 + RO_2 → products	1×10^{-12}
RO_2 + HO_2 → ROOH	1.7×10^{-11}

a.)estimated equivalent to the rate constant of OH+CH_3OOH (Atkinson et al., 2006)

This model was run 40 times for 0.5 s, with the final concentrations of the different species obtained at each run being used as initial concentrations in the following run, always adding 1.4×10^{10} cm^{-3} OH radicals to the mixture and the evolution of the different species is shown inFigure III- 6.

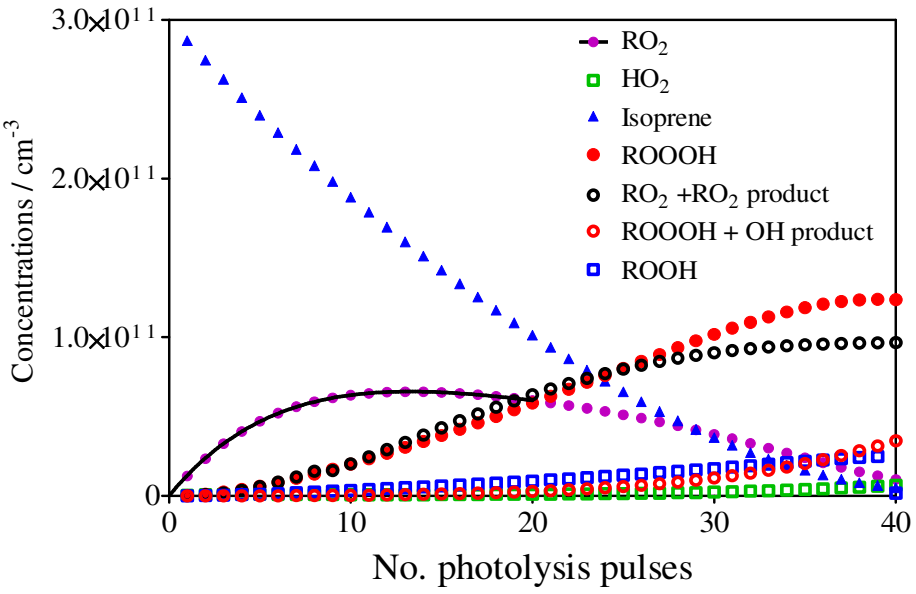

Figure III- 6: Evolution of different species in the photolysis cell as a function of the number of photolysis pulses. Full black line describes evolution of RO_2 by exponential rise (see section on CH_4 experiments)

The model has been run very basically: all OH radicals react with species present in the model, i.e. no wall loss or reaction with impurities is taken into account. The possible photolysis of ROOOH at 266 nm or a heterogeneous loss on the reactor walls are not considered. Also, no reaction of the products of RO_2 self-reaction with OH are considered. The possible inhomogeneity of the beam profile of our photolysis laser has not been considered, which can lead to uncertainties. All these

simplifications can lead to an overestimation of the final ROOOH concentration, possibly up to a factor of 10. With these assumptions the model predicts the consumption of most isoprene and the formation of around [ROOOH] ≈ 1×10^{11} cm^{-3}. The other major reaction path for the RO_2 radicals under these conditions is the self-reaction. The reaction of ROOOH with OH radicals has been estimated (in comparison with ROOH) to 1×10^{-11} cm^3s^{-1}, but only a small fraction of ROOOH will have reacted with OH after 40 photolysis pulses.

III.3.1.2 Experimental results in conditions favorable to the reaction of RO_2+OH

The initial isoprene concentration (3×10^{11} cm^{-3} inFigure III- 5) was chosen to make the reaction of RO_2 with OH compete efficiently with that of isoprene with OH after several photolysis pulses: with initial OH concentrations of around 1.4×10^{10} cm^{-3} (obtained from calibration in separate experiments), the isoprene concentration decreases with each photolysis shot, while the RO_2 radical concentration increases. It can thus be expected that, if formed, the concentration of ROOOH increases with every photolysis pulse, as shown by the model.

A mono-exponential decay was fitted to the OH profiles from Figure III- 5and the resulting pseudo-first order decay rates are shown as blue dots inFigure III- 7. It can be seen that the decay rate decreases with increasing number of photolysis pulses. This is expected due to the ongoing transformation of reactive isoprene (and RO_2 radicals) into less reactive species. The decrease of ~20 s^{-1} corresponds to a decrease in isoprene concentration of around 2×10^{11} cm^{-3}, in good agreement with predictions of a kinetic model (Figure III- 6). The OH LIF signal at long reaction times, obtained as the average of the LIF intensity between 0.2 – 0.4 s and shown as red dots inFigure III- 7, increases with increasing number of photolysis pulses. This can be interpreted as interference due to decomposition of the increased concentration of ROOOH within the FAGE.

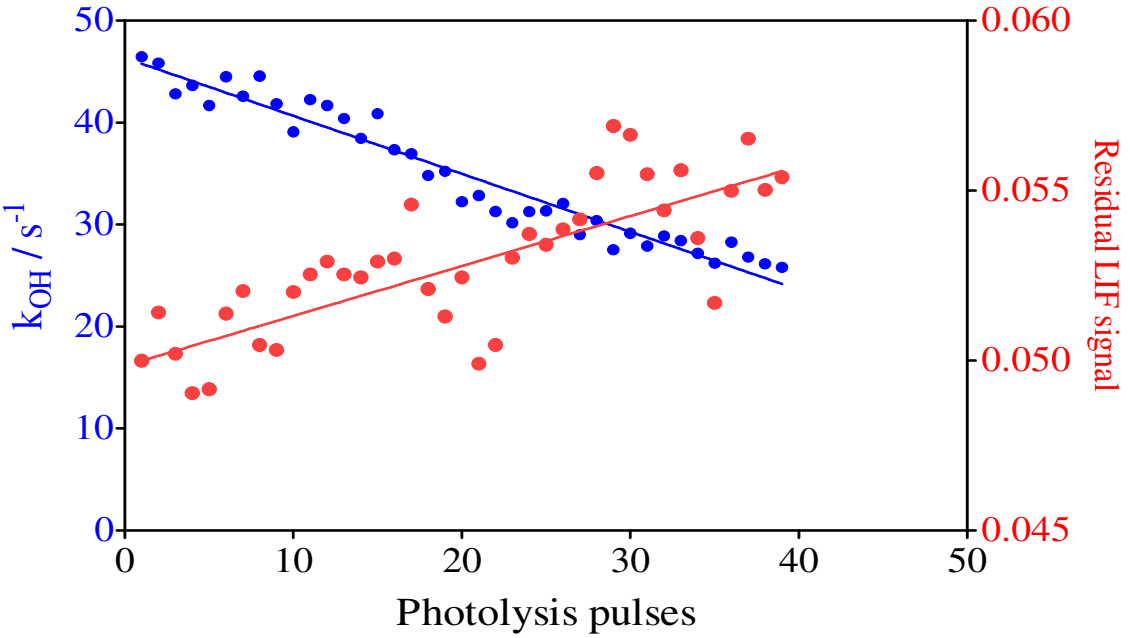

Figure III- 7: Results of fitting a mono-exponential decay to the raw signal of the experiments shown inFigure III- 5. Blue dots: OH decay rates from the mono-exponential fit (left *y*-axis). Red dots: average of the fluorescence signal between 0.2 and 0.4 s (right *y*-axis)

The increase in residual LIF signal in Figure III- 7over the 40 photolysis pulses is around 0.005 arb. units. This can be compared with the raw OH decays shown inFigure III- 5: an initial OH concentration of 1.4×10^{10} cm^{-3} leads to a LIF signal of ≈ 1.7 arb. units. Therefore, the increase in residual signal corresponds to an OH concentration of ≈ 4×10^{7} cm^{-3}. From thesimple model (Figure III- 6), it corresponds to conditions with the concentration of ROOOH after 40 photolysis pulses estimated to be [ROOOH] ≈ 1×10^{11} cm^{-3}.An interference signal corresponding to [OH] = 1×10^{6} cm^{-3} in the UL-FAGE (order of magnitude of the disagreement between model and measurements) could be generated by less than 100 ppt of ROOOH. To support this hypothesis, as ROOOH yield is not known for isoprene peroxy, experiments have been carried out with C_4H_{10} instead of isoprene (see paragraph III.3.3) for which high ROOOH yield is expected and with CH_4 (low ROOOH yield expected, see paragraph III.3.3.2). The same increase in residual signal with increasing photolysis pulses is observed for butane, while experiments with CH_4 do not show such behavior. Furthermore, as many secondary products are formed in the photolysis cell, other tests have been made to confirm the role of RO_2+OH products as described in the following paragraph.

III.3.1.3 Conditions unfavorable to the reaction of RO_2+OH

Additional experiments have been carried out with identical OH concentrationsbut much higher isoprene such that the hydrocarbon concentration always stays high compared to the RO_2 concentration. Under these conditions, no ROOOH would be formed, but still comparable

concentrations of RO_2 are generated, and with this, the products of their cross reaction or reaction with HO_2. Therefore, one can expect formation of all products from RO_2 self- or cross reaction or reaction with HO_2, but only very little or no products from the reaction of RO_2 with OH.In such conditions, no increase in residual OH signal should be observed if the interference is coming from the RO_2 + OH reaction.

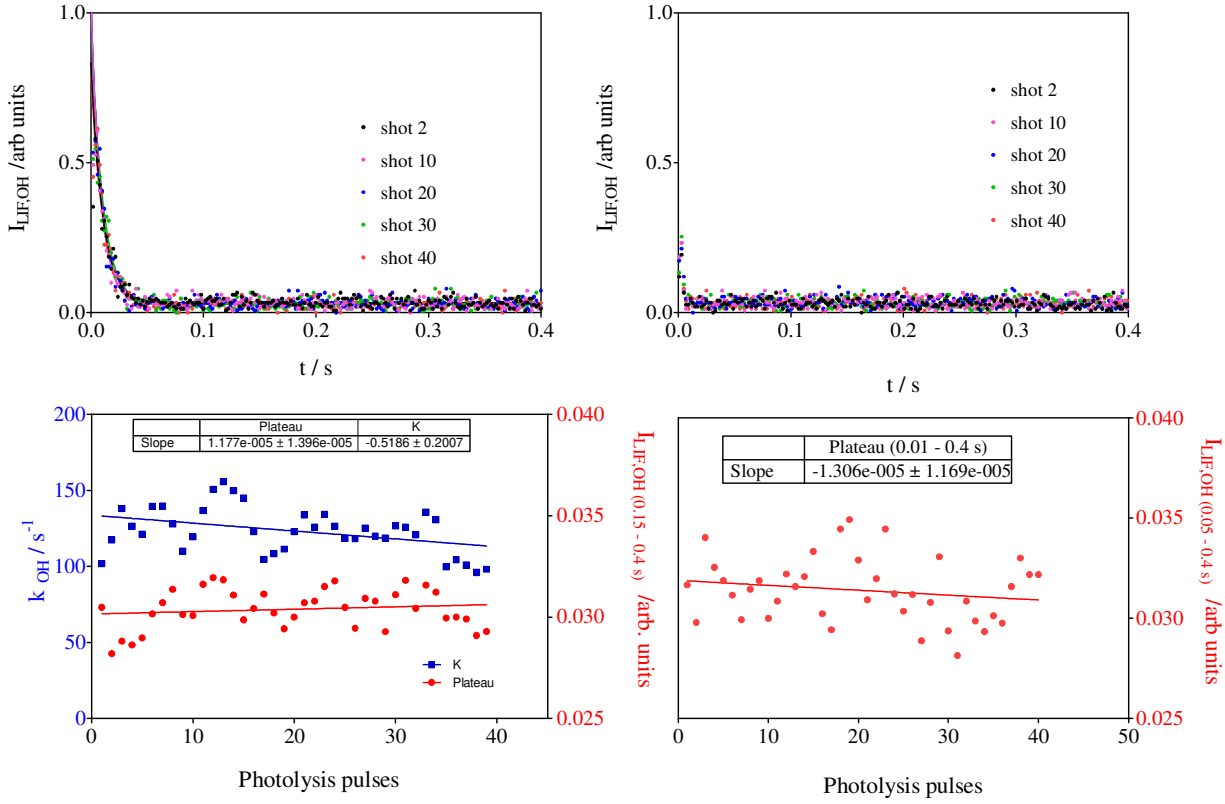

Figure III- 8: Experiments with high isoprene concentrations: $[C_5H_8] = 1.23 \times 10^{12}$and 1.23×10^{13}molecule.cm^{-3} for left and right graph, respectively. Upper graph LIF signals as a function of the number of photolysis pulses (for clarity, only every 10th pulse is shown), lower graph shows the rate constant in blue (left graph only, decay was too fast to be measurable under the conditions of the right graph) and the LIF intensity at long times (plateau from fitting for left graph, average of all data points between 0.01 – 0.4 s for right graph).

The results are shown inFigure III- 8where for the conditions in the left graph ($[C_5H_8] = 1.23 \times 10^{12}$ cm^{-3}) the OH decay rate decreases ((-0.5±0.2) s^{-1} pulse^{-1} = 20 s^{-1} after 40 pulses) in the same way than for the experiments above, and this is explained by the replacement of the reactive isoprene by less reactive products. For the conditions in the right graph the C_5H_8 concentration was so high ($[C_5H_8] = 1.23 \times 10^{13}$ cm^{-3}) that it leads to decay rates that are not measurable anymore with our time resolution. For both conditions however, the LIF-intensity at long times does not increase with the number of laser pulses ((1.2±1.4) × 10^{-5} and (-1.3±1.2) × 10^{-5} for the left and right graph, respectively).

From these observations, it can be concluded that the increase in LIF intensity at long reaction times is indeed due to the product of the reaction between RO_2 radicals and OH radicals.

However, if the interference is due to these products, it can be due to either their decomposition within the FAGE cell or due to a photolysis process by the FAGE excitation laser. In order to rule out this last possibility, the relationship between signal and laser energy has been investigated.

III.3.2 Is the interference a 1- or 2-photon process?

A photolysis process can be highlighted by quadratic dependence of the signal intensity with the laser power or through changing the repetition rate of the excitation laser. The behavior of our FAGE has been studied with a known photolytic source of interference: acetone and with the chemical system favoring the reaction of RO_2 from isoprene with OH.

III.3.2.1 Study of a known 2 photon process with acetone

In order to characterize the refreshing time in our FAGE instrument and to determine if photolytic interferences can be clearly identified, we have used acetone, CH_3COCH_3, known to lead to photolytic interference in the FAGE cell (Ren et al., 2004), in separate experiments as tracer for OH radicals generated photolytically by the excitation laser within the FAGE cell. Acetone is photolysed at the excitation laser wavelength (308 nm):

$$CH_3COCH_3 \rightarrow CH_3CO + CH_3 \qquad \text{R III- 4}$$

with CH_3CO leading in subsequent reaction with O_2 to fast formation of OH with a yield close to 1 at zero pressure(Carr et al., 2007):

$$CH_3CO + O_2 \rightarrow \text{product} + OH \qquad \text{R III- 5}$$

If the gas mixture in the excitation volume is not completely renewed between two shots (200µs), the OH radicals formed this way can be excited with one of the next excitation laser pulse. The resulting fluorescence intensity should (a) not be linear with the excitation laser fluence and (b) should decrease with decreasing repetition rate. This has been tested in our system with acetone:

a) Clean air containing stable concentration of $CH_3COCH_3$is pumped into the FAGE cell, and the resulting fluorescence intensity is plotted as a function of the laser power. Figure III- 9clearly shows a non-linear increase in fluorescence signal with laser power.

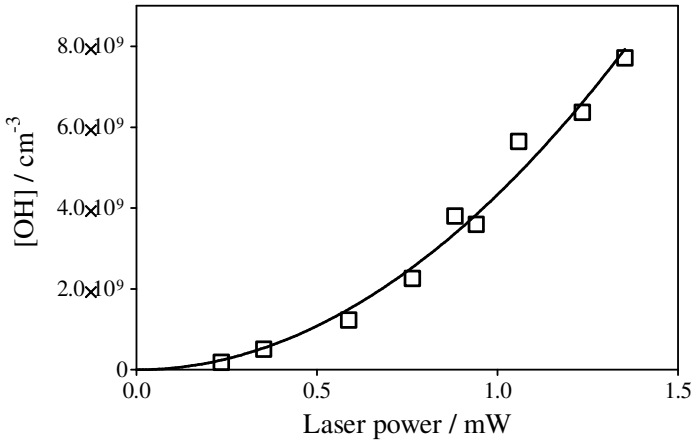

Figure III- 9: Formation of OH radicals from 308 nm photolysis of CH_3COCH_3 within the FAGE detection volume as a function laser energy within the FAGE cell. Repetition rate of the dye laser was 5 kHz, $[CH_3COCH_3] = 1.5\times10^{16}$ cm^{-3}.

b) Clean air containing stable concentration of CH_3COCH_3 is pumped into the FAGE cell, and the resulting fluorescence is measured at different excitation laser repetition rates. In these experiments, the pump laser energy has been adapted to obtain the same pulse energy for different repetition rates. It can be seen that the OH concentration decreases, but even at 1 kHz, i.e. 1 ms between two excitation laser pulses, there is still a small OH signal observed, as shown in Figure III- 10.

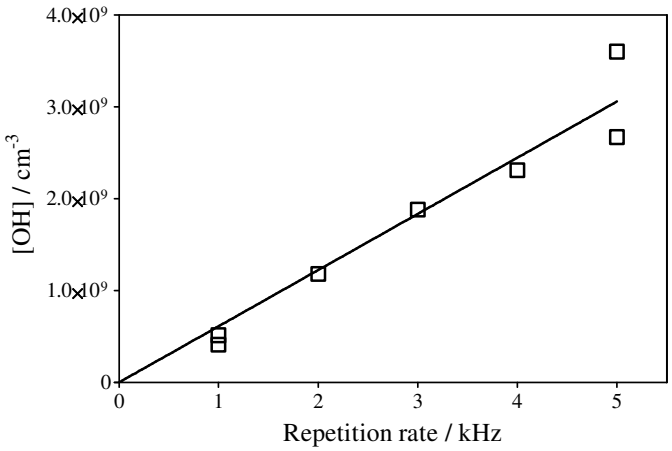

Figure III- 10: Formation of OH radicals from 308nm photolysis of CH_3COCH_3 as a function of the repetition rate. The YAG-laser energy has been adjusted in order to obtain for all repetition rates the same energy (0.8 mW within the FAGE cell). $[CH_3COCH_3] = 1.3\times10^{16}$ cm^{-3}.

From these experiments, it can be deduced that in the UL-FAGE photolytically generated OH radicals can be identified by either varying the fluence or the repetition rate of the fluorescence excitation laser.

III.3.2.2 Test with isoprene

In order to identify if similar interferences could explain the results of the experiments with isoprene and to check whether the observed increase in background fluorescence is a 1- or 2-photon process, i.e. due to interference by photolysis or by decomposition of an unknown species, we have carried out the same type of experiments than with acetone, but with isoprene (3.2×10^{11} cm^{-3}) in conditions in favor of the RO_2+OH reaction using 2 different laser energies at 5 kHz (1.7 and 0.8 mW) and with lower repetition rate (1 kHz, 0.4 mW). The obtained results are shown inFigure III- 11.

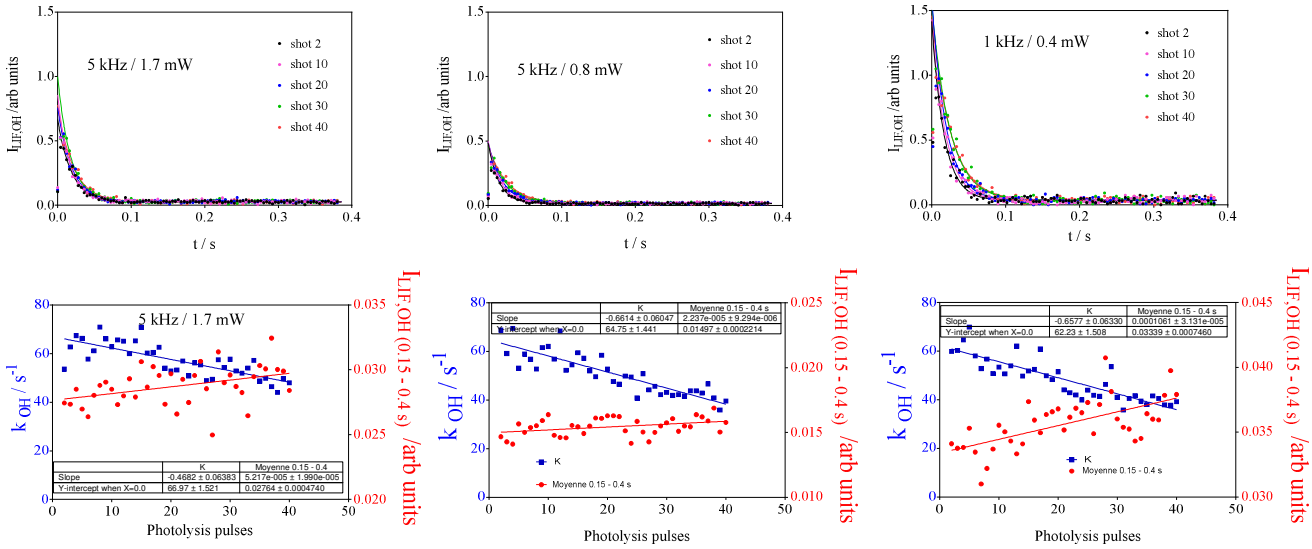

Figure III- 11: Photolysis of O_3 in the presence of isoprene using different excitation laser energies and repetition rates. Upper graphs: OH decays (for clarity, only every 10th decay is shown), lower graph OH decay rate as a function of Photolysis pulses (blue dots, left y-axis) and fluorescence intensity averaged over 0.15 to 0.4 s (red dots, right y-axis).

The lower graphs show the decrease in the decay rate with increasing number of photolysis pulses (blue dots), on the same order of magnitude for all three series, as expected (photolysis energies as well as isoprene and O_3 concentration were identical for all three series). Also, the background signal increases with increasing photolysis shots for all three series, but the slope is different. However, the slope is directly proportional to the sensitivity of the LIF detection, and for comparison needs to be normalized to the initial OH intensity. The results are summarized in Table III- 3.

Table III- 3: Summary of results from Figure III-11

Experiment	OH_0 LIF intensity [a]	Slope [b]	Slope / OH_0
5 kHz, 1.7 mW	0.85 ± 0.08	$(5.2 \pm 2.0) \times 10^{-5}$	$(6.1 \pm 2.5) \times 10^{-5}$

5 kHz, 0.8 mW	0.48 ± 0.04	$(2.2\pm0.9) \times 10^{-5}$	$(4.6 \pm 2.3) \times 10^{-5}$
1 kHz, 0.4 mW	1.50 ± 0.17	$(10.0\pm3.1) \times 10^{-5}$	$(6.7 \pm 2.7) \times 10^{-5}$

[a] OH_0 LIF intensity obtained as the average of the LIF intensity at t=0 for all 40 photolysis pulses, obtained by fitting to a mono exponential decay between 0.01 – 0.4 s, in arbitrary units, [b] Slope obtained by linear regression of red dots in Figure III- 11, in arbitrary units

By comparison between the three different conditions, we see that the increase in the fluorescence signal was of the same order of magnitude. From the observation, we conclude that the increase in residual LIF signal with increasing number of photolysis pulses is independent of both (a) the fluorescence laser excitation energy and (b) the repetition rate of the excitation laser. As a conclusion, the observed interference is not originating from a photolytic process.

III.3.3 Is the interference due to ROOOH ?

III.3.3.1 Test with n-butane (high ROOOH yield)

The chemistry of RO_2 radicals with OH radicals is not very well investigated. For isoprene, the reaction products are not known at all, and the assumption made in this work, ie. that a trioxide is formed which subsequently leads to interference in the FAGE, is speculation based on a recent theoretical study. Assaf et al.(Assaf et al., 2018b) highlighted an increase in stabilization of the adduct ROOOH formed by the reaction RO_2+OH with increasing size of the alkyl group between C1 and C4 (Table III- 1). This result is consistent with the measured HO_2 yield which decreased with increasing size of the alkyl moiety in the peroxy (C1 to C4). For butylperoxy radicals, the HO_2 yield was close to zero, leading to a supposed yield of ROOOH close to one. In the case of isoprene however one can still imagine the addition of OH radicals to the second double bond instead of reaction to the peroxy site and thus the yield of ROOOH may be less than one.

Therefore, we have investigated in the frame of this work the reaction of butane peroxy radicals with OH radicals. Different concentrations of butane have been added such that at the lowest concentration (left graphs in Figure III- 12) a high formation of ROOOH can be expected: under these conditions OH radicals react slowly with butane and the reaction with the nascent RO_2 radicals becomes rapidly competitive.

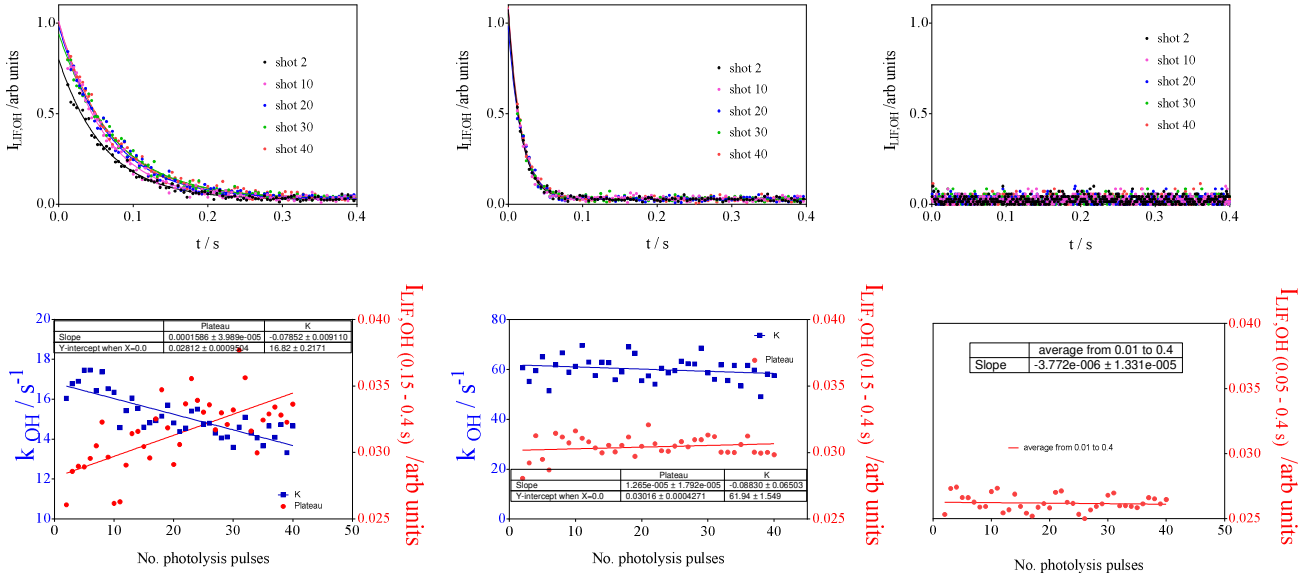

Figure III- 12: Photolysis of O_3 in the presence different concentrations of n-butane (7×10^{12}, $2 \times 10^{13}$and 7.5×10^{15} cm^{-3} from left to right). Upper graph: OH decays (for clarity only every 10^{th} decay is shown), lower graph: decay rates of OH radicals as a function of photolysis pulses (blue dots, left y-axis), residual LIF intensity taken from mono exponential fit for left graph and as the average LIF intensity between 0.15 – 0.4 s and 0.01 and 0.4 s for the center and right graph, respectively.

The concentration has been increased in the middle graph of Figure III- 12 such that only a low concentration of ROOOH is expected. In the right graph, finally, a very high concentration of butane has been used, too high to detect the decay of OH radicals with our time resolution. Under these conditions, it is expected that OH radicals react nearly exclusively with butane and no ROOOH is formed. Note that in all three experiments the initial OH radical concentration is the same. The interference is clearly visible in the left graph (slope m = (15.8±4)×10^{-5} arb. units), barely in the center graph (m = (1.2±1.7)×10^{-5} arb. units) and not present anymore in the right graph (m = -(0.4±1.3)×10^{-5} arb. units). Note that in the experiment of the right graph, the concentrations of all other species are similar to the concentrations in the left graph, i.e. the RO_2 and HO_2 concentrations are similar and with this all products obtained from self-and cross reactions. This is a strong indicator that the observed increase in residual LIF intensity is indeed due to the product of the reaction of RO_2 with OH.

III.3.3.2 Test with CH_4 (low ROOOH yield)

The reaction of CH_3O_2 + OH has been investigated in some detail (Assaf et al., 2016, 2017a; Müller et al., 2016) and it is now accepted that this reaction leads to formation of CH_3O + HO_2 (80-90%) with possibly small yield of CH_3OH and CH_3OOOH. Therefore, it is not expected to observe interference in the FAGE system. Two series of experiments with different CH_4 concentrations have been performed,

the results are shown in Figure III- 13. In both series, one observes for the OH decay rate an increase over the first few photolysis shots. This is expected due to the formation of CH_3O_2 radicals that are more reactive than CH_4. In Figure III- 6**,** it can be seen that the model predicts (for an overall reactivity of 30 s^{-1}) an increase of RO_2 radicals over the first 10 pulses, followed by a steady state period and a slow decay. The decay rates are plotted as a function of the photolysis pulses in Figure III- 13(lower graphs) and have been fitted by forcing to the same rise time as the one obtained from the mono exponential fit of the RO_2 profile inFigure III- 6.

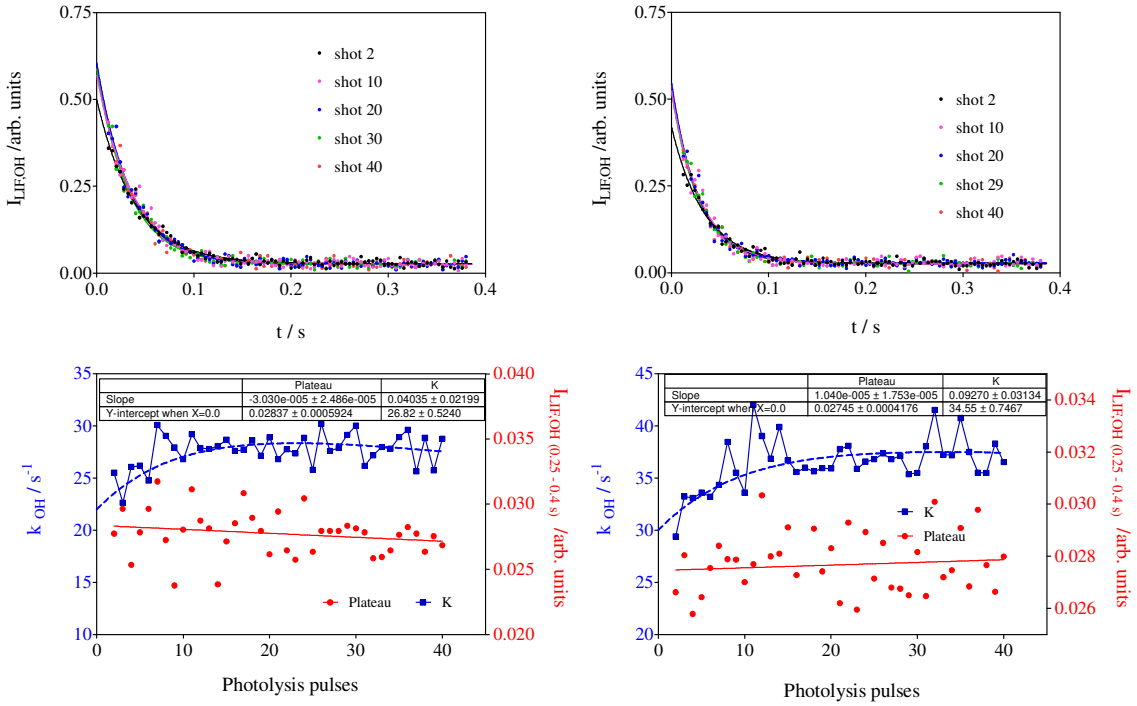

Figure III- 13: Photolysis of O_3 in the presence different concentrations of CH_4 (3.3×10^{15} cm^{-3} and 4.9×10^{15} cm^{-3} for the left and right graph, respectively). Upper graph: OH decays (for clarity only every 10^{th} decay is shown), lower graph: decay rates of OH radicals as a function of photolysis pulses (blue dots, left y-axis), residual LIF intensity taken as the average LIF intensity between 0.25 – 0.4s.

A rough estimation of the increase in the decay rate of 8 s^{-1} is obtained, corresponding to a CH_3O_2 concentration (using $k(CH_3O_2+OH) = 1.5\times10^{-10}$ cm^3s^{-1}) (Assaf et al., 2016) of 5×10^{10} cm^{-3}, in excellent agreement with the predictions of the model for RO_2 concentration (Figure III- 6). This good agreement gives more confidence in the principle idea of the experiments and the conditions chosen to enhance the formation of ROOOH.In both series, the LIF intensity at long times does not change ($(-3.0\pm2.5\times10^{-5}$ and $1.0\pm1.7\times10^{-5}$ for left and right graph, respectively). This is expected due to the small yield of CH_3OOOH in the case of methane + OH.

From the tests with butane and methane, with different ROOOH yield, we can confirm that ROOOH is very likely a source of interference in the UL-FAGE and that it is probably why an interference is seen in biogenic, low NOx environments (Feiner et al., 2016a).

III.4 Global modeling

As mentioned above, in the UL-FAGE, an interference signal which corresponds to [OH] = 1×10^6 cm^{-3} could be generated by less than 100 ppt of ROOOH in the atmosphere. Then in order to estimate if ROOOH concentrations in this range can possibly be accumulated in remote biogenic environments, calculations using global and box models have been performed.

III.4.1 Modeling methodology

The global distribution of ROOOH species produced by the RO_2 + OH reaction was investigated in collaboration with A. Archibald and colleagues using the Met Office's Unified Model with the United Kingdom Chemistry and Aerosols scheme (UM-UKCA), version 8.4.(Abraham et al., 2012).UM-UKCA is a global chemistry-climate model with a horizontal resolution of 1.875° in longitude × 1.25° in latitude on 85 vertical levels from the surface up to a height of 85 km (in its N96-L85 configuration). The chemistry scheme and emissions used in the present study were described in detail in a recent work(Ferracci et al., 2018) and included isoprene oxidation(Archibald et al., 2010) and isoprene emissions.

The UM-UKCA model included the formation and subsequent photochemistry of the following peroxy (RO_2) radicals:CH_3O_2 (methyl peroxy), $CH_3CH_2O_2$ (ethyl peroxy), $CH_3CH_2CH_2O_2$ (n-propyl peroxy), $(CH_3)2CHO_2$ (i-propyl peroxy), $CH_3C(O)O_2$ (acetyl peroxy), $CH_3CH_2C(O)O_2$ (propionyl peroxy), $CH_3C(O)CH_2O_2$ (propyldioxy peroxy). Peroxy radicals from the first oxidation of isoprene were lumped into one species, as those from the oxidation of isoprene oxidation products (methacrolein and methyl vinyl ketone).

Crucially, the model simulated the abundances of a number of peroxy radicals (listed above) resulting from the oxidation of emitted VOCs. These were used, along with the modelled number densities of OH and a rate constant k_1 of 1.5×10^{-10} cm^3 s^{-1} for all RO_2 + OH reactions (consistent with laboratory studies(Assaf et al., 2016, 2017b)) to calculate the total rate of production of ROOOH species. The total atmospheric abundance of trioxide species, $[ROOOH]_{ss}$, was then calculated offline using the modelled abundances of hourly [OH] and $[RO_2]$assuming steady state between the production and loss (L) processesof ROOOH, according to the equationEq III- 1:

$$[\mathrm{ROOOH}]_{\mathrm{SS}} = \frac{k_1[\mathrm{OH}]\sum_{i=1}^{n}[\mathrm{RO}_{2,i}]}{L} \qquad \text{Eq III- 1}$$

where the sum is across all RO_2 radicals in the model excluding methyl peroxy radicals, for which it has been shown that the production of a trioxide species is only a minor product channel. As the rate of loss of trioxide species is currently unknown, *L* was systematically varied across a few orders of magnitude (from 10^{-5} s^{-1} to 10^{-2} s^{-1}) using a global model simulation to account for ROOOH loss *via*photolysis, wet and dry deposition, chemical reaction and thermal decomposition as shown in Figure III- 14.

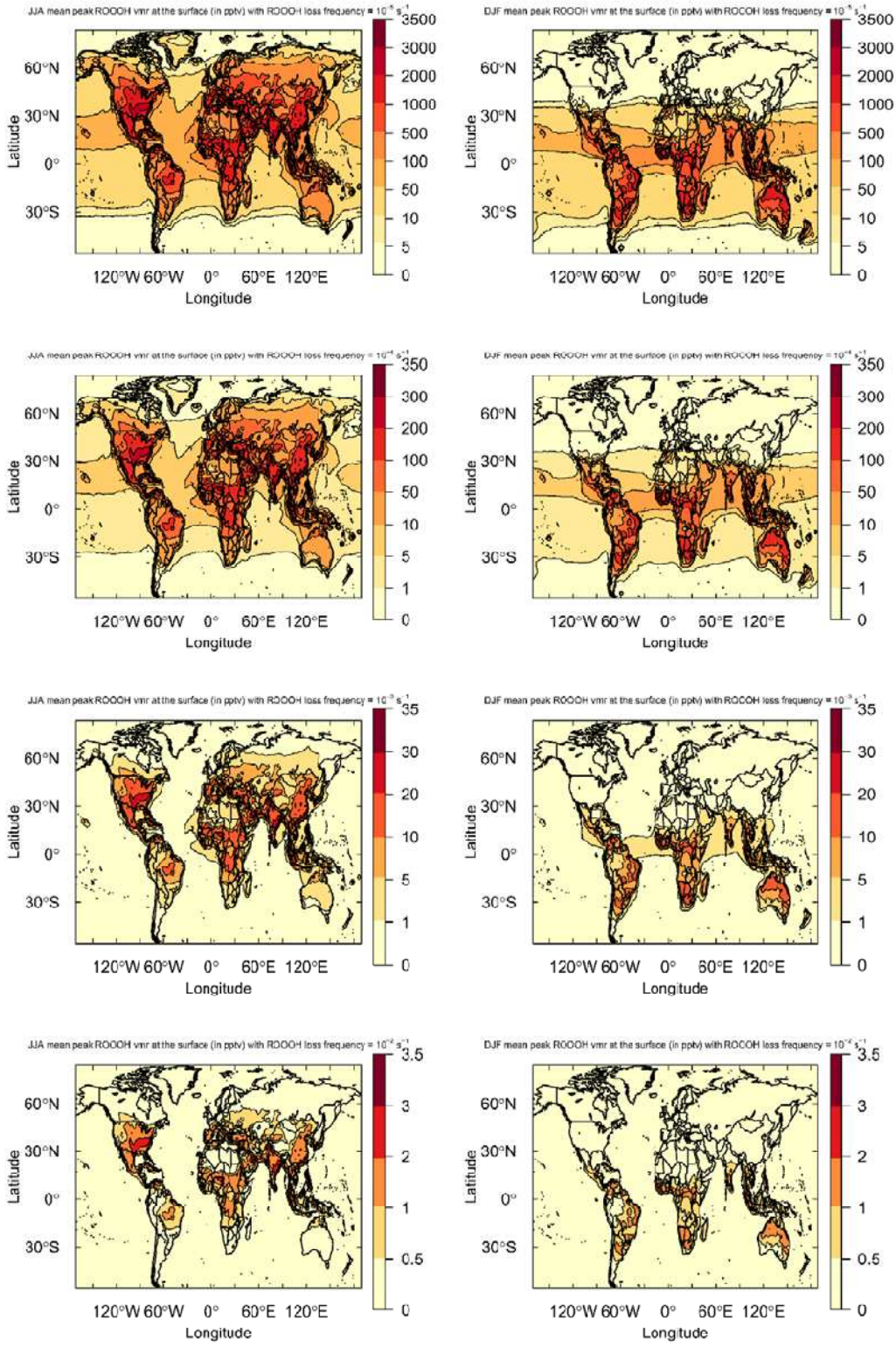

Figure III- 14: Modelled mean diurnal peak ROOOH volume mixing ratio (in ppt) during the Northern (left hand side) and Southern (right hand side) summer months. Each row shows steady state ROOOH abundances obtained with different ROOOH removal rates, ranging from 10^{-5} to 10^{-2} s^{-1}.

To confirm these global model results, a steady-state box model, constrained to observations made in the South East USA(Feiner et al., 2016a), was developed. The results of the calculations with the

steady-state model are shown inFigure III- 16, which highlights that at low levels of [NO] (< 200 ppt), typical in BVOC rich environments, levels of [ROOOH] are predicted to be on the order of 50-200 ppt. The two datasets plotted in Figure III- 16span a range of different NMVOC (isoprene) mixing ratios and highlight that ROOOH levels increase with increasing [VOC] and decreasing [NO], in agreement with the global 3D modelling results shown in Figure III- 15.

III.4.2 Global modeling results

The modelled [ROOOH] followed a diurnal and seasonal cycle similar to that of its precursors (OH and RO_2). Therefore, the highest [ROOOH] values were found around midday-2pm in the summer months (JJA in the Northern Hemisphere, DJF in the Southern Hemisphere). The peak [ROOOH] values shown in Figure III- 15were determined by producing an average seasonal diurnal cycle for each model grid cell and then plotting only its peak [ROOOH] value. Figure III- 15shows the average diurnal peak concentration of ROOOH in the Boreal (left) and Austral (right) summer obtained using a removal rate of 10^{-4} s^{-1}, leading to ROOOH lifetimes of around 3 hours. Peak concentrations of several 100 ppt are reached in this scenario, especially at tropical latitudes, which would lead to interference in the UL-FAGE system of the order of 1×10^{6} cm^{-3}.

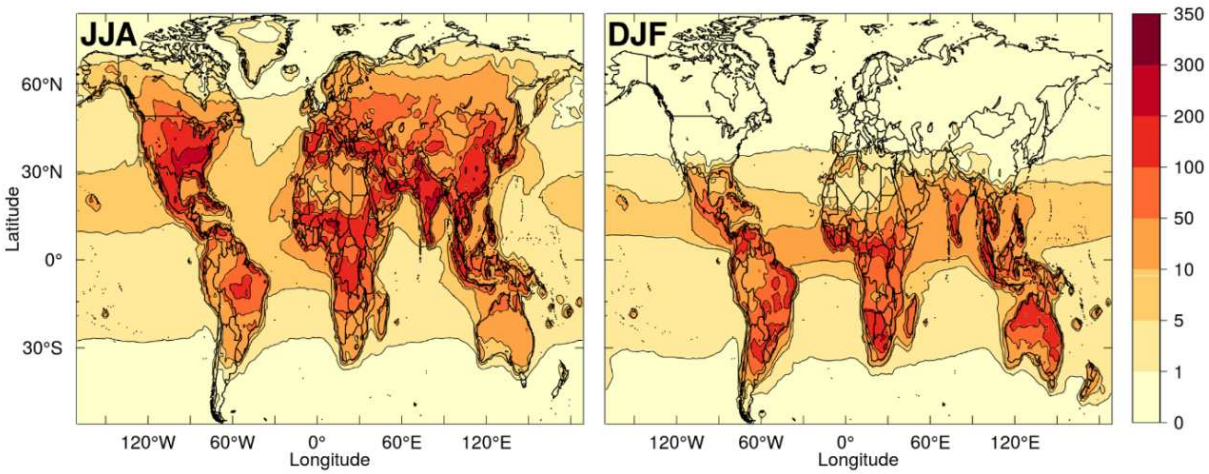

Figure III- 15: Modelled mean diurnal peak ROOOH volume mixing ratio (in ppt) during Northern (left) and Southern (right) summer months, using a combined removal rate for all ROOOH of 10^{-4} s^{-1}.

To confirm these global model results, the steady-state box model described above has been used. The results of the calculations with the steady-state model are shown inFigure III- 16, which highlights that at low levels of [NO] (< 200 ppt), typical in BVOC rich environments, levels of [ROOOH] are predicted to be on the order of 50-200 ppt. The two datasets plotted in Figure III- 16span a range of different NMVOC (isoprene) mixing ratios and highlight that ROOOH levels increase with

increasing [VOC] and decreasing [NO], in agreement with the global 3D modelling results shown inFigure III- 15.

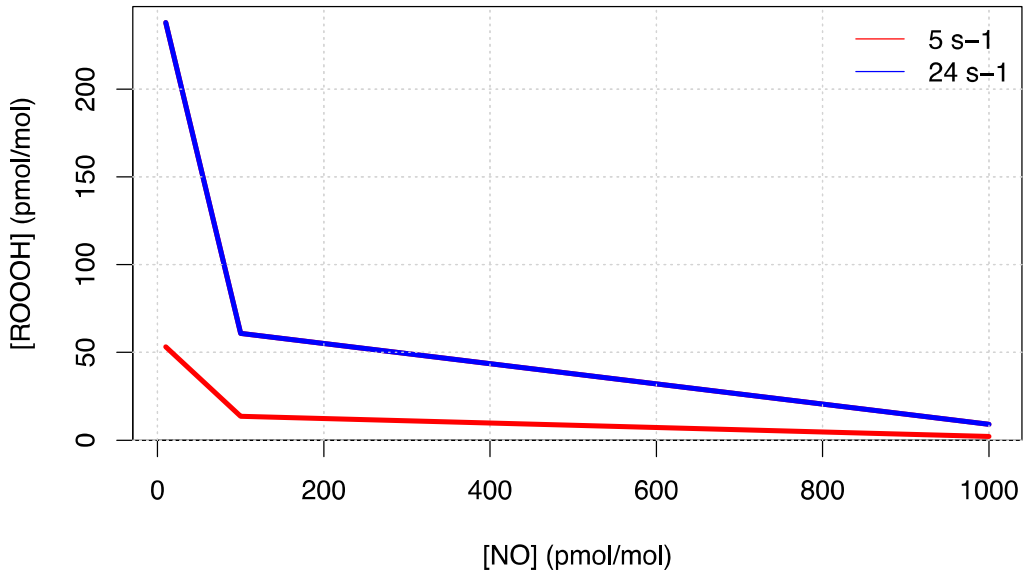

Figure III- 16: Variation in ROOOH as a function of NO (x-axis) and VOC reactivity (different colors) constrained by data from (Feiner et al., 2016a). Those data in red reflect a situation of VOC reactivity of 5 s^{-1} whilst the blue data reflect VOC reactivity of 24 s^{-1} (similar to that seen in regions like the Amazon).

III.5 Conclusion

In this work we have shown that the product of the reaction of RO_2 radicals with OH radicals leads to an OH interference signal in the UL-FAGE instrument. If occurring also in other FAGE instruments, it can be high enough to explain numerous observations obtained with FAGE instruments from other laboratories including:

a. Underestimation by models of OH concentrations measured in remote, biogenic environments: the global model predicts ROOOH peak concentrations in remote environments that are probably high enough to explain, at least partially, the observed disagreement between model and measurements(Hofzumahaus et al., 2009; Lelieveld et al., 2008; Whalley et al., 2011).
b. Variability of interferences observed in field campaigns: The box model calculations have shown that the concentration of ROOOH species varies with NO, VOC concentration and $J(O^1D)$ in the same way as the amplitude of the interference such as observed by the group of W. Brune(Feiner et al., 2016a).
c. Interference observed from O_3 + alkenes: the tentative explanation of alkene ozonolysis being the source of internally formed OH radicals through decomposition of the stabilized

Criegee intermediate[21] is possibly due to ROOOH formed in a secondary reaction from RO_2 and OH, both generated during the ozonolysis(Johnson and Marston, 2008) of the very high VOC and O_3 concentrations in laboratory experiments(Fuchs et al., 2016; Novelli et al., 2014a; Rickly and Stevens, 2018). Indeed, it is observed in these experiments that the interference scales with the O_3+alkene turnover rate, i.e. the time that ROOOH can accumulate.

d. Interferences observed in SAPHIR chamber: Fuchs *et al*. have carried out experiments under low NO conditions by comparing OH concentrations measured by FAGE and DOAS(Fuchs et al., 2012). Most of the time the agreement between both techniques was excellent, but on a few days towards the end of the campaign higher OH concentrations were measured by FAGE compared to DOAS. The NO concentrations on these days were lower, making the formation of ROOOH more likely, than on days with excellent agreement between FAGE and DOAS (Table 2 in(Fuchs et al., 2012)).

The results presented in this work thus propose an appealing solution to answer many open questions. Of course, currently the uncertainties are high on both, the observed FAGE interference per ROOOH molecule as well as the maximum ROOOH concentration that can accumulate in real environments. The first point could be improved through well-designed chamber studies under very low NO concentrations. The second point is more difficult to ameliorate because the steady state ROOOH concentration directly scales with its removal rate, and currently nothing is known about the fate of ROOOH. Maybe the table can be turned by using the evolution of the interference to learn about the fate of ROOOH.

Chapter IV: characterization of UL FAGE and different calibration cells for HO_x and RO_2 measurements

IV.1 Introduction

As highlighted in Chapter I, measurements of HO_x radicals can provide an essential test of the reliability of atmospheric chemical models. However, their very low mixing ratio in the atmosphere makes their measurements extremely difficult. Only a few instruments are capable of making in situ measurements of OH and HO_2 with the required sensitivity (FAGE, CIMS, and DOAS). If the DOAS technique is absolute, FAGE and CIMS techniques require a calibration.

Different intercomparisons have been done between the different instruments measuring HO_x radicals(Fuchs et al., 2010a; Heard and Pilling, 2003). A good agreement has been found most of the time under normal conditions. while under specific conditions such as dark conditions and during the night, disagreements were observed between different instruments (Fuchs et al., 2010b). These intercomparisons give confidence regarding the HO_x measurements and consequently to the calibration method used for CIMS and FAGE instruments. The standard calibration technique is based on the use of a calibration cell in which flows humidified zero air with the water vapour being photolysed at 184 nm by a Hg lamp, thus producing equal concentrations of OH and HO_2 radicals. This calibration cell can also be used to test the sensitivity of the instruments to the RO_2 radicals by adding a VOC which will be converted to its respective RO_2 by reaction with the generated OH. This method is used to calibrate instruments dedicated to RO_2 detection such as PERCA instruments.

Nevertheless, as mentioned during the HO_x workshop which took place in Jülich in 2011, more studies are necessary to ensure that the calibrations are correctly performed. It has even been proposed to build a common calibration cell to share between the different groups involved in HO_x quantification. This possibility is still under consideration.

Before having this common calibration cell, a first step is to intercompare existing calibration cells already used in the community. For this purpose, an intercomparison was conducted at Lille University in PC2A laboratory between three different calibration cells used for instruments measuring HO_x or RO_x radicals (FAGE of PC2A, CIMS of LPC2E and PERCA of IMT-Lille-Douai). The characteristics of the calibration cell used with our FAGE have been first studied and have then been compared with the 2 others by using them on our FAGE. Ambient measurements using the UL-FAGE and the PERCA took place at the end of the campaign during half a day.

Afterwards, in separated experiments, our calibration cell and the one used for the PERCA have been tested on the CIMS instrument located in Orléans (LPC2E laboratory).

In this chapter, the different calibration methods and in particular the cells used in the intercomparison are described, then the tests made on our calibration cell and the two others are presented for HO_x measurements. In the last part of the chapter, the behavior of the FAGE instrument for the detection of RO_2 species has been characterized with our calibration cell and the results obtained were compared with those obtained with the 2 other calibration cells.

IV.2 Calibration methods used for HO_x and RO_2 quantification

Calibration techniques can differ from one instrument to another and are summarized in Table IV-1. The most common calibration method used to calibrate HO_x instruments is the water vapour photolysis while the others are only occasionally used due to their poor accuracies and artifacts. Some HO_x generations such as water vapor UV-photolysis and ozone-alkene techniques have been intercompared (Dusanter et al., 2008). They found that both techniques to agree within their experimental uncertainties, although the sensitivities derived from the ozone-alkene technique were systematically lower than those derived from the water-vapor UV-photolysis technique. And it was reported that the water-vapor UV photolysis technique exhibits the highest accuracy and lowest degree of secondary chemistry (Dusanter et al., 2008).

Cross-calibrations of different field instruments using the same calibrator was not done so far, even if it is essential to ensure that the different calibrations have no significant biases on the measurements. Table IV- 1 summarize of the OH sources used for calibration of HO_x instruments.

Table IV- 1: Techniques employed to calibrate OH instruments (Dusanter et al., 2008), first 5 rows corresponds to methods no more used.

Calibration techniques	Principle	Uncertainty (1σ)	Generated radicals	Laboratory/Field (drawbacks)	References
I. Low-pressure flow-tube RF discharge	H atoms are produced by a microwave discharge in a low-pressure flow tube. OH radicals are produced by titration of the H atoms with NO_2	30 %	OH	Laboratory (low ambient pressure calibration)	(Stevens et al., 1994)
II. Pulsed N_2-H_2O RF discharge	OH and NO are produced at low pressure with a low power RF discharge. The OH density is related to the NO density in the discharge	20 %	OH	Laboratory (low ambient pressure calibration, require measuring NO by LIF)	(Dilecce et al., 2004)
III. Steady-state O_3-alkene	OH is produced inside a flow tube reactor by the ozonolysis of alkenes	42 %	OH	Laboratory/field (time consuming)	(Heard and Pilling, 2003)
IV. Continuously Stirred Tank Reactor (CSTR)	OH is produced in a CSTR by UV-irradiation of an Hydrocarbon /H_2O/NO mixture. The OH concentration is calculated from the loss of the hydrocarbon	36 %	OH	Laboratory/field (bulky, time consuming, potential gradient of OH near the wall of the reactor)	(Hard et al., 1995, 2002)
V. Laser photolysis of O_3	Ozone is photolysed at 248 nm and OH is produced by subsequent reaction of excited atomic oxygen with water $O_3 + hv \longrightarrow O(^1D) + O_2$	40-50 %	OH	Laboratory (bulky, expensive)	(Tanner and Eisele, 1995)
VI. Water UV-photolysis	See chapter II	10-30 %	OH, HO2	Laboratory/field (Photon flux measurements, lamp dependent absorption)	(Faloona et al., 2004; Heard and Pilling, 2003; Tanner and Eisele, 1995)

In this chapter, results based on the use of different cells with a similar calibration technique but different calibrator design and different measurement method for UV lamp fluxes are presented. The 3 calibration cells used are based on the photolysis of water to 184.9 nm to generate a known concentration of OH and HO_2, or a mixture of known concentrations of HO_2 and RO_2 when VOCs are added in concentration high enough to consume all the OH during the residence time within the calibration cell. The characteristics of the different calibration cells will be explained briefly in the following paragraphs.

IV.2.1 UL-FAGE calibration cell

The calibration cell was already described in details in chapter II and is briefly presented here. It is a rectangular aluminium tube (1.2 × 1.5 × 50 cm) with 5 rectangular openings in which 6 cm height windows are placed in between rubber seals. Two blocks of aluminium are placed on each side of the tube to maintain the windows (Figure IV- 1). The Hg lamp is placed in an aluminium block fixed to the calibration cell. This block can slide along the cell to place the lamp in front of the different windows. It is equipped with a photodiode placed on the opposite side of the mercury lamp to measure the Hg lamp flux in order to calculate the radical concentration produced. The aluminum housing of the lamp is continuously purged with dry nitrogen to avoid (a) the diffusion of air, containing absorbing species like oxygen, into the housing and (b) help maintaining the Hg lamp at constant temperature. The light is filtered at 182.4 nm with a band pass filter. The PC2A calibration system is limited to a maximum relative humidity equal to 15 % due to its humid air generation system. The flow rate used is 40 L/min.

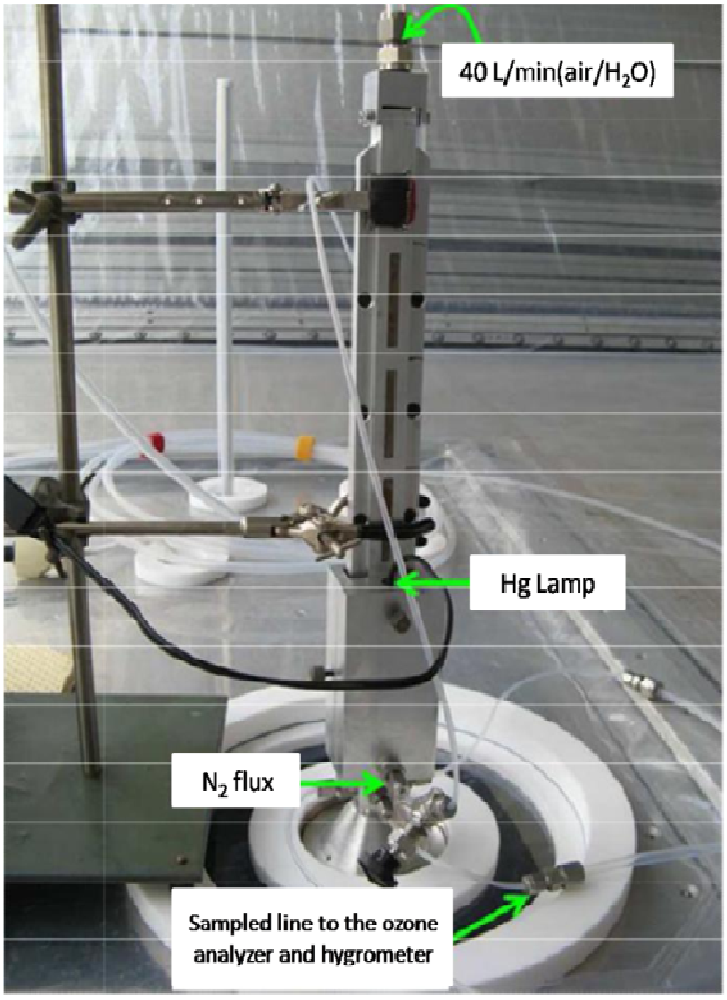

Figure IV- 1: Calibration cell for the UL-FAGE instrument (version1)

IV.2.2 IMT Lille Douai calibration cell

The calibration cell is based on the same principal than the one used for the UL-FAGE with some technical differences. It consists of a rectangular flow reactor made of aluminum (1.27×1.27×30 cm) and is equipped with a suprasil window on two sides (Figure IV- 2). At the exit of the calibration cell, a humidity sensor measures the relative humidity of the incoming air. Water vapor is generated by a handmade bubbler system. The humidity is changed by varying the flow entering to the bubbler mixed with the main flow. The light source is a mercury lamp housed in an aluminum housing that is continuously purged with dry nitrogen to avoid that the air from outside with absorbing species like oxygen is diffusing into the unit. In addition, the light is filtered at 182.4 nm with a band pass filter. The flow rate with IMT Lille Douai calibration system is 35 L/min.

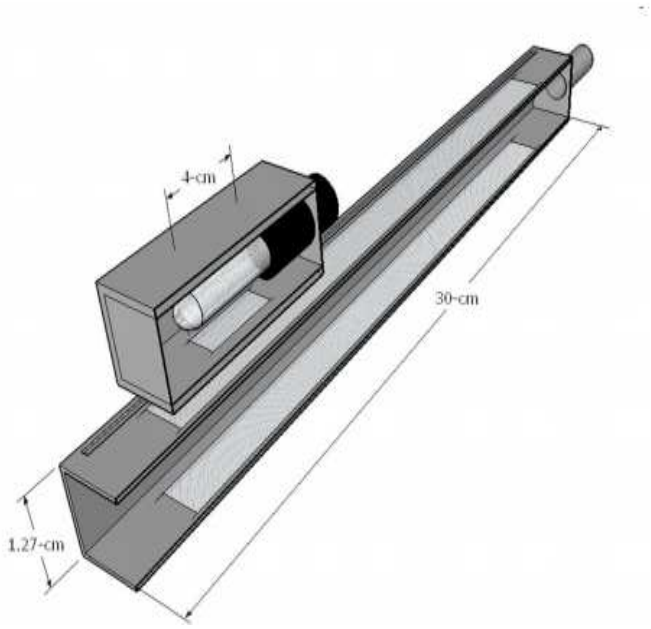

Figure IV- 2: Cross- section of the calibrator based on the water- vapor UV-photolysis technique (Dusanter et al., 2008).

IV.2.3 LPC2E calibration cell

Similar to previous cells, the radicals are generated by the photolysis of humid air in a flow tube (1.8 × 2.0 × 70 cm). UV light is emitted by a mercury lamp through 10 × 5 mm window of the lamp enclosure (Figure IV- 3). The UV light intensity can be varied using a N_2O UV absorption cell with variable N_2O concentration in nitrogen flow.

1 – gas flow inlet; 2 – humidity and temperature sensors; 3 – band pass filter; 4 – entrance lens; 5 – aperture; 6 – N_2O cell; 7 – Pen-Ray lamp; 8 – phototube; 9 – exit lens; 10 – exit of the flow tube. a) – cross section of the illuminated volume inside the flow tube (dimensions in mm)

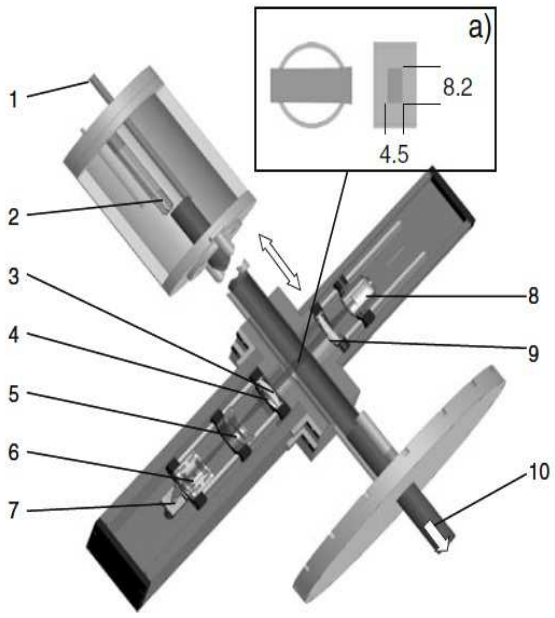

Figure IV- 3: LPC2E calibration cell based on N_2O actinometry with water mass flow controller (Kukui et al., 2008).

The light is filtered at 182.4 nm with a band pass filter to be detected by a phototube after the photolysis zone. Water vapor is generated by a set of a liquid water mass flow controller and an evaporator (Bronkhorst). The water vapor is measured by humidity sensor placed at the entrance of the calibrator. The flow rate used with this system was between 24 -40 L/ min. The water system allows generating relative humidities ranging from 1 to 70 %.

IV.2.4 Summary of the calibrations cells and conditions used for the intercomparison

Table IV- 2 summarizes the different calibration cell characteristics and configurations used during the intercomparison campaign on different instruments dedicated to measure HO_2 radicals.

Table IV- 2: Characteristics and configurations of the calibration cells used during the intercomparison

	Mines Douai	PC2A	LPC2E
Wand material	Aluminum	Aluminium	St. Steel
Wand geometry	Square pipe	Square pipe	Round Pipe
Wand dimensions (cm)	1.27(L)x1.27(W)x30(H)	1.2(L) x1.2(W) x43(H)	D=1.8cm; L=5-40 cm
Mercury lamp	UVP 11sc1	UVP LSP035+ alim LSP060	Uriel, LSP035, Hg(Ar)
Lamp housing purged with N_2	yes	yes	yes
185 bandpass filter on lamp housing	yes	yes	yes
Photodiode to track the lamp flux	yes	No (done after the intercomparison)	yes
Determination of photon flux and irradiation time	O_3 actinometry	O_3 actinometry	N_2O actinometry
Flow rate (SLPM)	35	40	24 (can vary up to 50) slm
Transit time from irradiated region to wand exit (ms)	20-50 ms (can be varied depending on the lamp position)	10-60 ms (can be varied : 5 windows)	60 – 260 ms (variable depending on the lamp position)
OH loss	20-35% at 40 ms	20% at 60 ms	K_{loss} = (3.2±0.2) s^{-1}
Achievable relative humidity (%)	1-70 %	1-15 % (with 1 bubbler)	RH=1%-70%
Range of [OH], [HO_2] (cm^{-3})	0.1-1.5×10^{10}	0.1-1×10^{10}	10^6 - 10^8
Uncertainty (1σ) on calculated [OH] and [HO_2]	≈ 15-18%	25%	20-30%

The main differences consist in the radical concentration generated, which is function of the exposure zone (highest for the PC2A) and the potential attenuation (N_2O filter for the LPC2E).

The tests that have been made with the three different calibration cells at the top of the UL-FAGE instrument are summarized in Table IV- 3.

Table IV- 3: test made with different calibration cells with the UL-FAGE instrument

Calibration cells / Tasks	PC2A	IMT-Lille Douai	LPC2E
Task 1: HO_x mode FAGE response as a function of lamp flux at constant humidity	×	×	×
Task 2: HO_x mode FAGE response as a function of humidity or humidity and lamp flux together	×	×	×
Task 3: HO_x mode FAGE response as a function of total flow			×
Task 4: HO_2* mode (presence of toluene or isoprene or cyclohexene) FAGE response as a function of the VOC and NO injected	×	×	×
Task 5: HO_2 mode (addition of CO) FAGE response as a function of NO injected (wall losses)	×	×	×

Tasks 1- 3 will be discussed in section IV.3 and task 4 and 5 will be discussed in section IV.4 of this chapter.

IV.3 Characterization of the calibration cells on the UL-FAGE for HO_x measurements

The UL-FAGE was first used for the characterization of the OH and HO_2 measurement, the objective being to compare the radical generation and the estimation of their concentration using the different calibration cells in absence of VOC. These conditions correspond to the so-called HO_x mode (zero air in the calibration cell, presence of OH and HO_2) and HO_2 mode (addition of CO to convert OH in HO_2).The intercomparison begins by using the PC2A calibration cell on the top of the UL-FAGE instrument, different tests were performed (normal calibrations) to ensure the reproducibility of the calibration factor of the UL-FAGE which is then used to determine the concentrations measured with

the other calibration cells. Then, for different conditions of the 2 other calibration cells on top of the FAGE, we are able to compare the expected concentration (calculated by each group) with the response of the FAGE. The tests realized have been chosen depending on the limitations of each calibration cell (flow rate, maximum humidity, lamp flux,…). The results obtained are presented and discussed in the following sections.

IV.3.1 Characterization of the PC2A calibration cell for wall losses and water effect

In order to better characterize the calibration cell used with the UL-FAGE after its modifications (see Chapter II), losses in the calibration cell have been redetermined.

IV.3.1.1 Radical losses in the calibration cell

As described in Chapter II, the mercury lamp can be moved along the calibration cell to be placed in front of the 5 windows. The ability to change the lamp position allows the determination of the radical losses through the calibration cell from the photolysis region to the sample inlet. It is very important to know the magnitude of the losses to calculate accurately the concentration of radicals available at the output of the calibration cell. As the calibration cell has been modified during my thesis, the radical losses have been determined again by measuring the OH and HO_2 signals in the FAGE cells at different lamp positions along the calibration cell. The distance between the photolysis region and the exit of the calibration cell varied from window 1 near the exit to window 5 at the top (6 to 32 cm respectively, corresponding to the distance between the center of the respective window and the exit of the calibration cell). OH and HO_2 radicals can be lost either by self or cross reactions or on the cell wall. From the lower window to the upper one, the time between the center of the irradiation and the exit of the cell varies from 10 to 60 ms with a flow of 40L/min. On this time scale, radical-radical reactions are normally minor with the concentration range generated (less than 0.1 % for [OH] = [HO_2] = 1×10^9 molecule.cm^{-3} for 60 ms) and the losses within the calibration source are mainly on the cell wall.

$OH + OH \rightarrow H_2O + O(^3P)$	R IV- 1
$OH + HO_2 \rightarrow H_2O + O_2$	R IV- 2
$HO_2 + HO_2 \rightarrow H_2O_2 + O_2$	R IV- 3
OH + wall → losses	R IV- 4
HO_2 + wall → losses	R IV- 5

The lamp housing was moved along the calibration cell to characterize the loss of radicals, changing the exposure time of the radicals to the reactor walls. 2 calibration experiments were done with different instruments (UL-FAGE and CIMS). The upper graph of Figure IV- 4 shows the evolution of

the OH and HO_2 signal as function of the mercury position through the calibration cell using PC2A calibrator on UL-FAGE instrument. While the lower graph of the same figure represents similar test for OH wall losses using the PC2A calibration cell on CIMS instrument. By extrapolating the signal to the origin (top of the cell) and normalizing by the signal at the exit of the cell (x=6 cm), we can measure the losses for OH radicals between the source of irradiation and the exit.

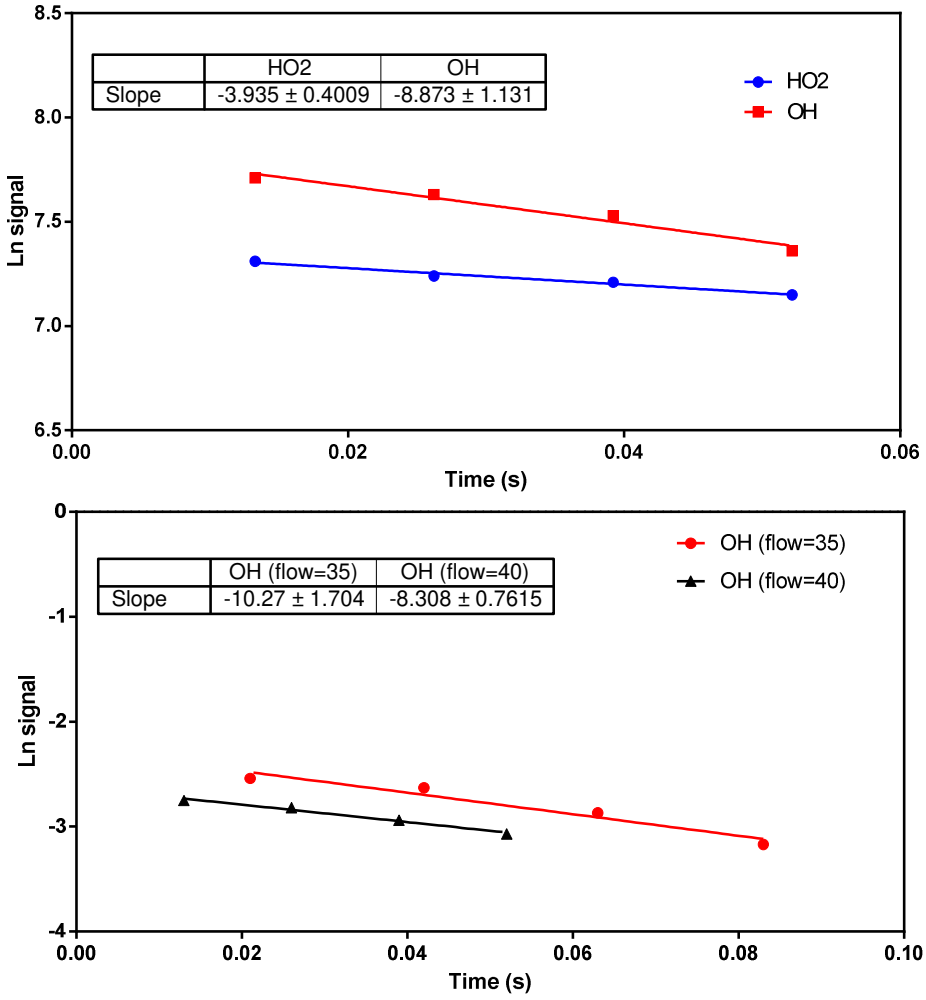

Figure IV- 4:upper graph represents theOH and HO_2 wall losses as function of the mixture residence time in PC2A calibrator on FAGE instrument. The lower graph shows the OH wall losses in PC2A calibration cell used on CIMS instrument.

OH wall losses found to be consistent using PC2A calibrator on both instruments, the average OH wall losses were found to be 9.1 s^{-1}. A NO flow of 80 sccm (4.3 x 10^{14} molecule.cm^{-3}) was injected downstream the first cell to measure the variation of the HO_2 signal in the HO_2 cell. The high concentration of NO enables the complete conversion of HO_2 into OH in the cell. The upper graph of Figure IV- 4 shows the evolution of the HO_2 signal as function of the lamp position and the losses were found to be about 4 s^{-1}. The normal calibration experiments in the laboratory where done with

lamp positioned on the first window where the wall losses for both radicals are expected to be minor. The wall losses of the radicals generated in PC2A calibration cell are summarized in Table IV-4.

Table IV- 4: OH and HO_2 wall losses in PC2A calibration cell for different lamp positions through the calibrator, the total flow was set to be 40 slm.

	loss rate (s^{-1})	9.10	4.00
Cell X	t, s	remaining OH	remaining HO_2
6	0.013	0.89	0.95
12	0.026	0.79	0.90
18	0.039	0.70	0.86
24	0.052	0.62	0.81

IV.3.1.2 Effect of water vapor concentration on HO_x calibration

A change in sensitivity with varying water vapor concentration is expected in the FAGE instrument due to changing quenching phenomenon. Quenching occurs when excited OH collides with molecules such as H_2O and results in a reduction in the fluorescence lifetime of OH. This water vapor -dependent behavior can be corrected by calculating the quenching as a function of the water vapor concentration. The measurements can then be corrected for this quenching effect as a function of the water concentration measured according to the equation (Amédro, 2012a):

$$C(H_2O) = -0.005 \times [H_2O]^2 - 0.0819 \times [H_2O] + 1 \qquad \text{Eq IV- 1}$$

The dependence of the UL-FAGE instrument on water vapor has been investigated previously (Amédro, 2012a). The OH and HO_2 sensitivity were measured over a large range of humidity between 0 up to 2.5 % of mixing ratio. The results show a polynomial dependence of the sensitivities of the FAGE to $[H_2O]$, with both sensitivities (OH and HO_2, respectively in OH cell and HO_2 cell) decreasing more with increasing water concentration than would be expected due to the quenching of OH by H_2O alone. The following dependence has been determined:

$$C(H_2O) = -0.05 \times [H_2O]^3 + 0.34 \times [H_2O]^2 - 0.86 \times [H_2O] + 1 \qquad \text{Eq IV- 2}$$

The reasons for this dependence are not clear: it can be due to a decrease of the FAGE instrument sensitivity or an artifact during the calibration. As previous comparisons with other instruments (Forschungzentrum FAGE instrument, LPC2A CIMS instrument) in atmospheric conditions have shown a good correlation between the instruments within a large range of humidity, the decrease of sensitivity of the UL-FAGE instrument can be discarded. This unexpected dependence is thus

probably due to an artifact in the calibration. Until now, the correction of the calibration factor by the polynomial dependence has been considered to determine the equivalent sensitivity in dry conditions and calibrations have been done at low humidity to limit the HO_x concentration and the correction.

The artifact observed during the earlier calibration could be due to radical-radical reactions between the calibration cell and the nozzle (due to possible turbulences leading to higher residence time than calculated) or to saturation of the detectors as these experiments have been done at very high OH concentrations (high lamp flux and high water vapor level). However, the experiments have been done in conditions limiting this saturation by delayed detection, and so the detector saturation is probably not the reason. In order to check if the method used is still consistent, several calibrations were done to analyze the water dependence effect on the sensitivity. The water concentration was varied using a homemade bubbler which limits the measurements to low humidities (the water vapor generator used during the previous tests was not available anymore in the laboratory). As shown in Figure IV- 5, the effect of water vapour on the instrument sensitivity is not considerable within the water concentration range tested.

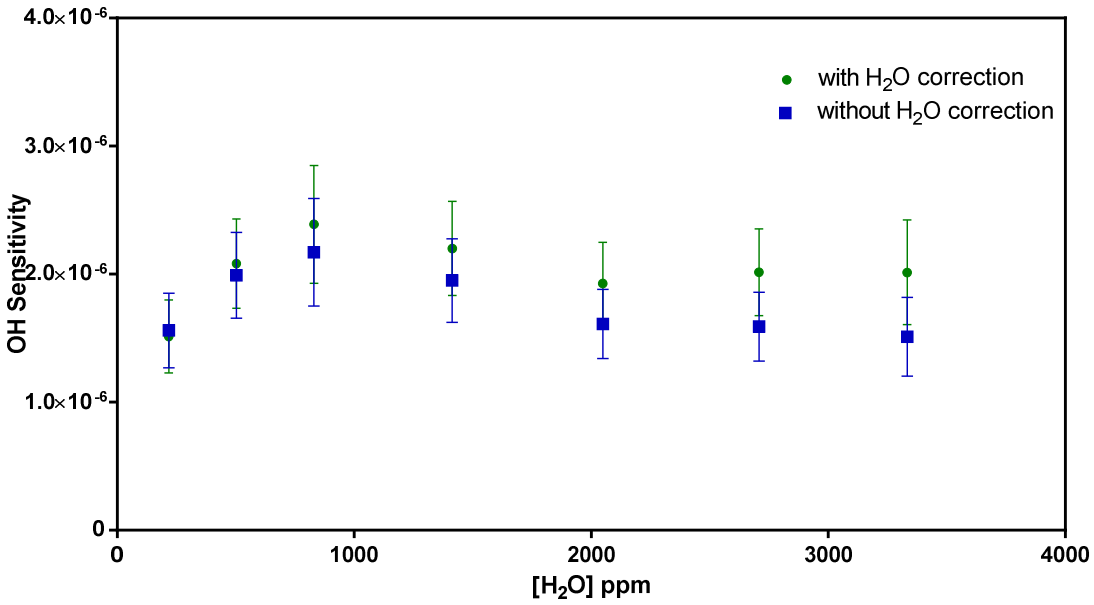

Figure IV- 5: effect of the water vapour on the LIF signal for small range of water concentration (300-4000 ppm). Green dots include the correction for H_2O quenching, using equation IV-2

The experiment was repeated several times and the results were reproducible. The correction using the polynomial dependence of H_2O has been used during my thesis but as only a low range of relative humidity (between 0.5 up to 5 % at ambient temperature about 22 °C) is used, this correction is weak.

The next step is to investigate the same measurement on a larger range of water concentration using a humidity generator similar to the one used at the LPC2E (under acquisition in PC2A) and adding CO to study the radical-radical reactions and reanalyze this behavior.

IV.3.2 LPC2E calibration cell on the UL-FAGE

The LPC2E calibration cell has been installed on the top of the FAGE and measurements varying the lamp flux, the humidity and the total flow were performed. Most of the tests were performed with a constant flow (24 L/min) used normally to calibrate the CIMS instrument. The lamp was fixed on the exit of the calibrator during the entire intercomparison.

IV.3.2.1 FAGE response as a function of the lamp flux at constant humidity

The first test consisted in varying the lamp flux with a constant relative humidity equal to 18 %. To vary the lamp flux, the LPC2E calibration cell is equipped with a N_2O filter located between the photolysis region and the mercury lamp. The lamp flux was measured by a photodiode placed in front of the mercury lamp on the other side of the calibration cell. Under these conditions, [OH] and [HO_2] produced varied between 2 × 10^7 and 6 × 10^8 cm^{-3}. The results are shown in Figure IV- 6(the measured radicals with the FAGE considering our calibration factor are plotted versus the calculated ones provided by the LPC2E). Calculated radical concentrations were done using N_2O actinometry. All the data were corrected to the water quenching for experiments done with LPC2E calibrator.

	HO_2	OH
Slope	1.061 ± 0.06537	0.8545 ± 0.07877
Y-intercept when X=0.0	2.370e+007 ± 1.741e+007	-5.002e+006 ± 2.554e+007

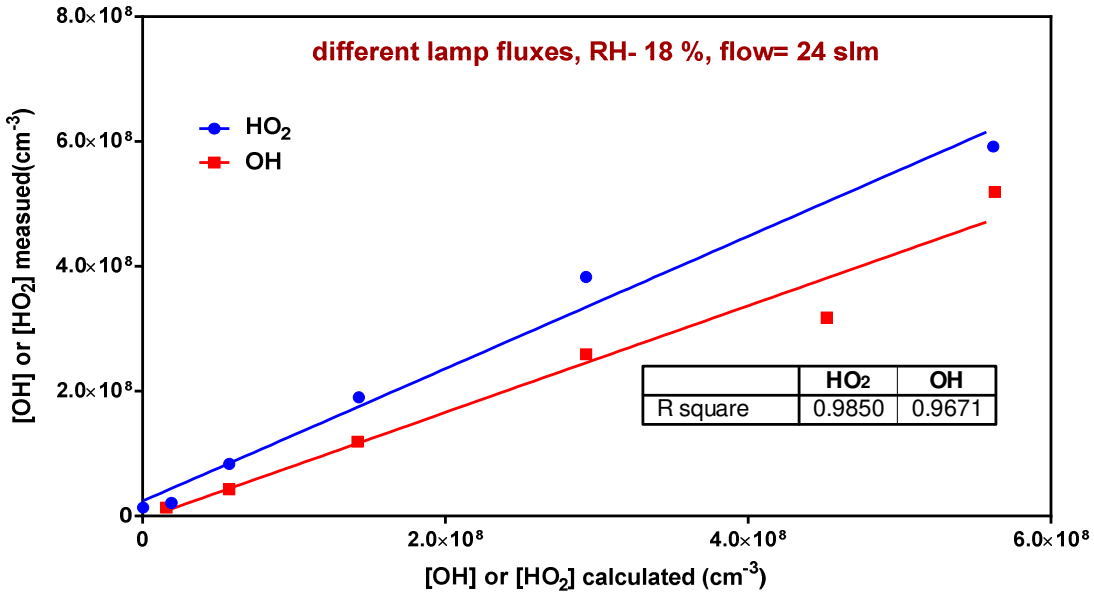

Figure IV- 6: Radical concentrations measured by UL-FAGE with the calibration cell of the LPC2E as the function of the calculated radical concentrations from the LPC2E with different lamp flux and constant humidity and flow rate. OH contribution is subtracted from the HO_2 measurement in HO_x mode (NO = 4.3×10^{14}).

Figure IV- 6 shows that the concentration measured by the UL-FAGE is consistent with the calculated concentration generated by the LPC2E calibration cell. The agreement is very good with the slope of 1.06 and 0.85 for HO_2 and OH radicals respectively. The linear fit shows a small offset which is within the uncertainty of the value provided by the fit calibration for both cells.

IV.3.2.2 FAGE response as a function of the calibration cell flow at constant lamp flux

In the second test, flow rates were varied between 24 and 47 L/min with a constant humidity of approximately 20 % and a constant UV lamp flux. This test had two purposes: to test the response of the FAGE with different operating conditions of the calibration cell and to ensure that the air probed by the FAGE comes only from the calibration cell.

	HO_2	OH
Slope	1.260 ± 0.4340	1.045 ± 0.1294
Y-intercept when X=0.0	-5.267e+007 ± 2.093e+008	3.097e+007 ± 6.662e+007

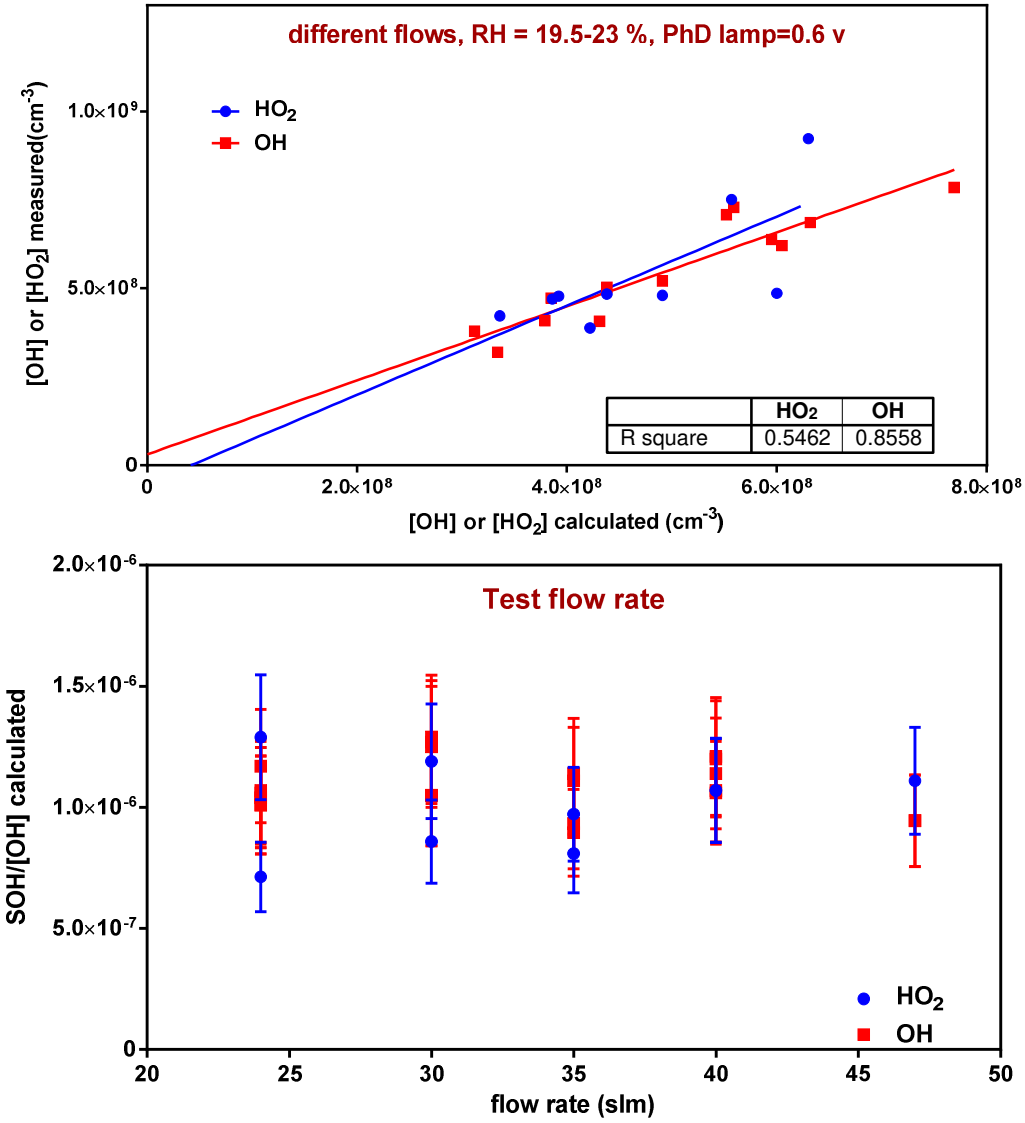

Figure IV- 7: Measured radical concentrations by the UL-FAGE as function of the calculated radical concentrations with different flow rates entering the calibration cell (upper graph) and measured signal normalized by the calculated concentrations as function of the flow rates used (lower graph).

As shown in the upper graph of Figure IV- 7, the measured OH and HO_2 concentrations by the FAGE and the calculated ones from LPC2E cell shows a good agreement. The linear fit gives a slope of 1.2 and 1.04 respectively for OH and HO_2, but the uncertainty on the HO_2 measurement was high with a high offset while for the OH measurement the offset was in the range of uncertainty of the calibration (≈ 20%).The lower graph of Figure IV- 7 shows the measured OH and HO_2 signal by the UL-FAGE instrument normalized by the calculated OH concentration from LPC2E calibrator versus the different total flows used (24, 30, 35, 40, 47 slm). For all the different flows, the measured signal normalized by the calculated radical concentrations was in the same range varying between 8×10^{-7}

to 1.2 × 10^{-6} counts $s^{-1}cm^3$. This means that with different range of flows, all the sampled air entering the FAGE cells is coming exclusively from the calibration cell, even at the lowest total flow.

IV.3.2.3 FAGE response as a function of the humidity in the calibration cell

A third experiment was conducted with the same calibrator in which the flow rate (24 slm) and the UV lamp flux were kept constant, and the relative humidity was varied over a wide range (1 to 70 %).The relative humidity of the air injected in the calibrator was varied by varying the water mass flown through the liquid mass flow controller (Bronkhorst) and measured by an humidity sensor. As for the previous analysis, the radical concentrations measured by the FAGE were plotted versus the calculated concentrations (Figure IV- 8).

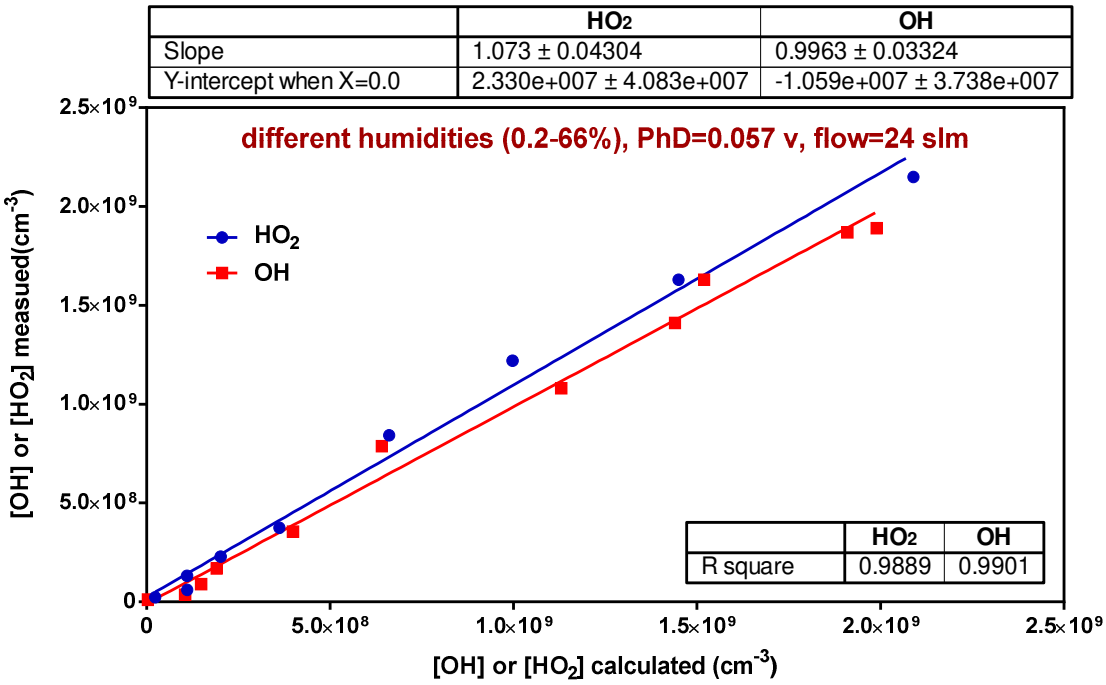

Figure IV- 8: OH and HO_2 signal measured in the FAGE as a function of the calculated concentrations varying the humidity, OH contribution to HO_2 cell was subtracted. Quenching sensitivity was used for the measured concentrations.

Similarly, to previous tests, we obtain a very good agreement between the measured concentration and the calculated one showing the consistency between the calibration cells used at PC2A and LPC2A despite the different design and concentration ranges generated. The linear regression gives a slope of 0.99 and 1.07 for OH and HO_2 radicals respectively with a correlation coefficient R^2, of 0.99 for OH and 0.98 for HO_2.

One further experiment was done, where the humidity and the lamp were varied in order to keep approximately the same HO_x radicals concentration. This test has been performed to see if the variation of the humidity influences the response of the instrument and it was found that at

maximum humidity the change coming from quenching is 10 %. The relative humidity varied between 21 and 60 %, while the lamp flux changed from 10 to 100 % with a constant total flow rate (24 L/min). The comparison between the calculated and the measured concentrations are shown in Figure IV- 9.

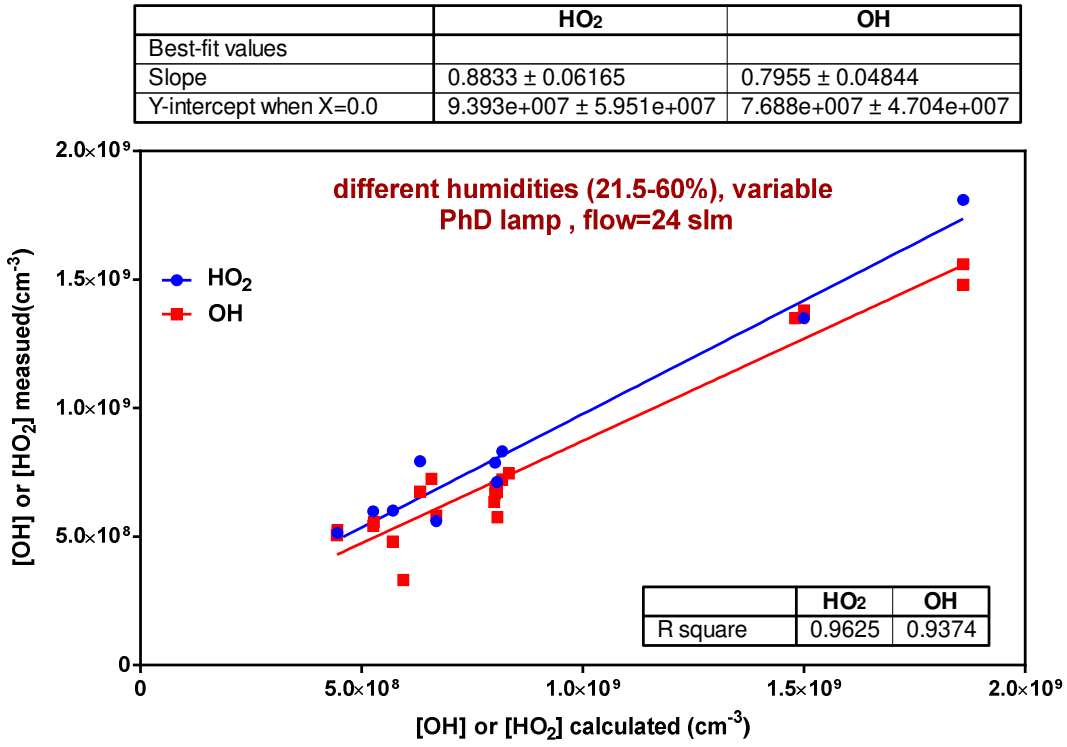

Figure IV- 9: Measured radicals by the UL-FAGE as a function of the calculated radical concentrations with different lamp flux and humidity generating approximately constant radical concentrations. OH contribution is subtracted from the HO_2 measurement (NO = 4.3×10^{14}).

The linear fit of OH and HO_2 radicals gives a slope of 0.79 and 0.88 respectively, which agrees with the other tests. However, agreement is a bit worse, probably due to the small range of concentration studied. Therefore, despite the large range of humidities used and low radical concentrations generated, the results showed a good agreement with the previous tests.

In order to conclude, the set of all the experiments performed with the LPC2E calibration cell were plotted together (Figure IV- 10). The HO_x radicals generated in the different conditions varied between 1.5×10^7 and 2×10^9 molecule.cm^{-3}. The comparison between the measured concentrations by UL-FAGE and the calculated concentration indicates a very good agreement. The linear regression fit through these data has a slope of 0.93 and 0.99 for OH and HO_2 radicals respectively with a correlation coefficient, R^2, of 0.95 for OH and 0.96 for HO_2. The offset is close to zero considering the uncertainty of the fit.

	HO_2	OH
Slope	0.9992 ± 0.03485	0.9319 ± 0.03454
Y-intercept when X=0.0	4.220e+007 ± 2.669e+007	2.315e+007 ± 2.784e+007

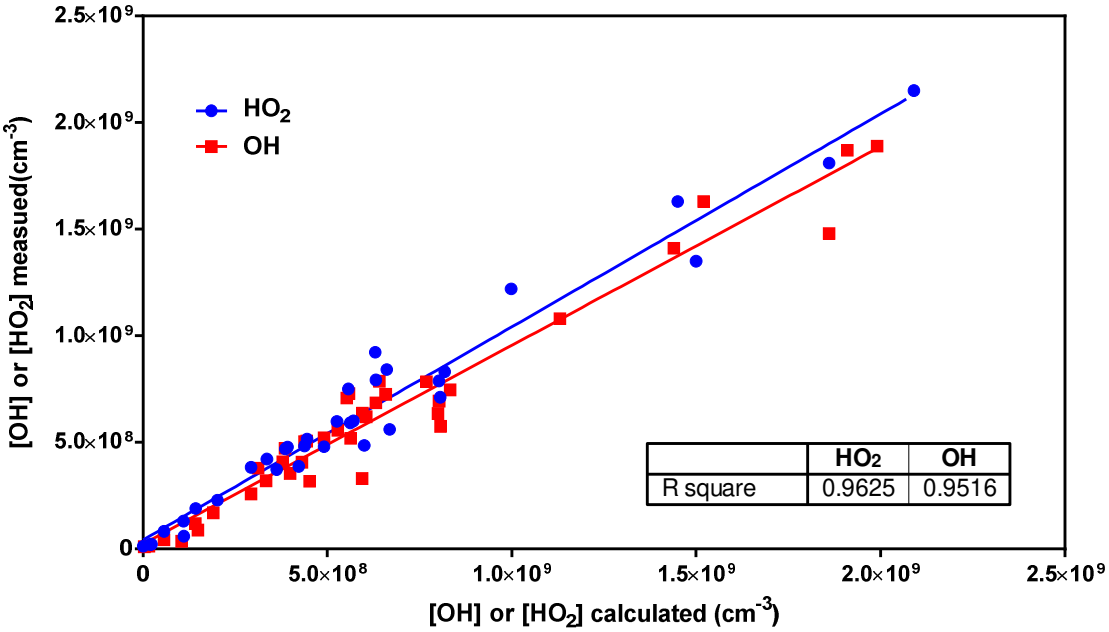

Figure IV- 10: Summary of the data from all the experiments that have been done with LPC2E calibration cell. The measured concentration of radicals is plotted versus the calculated concentrations based on LPC2E calibrator.

As a conclusion, there is a very good agreement between PC2A and LPC2E calibration cells, this gives us confidence in the absolute instruments calibration with both calibration cells. Similar tests were done with IMT Mines Douai calibration cell.

IV.3.3 IMT Lille Douai calibration cell on the UL-FAGE

The same experiments and methodologies were done using the IMT-Lille-Douai calibration cell under similar conditions than those used with LPC2E calibrator except for the flow variation as the one normally used on the PERCA is close to the one used in our calibration cell (35 L/min and 40 L/min) and no effect of the flow between 24 and 40 L/min has been found with the LPC2E calibration cell. As the calibration cell is used with the lamp at a position of 22 cm from the exit for PERCA calibrations, tests have been made at this position as well as close to the exit.

IV.3.3.1 Determination of the wall losses

In order to determine the wall losses and correct the calculated concentrations, measurements have been made with the FAGE and the mercury lamp on the IMT calibration cell at different positions. The lamp was moved along the calibrator with all other conditions constant. The obtained results are shown in Figure IV- 11.

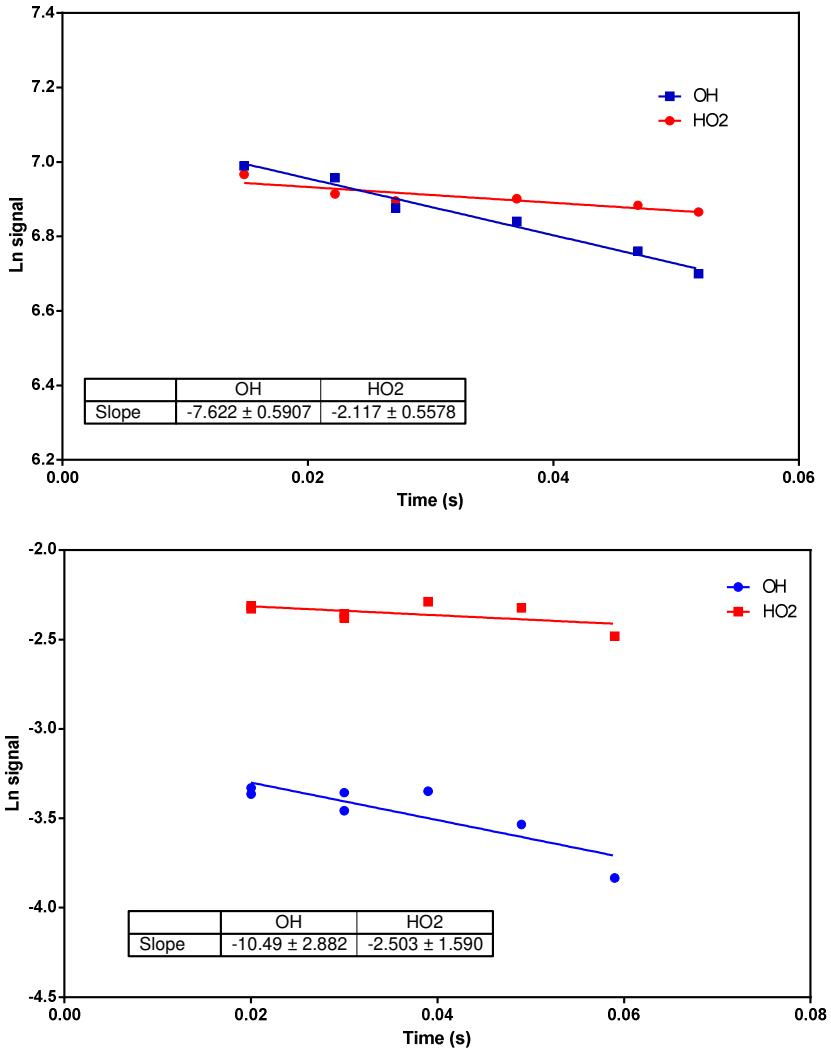

Figure IV- 11: Wall losses on the IMT-Lille-Douai calibration cell. The upper graph represents the results using the calibrator on the FAGE instrument, while the lower graph represents the results using the CIMS instrument.

As expected, the losses obtained for HO_2 radicals were less than the losses for OH radicals using the IMT-Douai calibration cell. Similar results have been found on the UL-FAGE and the CIMS instrument. The average losses were 9 s^{-1} and 2.3 s^{-1} for OH and HO_2,respectively (Figure IV- 11) Comparing these results of IMT-Douai calibration cell to the results found for PC2A calibration cell shown in Figure IV-4 (OH losses = 9.1 s^{-1}, HO_2 losses = 4 s^{-1}), we found that the two calibration cells show the same behavior and have almost the same wall losses for OH and HO_2 radicals respectively.

Table IV- 5 shows the summary of the losses in percentage as function of the lamp position for IMT-Douai calibration cell used the losses determined with the UL-FAGE or the CIMS instrument.

Table IV- 5: Comparison for the OH and HO_2 wall losses effect in the IMT-Douai calibration cell determined with the UL-FAGE or the CIMS instrument. The total flow was fixed at 35 slm.

loss rate (s^{-1})	10.50	2.50	7.60	2.10

Cell X	t, s	remaining OH using CIMS	remaining HO_2 using CIMS	remaining OH using FAGE	remaining HO_2 using FAGE
6	0.015	0.86	0.96	0.89	0.97
8	0.020	0.81	0.95	0.86	0.96
12	0.030	0.73	0.93	0.80	0.94
10	0.025	0.77	0.94	0.83	0.95
14	0.035	0.70	0.92	0.77	0.93
16	0.039	0.66	0.91	0.74	0.92
20	0.049	0.60	0.88	0.69	0.90
22	0.054	0.57	0.87	0.66	0.89
24	0.059	0.54	0.86	0.64	0.88

The determined correction for OH and HO_2 radicals due to wall losses vary by less than 10 % and 1 % respectively for different experiments using UL-FAGE and CIMS instruments (Table IV- 5). This slight difference may come from a change in the wall conditions of the calibration cell with time (tests with FAGE were carried out in June 2018, tests with CIMS was carried out in September 2017.

IV.3.3.2 FAGE response as a function of the calibration cell lamp flux

During the first calibration test, the water concentration (Figure IV- 12) and the flow rate were kept constant. The concentration of the generated HO_x radicals were varied by changing the lamp flux by varying the voltage applied to the lamp (110 to 220 v) using a variac while the total flow was adjusted to be 35 slm as normally used to calibrate the PERCA instrument. Same calibration was done under different humidites which range from 16 % to 60 %.

All the measured concentration data were corrected for the water quenching for all the experiments done with IMT-Douai calibrator. The lamp housing was placed 21 cm from the exit of the calibrator. Under such conditions, produced OH and HO_2 concentrations varied between of 9×10^8 to 1×10^{10} molecule.cm^{-3}.

	RH = 25 %	RH = 17 %	RH = 55 %	RH = 60 %
Slope	1.002 ± 0.07206	0.7020 ± 0.04043	0.9674 ± 0.03940	0.8226 ± 0.02936
Y-intercept when X=0.0	7.526e+008 ± 1.694e+008	6.686e+008 ± 6.404e+007	1.631e+009 ± 2.014e+008	3.079e+009 ± 1.616e+008

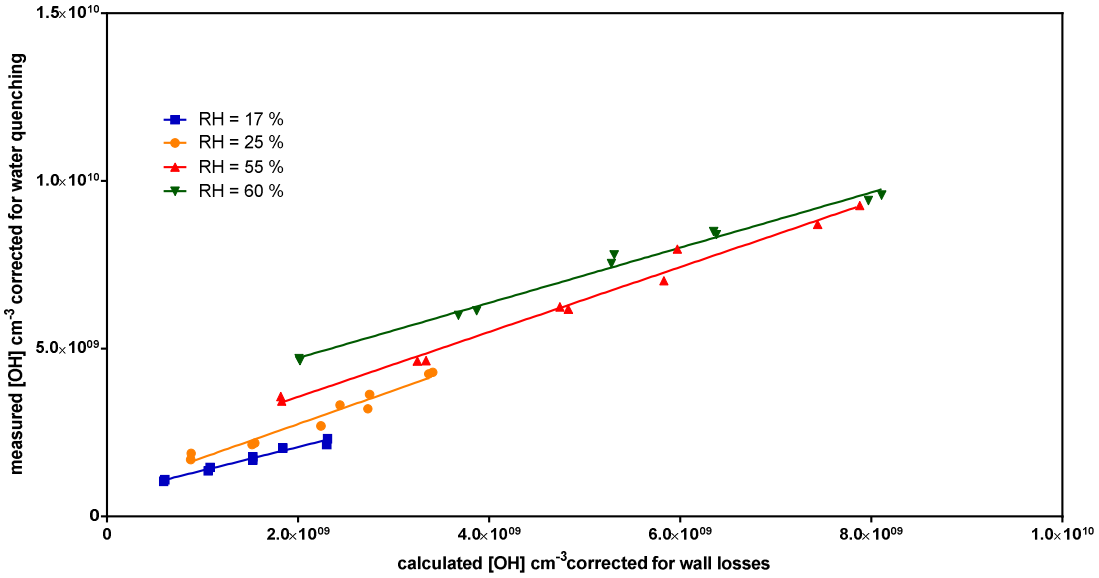

	RH = 17 %	RH = 25 %	RH = 55 %	RH = 60 %
Slope	0.2449 ± 0.02404	0.3169 ± 0.03954	0.2772 ± 0.04777	0.2299 ± 0.04531
Y-intercept when X=0.0	3.188e+008 ± 6.477e+007	4.919e+008 ± 1.571e+008	8.413e+008 ± 4.682e+008	1.706e+009 ± 4.738e+008

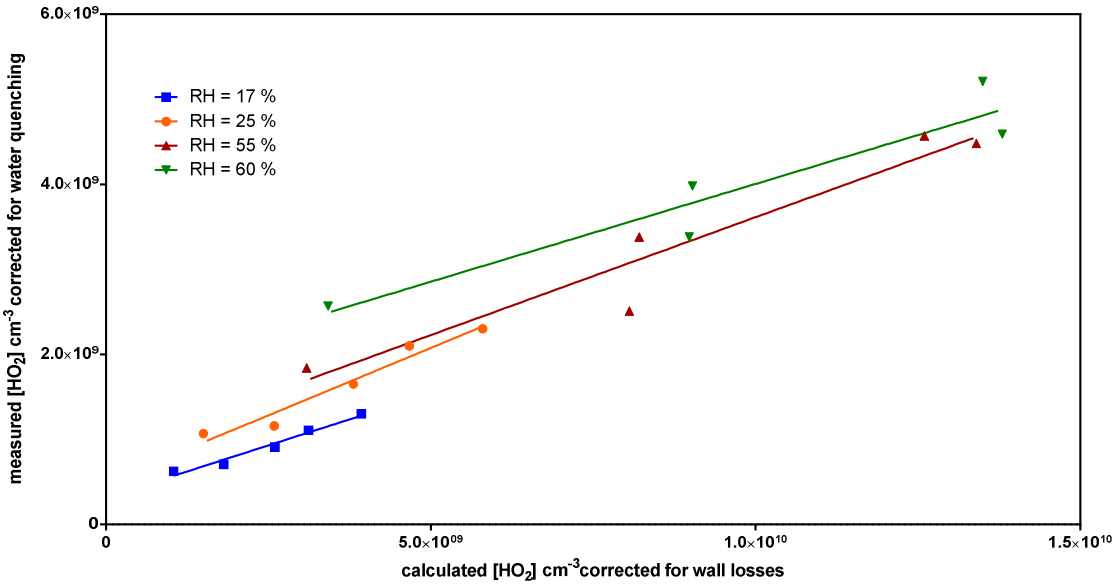

Figure IV- 12: Measured OH (upper graph) and HO_2 (lower graph) concentrations by UL-FAGE as function of the calculated OH and HO_2 concentrations. The total flow is 35 slm, and the Hg lamp position on x = 21 cm.

The obtained results are shown inFigure IV- 13, where measured OH and HO_2 concentrations are plotted versus the calculated ones. The calculated HO_x concentrations were corrected for the wall losses determined for the IMT-Douai calibration cell. The results showed different slopes for OH and HO_2 radicals with different humidities (Figure IV- 12), and high y-intercepts. Therefore, the results were inconsistent. This inconsistency is thought to be coming from the variation of the lamp voltage.

For this reason, the effect of the different voltages applied to the lamp has been analyzed by plotting the same results for each voltage separately at the different humidities.

	110 v	140 v	170 v	190 v	220 v
Slope	2.311 ± 0.1816	1.624 ± 0.08491	1.494 ± 0.06995	1.375 ± 0.05174	1.214 ± 0.04256
Y-intercept when X=0.0	-3.115e+008 ± 2.652e+008	-3.577e+008 ± 2.271e+008	-5.536e+008 ± 2.681e+008	-4.345e+008 ± 2.402e+008	-2.455e+008 ± 2.520e+008

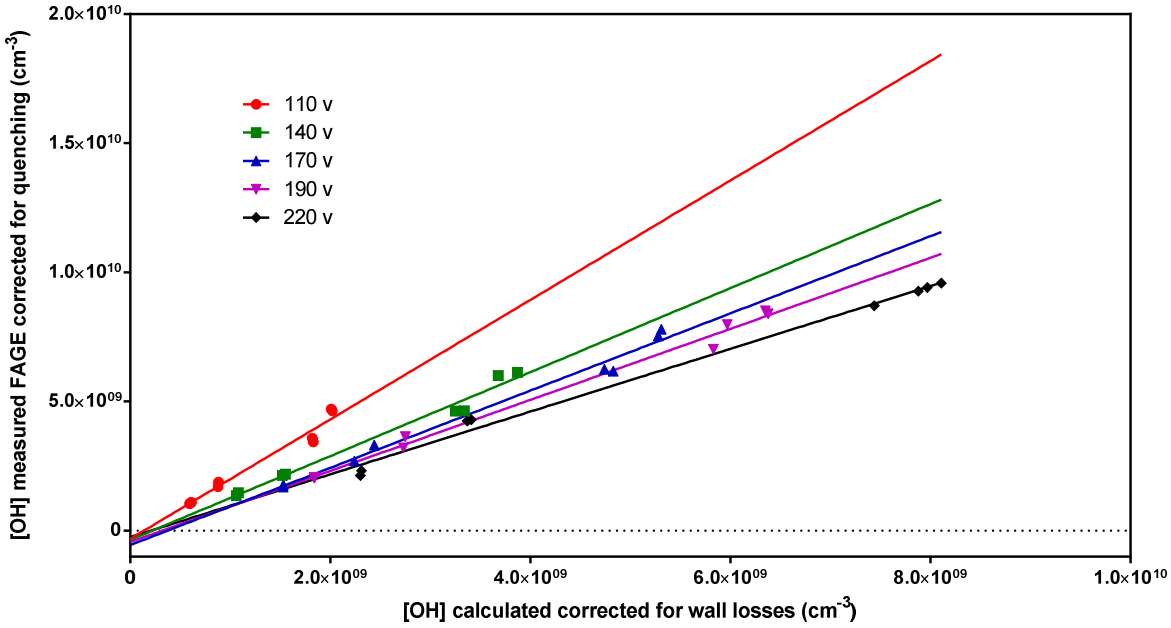

	110 v	140 v	170 v	190 v	220 v
Slope	0.7097 ± 0.1252	0.5250 ± 0.04990	0.4583 ± 0.02413	0.4565 ± 0.03094	0.3719 ± 0.02496
Y-intercept when X=0.0	-8.100e+007 ± 3.109e+008	-2.459e+008 ± 2.306e+008	-2.066e+008 ± 1.559e+008	-1.818e+008 ± 2.447e+008	-3.648e+007 ± 2.490e+008

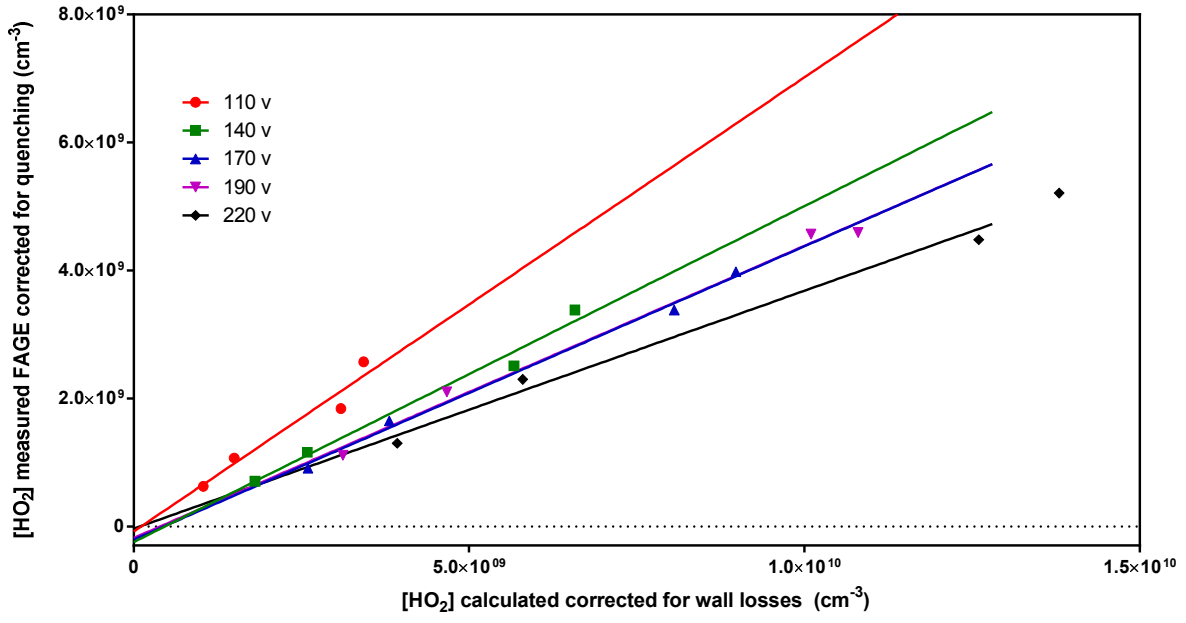

Figure IV- 13: Measured OH (upper graph) and HO_2 (lower graph) concentrations by UL-FAGE using the IMT-Douai calibration cell as a function of the calculated OH concentrations by varying the mercury lamp voltage.

The obtained results showed that for OH measurements, there is a good agreement between the measured and calculated concentration with lamp voltage at 220 V with a slope of 1.2 (within the

uncertainty of the calibration). However, with decreasing lamp voltage, the disagreement between the measured and the calculated concentrations becomes more important as shown in the upper graph of Figure IV- 13, the slope increases from 1.2 at 220 V to 2.3 at 110 V.

Similar results were observed for the HO_2 measurements, the obtained slopes for the different lamp voltage conditions were increasing as the lamp voltage decreased (from 0.37 at 220 Vto 0.7 at 110 V) as shown in the lower graph of Figure IV- 13. However, there is a strong disagreement between the measured and calculated HO_2 concentrations even at lamp voltage 220 V. The y-intercepts for OH and HO_2 measurement of different lamp voltages were close to 0 and within the uncertainty given by the fit.

From these results, we can conclude that the generated OH and HO_2concentrations were significantly affected by the variation of the lamp voltage, which involves probably a change in the spectral distribution of the lamp. Thus, we cannot conclude on the tests at different lamp fluxes and all the following tests were done with a lamp voltage of 220 V.

IV.3.3.3 FAGE response as a function of the calibration cell humidity

The OH and HO_2 concentration generated by the IMT-Douai calibration cell were measured with a constant lamp flux (voltage applied=220 V). HO_x radical concentrations were varied by adjusting the fraction of air passing through the bubbler to produce different water concentrations from RH= 17 % to 70 %. A LI-COR 840A instrument measured the water concentrations in the calibration cell. The experiment was done for 2 different lamp position on the calibrator: 1) - near the exit at position 1 (x=7 cm from the exit, measured at the center of the exposure zone), 2) - 21 cm from the exit (position 2). The obtained results are shown in Figure IV- 14. Tests adding CO have been performed to study the potential radical-radical reactions effects comparing HO_2 results without CO (presence of OH) and with CO (only HO_2).

	OH	HO2	HO2 (CO added)
Slope	1.035 ± 0.03423	1.059 ± 0.1701	1.004 ± 0.04659
Y-intercept when X=0.0	7.967e+007 ± 3.558e+008	-5.259e+008 ± 1.750e+009	-5.054e+008 ± 9.636e+008

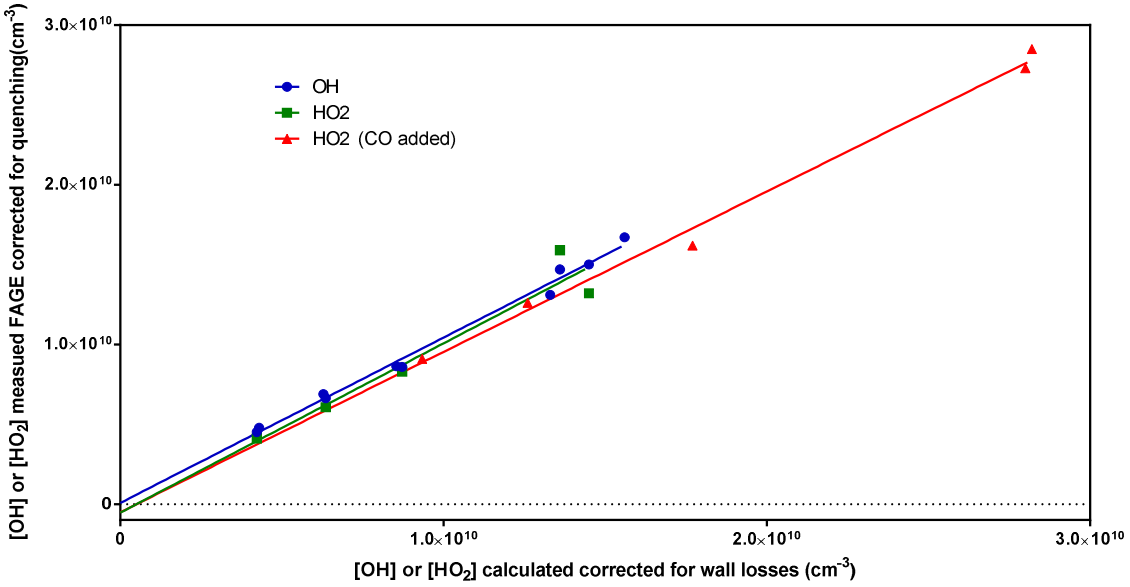

	OH	HO2	HO2 (CO added)
Slope	1.152 ± 0.05695	0.5842 ± 0.07945	0.5336 ± 0.04959
Y-intercept when X=0.0	2.806e+008 ± 2.764e+008	3.064e+008 ± 6.143e+008	6.350e+008 ± 7.671e+008

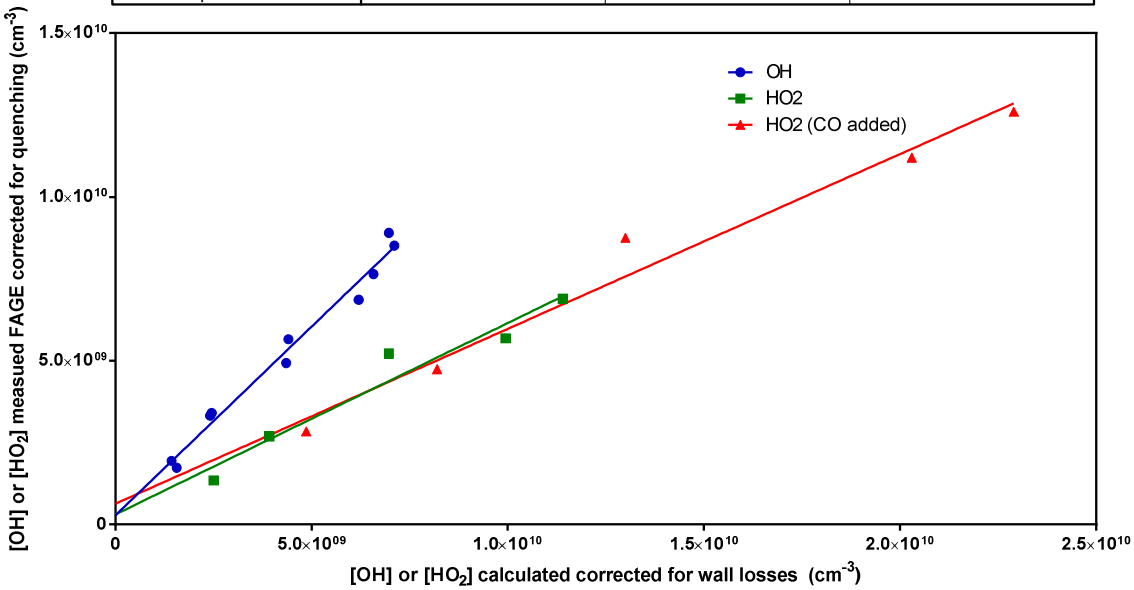

Figure IV- 14: Measured HO_x radicals by UL-FAGE as a function of the calculated concentration (upper graph represents lamp position 1 while the lower graph represents lamp position 2). OH contribution is subtracted from the HO_2 measurement (NO = 4.3×10^{14}).

The upper graph of Figure IV- 14 shows that the measured concentrations of OH and HO_2 radicals are in a good agreement with the calculated ones where we obtain slope of 1.03, 1.05, and 1.0 for OH, HO_2 in presence of OH, and HO_2 alone with CO addition respectively. The calculated concentrations are corrected by the wall losses. The linear regression has non-zero intercept which is in the range of the uncertainty given for the value. Under these conditions where the lamp is at the minimum

position on the calibrator (x = 7), the wall losses are very small and can be considered negligible. Therefore, the two calibration cells are in a good agreement.

On other hand, the lower graph represents the experiment when the lamp was adjusted to a higher position (21 cm from the exit of the calibrator, similarly to previous tests). We observe that the OH concentrations tends to be in reasonable agreement with slope equals 1.15 compared to the first condition with lamp at x = 7 cm. This slope is similar to what was obtained with the previous experiment changing the lamp voltage (slope =1.21 with 220 V, upper graph of Figure IV- 13). Therefore, there is reproducibility for the different experiments under the same experimental conditions.

HO_2 measurements showed strong differences between the measured and calculated concentrations as it has been observed in the previous tests but with a higher slope of 0.58. Results with and without CO are in agreement with slopes of 0.58 and 0.53 showing that radical-radical reactions are not responsible of this disagreement. This behavior is strange and was not expected as the losses had been characterized in similar conditions and corrections applied. No clear explanation can be provided and more experiments are still needed to understand the origin of the disagreement only observed with the lamp at far distance from the exit.

However, the results obtained for the lamp position near the exit of the calibration cell are in agreement with PC2A calibration cell (used also near the exit) which gives confidence in the calibration procedure.

IV.3.4 Summary of the results on the HO_x measurements

The overall goal of this study was to improve the confidence of current OH calibration cells through an intercomparison between three different cells. The tests performed with the different calibration cells have shown that:

I. There is an excellent agreement between PC2A and LPC2E calibration cells under different conditions, the linear regression fit through all the data obtained by LPC2E calibrator data has a slope of 0.93 and 0.99 for OH and HO_2 radicals, respectively with a correlation coefficient, R^2, of 0.95 for OH and 0.96 for HO_2.

II. The PC2A and IMT-Douai intercomparison showed that there is a very good agreement for the HO_x tests done with lamp position on x = 7 cm and less good agreement for HO_2 measurement for lamp position on x = 21 cm with inconsistencies between the walls losses

measurements and the correlation between measured and calculated concentrations. This inconsistency is not due to radical-radical reactions and needs to be understood.

Another possible application of the calibration cells is the generation of known concentrations of RO_2 when VOCs are added. It has been used to characterize the sensitivity of our FAGE to RO_2 and similarly to the tests with HO_x, an intercomparison of the different calibration cells on the RO_2 measurements has been done.

IV.4 Characterisation of the UL-FAGE for RO_2conversion

IV.4.1 State of the Art

As described in Chapter I, peroxy radicals are produced in the troposphere from the oxidation of VOCs by OH radicals (or O_3 or NO_3) and are present in the atmosphere in similar concentrations as HO_2.

For a long time, it was thought that the FAGE instruments were only selective to HO_2 radicals when adding NO and the reactions that convert peroxy radicals to HO_2 in the presence of NO at low pressure were too slow (Fuchs, 2006). Indeed, laboratory experiments investigating C1 to C4 alkyl peroxy radicals did not suggest a significant interference (Faloona et al., 2004; Kanaya et al., 2001). Therefore, it was assumed that other peroxy radicals would follow the same behavior. More recently, the conversion of more complex peroxy radicals to OH upon reaction with NO in FAGE detection cells (Fuchs et al., 2011; Whalley et al., 2013) have shown a significant enhancement of the HO_2 signal in the presence of RO_2 derived from double bounds or aromatic hydrocarbons due to a conversion faster than expected.

The RO_2 interferences on HO_2 measurements identified in Leeds and Jülich FAGE instruments have initiated the study of RO_2 conversion to HO_2 in the different FAGE instruments and the potential use of this interference for some RO_2 quantification measurements (Whalley et al., 2016, 2013). The overall rate at whichRO_2 isconverted to OH and the magnitude of the interference depends on the residence time and the NO concentration injected. The comparison done by Fuchs et al., 2011 with two nozzles shows that the inlet nozzle (and then the pressure) has a strong effect on the conversion of peroxy radicals. Also, calculations based on the Master Chemical Mechanism have been used to determine reaction times in the cells. And then, the modelled profiles have been compared with measured ones for RO_2 conversion with the measurements (Figure IV- 15).

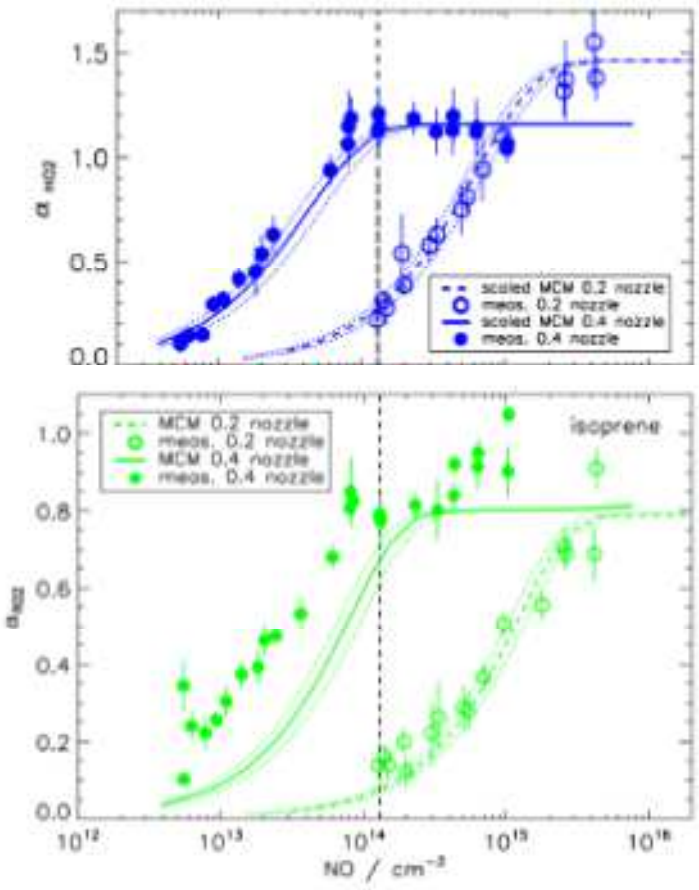

Figure IV- 15: Relative detection sensitivity for HO_2 (upper panel) and RO_2 (lower panel) radicals produced by isoprene depending on the NO concentrations in the detection cell. 2 types of nozzles were tested and compared to MCM model (Fuchs et al., 2011)

The lower graph of Figure IV- 15 shows the measured dependence of the conversion efficiency of peroxy radical derived from isoprene as function of NO concentration, which was globally in agreement with the model when using the 0.2mm nozzle. However, the RO_2 conversion predicted by the model were smaller that the measured ones in case of isoprene with a 0.4 mm inlet nozzle with reactions probably faster in reality than in the model (Fuchs et al., 2011).

Moreover, the effect of water vapor mixing ratios on RO_2 detection sensitivity was tested. It was reported that the relative detection sensitivity for isoprene peroxy radicals does not show any significant trend with the water vapor mixing ratios for both inlet nozzles. Finally, Fuchs et al. concluded that interference from RO_2 species can be significantly reduced if the reaction time and the NO concentration in the detection cell are reduced.

As the interference differs between different nozzles for the same instrument, it will also differ from one FAGE instrument to another, depending on the instrumental configuration.This interference has

been characterized in the UL-FAGE during my thesis for different nozzles as well as the potential of using variable NO concentrations to selectively measure HO_2 and the contribution of some RO_2.

IV.4.2 Protocol to generate and study the RO_2 interference

The quantification mode (2 cells on top of each other) has been used for these experiments with the calibration cell on top of the FAGE nozzle. Different conditions are used in the calibration cell in order to generate mixtures of OH/HO_2 (HO_x mode), HO_2 (HO_2 mode), and HO_2/RO_2 (HO_2* mode: HO_2 + contribution of some RO_2).

In the first cell, OH alone in measured whereas in the second cell OH (without NO above the second cell) or OH/HO_2 (NO addition above the second cell) respectively are measured during the HO_x generation. To characterize the interference due to the RO_2 in the HO_2 cell of the UL-FAGE, different VOCs (isoprene, toluene, methane, butane) have been injected in the calibration cell (Figure IV- 16), their reaction with OH in presence of O_2 produce RO_2 radicals. High enough concentrations of hydrocarbons were introduced to completely consume OH, so that $[RO_2] \approx [HO_2]$. The HO_2 radical signal is subtracted from the RO_2 signal to calculate the RO_2 radical interference. A set of experiments has been done by adding CO (or methanol) instead of VOCs to convert all OH radicals into HO_2. The conditions that were used to study the RO_2 interference to HO_2 measurements are listed in Table IV-6.

Table IV- 6: measurement conditions in the UL-FAGE instrument

MODE	Added Reagent in the calibration cell	Species at the output of the calibration cell	Signal S1 measured in the FAGE cell 1 (OH cell = cell 1)	Signal S2 measured in the FAGE cell 2 (HO_2 cell = cell 2)
HO_x	Humidified zero air	OH/HO_2	$S1_{OH}$	$S2_{\alpha HO2}+S2_{OH}$ (α being the conversion of HO_2 variable as function of the NO level)
HO_2	Humidified zero air +CO (or methanol)	HO_2	x	$2\times S2_{\alpha HO2}$
HO_2^*	Humidified zero air + VOC (called RH)	RO_2/HO_2	x	$S2_{HO2*}$ (=$S2_{\alpha HO2}+S2_{\alpha' RO2}$, α' being the contribution of RO_2 variable as function of the VOC studied and the NO level)

Similarly to the calibration for HO_x described previously, a flow of 40 L/min (at 1 atm, 20°C) of humidified zero air goes through the calibration cell. Reagent gases are introduced to the main flow at the top of the calibration cell (Figure IV- 16). The type of the reagent gas used is selected by a 3 ways valve which is controlled manually and enables to change between the HO_x, HO_2 and HO_2* mode. In the HO_2* mode, hydrocarbons are mixed with the main flow upstream the calibration cell. 10 to 100 sccm of hydrocarbons (controlled by mass flow controllers, Bronkhorst) are added depending on the reactivity of the VOC (to get a reactivity in the range of 500 to 1000 s^{-1}). As the flow reaches the photolysis region, equal amounts of OH and HO_2 are produced by water vapor photolysis. The OH initiates the oxidation of VOCs, creating peroxy radicals in the presence of O_2. The resulting mixture of zero air and VOCs produce identical concentrations of RO_2 and HO_2.

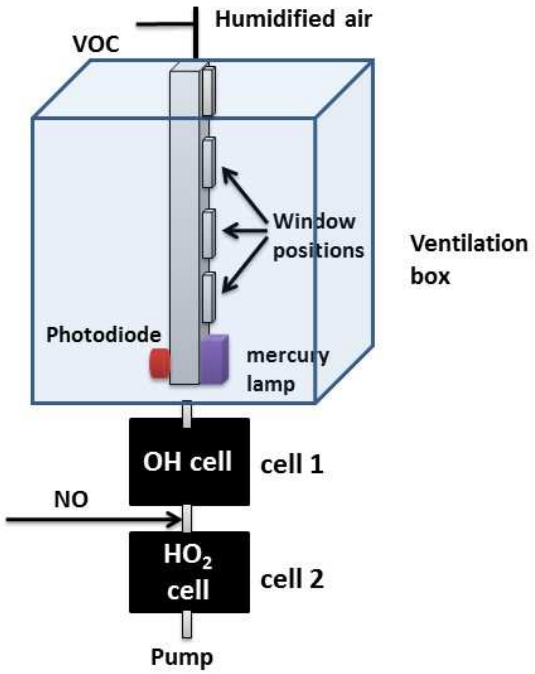

Figure IV- 16: schematic of the experimental setup used to study the RO_2 conversion in the UL-FAGE

The air is sampled from the calibration cell through the nozzle (1 mm) from atmospheric pressure to reduced pressure of 2 Torr. In the first cell which is dedicated to OH measurement, it can be controlled by the absence of the signal that all the produced OH radicals are converted to RO_2 by the absence of signal. Pure nitrogen oxide (NO-99.99%) was injected upstream the second cell to convert HO_2 into OH and potentially the RO_2 also. The NO flow (1-400 sccm) was controlled by a set of mass flow controllers (Brooks and Bronkhorst) which enable the injection of NO at different concentration ranges (3×10^{12} up to 3×10^{15} molecules.cm^{-3} at 2 Torr). The fluorescence signal observed in the second cell in absence of VOC, but with NO added,originates from OH and converted HO_2 (OH + α HO_2), where α is equal to the titration efficiency of Reaction (R I- 13), which is a function of the

amount of NO added and the reaction time in the cell. The experiments in absence of VOC were done over large range of NO to identify the magnitude of interference of RO_2. The relative OH yield from each RO_2 was determined by comparing the HO_2 signal with ($S_{HO2+RO2}$) and without RO_2 (S_{HO2}) as follows:

$$RO_2\ conversion\ efficiency = \frac{S_{HO_2+RO_2} - S_{HO_2}}{S_{HO_2}} \qquad \text{Eq IV- 3}$$

However, for some VOCs, HO_2 is directly formed by its reaction with OH (prompt HO_2) and this contribution has to be subtracted from the signal measured. In that case:

$$RO_2\ conversion\ efficiency = \frac{S_{HO_2+RO_2} - S_{HO_2\ prompt} - S_{HO_2}}{S_{HO_2}} \qquad \text{Eq IV- 4}$$

IV.4.3 Preliminarily tests with CO and methanol

In order to check if the addition of species reacting with OH is efficient in the calibration cell, a first series of tests consisted in injecting species (CO or methanol) which do not produce RO_2 but produce HO_2 with a yield of 1 by reaction with OH in the calibration cell. For the HO_2 mode with CO, pure CO (99.99 %) is injected to the main flow to reach a concentration of about 9.4×10^{15} molecule cm^{-3} in the calibration cell, which is sufficient to convert all OH radicals into HO_2 in the calibration cell(k_{OH}≈1000 s^{-1}). HO_2 is then detected in the HO_2 cell of the FAGE.

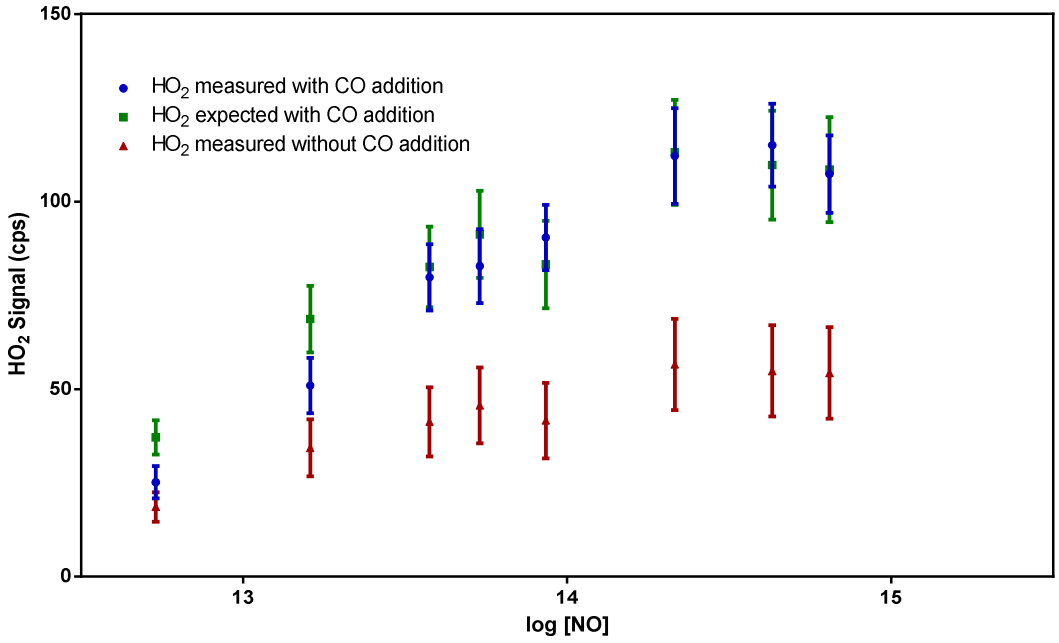

Figure IV- 17: OH signal measured in cell 2 with and without the addition of CO. Red triangles refer to the HO_2 signal measured without adding CO, blue points correspond to the HO_2 signal coming from conversion of OH into

HO_2 with CO addition, and green squares are the signal expected upon the CO addition considering that HO_2 is completely converted to OH.

The HO_2 signal measured in the presence of CO should double compared to the one measured in HO_x mode. The experimental results showed a good agreement with the theoretical assumptions (Figure IV- 17) with the signal of HO_2 doubled in cell 2.

In Figure IV- 17, we see that as the NO concentration increases, the conversion efficiency of HO_2 increases reaching a plateau with NO concentration around 1×10^{14} molecule.cm$^{-3.}$

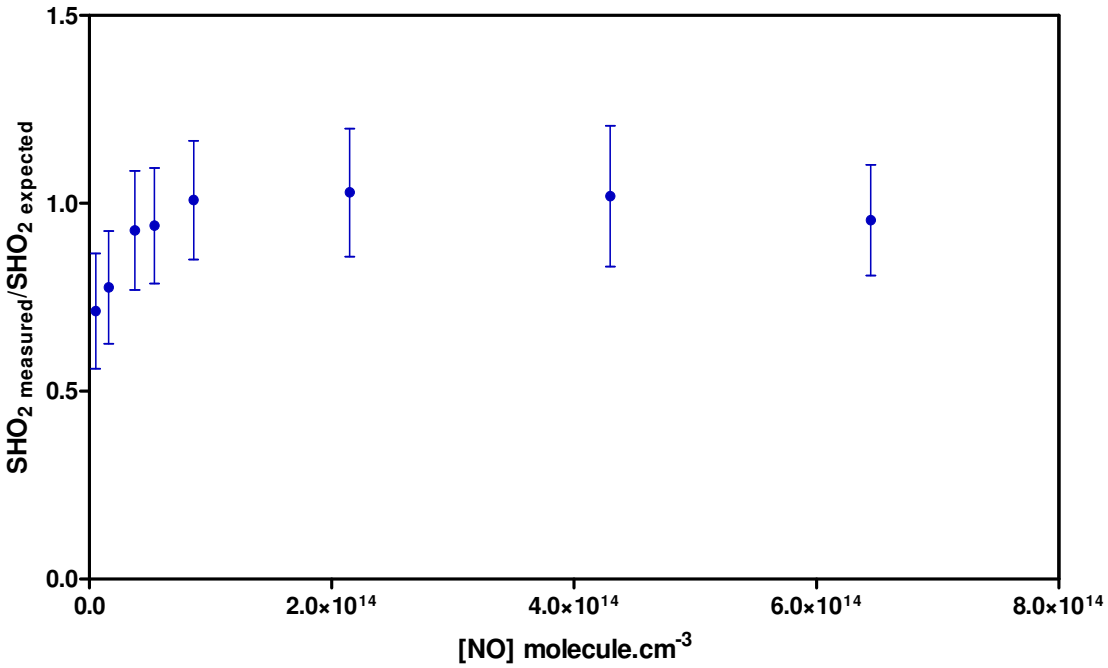

Figure IV- 18: Ratio of the signal of HO_2 coming from the CO addition over the expected signal in the detection cell assuming a total conversion of CO into HO_2.

The first two points in Figure IV- 18 are below 1 because the injected NO concentrations are very low and maybe the fluctuations of the flow of NO injected is higher. The expected signals were close to the measured ones as shown in Figure IV- 18. This observation validates our setup for further testing with more compounds such as VOCs.

A similar test has been made using methanol which plays the same role as CO, reacting with OH to give HO_2 in the calibration cell via:

$$OH + CH_3OH \rightarrow CH_2OH + H_2O \qquad \text{R IV- 6}$$

$$CH_2OH + O_2 \rightarrow HO_2 + CH_2O \qquad \text{R IV- 7}$$

$$OH + CH_3OH \rightarrow CH_3O + H_2O \qquad \text{R IV- 8}$$

$$CH_3O + O_2 \rightarrow CH_2O + HO_2 \qquad \text{R IV- 9}$$

OH reacts with methanol, predominantly forming CH_2OH (R IV- 6) (reported yields of 0.85) (Atkinson et al., 2006) which then rapidly reacts with O_2 (9.6×10^{-12} cm^3 $molecule^{-1}$ s^{-1}) (Atkinson et al., 2006) to form HO_2 (R IV- 7). The other minor reaction produces CH_3O, which reacts slower with O_2 (1.92×10^{-15} cm^3 $molecule^{-1}$ s^{-1}) (Atkinson et al., 2006) to also produce HO_2 (R IV- 8 and R IV- 9). HO_2 generated in the system was detected in the same way by adding NO to the HO_2 cell (cell 2). As for the CO addition, the conversion of OH into HO_2 by reaction with methanol in the calibration cell should be equal to 1 and the signal of HO_2 in the FAGE (cell 2) in presence of methanol should double compared to the signal with only water vapor (HO_x mode). But the results show a higher fluorescence signal than expected in the case of methanol addition (Figure IV- 19): the measured signal was about twice the expected one.

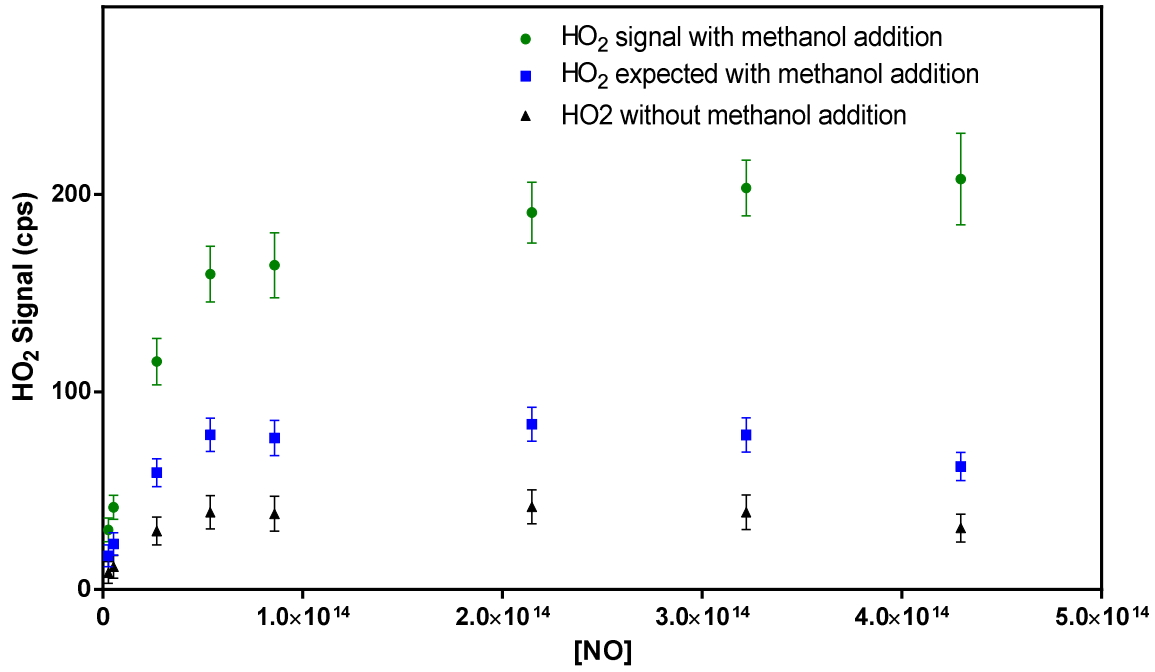

Figure IV- 19: OH signal in cell 2 with methanol addition and the expected signal if OH is converted into HO_2 with a yield of 1 in the presence of methanol

As methanol can be photolysed by the mercury lamp at λ= 184.9 nm, this potential contribution has been quantified. The methodology was the following: dry air was sent directly to the calibration cell without the addition of any reagent (no production of OH and HO_2 radicals). NO (80 sccm) is injected in the second cell to maintain the maximum conversion of HO_2 to OH. The OH signal measured was in the range of noise in both cells for OH and HO_2, which ensure than there is no residual signal from trace water vapor photolysis. Following that, methanol was injected to the dry air with different flow

rates (1-100 sccm), the signal in cell 2 increases linearly with the increase of the methanol concentration (Figure IV- 20).

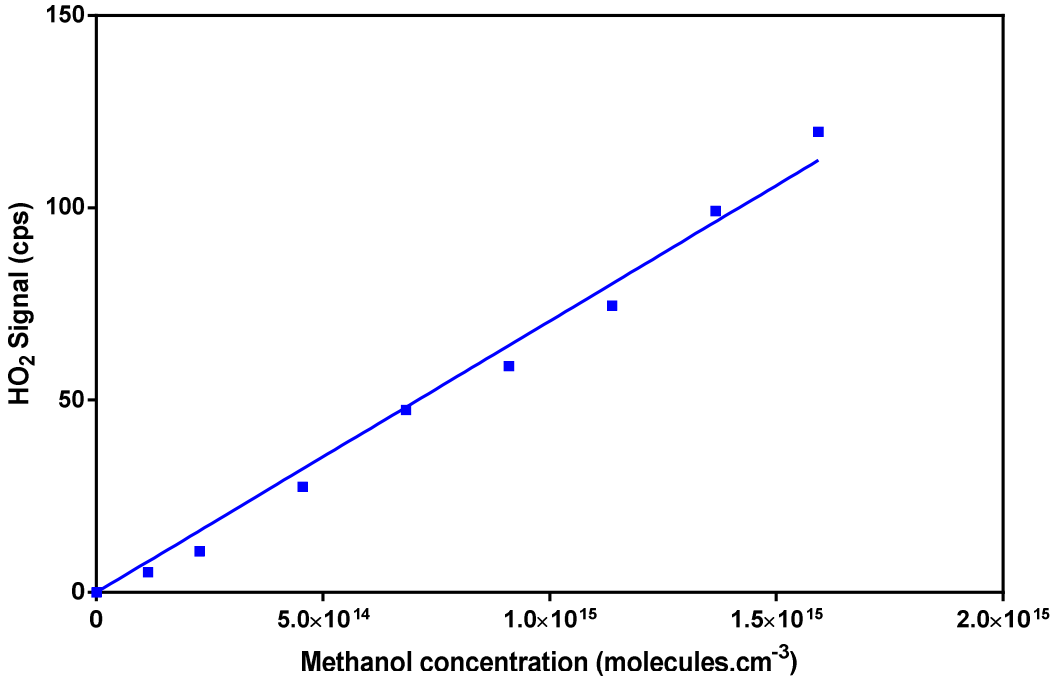

Figure IV- 20: Generation of HO_2 by methanol photolysis as function of CH_3OH concentration

Methanol photolysis at λ= 185 nm gives CH_2OH and CH_3O according to reactions R IV- 10 and R IV- 11 which then react with O_2 in the air to give HO_2(Buenker et al., 1984). This phenomenon was not observed by Fuchs et al. (Fuchs et al., 2011) probably due to lower lamp flux in their calibration cell. On the other hand, Whalley et al. (Whalley et al., 2013) avoided this photolysis effect by injecting the hydrocarbons after the photolysis region in the calibration cell.

$$CH_3OH + \lambda\ (185\ nm) \rightarrow CH_2OH + H \qquad \text{R IV- 10}$$

$$\rightarrow CH_3O + H \qquad \text{R IV- 11}$$

The same methodology has been repeated with a constant methanol flow injection of 50 sccm and varying the NO concentration in the FAGE cell from 1 to 400 sccm. By this method we are able to determine the contribution of the photolysis of methanol (for each NO concentration) to the HO_2 signal (Figure IV- 21).

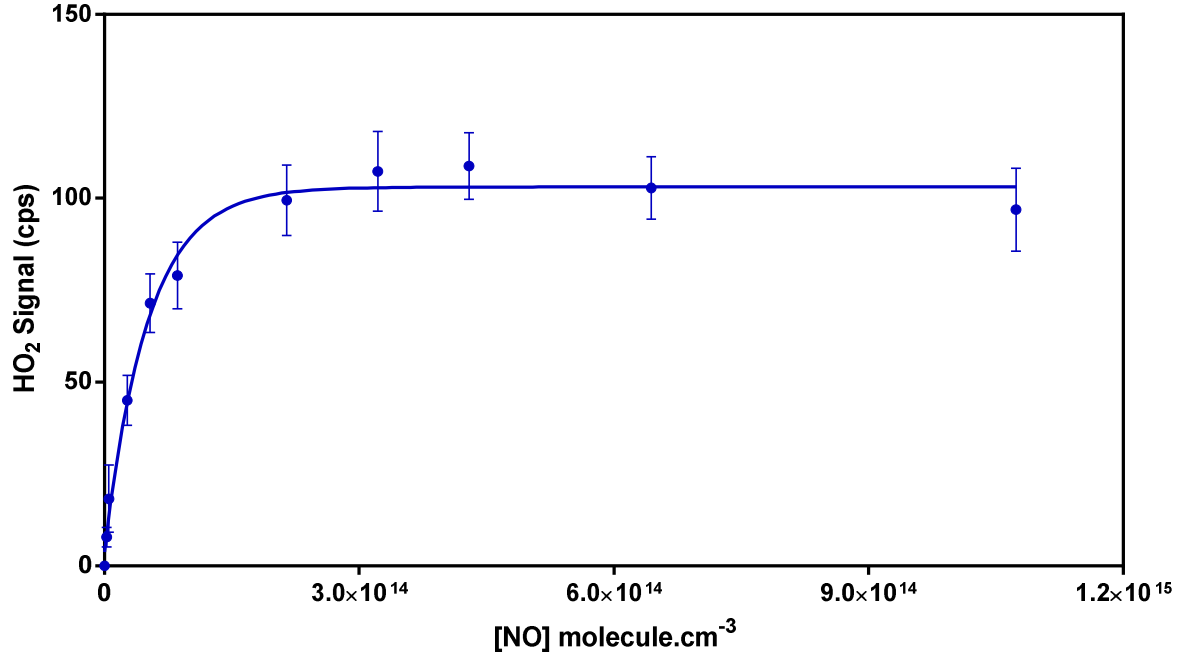

Figure IV- 21: HO_2 signal upon methanol photolysis (dry conditions) in the second cell as function of the nitrogen oxide concentration.

Therefore, the OH signal due to HO_2 measured in cell 2 with methanol addition can be corrected from the photolysis by subtracting its contribution. The experimental results were then consistent with the expected signal.

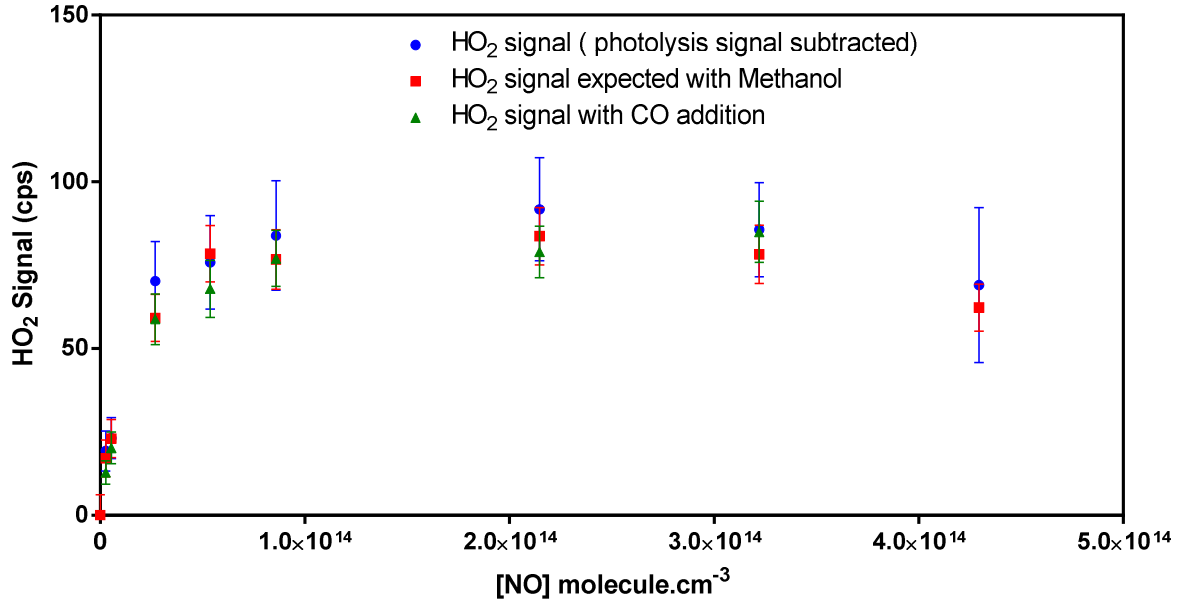

Figure IV- 22: HO_2 signal in cell 2 during the CO addition, methanol addition and signal expected with the reagent additions as function of NO concentration.

Besides, the OH signal measured in case of CO addition was compared to the corrected signal in case of methanol addition under the same conditions. The result showed a good agreement (Figure IV-22). As a conclusion, after subtracting the photolysis signal from the measured signal, we are able to extract the converted fraction of the $RO_2$to HO_2. These results validate our setup to test different VOCs under the same conditions. The parameters and instrumental conditions of the UL-FAGE instrument used for characterizing different RO_2 are listed in Table IV- 7.

Table IV- 7: Experimental parameters of the UL-FAGE instrument maintained for RO_2 characterization.

	Parameter	Value
UL-FAGE Instrument	Reagent reactivity with OH	500 to 1000 s^{-1}
	Inlet nozzle orifice	1 mm
	Sample flow rate	9.2 L/min
	NO concentration	(0.5-400 sccm) maximum = 2×10^{14} cm^{-3}
	Laser power	0.5-1 mW
	Laser repetition rate	5 kHz
	Pressure	1.5-1.7 torr
	Temperature	Room temperature

IV.4.4 Characterization of the RO_2 interference in the UL-FAGE with our calibration cell

The potential formation of HO_2 from RO_2 radicals in the FAGE instruments is different from one compound to another, depending on the structure of the RO_2. In order to investigate the interference in the UL-FAGE instrument, a wide range of RO_2 compounds have been studied by injecting the VOC precursor in the calibration cell. Interferences caused by RO_2 radicals derived from methane, butane, isoprene, toluene, and cyclohexene were tested. The potential photolysis of each parent hydrocarbon at 185 nm as a source of HO_2 has been quantified in dry air conditions. This contribution has been subtracted from the signal obtained in presence of VOC and OH (with production of RO_2) similarly to what has been done for methanol. For butane and methane, the photolysis magnitude was not significant and it was considered to be negligible. The results of the conversion efficiency of the different RO_2 radicals in UL-FAGE are shown in Figure IV- 23.

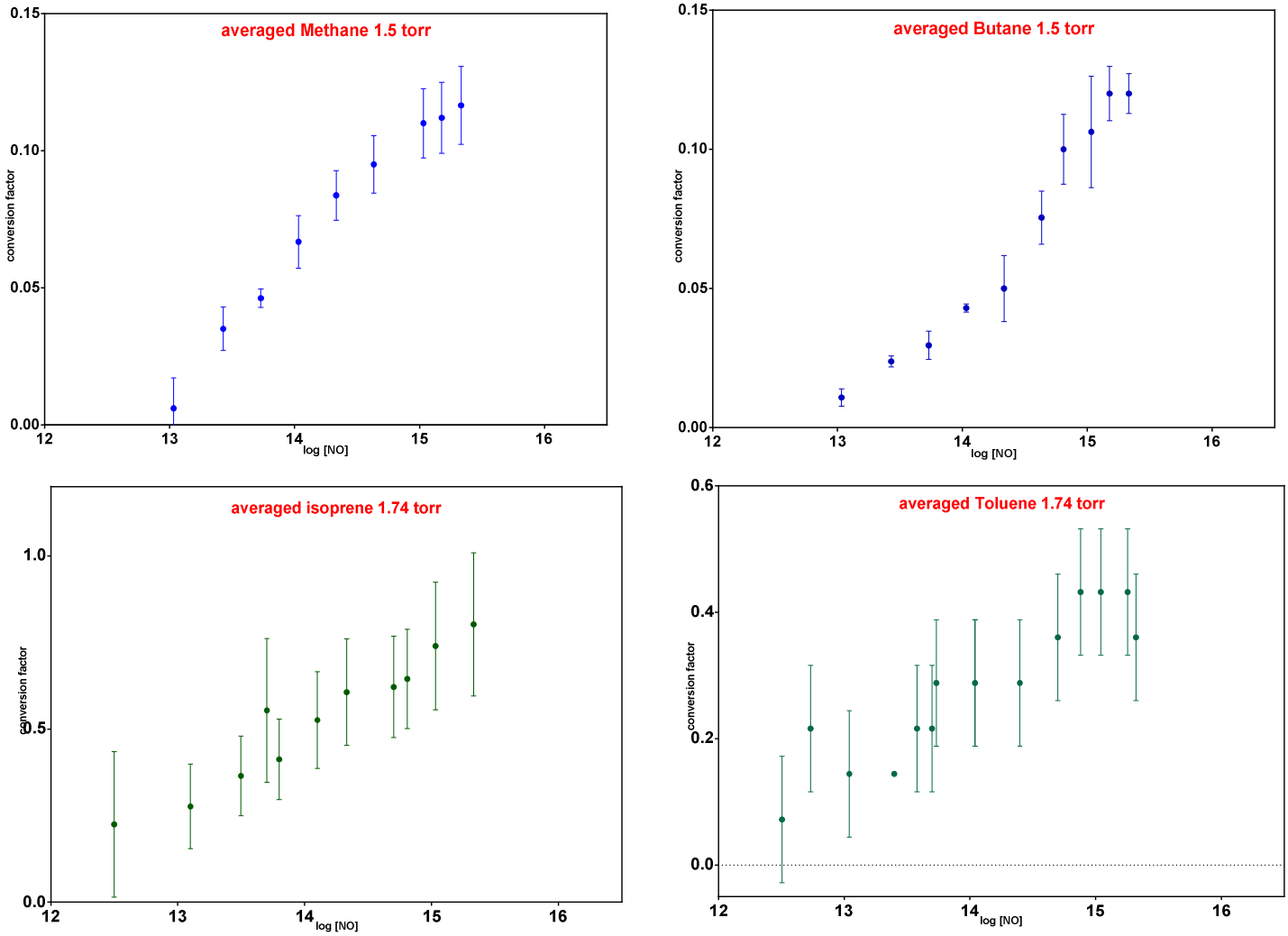

Figure IV- 23: conversion efficiency of different RO_2 precursors from RO_2 to HO_2 in UL-FAGE cell as function of NO concentration. Pressure differs between the experiments due to a change in the pumping system.

Same behavior was seen for all RO_2 radicals investigated, where the conversion efficiency of RO_2 to HO_2 increases as the NO concentration increases reaching a plateau around [NO] = 1 x 10^{15} cm^{-3}. Weak interference was observed from methylperoxy and butylperoxy for UL-FAGE instrument as expected. This behavior was in agreement with the results reported by other groups (Fuchs et al., 2011; Whalley et al., 2013). In contrast to alkylperoxy radicals, RO_2 from alkenes and aromatics showed a significant interference on HO_2 measurement. The relative OH yield from isoprene and toluene was determined to be 0.6 ± 0.2 and 0.36 ± 0.2 respectively with cell pressure of 1.74 torr and a NO concentration varied between 7 x 10^{14} to 1 x 10^{15} cm^{-3}. The prompt HO_2 formed by the reaction of isoprene and toluene with OH is subtracted from the signal measured in case of isoprene and

toluene addition. The prompt HO_2 for isoprene and toluene was 6 % and 28 % respectively, according to MCM mechanism. The conversion efficiencies for each RO_2 are summarized in Table IV- 8.

Table IV- 8: conversion efficiency of different RO_2 in UL-FAGE HO_2 cell with medium NO concentration.

RO_2 precursor	[NO] molecules.cm^{-3}	Conversion efficiency	error
Isoprene	7 x 10^{14}	0.6	± 0.2
Toluene	1 x 10^{15}	0.36	± 0.2
Butane	1 x 10^{15}	0.13	± 0.05
Methane	1 x 10^{15}	0.1	± 0.05

All the conversion efficiencies listed in Table IV- 8 are under conditions of medium NO concentrations where it is sure that the maximum fraction of RO_2 is converted to HO_2. Values do not include the prompt HO_2 formation in the radical source, the HO_2 prompt is subtracted for isoprene and toluene. The obtained results were in a good agreement with the results that have been reported by Fuchs et al., (Fuchs et al., 2011) where the conversion efficiency of isoprene and methane were found to be 0.79± 0.05 and 0.04 ± 0.04 respectively.

As already mentioned, Fuchs et al., (Fuchs et al., 2011) reported that RO_2 conversions can be suppressed at low NO concentrations, and Whalley et al., (Whalley et al., 2013) highlighted that decreasing NO concentration in the detection cell only reduces the OH yield from RO_2 conversion and in return reduces the sensitivity of the instrument to the interference, thus allowing to discriminate between HO_2 and RO_2.

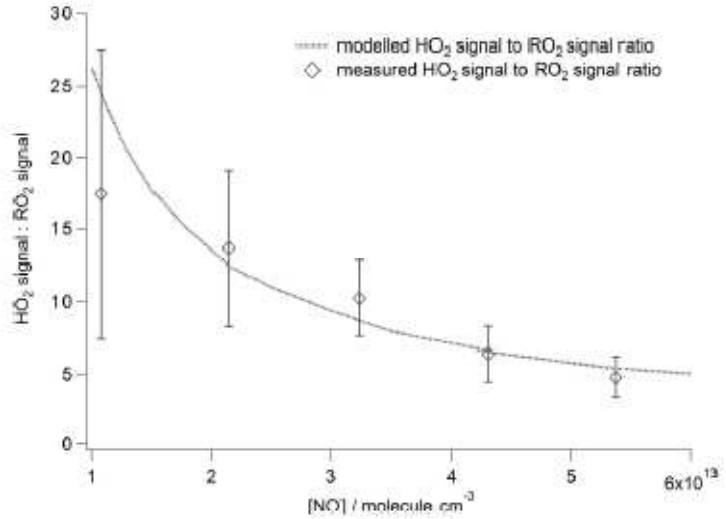

Figure IV- 24: modelled (dashed line) and measured (open diamonds) ratio of the OH yield from HO_2 signal : RO_2 signal as function of NO concentration (Whalley et al., 2013).

Under the operating conditions employed during the RO_2 characterizations, the RO_2 and HO_2 conversions were seen to have similar conversions at low NO concentrations (3 x 10^{12} to 1 x 10^{13} cm^{-3}) which disagree with the previous studies. As the NO concentrations increased, the conversion between both radicals start to be different and therefore allows to discriminate between RO_2 and HO_2 conversions as shown in Figure IV- 25. It shows the conversion efficiency of RO_2 coming from the reaction of toluene with OH (red points) and the conversion efficiency of HO_2 (blue points). The measurement for both conversions was done at the same time and under the same conditions. The same methodology was done for the other parent hydrocarbons (isoprene, methane, and butane) and the same results were obtained.

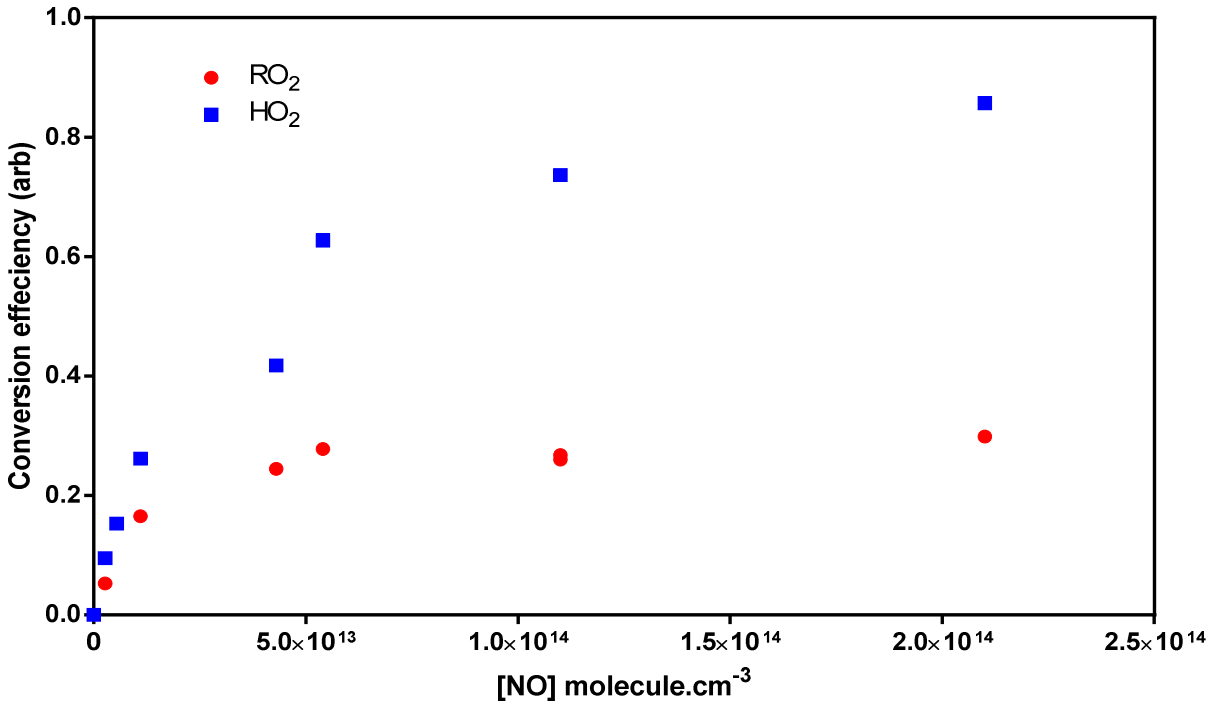

Figure IV- 25: Conversion efficiency of toluene as function of NO concentration; red points represent the toluene conversion efficiency, and the blue points represents the HO_2 conversion efficiency under the same conditions using the normal nozzle.

These findings suggest that even with low NO concentration injected in the detection cell, we are not able to distinguish between the RO_2 and HO_2 conversion and in return we cannot suppress the interference as it was reported (Fuchs et al., 2011; Whalley et al., 2013) for this type of nozzle. However, with increasing NO, the conversion of RO_2 will have less weight than the one of HO_2 and the comparison between low and high NO could be a way to extract RO_2 concentrations.

The previous experiments were done using the normal 1 mm nozzle (Figure II-4) but with different nozzles and pressures, the conversion of peroxy radicals can be different as reported in Fuchs et al., 2011 (Figure IV- 15). For this reason, the UL-FAGE was characterized for the conversion of isoprene and alpha-pinene (no prompt HO_2, MCM mechanism) in conditions used during the LANDEX campaign (using a pre-injector and another nozzle, at higher pressure, 2.2 Torr, due to the different pinhole and tubing length, see chapter V). This higher pressure increases the residence time of the mixture inside the cell which can change the conversion efficiency profile. Also, the design of the nozzle can directly affect the RO_2 conversion. The obtained results for conversions using the conditions of the LANDEX campaign are shown in Figure IV- 26.

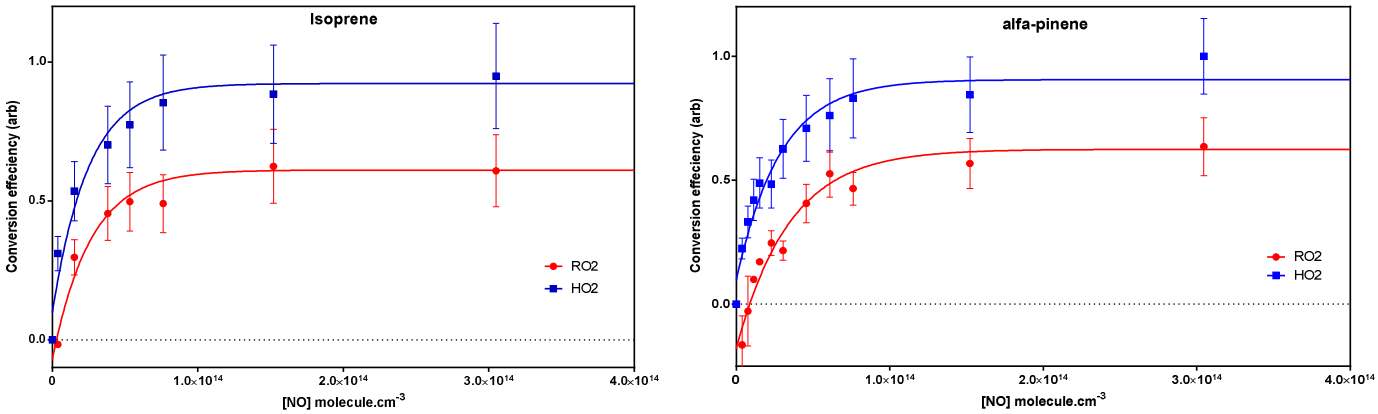

Figure IV- 26: Conversion efficiency (red points) of isoprene peroxy (left graph) and α-pinene peroxy (right graph) compared to HO_2 conversion efficiency as a function of NO concentration, corresponding to the LANDEX configuration.

It is clearly seen that with low NO concentrations, the conversion of RO_2 is close to zero (within the uncertainty of the measurement). The conversion efficiency of both peroxy radicals starts to increase with increasing the NO concentrations reaching a maximum conversion around 2 x 10^{14}molecules cm^{-3} of NO. The maximum conversion of isoprene was 0.62 while for α-pinene it was 0.63. From these data we noticed that under these operating conditions we are able to extract the RO_2 contribution to the HO_2 measurements (see results of the LANDEX campaign in Chapter V). The conversions were corrected to the prompt HO_2 produced from the reaction of the VOCs with OH.

In a similar way than what has been performed for the calibration of HO_x radicals, tests have also been done on the UL-FAGE during the intercomparison campaign with our calibration cell and other calibration cells used to calibrated RO_2 in other instruments (CIMS at LPC2E and PERCA at IMT-Lille-Douai). Results are presented in the following paragraph with the first nozzle.

IV.4.5 Characterization of the different calibration cells with the UL-FAGE for RO_2 generation

The second objective of the intercomparison described in paragraph IV.2.4 was to test the different calibration cells for the measurement of $HO_2^* = HO_2 + \Sigma\alpha RO_2$ by the UL-FAGE and RO_2 on the other instruments to highlight potential calibration problems due to the calibration cells themselves. For each combination calibration cell – detection device, peroxy radicals were generated by successively injecting different types of VOCs such as isoprene, toluene, and cyclohexene in the different calibration cells. This type of comparison of different techniques is essential to verify that measurement artifacts are well characterized on the instruments commonly used in field campaigns.

To determine the OH yield from different RO_2 radicals in the presence of NO, RO_2 radicals were generated by the addition of different parent hydrocarbons to the calibration cell as described previously. Peroxy radical conversion measurements were investigated for three VOCs: isoprene, toluene and cyclohexene and different concentrations of NO.

The signal in the HO_2 cell has been recorded for the 3 RO_2 generated in the LPC2E and IMT-Lille-Douai calibration cells over the accessible range of NO and compared with those observed with our calibration cell (Figure IV- 27). The main difference between the three systems was the relative humidity range, where the PC2A calibration system was limited to a maximum relative humidity equal to 9 %.

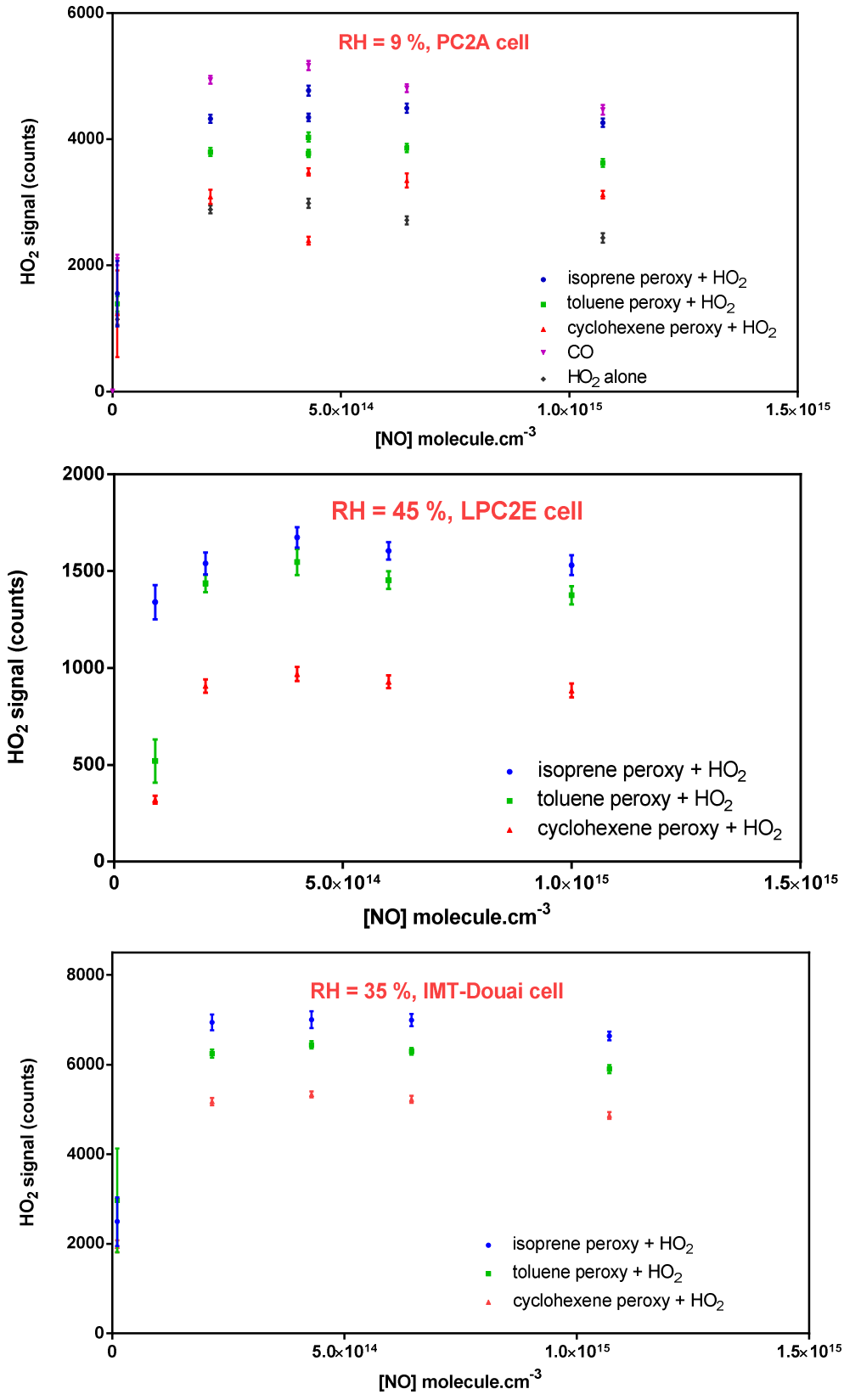

Figure IV- 27:HO_2 signal coming from RO_2 precursors as a function of [NO] in the second cell using PC2A calibration cell (RH = 9 %), IMT Douai calibration cell (RH = 35 %), and LPC2E calibration cell (RH = 45 %). (The photolysis signal and the OH contribution in the second cell in the case of HO_x mode are subtracted).

The conversion efficiency of RO_2 radicals coming from isoprene, toluene and cyclohexene increased with NO and it was approximately constant for high NO (6×10^{14} molecules.cm^{-3}). As the NO concentration continue to increase, the signal starts to decrease slightly (Figure IV- 27) due to the reaction of OH with NO producing HONO. The HO_2 signal coming from photolysis of VOCs by the Hg lamp are not subtracted for all the tests with the different calibration cells.

The results obtained with the different calibration systems were in a good agreement, with a conversion efficiency for isoprene peroxy higher than the one for toluene peroxy, and higher than the one for cyclohexene peroxy. As the reaction rate constant of the decomposition of the β-hydroxyalkyl alkoxy radical formed in the FAGE after reaction of RO_2 with NO differ from one RO_2 to another (Fuchs, 2006), the conversion efficiency of the RO_2 radicals produced from isoprene was more than for RO_2 derived from toluene and cyclohexene. As the measurement of HO_2 without RO_2 has not been done for the tests with the calibration cell from Douai and Orléans, we have calculated the ratio of conversion efficiency of toluene and cyclohexene taking isoprene as reference (Figure IV-28).

The measured ratio of conversion efficiencies for the three RO_2 with the different radical calibrations were equal within the range of 5 %.

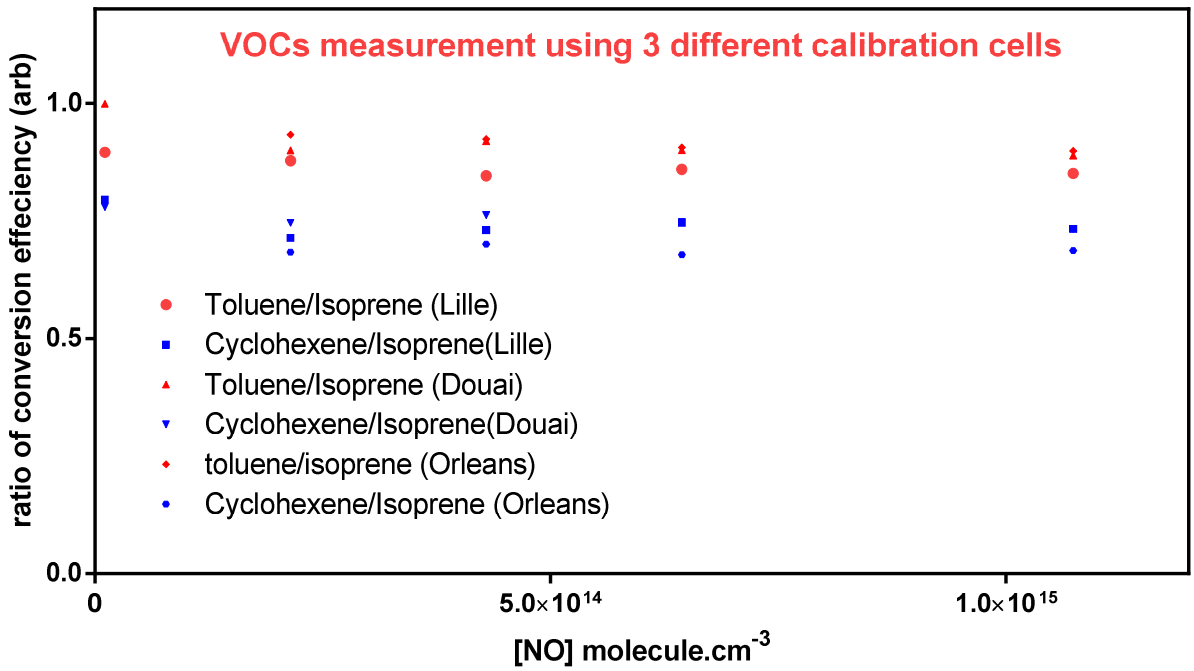

Figure IV- 28: ratio of conversion efficiency for different RO_2 (toluene, and cyclohexene) on isoprene conversion efficiency.

High conversion efficiency from isoprene peroxy was observed when high NO concentrations was present in the FAGE cell. Smaller, but still significant conversions were also observed for RO_2 radicals derived from toluene and cyclohexene. The results for the three calibration cells were close as seen in Table IV- 9.

Table IV- 9: ratio of conversion efficiency from toluene and cyclohexene RO_2 normalized to isoprene conversion efficiency.

group	Toluene/Isoprene	Cyclohexene/Isoprene
Lille	0.86	0.74
Douai	0.96	0.75
Orleans	0.91	0.69

The 3 calibration cells from the different groups showed close results to the RO_2 conversion in the FAGE instrument. To resume, the three different calibration cell systems show close behavior with the UL-FAGE instrument for OH, HO_2, and RO_2 calibration experiments with different parameters and covering a wide range of radical concentrations (10^8-10^9 molecules.cm^{-3}). The conversion efficiencies obtained were in good agreement with the literature for the RO_2 studied.

IV.5 Conclusion

The calibration cell used for the UL-FAGE instrument has been characterized for different parameters (water vapor, wall losses). Also, it has been successfully calibrated for different RO_2 radicals coming from the reaction of OH with methane, butane, isoprene and toluene hydrocarbons.

I. The influence of H_2O on OH fluorescence lifetime was obtained by varying the H_2O concentration from 300 to 4000 ppm within the calibration cell. Under these conditions, the effect of water concentration is weak on the sensitivity of the UL-FAGE instrument.

II. Radical wall losses were found to be minor, where the losses obtained were about 9 s^{-1} for OH and 2.3 to 4 s^{-1} HO_2 radicals with different humidities and using the calibration cells on CIMS and UL-FAGE.

III. The intercomparison between PC2A and LPC2E calibration cells for HO_x measurements showed a very good agreement. The agreement between the 2 calibrators was 0.93 and 0.99 for OH and HO_2 radicals respectively with a correlation coefficient, R^2 of 0.95 for OH and 0.96 for HO_2.

IV. The intercomparison between PC2A and IMT-Douai calibration cells for HO_x measurements showed a good agreement for lamp position near the exit of the calibrator (x=7), while at higher lamp positions we see a very strong disagreement for HO_2 measurements. In addition, it was highlighted that the use of a variac to change the lamp flux can affect the measurement because probably not only the intensity, but also the Hg lamp spectral distribution is modified.

V. The interference of HO_2 measurements from RO_2 produced by the reaction of OH with alkanes (methane and butane) was tested and it was found to be within the range of few percent under the operated conditions. Subsequently, the interference from small alkanes was considered to be negligible in agreement with the results reported by other groups.

VI. The interference from RO_2 radicals produced by the reaction of OH with alkenes and aromatic hydrocarbons was determined and found to be significant to the HO_2 measurement in UL-FAGE. Interference from RO_2 produced by the reaction of isoprene and toluene with OH are 0.6 and 0.36 respectively under the operated conditions.

VII. With our nozzle, the RO_2 interference could be deduced by studying the variation of the signal at different NO levels. The concentration of HO_2 extracted using HO_2 calibration factor should be significantly lower at high NO (RO_2 conversion efficiency lower than HO_2). With the nozzle used during the LANDEX campaign, RO_2 levels can be deduced by the difference of HO_2 concentration obtained at low NO (only HO_2) and high NO (HO_2+RO_2)

VIII. The three different calibration cell systems showed close behavior with the UL-FAGE instrument for RO_2 calibration experiments with different parameters and covering a wide range of radical concentrations (10^8-10^9 molecules.cm^{-3}). The conversion efficiencies obtained were consistent for the three calibrators.

In the future, more hydrocarbons will be investigated in order to determine the relative sensitivity of a wide range of RO_2 radicals in the UL-FAGE instrument. In the meantime, a RO_x-LIF instrument is under characterization in order to have complementary measurements for RO_2 obtained from hydrocarbons containing a double bound and the sum of RO_2.

Chapter V: LANDEX campaign

V.1 Introduction

Several field measurement campaigns have involved measurements of OH, HO_2, and RO_2 in biogenic environments and highlighted difficulties to interpret the chemistry observed (Feiner et al., 2016b; Fuchs et al., 2017a; Mao et al., 2012; Stone et al., 2012; Whalley et al., 2016; Yang et al., 2017). Concerning HO_x measurements, discrepancies between measurements and models were reported in low NO_x environments (see chapter I for more details). For OH reactivity measurements, it was shown that there were still OH sinks unaccounted for in these areas. Thus, a missing reactivity have been reported in forest and in environments characterized by larger loadings of secondary oxidation products (Nölscher et al., 2016; Whalley et al., 2016; Zannoni et al., 2016).

Complex chemistry due to the presence of numerous biogenic VOCs involves oxidation processes which can lead to the formation of SOA. Therefore, in such type of environment, detailed characterization of both gas and particle phases is crucial. Chapter V of this thesis presents the results obtained from the deployment of the UL-FAGE instrument in the Landes forest where regular nocturnal particle formation (NPF) events have been observed (LANDEX 0 campaign, summer 2015, EPOC laboratory, Bordeaux University).

The LANDEX 0 campaign involved the measurement of different species such as VOCs by PTR-MS, ozone, NO_x by analysers, particles by SMPS but the information available did not allow to clearly explain these events. In order to better understand these events and more generally the chemistry in this particular environment, a more extensive campaign has been organized, including more measurements such as HO_x radicals and OH reactivity. The LANDEX project (CNRS INSU LEFE-CHAT) involved more than 10 research groups from France. The campaign was conducted from 28 June to 18 July 2017.

The UL-FAGE instrument was deployed for 4 weeks during this campaign to measure OH, HO_2, RO_2 concentrations and OH reactivity. This was the first time that UL-FAGE was deployed with a preinjector to quantify the OH interference and a modulation of NO to quantify RO_2 radicals in ambient air. A part of this campaign was dedicated to an intercomparison between the UL-FAGE and the CRM instrument from LSCE laboratory. This intercomparison was complementary to the intercomparison that has been done in the SAPHIR chamber (Fuchs et al., 2017b).

V.2 Context of the study

V.2.1 Role of forests in the atmosphere

Forest ecosystems occupy an important part of the continental surface and provide a considerable amount of resources. Sometimes called "lung of the planet", forests are primarily, through the photosynthesis process, a source of atmospheric oxygen, which allows us to breathe and live. They are also essential in our everyday life: paper, furniture, energy production, heating, etc. In France, according to the French Environment and Energy Management Agency (ADEME), it is estimated that nine million TOE (ton of oil equivalent) is supplied each year by burning wood (Branche, 2016). After hydropower, biomass combustion is the second most important renewable energy at the national level. From an ecological point of view, forest ecosystems harbor remarkable biodiversity, for both plants and animals, and represent on a global scale the main reservoir of biodiversity.

Evapotranspiration also allows other gas exchanges as absorbing the carbon dioxide (CO_2) necessary for photosynthesis. If forest ecosystems are also capable of emitting CO_2 via the breathing process, they nevertheless remain a net CO_2 sink (Heimann and Reichstein, 2008). Forests thus capture a considerable share of the atmospheric CO_2 emitted by anthropogenic activities, thus making it a major ecosystem service. However, carbon assimilated by plants is not entirely allocated to their structures or growth, but it also contributes to the synthesis of Volatile Organic Compounds (VOCs).

These biogenic VOCs (BVOC), which can contribute to 10 % of the net carbon flux, is emitted to the atmosphere and has a significant impact on air quality and climate. Globally, forests are the primary source of VOC (Sindelarova et al., 2014). In order to better characterize their impact, it is necessary to identify and quantify these compounds and understand how they are transformed.

Plants emit BVOCs for many reasons: to protect against oxidative stress, to protect against bacteria, as a blossom hormone, for thermotolerance, to defend against herbivores attacks, as antioxidant when exposed to high ozone levels, for signaling (Laothawornkitkul et al., 2009).

The BVOCs most widely emitted in the atmosphere include isoprene (C_5H_8), monoterpenes (C10 compounds, like pinenes, terpinenes, limonene), and sesquiterpenes (C15 compounds, like caryophyllene) (Sindelarova et al., 2014) . When terpenes are modified chemically, such as by oxidation or rearrangement of the carbon skeleton, the resulting compounds are generally referred to as terpenoids. Also, terpenes are synthesized from a common precursor with five carbon atoms, isopentenyl-pyrophosphate (IPP), according to the "law of isoprene" defined by Ruzicka (Ruzicka, 1953) .

IPP can rapidly isomerize to dimethylallyl-pyrophosphate (DPP), which is directly responsible for the production of isoprene. The addition of an IPP group on the DPP leads to the formation of geranyl pyrophosphate (GePP), precursor of the formation of monoterpenes in plants (Figure V- 1).

Finally, the addition of a C5 unit to the GPP forms farnesyl-pyrophosphate (FPP), which is responsible for the formation of sesquiterpenes. A complete description of the synthesis pathways of terpenes and other BVOCs, from the absorption of CO_2 through photosynthesis to the production of VOCs, is available in the literature (Dewick, 2002; Laothawornkitkul et al., 2009).

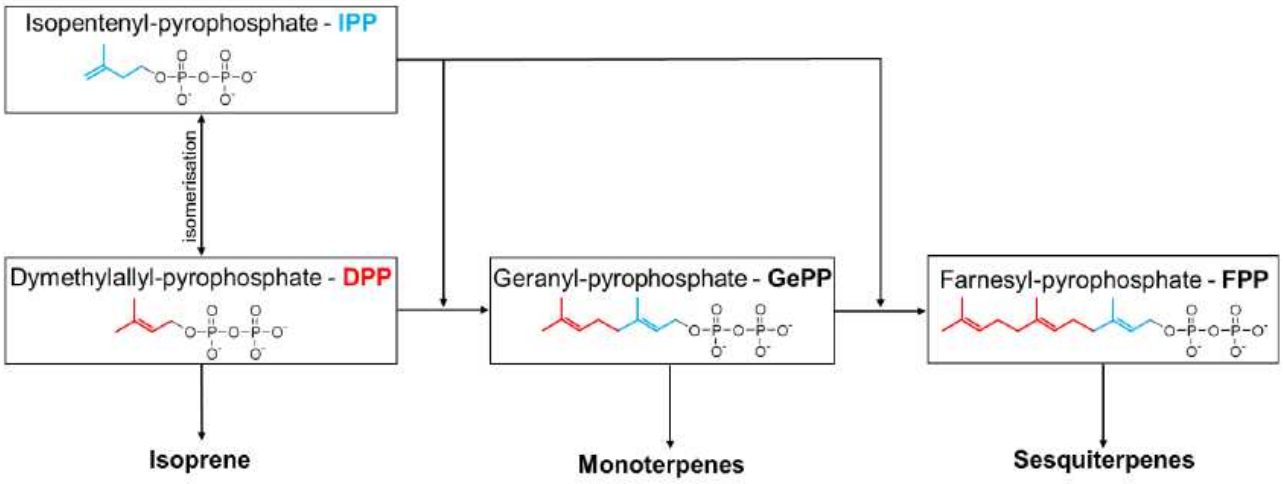

Figure V- 1: Schematic of the VOCs synthesis in the vegetable cells (Kesselmeier and Staudt, 1999).

The oxidation of BVOCs leads to the formation of different compounds such as aldehydes, ketones or carboxylic acids (Figure V- 2). Some of these oxygenated compounds derive from one or more oxidation steps. Heaviest secondary compounds have a relatively low saturating vapor pressure, giving them a semi-volatile character, implying their ability to be transferred to the particulate phase. The transfer of organic molecules from the gas phase to the particulate phase results in the formation of Secondary Organic aerosols (SOA), an aerosol being defined as a particle suspended in the air (Kim et al., 2011).

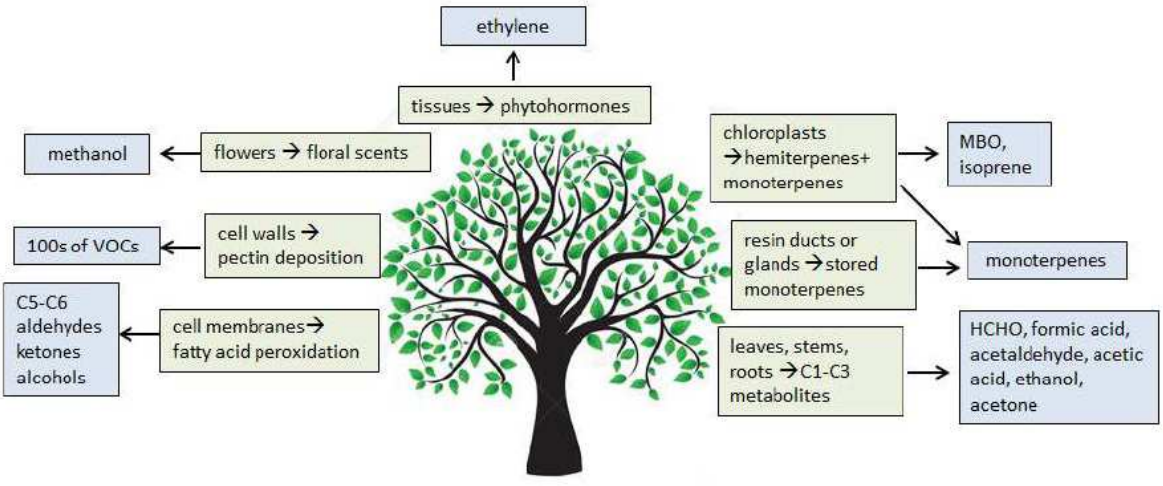

Figure V- 2: Schematic of biogenic VOCs emissions pathways (Zannoni, 2015)

Atmospheric aerosols play a predominant role on the climate, directly via the absorption, reflection or diffusion of solar radiation, or indirectly by acting as a condensation nucleus for the formation of water droplets. According to the Intergovernmental Expert Group on Climate Change (IPCC), it is precisely the action of these aerosols on the climate that today constitutes the greatest uncertainty in the assessment of terrestrial radiative forcing. Although their impact in urban areas is widely recognized, it has only recently been shown that fine particles can reduce life expectancy up to 14 months in rural areas. The health impact of fine particles is therefore not only an urban problem but a major challenge for all populations.

The biogenic organic compounds are highly reactive with the oxidants in the atmosphere such as hydroxyl (OH), nitrate (NO_3) and ozone (O_3). They have a significant influence on tropospheric chemistry on local and global scales (Dlugi et al., 2010).In this context, it is particularly interesting to study the particle formation in the Landes forest.

V.2.2 Specificities of the Landes forest – learns from LANDEX 0

The Landes forest is an artificial forest used for the forestry and the number of species is limited. For that, it can be considered as a laboratory ecosystem. From LANDEX 0, it has been shown that the main emissions are monoterpenes contrary to most of the forest emissions being governed by isoprene. α-pinene (55 %) and β-pinene (32 %) dominate the emissions of monoterpenes as shown inFigure V- 3.

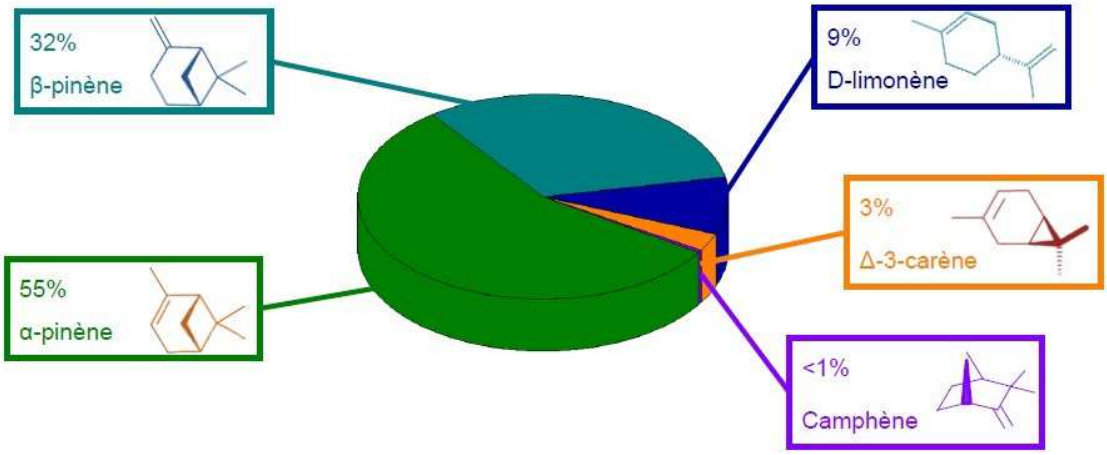

Figure V- 3:Characterization of BVOCs in Landes forest and speciation of the different types of emissions in the canopy level (Kammer, 2016)

The measurements of the particles size distribution during the field campaign LANDEX 0 have shown nucleation events starting the evenings as can be seen in Figure V- 4by the appearance of characteristic banana-shape on the aerosol particle size distribution graph.

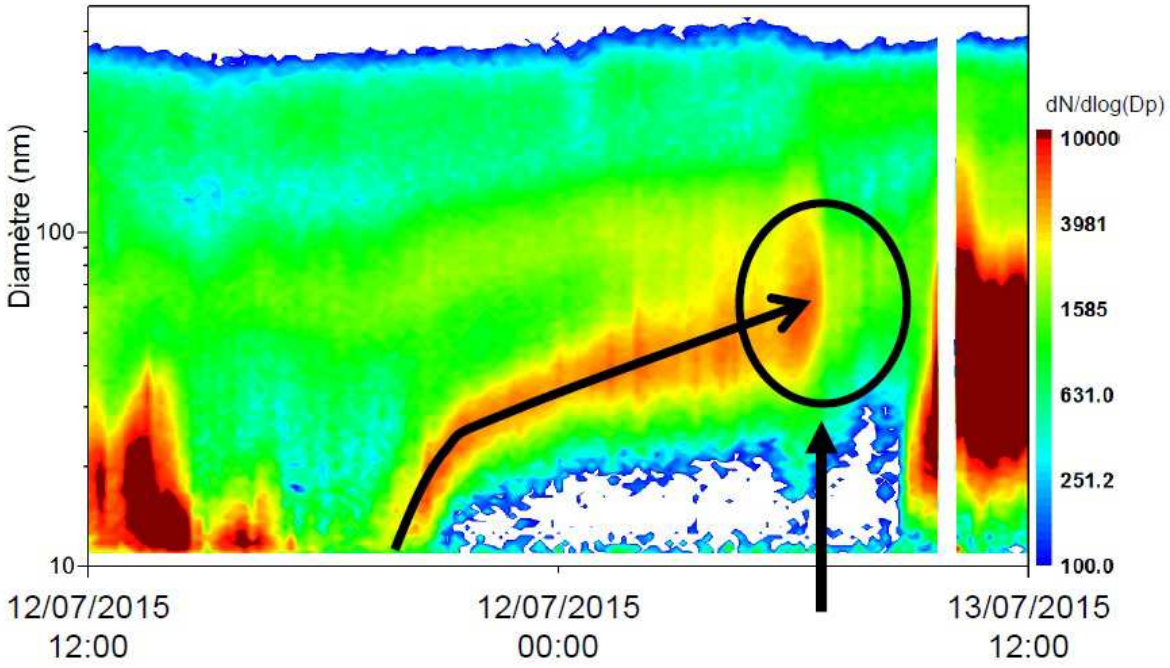

Figure V- 4:Particle formation during the night shown by the formation of a banana shape (Kammer, 2016)

This characteristic shape reflects the appearance of a mode of ultrafine particles (aerodynamic diameter of the order of a few nanometers) formed by nucleation, which is immediately followed by a magnification to a diameter of about 100 nm, sufficient to act as a condensation nucleus for cloud formation (Kammer, 2016).

Due to the important surface covered by the Landes forest and its role on the economic activities of the Nouvelle Aquitaine area, it is crucial to better characterize its emission and the production of secondary species. In addition, it is useful to identify the chemical mechanisms responsible for the secondary species formation and particle nucleation during the night.

LANDEX 0 and LANDEX 1 took place on the same field site described in the next paragraph.

V.3 Field site description

The LANDEX 1 campaign was conducted from June 28 to July 18, 2017. The measurement site was located at Bilos in the Landes forest (44°29'39.69"N, 0°57'21.75"W, and 37 m above sea level). The nearest big urban area is the city of Bordeaux, 50 km north east from the site, as presented inFigure V- 5. This site has remote characteristics with heavy influences of fresh emissions from pines trees. Monoterpenes were the major dominating emissions, while the NO_X and CO concentration were very low compared to urban environments.

Figure V- 5: Site location of the measurement campaign and LANDEX forest (Kammer, 2016).

The field site consists in a large area of 30.2 ha (570 × 530 m) composed of maritime pine ranges (pinus pinaster), with a dense understorey of gorse (ulex europae), grass (molinia caerula) and heather (calluna vulgaris) (Kammer, 2016). Trees height was around 12 m and the soil is a sandy acidic hydromorphic podzol with a discontinuous layer of iron hard pan at 75 cm depth. The climate is temperate with a maritime influence due to the proximity of the Atlantic Ocean (23 km). This site is also part of the European ICOS (Integrated Carbon Observation System) program.

V.4 Sampling and instrumentation

Instruments were setup inside trucks or shipping containers located in the measurement site surrounded by pine trees (Figure V- 6). There was no traffic by cars or trucks in the site, a nearby road was 1 km away.

Figure V- 6 : Trucks of different groups installed in the site between the pine trees.

For PC2A laboratory, we carried out measurements of total OH reactivity using pump-probe method and quantification of OH, HO_2, and RO_2. All the instruments were installed inside a shipping container and air sampled by Teflon tubes except for UL-FAGE-quantification. The FAGE cells for quantification were fixed on top of the container at about 5 m above the ground level (Figure V- 8) which is in the canopy (canopy level represents area below the top of the tree). Ozone and water concentration were recorded by gas analyzers (Thermo analyser TEI 42i for ozone and hygrometer, Michell Instruments, S8000 integral Precision Dewpoint Meter, 95% accuracy for water vapor).

V.4.1 HO_x measurements

OH, HO_2 and RO_2 radicals were measured by laser induced fluorescence (LIF) technique. LIF is a direct method to detect OH radicals, while HO_2 and RO_2 radicals can be detected by fluorescence after chemical conversion to OH. The UL-FAGE consists of two LIF measurement cells to detect OH (first cell), HO_2 and RO_2 (second cell). The UL-FAGE instrument was deployed for the first time to measure RO_2 radicals during this campaign. All the components of the FAGE instrument for quantification were housed in an aluminium box at the top of the UL-container (5 m) as shown in Figure V- 7.

For the OH, HO_2, and RO_2 detection cells, ambient air is sampled at a flow rate of 9 slm through a 1 mm nozzle, a pre-injector is fixed just above the nozzle (see details in Chapter II). The sampled air goes through the nozzle into low pressure cells (p = 2.1 torr). OH is then detected by LIF in the first detection cell, while HO_2 and RO_2 are detected in the second cell after conversion in OH by injecting different NO concentrations and detecting then OH by LIF.

The OH fluorescence is recorded by a gated photon-counting system starting approximately 100 ns after the laser pulse. The total photon count-rate is composed of the OH fluorescence, solar stray light that enters the cell through the orifice, and laser stray light. The solar stray light is detected separately during a second counting window, when the OH fluorescence signal has disappeared.

The remaining other background signals are separated from the OH fluorescence by wavelength modulation of the laser. Background and fluorescence signals are measured together, when the laser wavelength is tuned on the OH absorption line, and only background signals are detected, when the laser wavelength is tuned away. A full wavelength cycle gives a time resolution of 40 s for one radical measurement. UL-FAGE was calibrated several times during the measurement campaign for OH and HO_2 radicals (see more details in Chapter II).

Figure V- 7: PC2A measurement container installed in the center of the forest

V.4.2 Total OH reactivity measurements

Total OH reactivity was measured by two different techniques during this campaign, pump-probe reactivity (PC2A group) and comparative reactivity method (LCSE group). The pump-probe LIF measured OH reactivity in the canopy whereas the CRM measured alternatively the OH reactivity at two heights (see Figure V-9). The CRM technique is very different from the pump-probe method. It is based on the measurement of the concentration of reagent (pyrrole) in different environments (without artificially added OH radicals and with artificial OH in zero and in ambient air) using mass spectrometry. Table V- 1summarizes the performance of the 2 OH reactivity techniques that were intercompared during the LANDEX campaign.

Table V- 1: Performance of the 2 techniques during LANDEX campaign.

Group	Method	LOD(s^{-1}) (2 σ)	K' max (s^{-1})	Time resolution (s)	Uncertainty (1 σ)
LSCE, Paris	CRM/PTR-MS	3	300	600	20 - 30 %
PC2A, Lille	pump-probe /LIF	0.6	150*	30-120	15 %

***without dilution**

The pump-probe technique has a better limit of detection than the CRM, however the CRM has a larger dynamic range since it can measure OH reactivities up to 300 s^{-1}. The 2 instruments were intercompared, the CRM and pump probe technique (UL-FAGE) characteristics are given in the following paragraphs.

V.4.2.1 Pump probe-FAGE technique

Total OH reactivity was measured using pump-probe LIF (or laser photolysis LIF) reactivity technique which had already been used in several intercomparisons and field campaigns (Amédro, 2012a; Fuchs et al., 2017b) and described previously in Chapter II. The gas flow in the photolysis cell was 7.5 l min^{-1}, when it is connected to the ambient air sampling line (length = 5 m approximately, diameter = 1/2 of inches). The pressure in the photolysis cell was approximately 740 Torr, lower than the atmospheric pressure due to a restriction of the flow through the Teflon sampling line. The pressure in the FAGE cell was equal to 2.3 Torr. The sampled flow is completed by 20 ml min^{-1} of zero air previously passing through an ozone generator (Scientech, 60 ppb of O_3).

Air was sampled in the canopy near the sampling area of the UL-FAGE instrument at about 5 m, a PFA filter was installed at the entrance of the tube in order to avoid the sampling of particles or dust. For the measurement of reactivity in zero air, air from a cylinder was used and part of the flow (2 slm) passed through a bubbler with Milli-Q water to reach a water vapor concentration of about 3000 ppm.

In order to validate the experimental setup before the campaign, tests to measure the well-known CO + OH reaction rate constant were carried out according to the procedure described in Chapter II. Different CO concentrations allowed to measure reactivities ranging from 10 to 90 s^{-1} and to determine by linear regression (R^2 = 0.97) a rate constant of $k_{CO+OH} = 2.45 \times 10^{-13} \pm 1.14 \times 10^{-14}$ cm^3 $molecule^{-1}$ s^{-1}, in good agreement with the reference value of 2.31×10^{-13} cm^3 $molecule^{-1}$ s^{-1}(Atkinson et al., 2006).

During ambient measurements, only the ozone flow is added to the air to be analyzed in the cell, the ambient water vapor being sufficient to produce OH. The photolysis laser used is a Quantel Nd: YAG laser Brillant quadrupled at 266 nm with an energy of 20 mJ and a beam of 2.5 cm in diameter after expansion aligned to be in the center of the photolysis cell. The pulse duration is 20 ns. The repetition rate of the photolysis laser is 1 Hz with an acquisition time of 1 s per photolysis shot. The photolysis laser energy was measured using a photodiode before entering to the photolysis cell and was observed to be stable during the campaign. The renewal of air in the cell is provided every 6.6 s.

The OH reactivity time resolution was at the minimum set to be 30 s, meaning that each OH decay was accumulated over 30 photolysis laser shots. To obtain the OH reactivity data, a LabView based program was used to fit the decays considering the variation in the S/N ratio. Before fitting each set of 30 OH decays, the signal to noise ratio was checked and compared to a chosen value (typically 4). If the OH decay signal to noise ratio is higher than 4, the OH was fitted and the next OH decay was started. However, if the S/N was lower than the criteria (4), the present OH decay is added to the following one. Then the S/N test runs again and if S/N> 4, the signal was fitted. As the reactivity varied during the day, the signal to noise ratio (S/N) varied as a function of the ambient species concentrations. When the reactivity is high, the time resolution was lowered since 2 or 3 sets of 30 decays were needed to be added in order to fulfil the criteria.

To obtain the measured reactivity, it is necessary to subtract a "zero air" reactivity k_{zero} which represents the losses of OH not related to the reactions in the gas phase with the species present in the ambient air but due to losses at the walls, diffusion, etc.

$$k_{ambient} = k_{measured} - k_{zero} \qquad \text{Eq V- 1}$$

For determining k_{zero}, "zero air", ie considered free of reactive species with OH (in our case, synthesized air, purity of 99.8%), is introduced into the photolysis cell and the decay is measured.

Zero air tests were conducted twice a day (in the morning and at night) when the reactivity measurements took place: on 8 days from 11 to 19 of July. The average of all the experiments with zero air gives on average of $k_{zero} = 4.0 \pm 0.5\ s^{-1}$. This value was therefore chosen as k_{zero} for the whole campaign.

V.4.2.2 Comparative Reactivity Method (CRM)

Total OH reactivity was also measured by a CRM instrument from the LSCE. This technique has been described in Chapter I. It is based on the measurement of the concentration of a reagent reacting with OH (pyrrole) in different conditions (steps) at the output of a reactor by a PTR-MS instrument. The first step is to introduce only pyrrole and dry zero air to measure C1 corresponding to pyrrole concentration in absence of OH. Then humid zero air is added to produce OH by photolysis of water vapor through a mercury vapor lamp emitting at 185 nm, the pyrrole concentration C2 is then measured. C2 is less than C1 because pyrrole reacts with OH. In the last step, zero air is replaced by ambient air, there is then competition between the reactions of OH with pyrrole and OH with reactive species present in the ambient air and C3, higher than C2, is measured.The time resolution of the CRM was 10 minutes.

The total OH reactivity is determined from C1, C2 and C3 andrequires corrections due to:

(1) Changes in relative humidity between C2 and C3, leading to different OH levels, (2) The formation of spurious OH in the sampling reactor when hydroperoxy radicals (HO_2) react with nitrogen monoxide (NO), (3) Not operating the CRM under pseudo-first order regime, and (4) The dilution of ambient air inside the reactor by N_2 and pyrrole flow.

Intensive laboratory experiments as well as tests during the LANDEX field campaign were performed in order to characterize these corrections and assess the performance of the technique with time. During the LANDEX field campaign, a slightly modified version of the CRM-LSCE has been adopted compared to the operating conditions used during the Julich intercomparison (Fuchs et al., 2017b) and the description of the improvementsis given in this section.

The Julich intercomparison of 2015 (Fuchs et al., 2017b), performed in the SAPHIR chamber, showed that the agreement between CRM and UL-LIF instruments was less good in the presence of

monoterpenes and sesquiterpenes compared to other tested species. The reactivities measured by all CRM instruments tended to be significantly lower than those obtained by the other instruments. This discrepancy was mainly explained by potential losses of monoterpenes and sesquiterpenes in the inlet system, with a CRM-LSCE sampling system built with ¼" OD PFA non-heated tubing and a Teflon pump to introduce the sample into the CRM reactor.

In order to measure total OH reactivity in a monoterpenes environment, several technical improvements have been made on the previous version of CRM-LSCE described by Zannoni et al., 2015 (Zannoni, 2015). First, all the system's PFA lines which conduct the sampled air to the reactorhave been replaced by stainless steel lines 1/8" OD, they were insulated with black tubing, heated with 20W/m heating cables and their temperature was regulated continuously to around 50°C to prevent condensation to minimize possible losses of reactive compounds. Second, temperature (°C) sensors have been placed at several points inside the system to monitor potential variations, the dew point (°C) was measured in the flow out through the pump to follow up humidity fluctuations and the pressure (bar) was monitored as well to make sure that experiments are taking place at atmospheric pressure all the time. All the flows going in and out of the reactor, the temperature at various places, the humidity and the pressure in the reactor were registered all the time in order to keep a track of potential variations and make adequate corrections.

V.4.2.2.1 Ambient air sampling

Air samples were conducted through two stainless steel lines of 1/8" OD collocated on a mast close to the container (see Figure V-9). The lines entire lengths were 8m for the one inside canopy and 12m for the one above.

During sampling, the flow was driven through one line by two pumps. Together, the two pumps allowed air sampling at 1 – 1.2 L/min, with the excess going to an exhaust, ensuring a residence time of 2- 4s within the sampling lines (50°C).

V.4.2.2.2 CRM-LSCE system characterization

Several tests were performed before, during and after the campaign to assess the performance of the instrument operating during one month. The PTR-MS was calibrated at the beginning and at the end of the field campaign in dry and wet conditions. Regular C1 measurements were made to check the initial concentration of pyrrole after potential photolysis by the UV Hg lamp.

Small differences in humidity were observed between C2 and C3 and have to be considered while processing the raw data. In order to assess this correction, experimental determination of C2

variation with humidity was performed measuring ΔC2 at various Δ m/z 37-to-m/z 19 ratios (with m/z 37 being representative of $H_3O^+(H_2O)$ and m/z 19 of H_3O^+ and their ratio being proportional to the humidity). These tests were done by introducing various flow rates of dry zero air to dilute humid zero air entering the reactor. During this campaign, three humidity tests in ambient air samples were in good agreement.

To complete the assessment of the instrument performance, series of tests were made to determine the correction factor for the deviation from pseudo-first order kinetics. In fact, the pyrrole reaction assumes to be under pseudo-first-order conditions ([pyrrole]>> [OH]), which is not the case with current operating conditions of CRM instruments. To meet this goal, injections of known concentrations of isoprene ($k_{isoprene+OH}$ = 1 x 10^{-10} cm^3. $molecule^{-1}$. s^{-1}) and α-pinene ($k_{\alpha\text{-pinene+OH}}$ = 5.33 x 10^{-11} cm^3. $molecule^{-1}$. s^{-1}) were performed before and after the field campaign. Thus, measured OH reactivities obtained from these tests are compared to the injected/calculated OH reactivity, leading to a correction factor that is dependent on the pyrrole-to-OH ratio. Therefore, standard OH reactivity experiments were conducted at different pyrrole-to-OH ratios ranging from 1.7 to 4, which is the range observed most of the time during the LANDEX field campaign, leading to a correction factor (D) = -0.5199(pyrrole-to-OH) +3.3771**.**

Correction on reactivity values for dilution has to be applied as well, since ambient air is diluted inside the reactor. This correction factor (F) was around 1.46 during the LANDEX campaign.

V.4.3 Other gas species quantification

Gas-phase constituents were measured by other laboratories by combining a number of different techniques available at the site, including: Proton Transfer Reaction-Mass Spectrometry (PTR-MS) and Gas Chromatography (GC).

Aerosol properties were also measured during this campaign by different techniques: on-line by Scanning Mobility Particle Sizer, SMPS or Aerosol Mass Spectrometry, AMS or by sampling on filters analysed later in laboratory but results will not be described here (not yet available).

V.4.3.1 Proton Transfer Reaction-Mass Spectrometry

Proton Transfer Reaction Mass Spectrometry (PTR-MS) is a technique based on chemical ionization through proton transfer, initially developed for the detection of gaseous organic compounds in ambient air (Lindinger and Jordan, 1998) and extensively deployed for online atmospheric trace gas measurements (Holzinger et al., 2002; Karl et al., 2009). A PTR-ToF-MS from IMT-Mines Douai was

used with a sampling located on mast 2 as shown inFigure V- 8. It measured VOCs including biogenic and oxygenated volatile organic compounds at 4 different levels as shown in the right side of Figure V- 8 (L1=12 m, L2=10 m, L3=8 m and L4= 6 m), the time resolution of each cycle was 30 minutes.

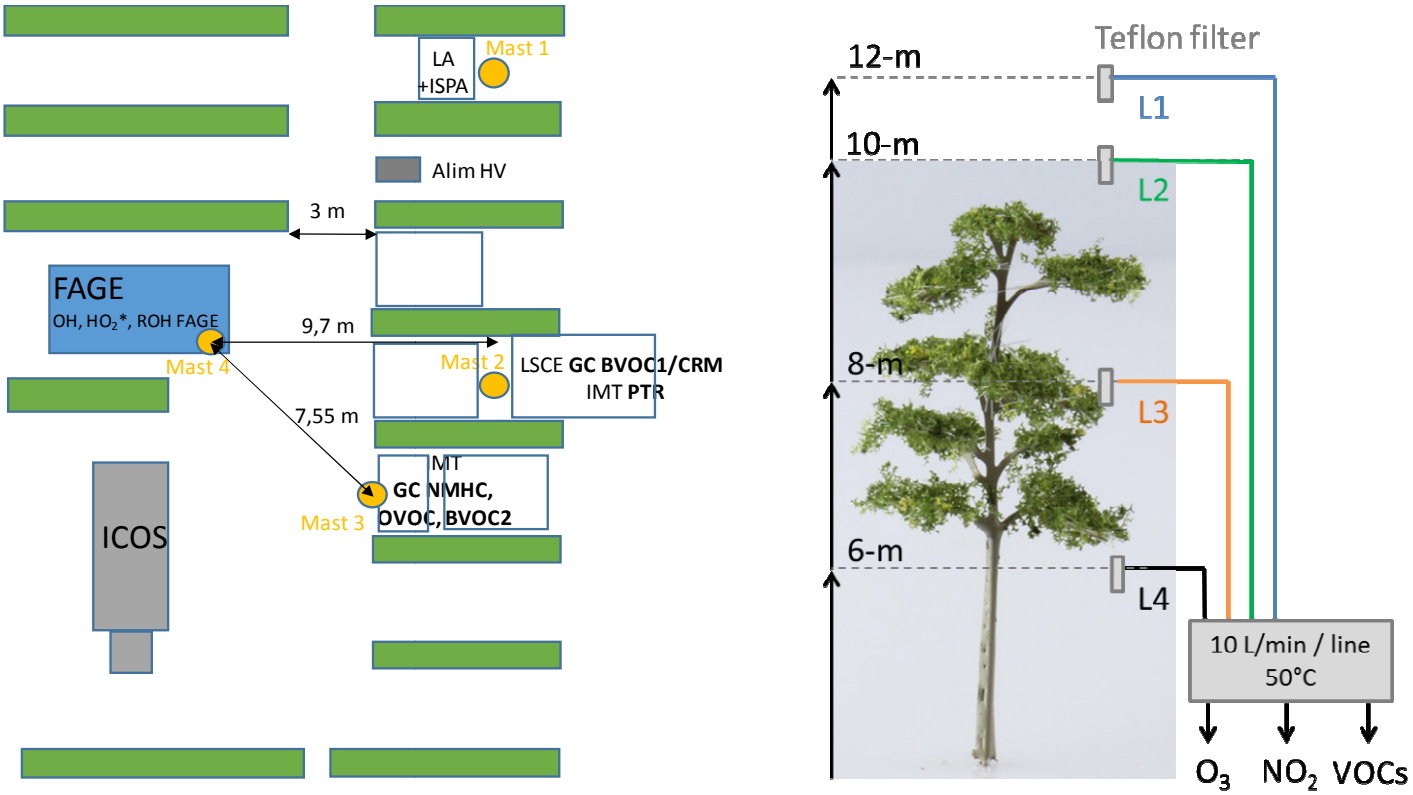

Figure V- 8:Left side corresponds to the map of the instruments distribution in the field site for all the different groups, the left side represents the different levels of the sampling points with respect to the trees size.

V.4.3.2 Gas chromatography

Additional measurements of different VOCs were obtained by several on-line gas chromatography instruments. Indeed, if the PTR-ToF-MS allows to access to a large number of species simultaneously, species with proton affinity lower than water cannot be detected, isobaric species cannot be speciated and some others are submitted to interferences. Four instruments have been deployed : GC-NMHC (non methane hydrocarbon), GC-OVOC (oxygenated VOCs), GC-BVOC1 from LSCE and GC-BVOC2 from IMT-Lille Douai (for biogenic VOCs). Gas chromatography instruments were distributed at different locations and the sample levels were above the canopy at 12 m (COVO, NMHC, and BVOC1), while BVOC2 instrument was sampling at 6 m level. Table V- 2summarizes the location and the sampling level for each gas chromatograph. The sampling levels are represented in the right side ofFigure V- 8.

Table V- 2: summary of the location and sampling level of each gas chromatography in LANDEX campaign

Gas chromatography	NMHC	COVO	[a]BVOC1	[b]BVOC2
location	mast 3	mast 3	mast 2	mast 3
level	L1	L1	L1	L4
Resolution time (min)	30	30	30	90

a: BVOC1 instrument is from LSCE laboratory for measurements of monoterpenes: α -pinene, β -pinene, myrcene, p-myrcene, limonene (co-eluted with cis-o-cymene), cineole.

b: BVOC2 from IMT-Mines Douai laboratory for the measurement of isoprene, monoterpenes: α-pinene, β-pinene, Myrcene, Limonene, Camphene, Sabinene, α-Phellandrene, 2 and 3-Carene, α-Terpinene, p-Cymene, Ocimene, 1,8-Cinéole(=Eucalyptol), γ-Terpinene, Terpinolene, Nopinone and other BVOC : Citral, Linalool and β-Caryophyllene.

Trace constituents (O_3, CO, NO_x,) were measured and collected by commercial analysers by different groups.

V.5 Results

OH, HO_2 and RO_2 concentrations were measured by UL-FAGE instrument for a limited period only: from 13 up to 19 of July, due to technical problems. The OH radical concentration was measured in the first cell, HO_2 radicals are detected as the sum of OH and HO_2 in the second cell (HO_x) after chemical conversion to OH by reaction with nitrogen oxide (NO). In order to quantify HO_2 without significant conversion of organic peroxy radicals (Fuchs et al., 2011), a "low NO" mode with the amount of NO adjusted to a conversion efficiency of 20 % has been used alternatively with a "high NO" mode to favor the conversion of RO_2 and quantify them. The instrument sensitivity was calibrated every 4 days by the calibration cell described in chapter II. We had technical problems with the reference cell dedicated to the OH wavelength precision, and the reactivity cell has been used instead to lock the laser to the OH line.

V.5.1 OH radical detection

Ambient air was sampled to the OH cell through a 1 mm nozzle with a sampling nozzle lent by the University of Indiana, allowing the use of an OH scavenger (pre-injector). The upper graph of

Figure V- 9shows the diurnal cycle of the measured OH radical from 13 up to 19 of July. Generally, OH concentration profiles were similar from the 13th up to the morning of 15th. The OH concentration profiles measured reached up to 3 × 10^7 cm^{-3} during the day from the 16th up to 18th. The minimum

concentrations were measured at night and were in the range of 10^6 cm^{-3}, while the maximum concentrations were observedin the midday of the 16th. The missing data in the OH concentration profile come from technical problems with the instrument. The chemical method to quantify the interferences on OH was applied during the 18th and 19th and the obtained results will be presented in the following section. The diurnal OH series in the upper graph of

Figure V- 9 shows negative data points, which is referred to noise in the measurement. This noise is mainly caused by the use of the reactivity cell for the on to off line modulation instead of the reference cell, not working.

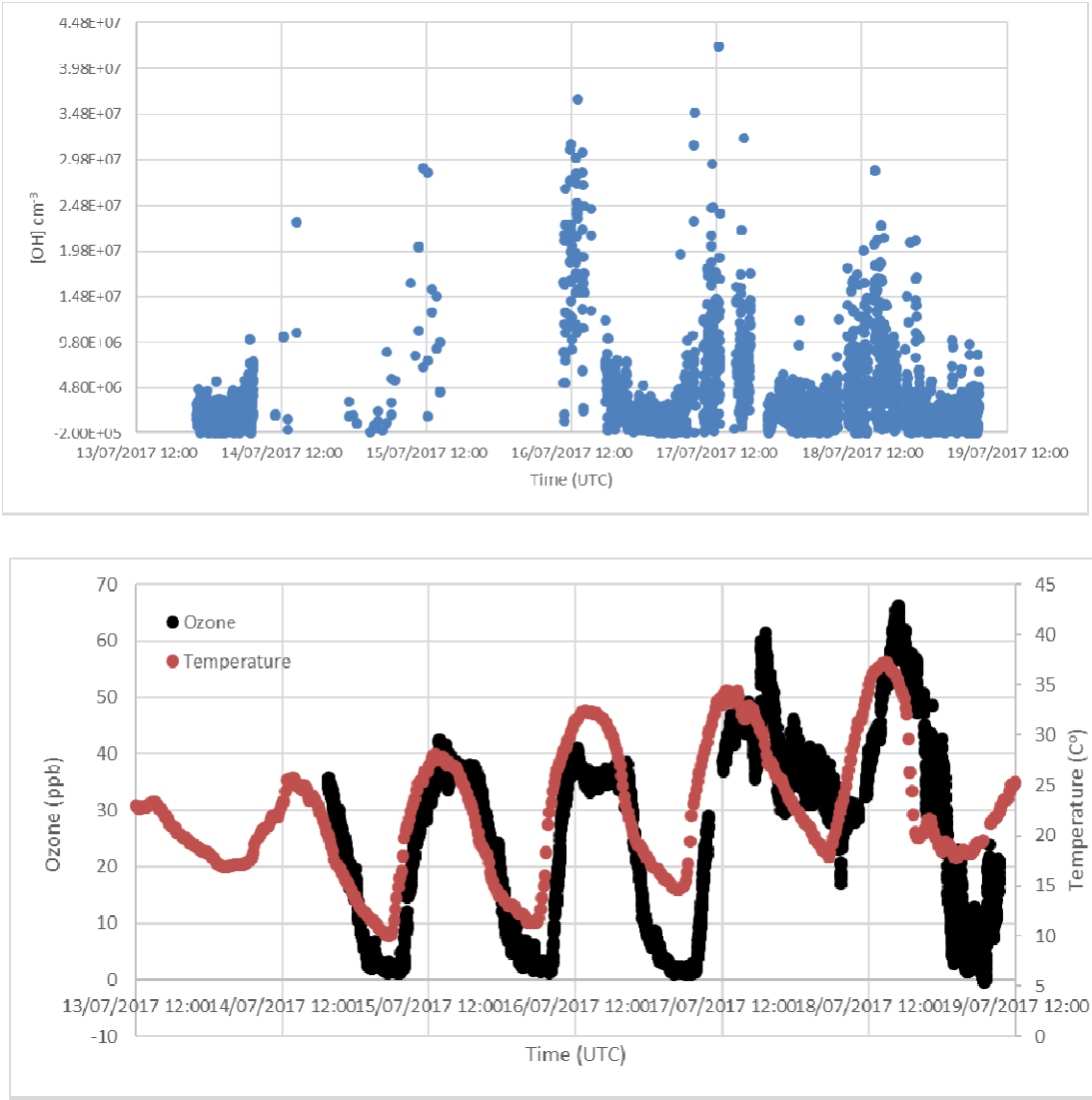

Figure V- 9: Time series of the OH signal (upper graph) in the first detection cell of UL-FAGE and time series (lower graph) of the ozone concentration and temperature evolution during LANDEX campaign from 13 to 19 July 2017.

The first 2 days, the weather was rainy and sky was mostly cloudy, while the mean temperature was around 20 C^o. On the 15th, the weather started to be moresunny and much hotter reaching the maximum of 37 C^o at 18th of July. The ozone concentration displayed a diurnal profile in correlation to the temperature diurnal profile with a maximum in the afternoon and a minimum at night as seen in the lower graph of Figure V- 10. The first 4 days (13-16 of July), the ozone concentrations observed were similar with a maximum of 35 ppb during the day and a minimum of 5 ppb at night. On the 17th, the O_3 concentration increased to reach 60 ppb during the day (lower graph of

Figure V- 9). When measured OH is compared to the ozone concentration and temperature, we find that OH concentration globally follows the ozone profiles. Some differences between the OH and ozone concentration profiles was seen in some periods. More analysis is needed to calculate the ozone production rate in the site, these calculations need to be done as all data from all participating groups are finalized.

Potential interferences overestimating the OH concentration can take place in such environment as seen in previous campaigns done in biogenic environments (Feiner et al., 2016a; Mao et al., 2012). Comparing the results of the measured OH concentrations in LANDEX to the ones measured in biogenic environments, we found slightly higher OH concentrations during LANDEX. The OH concentrations peak in the afternoon to reach 3 × 10^7 cm^{-3}, while the measured concentrations in other biogenic environments ranged between 1.5 to 2.5 × 10^7 cm^{-3} such as OP3, BEARPEX-2007, and PRIDE-PRD campaigns (Stone et al., 2012). Also, the concentrations measured are higher than the ones measured in a recent campaign in Wangdu (rural environment in China), were the OH profiles varied between 0.5 to 1.5 × 10^7 cm^{-3} (Tan et al., 2016).These differences of measured OH concentrations may come from the different site locations and seasonal measurements of the different campaigns.

V.5.2 OH interference

Forests emit abundant biogenic VOCs which react rapidly with OH. Besides that, forests have low levels of NO which can affect the pathways in the oxidation chemistry of these species. Several studies (Stone et al., 2012) have reported high discrepancies between the measured OH profiles and the modeled one in forest environment. It was suggested that these discrepancies may come from an additional source of OH such as: primary sources, photolysis of an unknown chemical species, or secondary sources, such as recycling of HO_x to OH within the BVOC oxidation mechanisms (Feiner et al., 2016b). The discrepancies may also arise from an instrumental interference in the FAGE

instrument (see Chapter III). For this reason, a pre-injector was used for the OH measurement in order to quantify the interference magnitude on the UL-FAGE instrument.

The pre-injector was used for the 18th and 19th of July, hexafluoropropylene (C_3F_6) was used as scavenger. C_3F_6 was injected into the ambient air to scavenge the OH before it is sampled through the instrument inlet. The amount of scavenger was chosen to maximize the fraction of OH (95 %) removed between the pre-injector and the inlet. By turning C_3F_6 injection on and off, the ambient OH signal is determined by subtracting the signal when injection is on from the signal when injection is off. Each mode was adjusted to be on for 20 mins followed by 1 min of flushing mode (see chapter II for more details). Figure V- 10shows the obtained results for the days where the chemical method was applied.

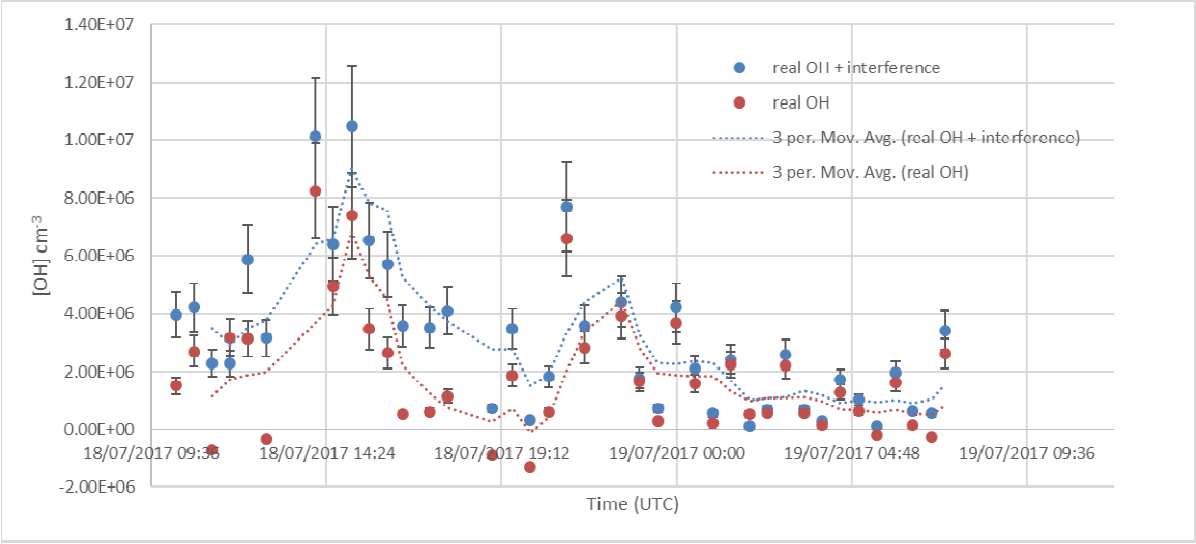

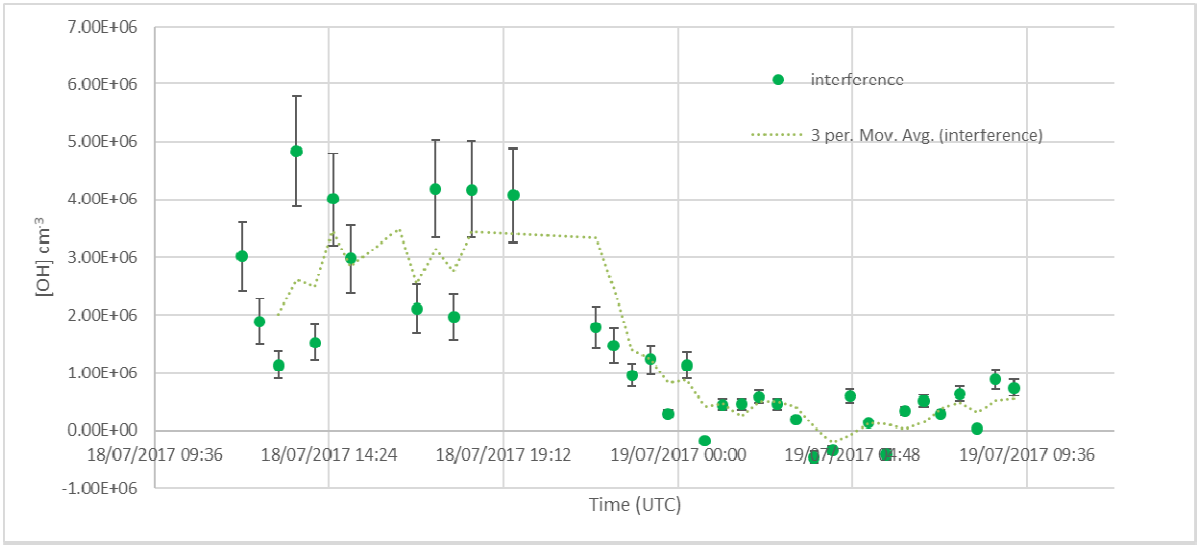

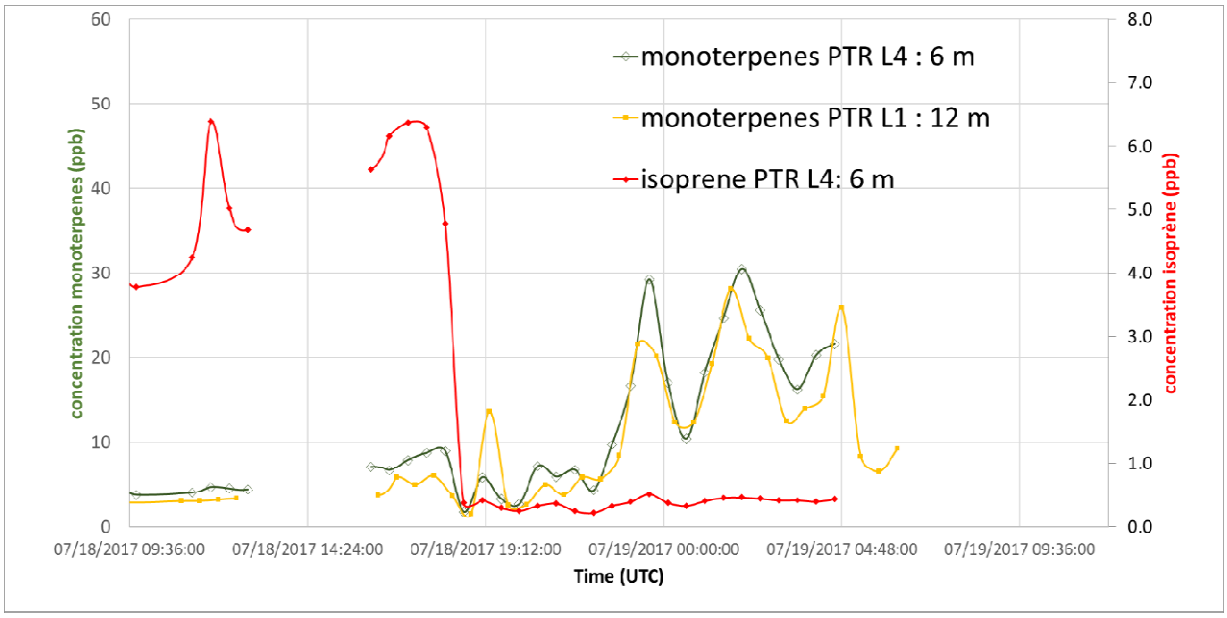

Figure V- 10: graph a, represents the OH + interference and real OH data, graph b, represents the interference observed using the pre-injector in the 18th and 19th of July, graph b, represents the VOCs concentrations measured at the same time by IMT-Douai laboratory.

The blue points represent the OH measured without using the scavenging gas (real OH + interference). The red squares represent the real OH measured which results from the subtraction of the signal measured without using the scavenging gas from the signal measured using the scavenger ($OH_{\text{mode on}} - OH_{\text{mode oFF}}$). Figure V- 10(upper graph) shows that the concentrations measured without scavenger (impacted by the OH interference) is high during the day of 18th and it starts to decrease to be on the same level as real OH during the night of 19th. The high interference observed corresponds to high level of VOCs during the day as seen in the lower graph ofFigure V- 10, were isoprene represented in red reached a maximum of about 6 ppb on the 18th. As we have shown that one source of the interference can be the presence of trioxides, ROOOH, (see Chapter III), the variation of the interference is consistent with this finding. Indeed, the presence of high level of VOC during the day with low NO (around zero most of the time with some peaks reaching 2 ppb) level is in favor of the production of trioxides from RO_2+OH reactions.

The OH measurements in absence of pre-injector may then be overestimated. This test is a proof that the pre-injector is needed in field campaigns with the UL-FAGE especially in environments where NO levels are low (during this campaign, most of the time below 1 ppb) and VOCs levels are high.

V.5.3 HO_2 and RO_2 detection

The UL-FAGE instrument was characterized for the interference of some RO_2 in the HO_2 detection cell as described in the chapter on laboratory experiments (see Chapter IV). During the campaign, HO_2

and RO_2 were measured in this cell by systematically varying the NO concentration. By this method we convert a significant portion of ambient RO_2 "double bound" in the FAGE cell at high NO concentration whereas it is negligible at low NO concentration. On the LANDEX site, there was a substantial emission of BVOCs and especially monoterpenes which can form peroxy radicals which can be converted to HO_2 then OH in the FAGE cell.

In order to detect ambient HO_2 or HO_2 coming from some RO_2 (HO_2*= sum of HO_2+ some RO_2 contributions), we used 3 different NO concentrations in the HO_2 cell (very low NO, low NO and high NO concentration). The 3 concentrations were 0.5 sccm, 2 sccm, and 8 sccm which correspond to conversion of HO_2 only, medium conversion of HO_2 + RO_2, and high conversion of HO_2 + RO_2 respectively. The NO flow was controlled to change the flow every 20 minutes.

This methodology allows to calculate separately the estimated concentration of HO_2 (with 0.5 sccm of NO, low level) and the estimated RO_2 converted in the cell (with 2 and 8 sccm of NO). The method used to extract HO_2 and RO_2 concentrations are described below.

From the signal measured at the different NO flows and the laboratory determination of the conversion efficiency of different RO_2, it is possible to obtain HO_2 and the sum of double bound RO_2 concentrations:

$$\text{Signal measured}_{(NO = x\ sccm)} = \text{Signal}_{RO2} + \text{Signal}_{HO2} \qquad \text{Eq V- 2}$$

From the tests in laboratory, we know that Signal $RO_{2(NO=0.5\ sccm)} = 0$.

Then:

$$[HO_2]_{(NO = 0.5\ sccm)} = \text{Signal measured}_{(NO = 0.5\ sccm)} / (\text{laser power} \times \text{Calibrations factor}_{(NO = 0.5\ sccm)}) \qquad \text{Eq V- 3}$$

The contribution of HO_2 to the signal measured at other NO flows can be subtracted to get the contribution of RO_2.

$$\text{Signal}_{RO2\ (NO = x) =} \text{Signal measured}_{(NO = x)} - ([HO_2]_{(NO = 0.5)} \times \text{laser power} \times \text{Calibrations factor}_{(NO = x)}) \qquad \text{Eq V- 4}$$

$$[RO_2]_{(NO = x)} = [(\text{Signal}_{RO2(NO = x)} / (\text{power laser} \times \text{Calibrations factor}_{(NO = x)})] \times \text{conversion factor } RO_{2(NO=X)} \qquad \text{Eq V- 5}$$

The conversion factor used was the one for isoprene and α-pinene which was equal to 0.6 at high flow (2 and 8 sccm, see Chapter IV). By analyzing the signal at 2 and 8 sccm, we have seen the same magnitude of RO_2concentration which validates the method as shown inFigure V- 11. We see that

the HO_2 concentration varied between 1 × 10^7 to 1 × 10^8 cm^{-3} from 13th to 16th of July where the ambient temperature was not high and the sky was cloudy. Then [HO_2] showed a dramatic increase during the daytime reaching 5 x 10^8 cm^{-3}on 18th of July.

The same behavior was seen for RO_2 concentrations with the two different NO concentrations. The results showed low concentrations from 13th to 16th of July reaching the maximum of 5 x 10^7 cm^{-3} on the 15th. As the temperature started to increase from 16thto 19th of July, the concentrations of RO_2 radicals showed an increase during the daytime reaching 1 x 10^8 cm^{-3} and started to decrease through the afternoon (Figure V- 11). This indicates that less RO_2 radicals are formed at night.

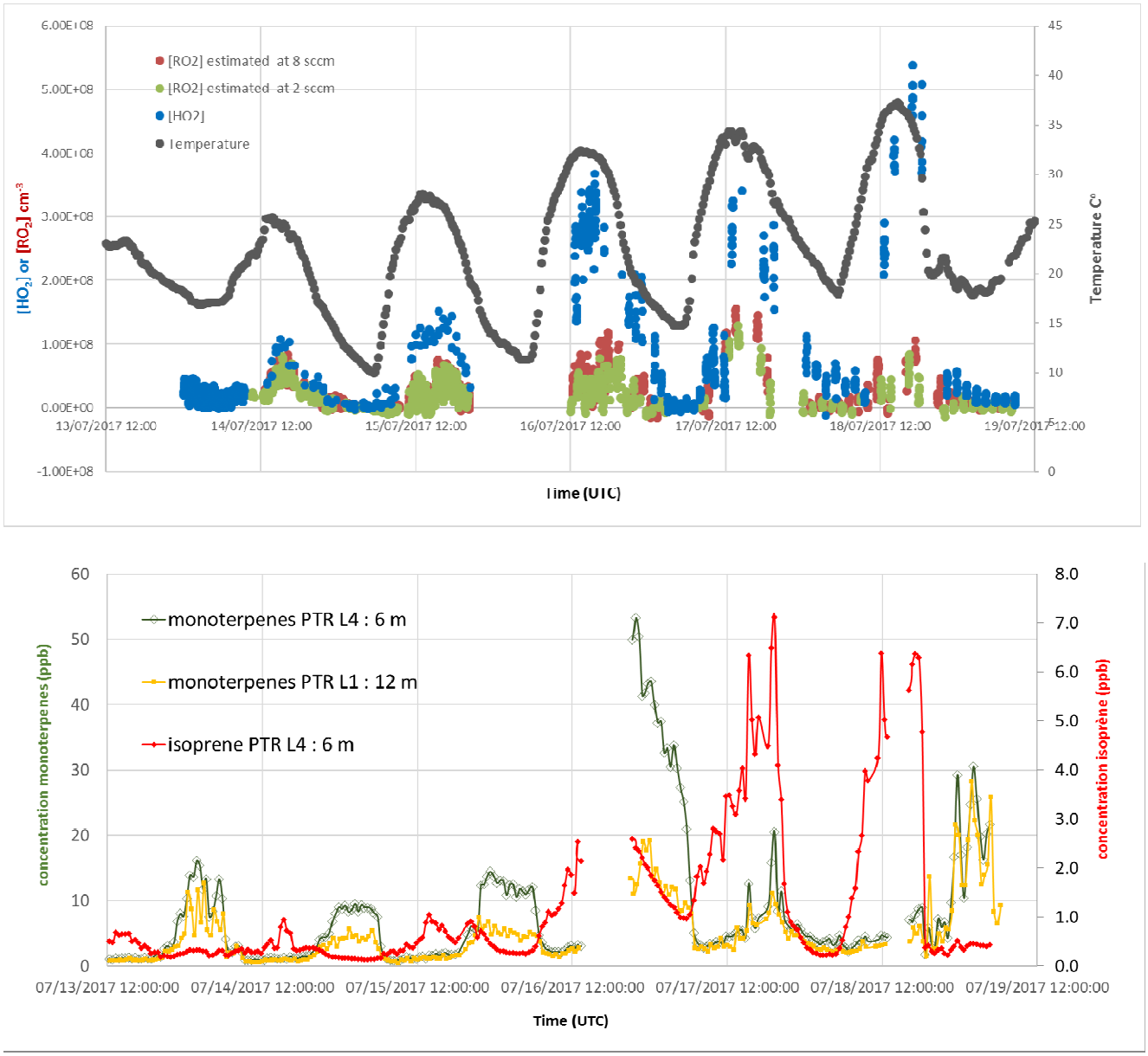

Figure V- 11: The upper graph shows the time series of HO_2 and peroxy radicals measured at LANDEX forest from 13 to 19 July 2017, the lower graph shows the measured VOCs (mainly monoterpenes and isoprene) at 2 different levels (L1 and L4).

Similar to other field campaigns, the measured HO_2 concentrations are in the range of 1.5 x 10^8 cm^{-3} in the afternoon. However the measured HO_2 radicals in biogenic environment campaigns varies between 1.2 x 10^8 cm^{-3} such as TOHPE campaign, to 28 x 10^8 cm^{-3} as one measured in AEROBIC and BEARPEX-2007 campaigns (Stone et al., 2012). Studies in different environments have also measured similar HO_2 concentrations, the measured HO_2 in rural environments ranged between 3-14 x 10^8 cm^{-3} (Tan et al., 2016). While in polluted environments, the measured HO_2 was lower by a factor of 3 to 10, the concentrations measured in PMTACS-2 2004 and MILAGRO-2006 campaign was around 2 x 10^7 cm^{-3} and 1.9 x 10^8 cm^{-3} respectively (Stone et al., 2012). Concerning the RO_2 profiles measured, there are not many published studies in biogenic environments. The measured peroxy radical concentrations ranged between 5-9 x 10^7 cm^{-3} in the afternoon. Comparing the concentration profiles measured in LANDEX to the one measured in rural environments such in WANGDU (3-15 x 10^8 cm^{-3}), we found that the concentrations measured in LANDEX are 10 times lower probably due to low NO levels.

Further analysis of these profiles will be performed when all data set from the different groups will be available. A comparison between concentrations measured and expected, from an analysis of the production and loss pathways will be done in collaboration with the LISA laboratory.

V.5.4 Total OH reactivity

This part will focus on the OH reactivity measurements and the intercomparison between the CRM and the pump probe method. The pump probe (UL-FAGE) and CRM are the main techniques available to measure the OH reactivity in the atmosphere. The OH reactivity measurement is particularly interesting for the understanding of the oxidation chemistry in the Landes forest as it allows to determine the level of understanding of the OH losses. The use of two instruments allows also to study the evolution of the reactivity with the height. Even if CRM and pump probe techniques have already been compared in the past and the results can be found elsewhere (Fuchs et al., 2017b), it was useful to have an intercomparison between these techniques again in this particular environment.Indeed, the intercomparison at the SAPHIR chamber highlighted a systematic underestimation of the reactivity measured by the CRM instruments for monoterpene mixtures(Fuchs et al., 2017b) andseveral improvements in the CRM have been done (see paragraph 4.2.2).

We will present first an overview of the results during the period of pump-probe measurements, then the comparison between CRM and UL-FAGE instruments in different locations and then an analysis of the calculated reactivity and the comparison with the measured ones.

V.5.4.1 Overview of the results obtained

The UL-FAGE instrument measured the OH reactivity from the 13th to the 19th of July, in the canopy. During that period, the CRM instrument measured or in the canopy or above the canopy but not at the same horizontal location. At the end of the campaign, the CRM probing line was moved to be at the same location than the UL-FAGE instrument. Results are shown in the upper graph ofFigure V-12. The OH reactivity measured was in direct correlations with the emitted VOCS as shown in Figure V- 12(lower graph), and will be analyzed in more details in paragraphV.5.5. Morning contributions to OH reactivity seem to follow isoprene concentration whereas it follows monoterpenesat night. The measured reactivities showed a low reactivity during the day of average 6 s^{-1} over the first 4 days (13th -16th of July), while it showed a higher reactivity during the night reaching 20 s^{-1} for the same period. The 17th of July, the reactivity increased as the temperature increased, the maximum reactivity recorded during the daytime was around 20s^{-1}. The total OH reactivity starts to increase in the afternoon at around 19 h to reach the maximum at 00 h and then starts to decrease to reach the minimum (12 s^{-1}) in the morning around 8 h. Largest variability was observed at night (19 h to 00h) in the 24 hours profile.

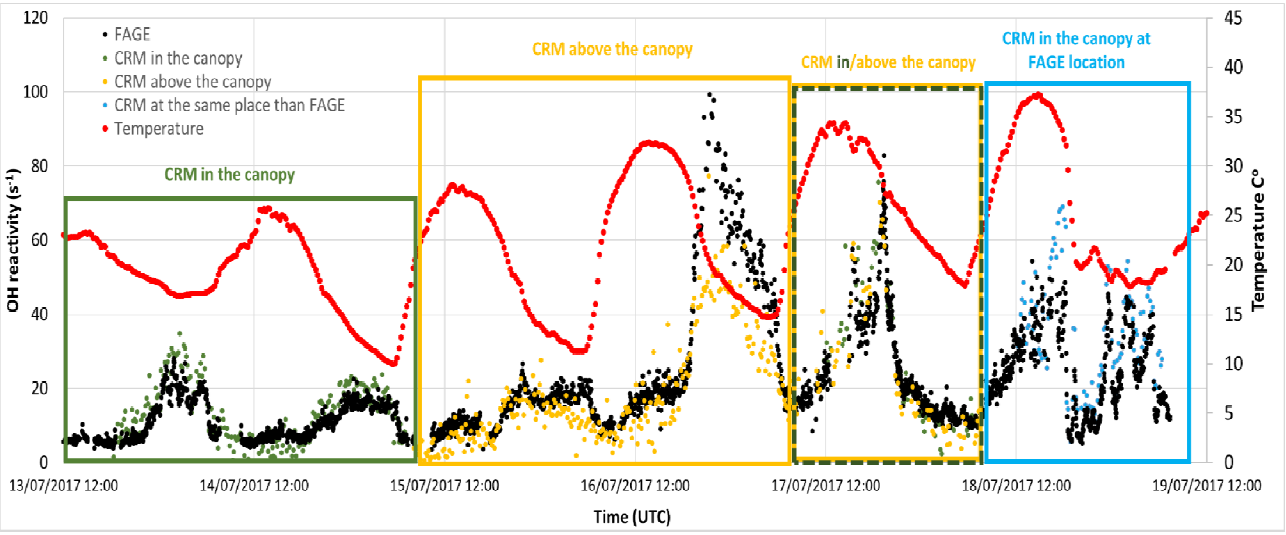

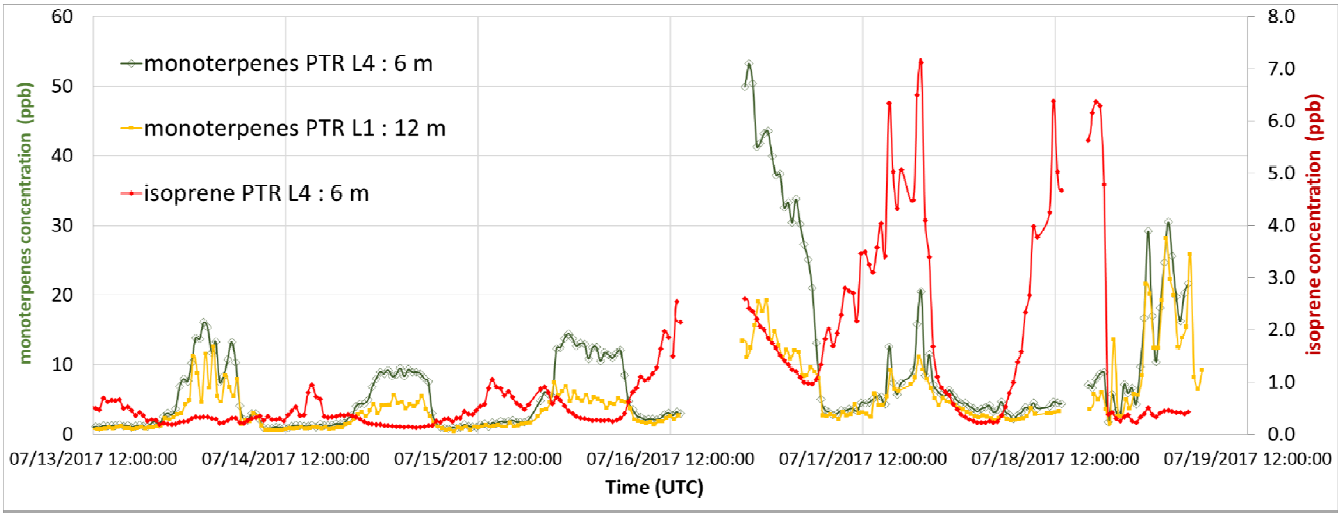

Figure V- 12: The upper graph represents the time series of total OH reactivity during LANDEX campaign measured by UL-FAGE and CRM instruments from 13 to 19 July 2017, black points represent the measured reactivity by UL-FAGE, green, yellow, and blue points represent the measured reactivity by CRM. The lower graph shows the measured monoterpenes and isoprene in the field. Green points correspond to the isoprene concentrations at L4 level, yellow and gray points represent the monoterpenes concentrations at L1 and L4 respectively.

The comparison between the CRM and UL-FAGE peaks in the last period and the results of the PTR-ToF-MS has been used to check the synchronization of the measurements. A shift of 4 min (delayed) has been observed on the pump-probe data and has been corrected for all the analysis.

The intercomparison between LIF and CRM methods at the same place was carried out the last 2 days of the measurement campaign (18th and 19th of July, paragraphV.5.4.2, blue frame inFigure V-13). In addition, a comparison for the reactivity measurement was done for different periods of the campaign: with both instrument at the same height but at different horizontal locations (paragraphV.5.4.3, green frames) and with the instruments at different heights (paragraph V.5.4.4, yellow frame).

V.5.4.2 Intercomparison of CRM and UL-FAGE measurements at the same location

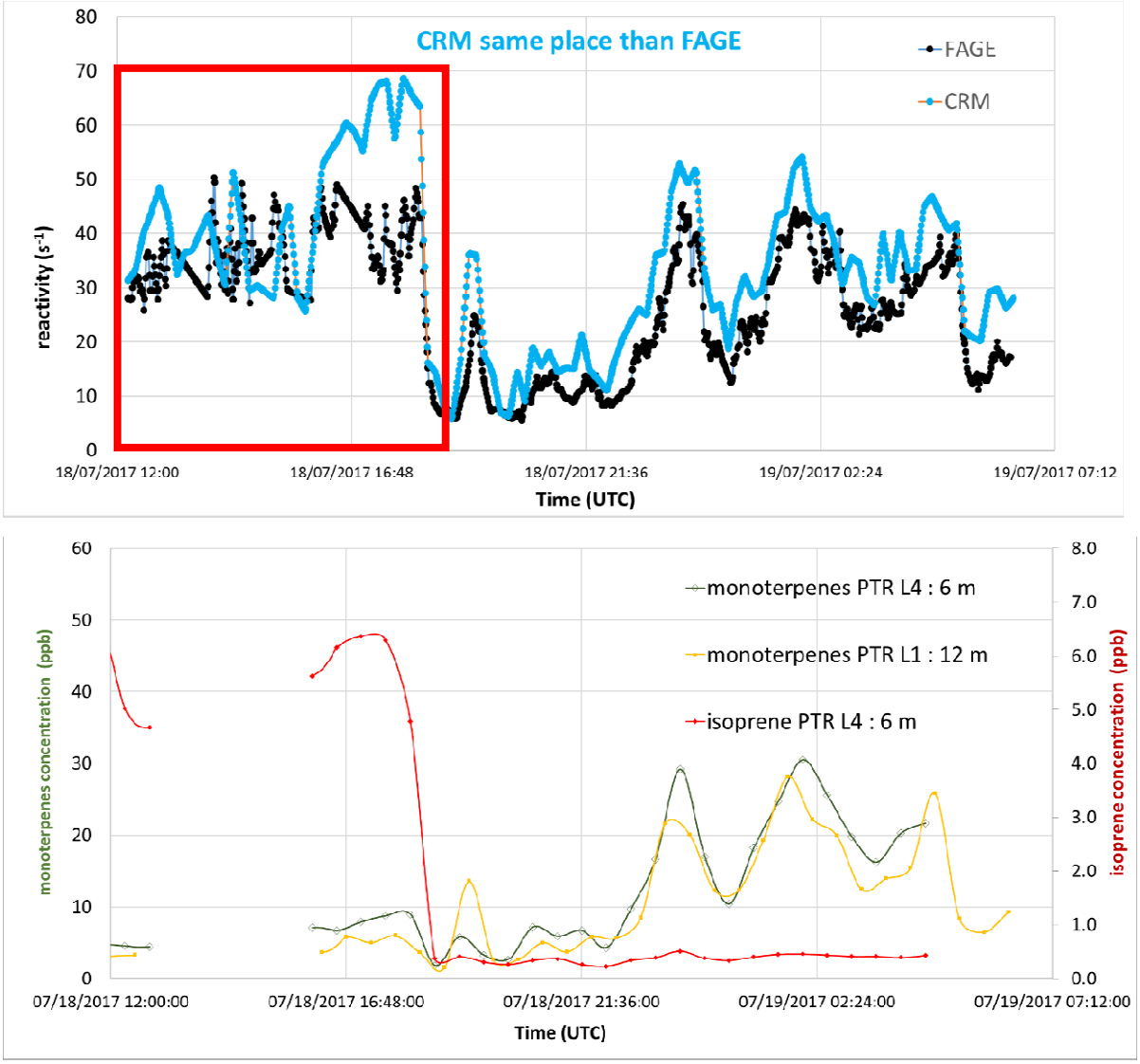

Figure V- 13:The upper graph represents the time series of total OH reactivity during LANDEX campaign measured by UL-FAGE and CRM instruments from 18 to 19 July 2017, black points represent the measured reactivity by UL-FAGE, blue points represent the measured reactivity by CRM.The lower graph shows the measured monoterpenes and isoprene in the field for the same period. Green points correspond to the isoprene concentrations at L4 level, yellow and gray points represent the monoterpenes concentrations at L1 and L4 respectively. The red square in the upper graph corresponds to the period where the pyrrole-to-OH ratios higher than 4.

This period represents the last 2 measurement days (18th and 19th of July) of the campaign where the 2 instruments were sampling at the same point. The sampling tube of the CRM was moved to be side to side to the Teflon tube of the UL-FAGE (above the container at 5 m from the ground, inside the canopy). This way we can have a direct comparison between the 2 methods without any variabilities which could be due to the heterogeneity of the air composition. As shown inFigure V- 13, almost the same reactivity was measured by both instruments despite the variation in the VOCs concentrations. On 18th of July, isoprene was the dominant species present reaching 6 ppb in the afternoon while the

monoterpene concentrations were low around 3 ppb. In contrast, the monoterpene concentrations were dominant on 19th of July showing 3 spikes reaching 30 ppb as shown in the lower graph ofFigure V- 13. Total OH reactivity in this period ranged between 60 and 15 s^{-1} within the canopy, minimum values were found during daytime, increasing throughout the night. A strong difference was seen in 18th of July (from 16:00 to 18:15, UTC). However, it corresponds to a period for which the CRM was working out of the characterized conditions, with a pyrrole-to-OH ratios higher than 4 from 12:09 to 18:31 (UTC). The total period with pyrrole-to-OH ratios higher than 4 has been excluded from the intercomparison.

Despite the variable species domination (isoprene, monoterpenes or mixture), we observe a good agreement in the measured reactivity by the 2 methods. The measured reactivity by CRM instrument as function of the measured reactivity byUL- FAGE instrument has been plotted (Figure V- 14).

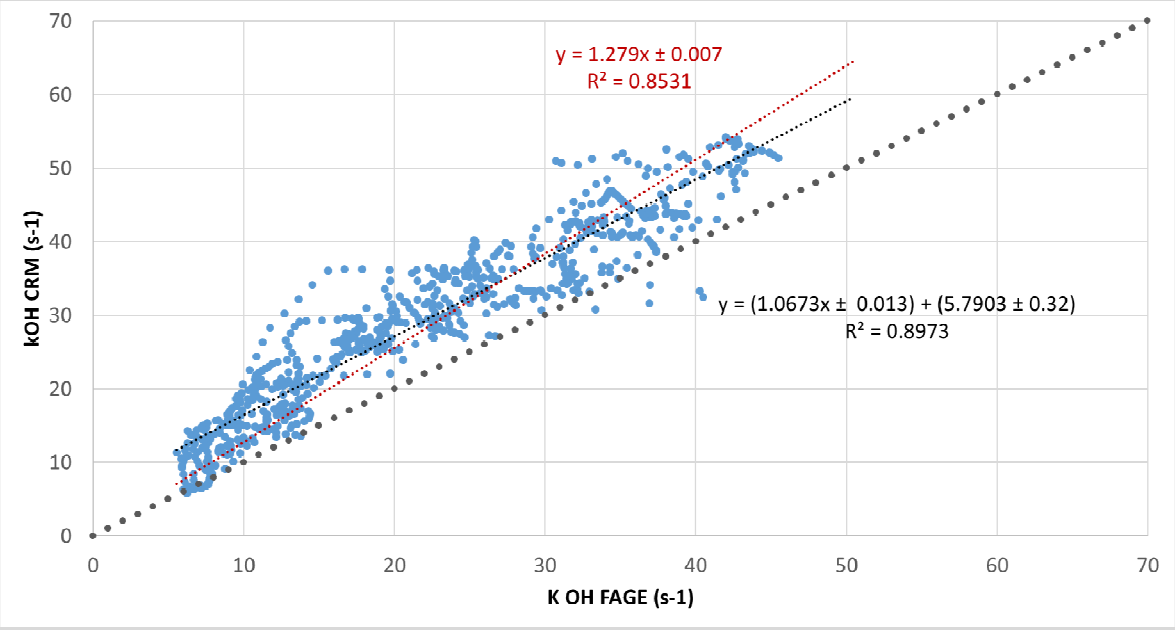

Figure V- 14: Measured reactivity by CRM instrument as function of the measured reactivity by UL-FAGE during the last period of the intercomparison.

A good agreement was obtained with the linear fit giving a slope of 1.05 (fit non-forced to zero) but with a high intercept. When forced to zero, the slope increases (1.27) but with a similar R^2. This intercept may come from underestimation of the zero air measurements done by the CRM or over-estimation of the zero measurements done by the FAGE instrument.

V.5.4.3 Comparison of CRM and UL-FAGE measurements at the same height but different horizontal locations

From 13th to midday of 15th of July and from 17th midday to 18th midday, the 2 instruments were at different locations but measured in the canopy (alternatively for the CRM for the second period). The horizontal distance between them was around 10 m as shown inFigure V- 8.

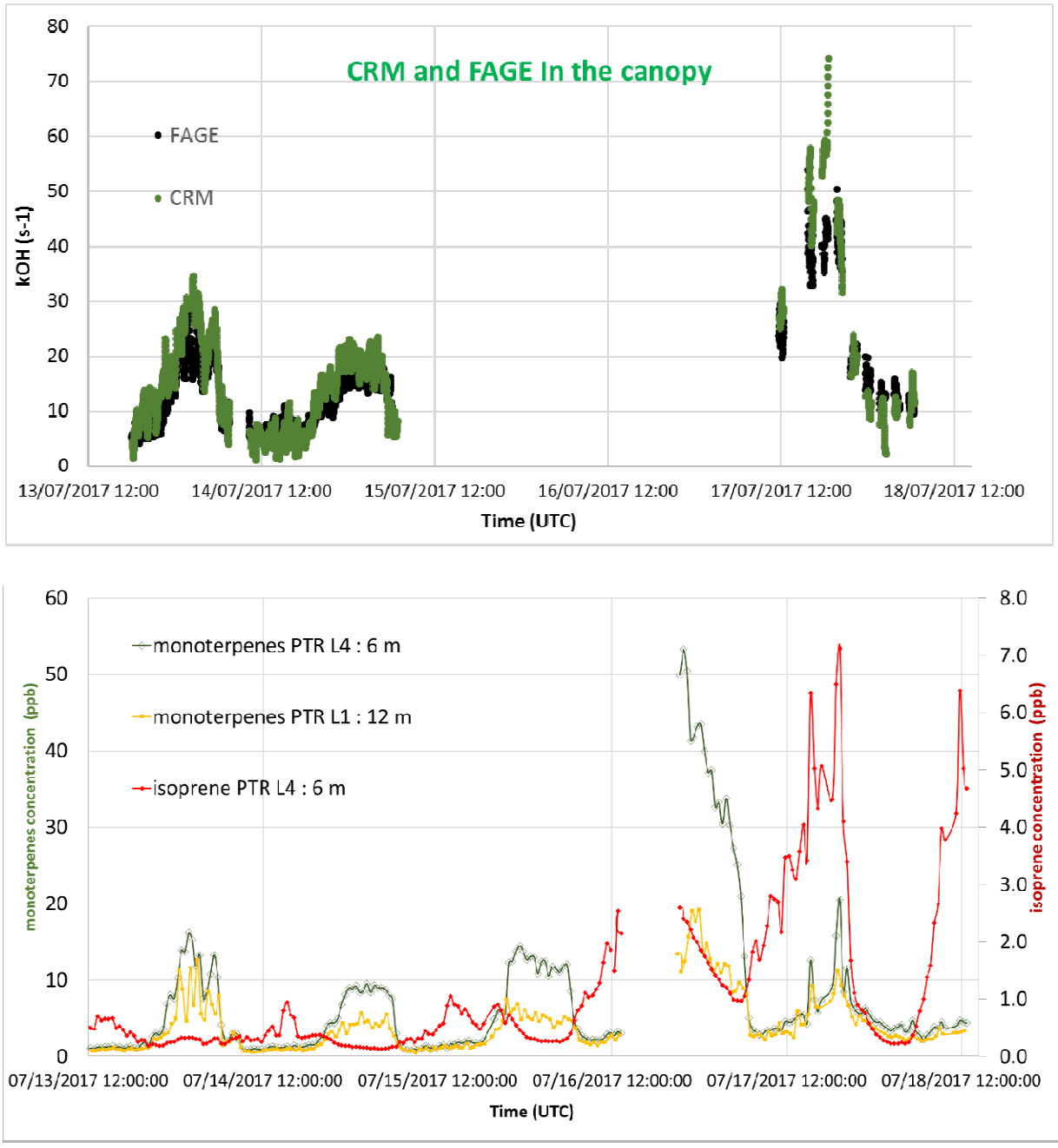

Figure V- 15:The upper graph represents the time series of total OH reactivity during LANDEX campaign measured byUL-FAGE and CRM instruments from 13 to 15 and 17 midday to 18 midday of July 2017, black points represent the measured reactivity by UL-FAGE, green points represent the measured reactivity by CRM.The lower graph represents the measured monoterpenes and isoprene in the field for the same period. Green points correspond to the isoprene concentrations at L4 level, yellow and gray points represent the monoterpenes concentrations at L1 and L4 respectively.

The sampling lines for both instruments were inside the canopy (5 mabove the ground). During these periods, the measured reactivity by both instruments found to be in a good agreement even if the conditions are contrasted:

1) - from midday of 13th to midday of 14th of July, we see that the measured monoterpenes at L1 (12 m) and L4 (6 m) are almost the same. From this, we conclude that there is no vertical stratification of the mixture. Therefore, there is a homogeneity in the field vertically and horizontally and we observe the same total OH reactivity at different horizontal locations.

2) - from 14th midday to 15th midday of July, we see during the night a difference in the measured monoterpenes concentrations between level 1 and level 4. The monoterpenes were higher by a factor of 2 in level 1 (lower graph ofFigure V- 15), thus there is a vertical stratification in the gas mixture. However, concerning the measured reactivity by UL-FAGE and CRM, we see that both instruments measured the same reactivity. Therefore, we can assume that even when there is a vertical stratification, it is not the case horizontally and we can consider the homogeneity of the gas mixture composition at a given height.

Concerning the period starting from 17th midday to 18th midday of July, the CRM sampling was 1 hour inside the canopy (5 m) / 1 hour above the canopy (12 m). The measured reactivity by both instruments showed a good agreement for the entire period (Figure V- 15). In the same figure, we see that the measured monoterpenes were also the same for the different levels (L1 and L4).

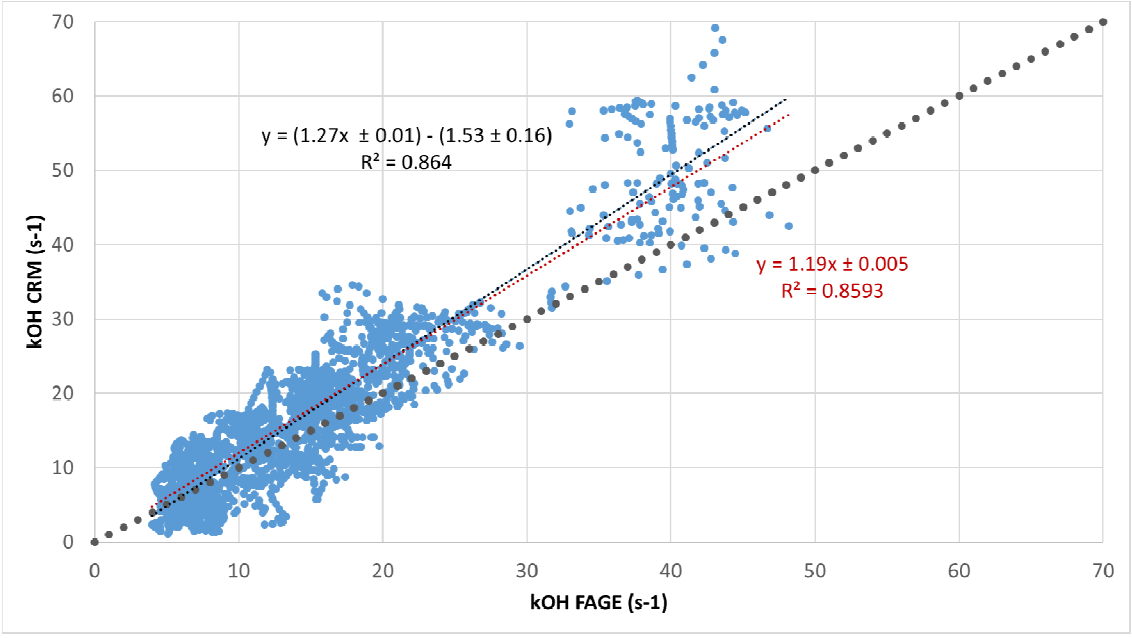

Figure V- 16: measured reactivity by CRM instrument as function of the measured reactivity by UL-FAGE during the first period of the comparison.

The reactivity measured by CRM instrument as function of the reactivity measured by UL-FAGE instrument was plotted when CRM was measuring in the canopy (Figure V- 16). The linear regression of these data shows a good agreement with a slope of 1.27 (fit non-forced to zero) and 1.19 (for fit forced to zero) and correlations coefficient, R^2, equals to 0.864 and 0.859respectively. The offset for the non-forced fit is -1.1 ±0.16.From these observations, we can conclude that when there is or not a vertical stratification, results in the reactivity measurements at different horizontal locations are consistent and that the mixture is horizontally homogeneous, which is very useful for the calculated reactivity at level L1 where less measurements are available (see paragraph V.5.5).

V.5.4.4 Comparison of CRM and UL-FAGE measurements at different heights

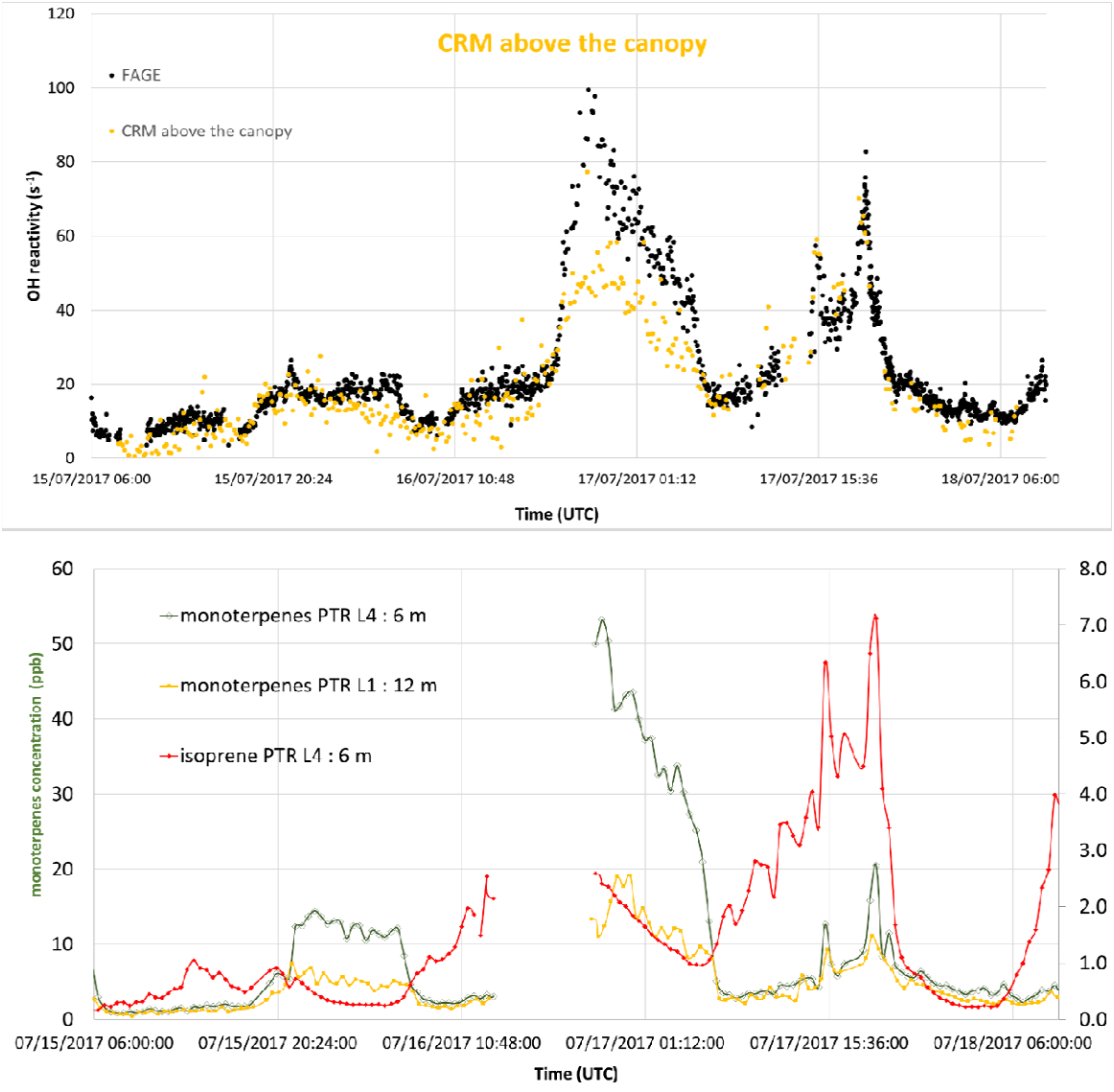

Figure V- 17: The upper graph represents the time series of total OH reactivity during LANDEX campaign measured by UL-FAGE and CRM instruments from 15 to 18 midday of July 2017, black points represent the measured reactivity by UL-FAGE, yellow points represent the measured reactivity by CRM. The lower graph represent the measured monoterpenes and isoprene in the field for the same period. Green points correspond to the isoprene

concentrations at L4 level, yellow and gray points represent the monoterpenes concentrations at L1 and L4 respectively.

Measurements with the CRM were carried out at two different heights in order to characterize total OH reactivity inside (6m) and above the canopy (12m). More specifically, measurements were performed above the canopy measurements from July 15th to 17th simultaneously to measurements in the canopy by the UL-FAGE instrument.

During this period, we can observe different conditions. The first night, both instruments measured similar levels of reactivities whereas the difference increased at night of the 16th of July where the measured reactivity by UL-FAGE is 2 times higher than the reactivity measured by CRM.

We clearly see that PTR-MS from IMT-Douai measured higher concentrations at L4 reaching maximum of 50 and 12 pbb monoterpenes at nights of 15th and 16th of July respectively while the measured monoterpene concentrations at L1 were at the maximum 5 and 20 ppb. This difference directly affected the measured reactivity by CRM and UL-FAGE at L1 and L4 respectively, particularly when high concentrations of monoterpenes are observed.

On the other hand, when there is stratification, we observe a big difference in the reactivity measured by both methods for the 2 levels with huge differences in the monoterpenes concentrations. These results have to be analyzedwith respect to the calculated reactivity to identify conditions of missing reactivity, which would highlight missing OH losses not identified by VOCs measurements.

V.5.5 Missing reactivity

The forest environments emit numerous hydrocarbon species including isoprene, monoterpenes and oxygenated compounds. At the study site, the most abundant and important hydrocarbons measured were the isoprene and monoterpenes whose daily maximum mixing ratios reached 7 and 50 ppb respectively. Thus, these trace gas concentrations were used to calculate the OH reactivity. The total OH reactivity is defined as the summation of all the species reacting with OH multiplied by their rate constant. Calculated OH reactivity is assessed based on the trace gases datasets and VOCs dataset from PTR-MS and GC-MS.

V.5.5.1 Trace gases considered for the calculated reactivity

Different instruments were available to quantify the VOCs during the LANDEX campaign, air was sampled in the field by 4 GC-MS instruments at different locations (Table V- 2) and one PTR-MS sampled at 4 different levels (Figure V- 8).

During the second part of the measurement campaign (16 July), the BVOC2 had a technical problem and stopped to measure at L4 (6 m), but the PTR-MS continued to measure during this period. As the aim of the comparison between the measured and the calculated reactivity is to identify missing reactivity and potential different behaviors at L1 and L4, it is also important to compare similar sets of data at the two levels. It is why a preanalysis of the VOCs data has been done to select the most appropriated data to calculate the reactivity.

As the PTR-MS was measuring all the time at the two levels where the OH reactivity was measured, this set of data is the most interesting. However, it suffers from different limitations:

1) The PTR-MS measures the total monoterpenes mass (z=137), while with GC-MS, monoterpenes are speciated.
2) Some species are not measured by the PTR-MS (alkanes for example)
3) Some species suffer from interferences of other species in the PTR-MS (case of isoprene)

To solve these different limitations, different tests have been done to evaluate the reliability of the PTR-MS data to calculate the OH reactivity.

1) To account for the speciation of the monoterpenes using the PTR-MS data, a comparison was done using the first part of the campaign where both instruments were measuring at the same level. By dividing the concentrations of the speciated monoterpenes (10 compounds) measured by the GC- BVOC1 and 2 over the total monoterpenes measured, we obtain ratios of the monoterpenes measured.

2) The OH reactivity calculated from each monoterpene has been compared with the one obtained from the average ratios for the GC BVOC data and the PTR-ToF-MS data for the overlapping period. Calculated reactivity for monoterpene ratios are done using a weighted rate constant. It represents the summation of the rate constant of each monoterpene multiplied by the corresponding concentration of the specific monoterpene. Weighted rate constant is defined as:

$$k_{weighted} = \sum_i k_{OH+\,X_i} X_i \qquad \text{Eq V- 6}$$

Where X_i represents the ratio of each monoterpene, and $k_{OH+\,X_i}$ is the corresponding rate constant for each monoterpene species. The reaction rate constant of the different trace species quantified in the field were taken from the literature (Atkinson et al., 1997, 2006). Then, the reactivity of the monoterpene ratios is calculated as the following equation:

$$k_{OH-monoterpenes} = \left[\sum_i k_{OH+\,X_i} X_i\right] \times [M] \qquad \text{Eq V- 7}$$

where [M] represents the sum of monoterpenes concentration. The comparison of the calculated reactivity from each monoterpene with the one obtained from the ratios for the GC BVOC data and the PTR-ToF-MS data for the overlapping period are shown inFigure V- 18.

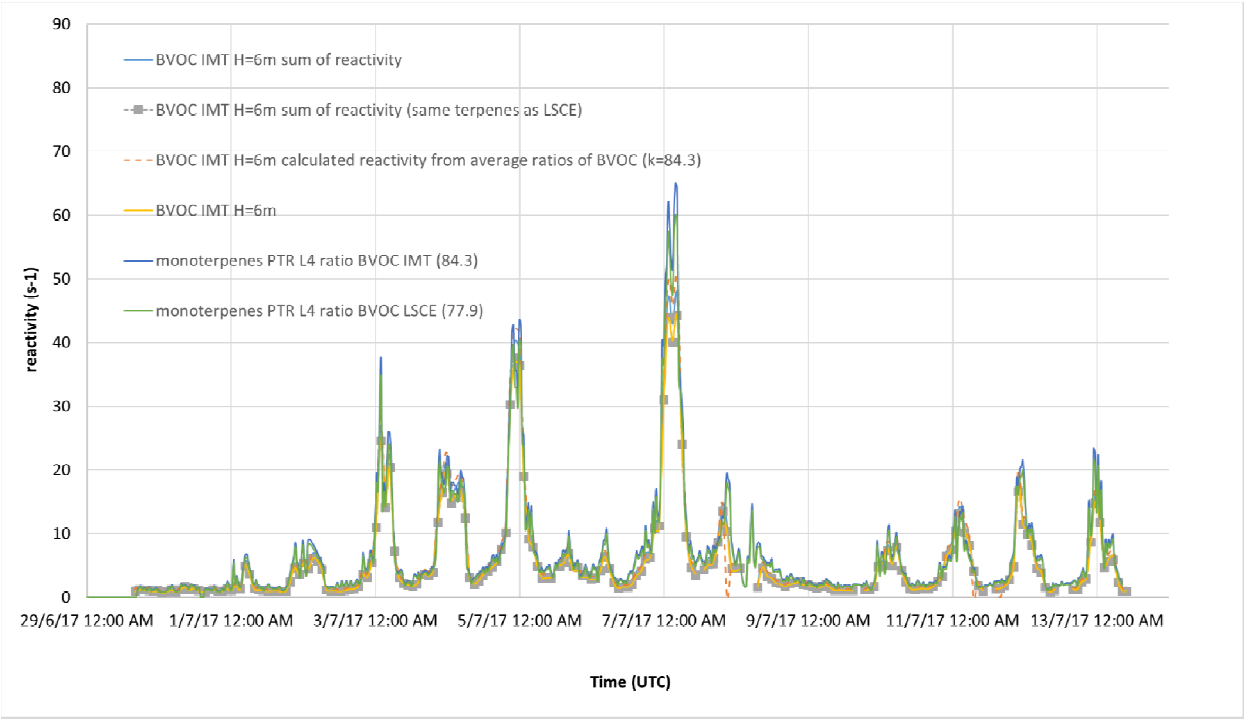

Figure V- 18: OH reactivity calculated for monoterpenes with the GC BVOC IMT at 6 m using the concentration and rate constant of each monoterpene (blue line), with the monoterpenes measured considering only the monoterpenes measured by the other GC-BVOC (gray dashed line), with the sum of the concentrations weighted by the ratio of each monoterpene multiplied by the respective rate constant (orange dashed line), with the monoterpenes measured by the PTR-MS considering or the weighted reactivity from the monoterpenes measured by the GC BVOC IMT (dark blue) or the restricted list (corresponding to those measured by the GC LSCE (green line).

The use of the ratios is in good agreement for the whole period with some overestimations at the peaks when using PTR-MS data. An overestimation of 1.4 s^{-1}(2.9%) at the maximum is observed when

using the ratios compared to the real concentrations. The use of only a part of the monoterpenes (those measured by the GC BVOC LSCE) leads to an underestimation of 1.6 s^{-1}(3.4 %). When using the data from the PTR-MS, the OH reactivity at the highest peak is overestimated by approximately 17.5 (36.7%) and 12.5 s^{-1} (26.3 %) at the maximum (Table V- 3) considering the weighted rate constant from all the monoterpenes measured with the GC BVOC IMT or only those measured by the GC BVOC LSCE.

Table V- 3: The maximum reactivity calculated using the monoterpenes measured separately of as ratios from the different GC-MS and PRT-MS instruments. $K_{weighted}$ for each condition are presented.

	Sum of reactivity GC BVOC IMT	*Sum of reactivity GC BVOC IMT reduced to LSCE*	*Reactivity GC ratio BVOC IMT ($k_{weighted}$=84.3)*	*Reactivity BVOC IMT ratio LSCE ($k_{weighted}$=77.9)*	*Reactivity PTR ratio BVOC IMT ($k_{weighted}$=84.3)*	*Reactivity PTR ratio BVOC LSCE ($k_{weighted}$=77.9)*
Maximum	47.55	44.31	50.24	44.08	65.00	60.06
difference		-3.24	2.69	-3.47	17.45	12.51

The use of the ratios shows a relatively good agreement between calculated reactivity from the GC-BVOC and weighted reactivity from the PTR-MS data. Similar results have been observed at 12 m. It has then been chosen to use the PTR-MS data for both heights with the monoterpene list measured by the GC BVOC from the LSCE.

3) To estimate the contribution of the species measured by the NMHC and OVOC GC (only at 12 m), calculated reactivities including or not these species have been compared as shown in Figure V- 19. The included species from each instrument are listed in Table V- 4.

Table V- 4: species used to calculate the reactivity in the site by three different instruments

Instrument	*Measured species*
PTR-MS (L1, L4)	Monoterpenes, Methanol, acetonitrile, acetaldehyde, acetone, isoprene, MAC+MVK[a], MEK
GC-NMHC (L1)	Ethane, ethylene, propene, isobutene, acetylene, 2-butene, isopentane, pentane, 1,3-butadiene, [c]2mt 2 butene+1 pentene, cyclopentene, hexane, hexane,2,4-dimethylpentane,benzene, 3,3-dimethylpentane, 2-methylhexane, isooctane, heptane, toluene, octane, ethylbenzene, xylene, styrene, o-xylene, nonane, 4-ethyltoluene, 2-ethyltoluene, 1,2,4-trimethylbenzene, 1,3-dichlorobenzene, undecane, isopropylbenzene, n-propylbenzene
GC-OVOC (L1)	Benzaldehyde, butanol+2hexanone[b], isopropanol, ethanol,2-butanone, tert-Amyl

	methyl ether, furan

a:the ratio has been calculated from the GC-OVOC, b: the rate constant of butanol is used, c: rate constant of 2 methyl 2 butene is used.

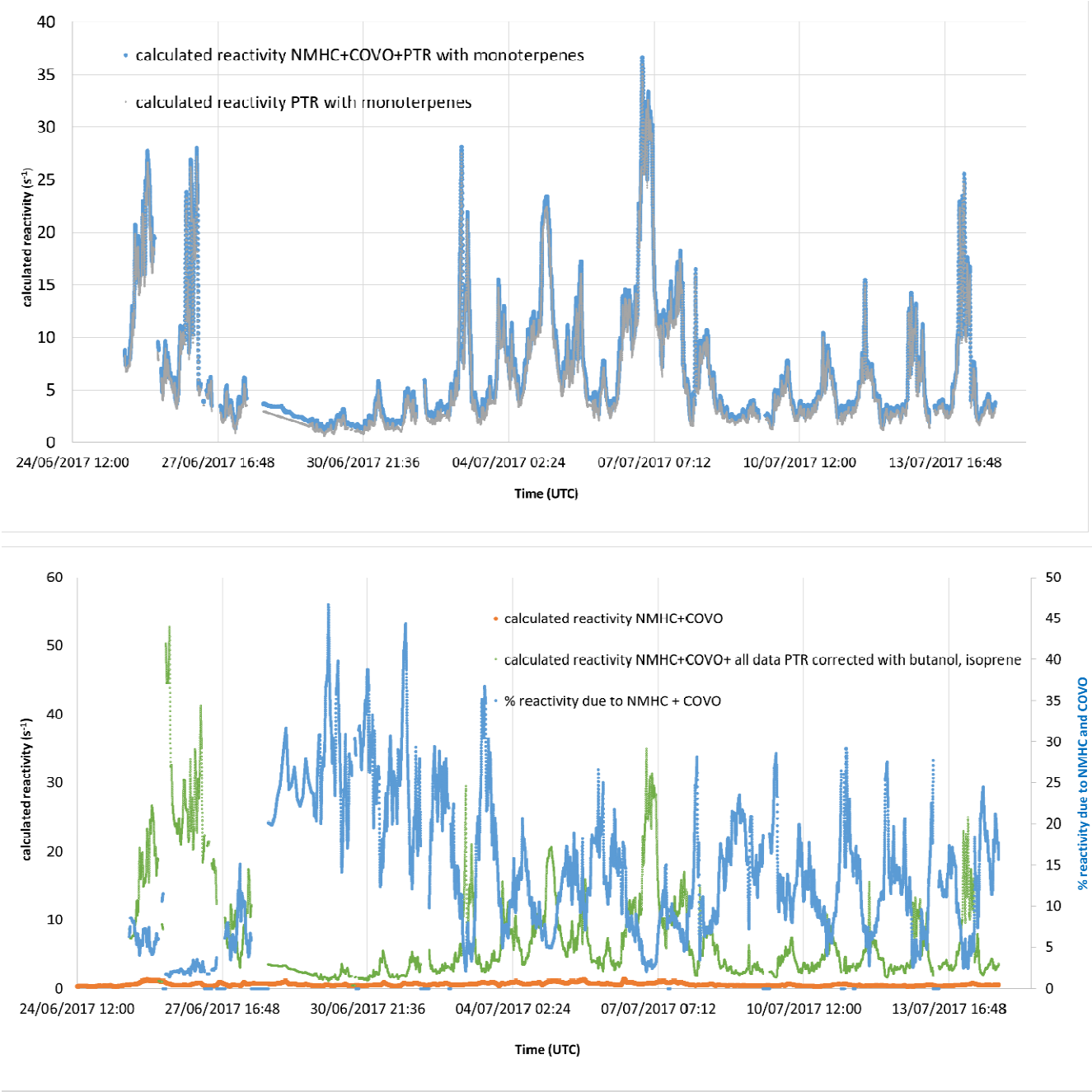

Figure V- 19: The upper graph represents the calculated reactivity at L1 (12 m) from the PTR monoterpenes (gray points) and the calculated reactivity done including the PTR, NMHC, and COVO data (blue points). The lower graph represents the calculated reactivity from NMHC, COVO, and PTR data corrected with butanol and isoprene (green points), from NMHC and COVO data alone (orange points), and the percentage of the reactivity due to NMHC and COVO data during the first period of the campaign.

The contribution of these species is weak (less than 2 s^{-1}) and will represent an important part of the reactivity only for weak reactivities. This contribution is within the uncertainties of the OH reactivity measurement and will not be considered in the analysis.

4) The isoprene measurement by the PTR-MS has been shown to be affected by interferences due to monoterpenes fragments. In order to use the PTR-MS data for this species (only data available at L4), the contributions of monoterpenes have been estimated by comparison between GC measurements and PTR-MS ones and a contribution of 4% of monoterpenes, giving a good agreement between the profiles, has been used.

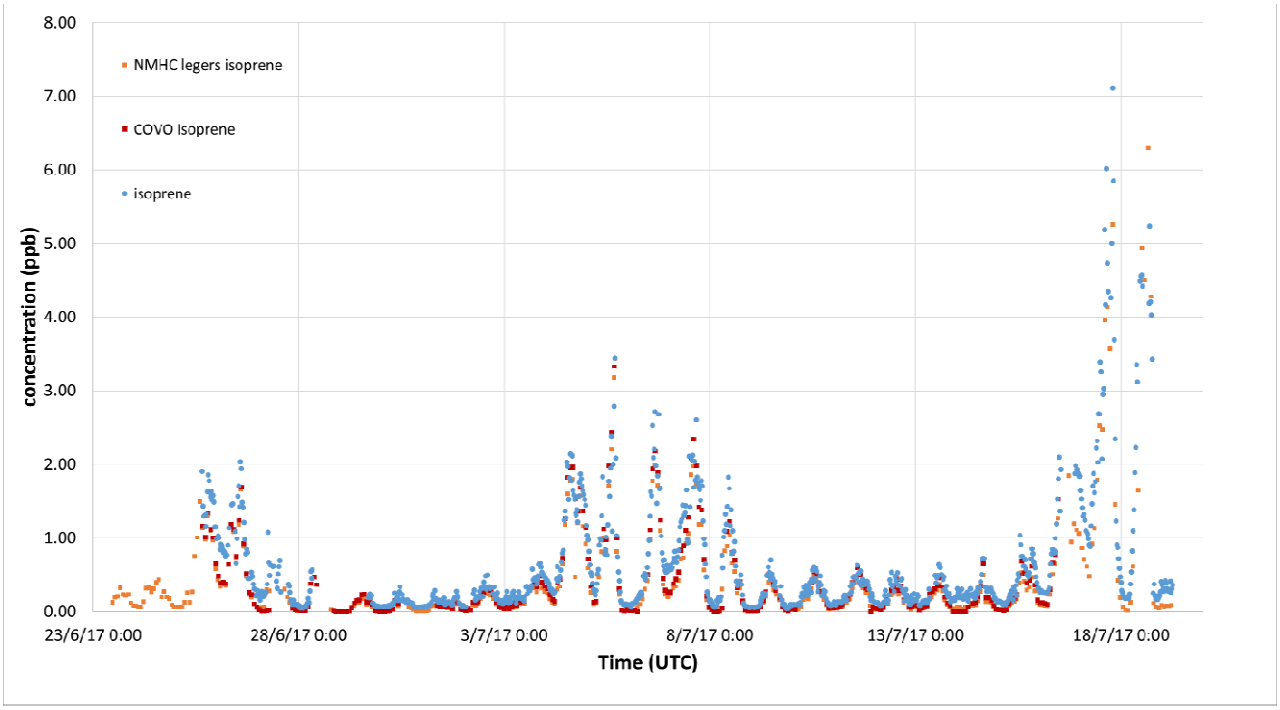

Figure V- 20:Comparison of isoprene concentration measured by three different instruments: PTR (blue points), NMHC (orange points), and COVO (red points) from 23 June to 18 July 2018.

With the PTR data and these assumptions, the calculated reactivity has been compared to the measured one during the period of pump-probe measurements. The contribution of butanol (from SMPS exhausts) has also been analyzed and found to be negligible at L1 and highly variable at L4. As the pump-probe and the CRM probing were not close to the SMPS exhaust, it has been chosen to not consider this contribution.

V.5.5.2 Comparison between the measured and calculated reactivity

By comparing the measured reactivity and calculated OH reactivity, derived from the chemical analysis, we can determine whether all of the trace species related to the formation of photochemical oxidants have been quantified. A comparison between the measured and the calculated reactivity is presented inFigure V- 21.

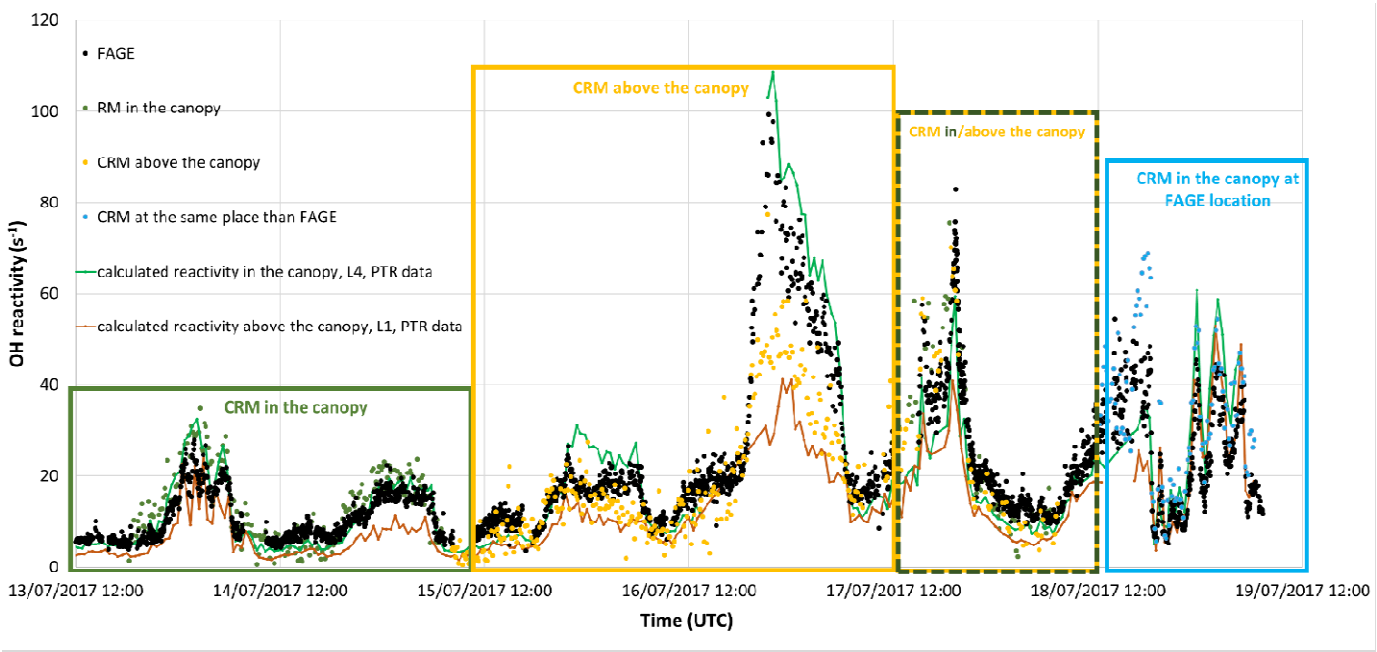

Figure V- 21 : Total OH reactivity for both UL-FAGE and CRM with the calculated reactivity from the measured trace gases. Green line represents the calculated reactivity at L4 level, while the orange line corresponds to the calculated reactivity at L1 level. Data corresponds to PTR data. The data are corrected for isoprene from monoterpenes contribution (4 %).

A comparison of the observed and calculated reactivity for the entire campaign shows that the difference between the calculated OH reactivity and the measured ones at L1 and L4 vary as a function of the conditions and the level. Therefore, each levelwill be discussed separately for the different periods in the following section.

V.5.5.2.1 Level 4, measurements at 6 m

We observe that the measured reactivity and the calculated one were similar most of the time but some differences are observed during the night as shown in the graphs ofFigure V- 22. The reactivity was measured by UL-FAGE and CRM at L4 and L1 respectively.

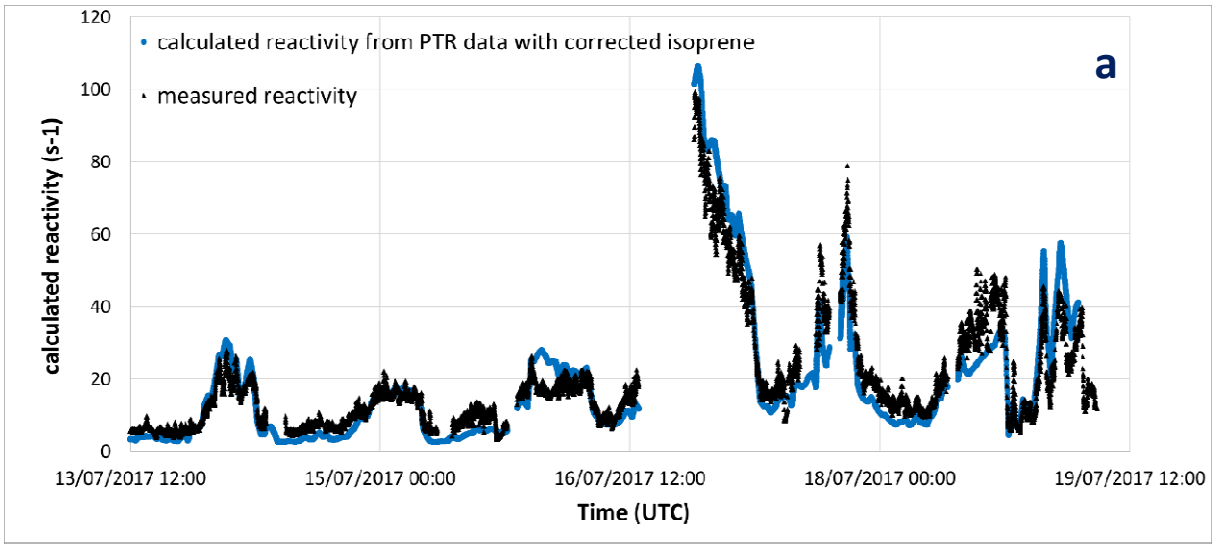

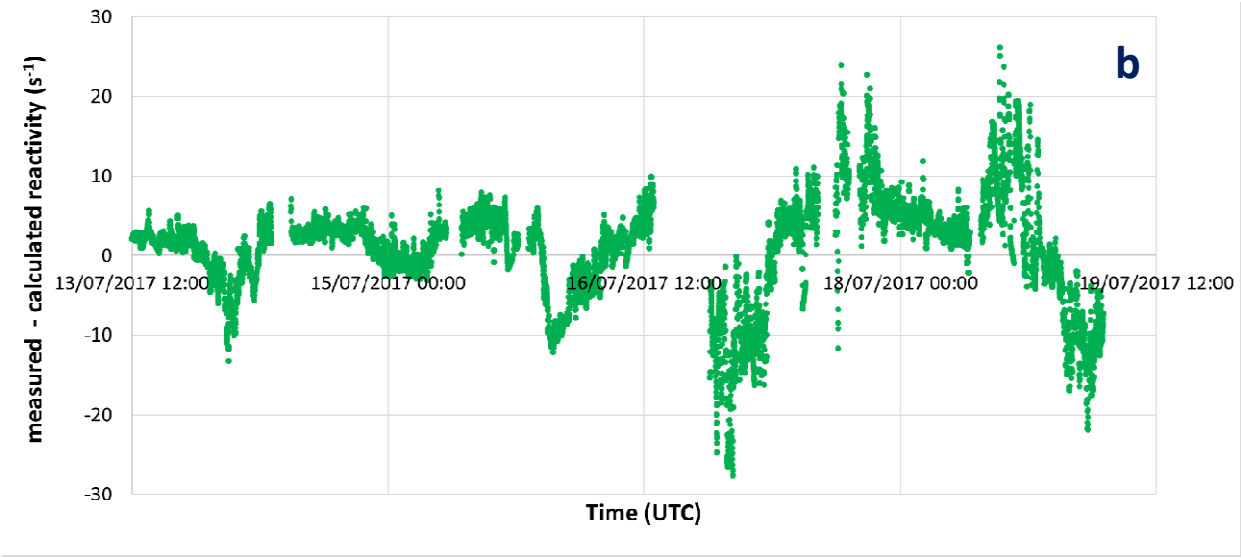

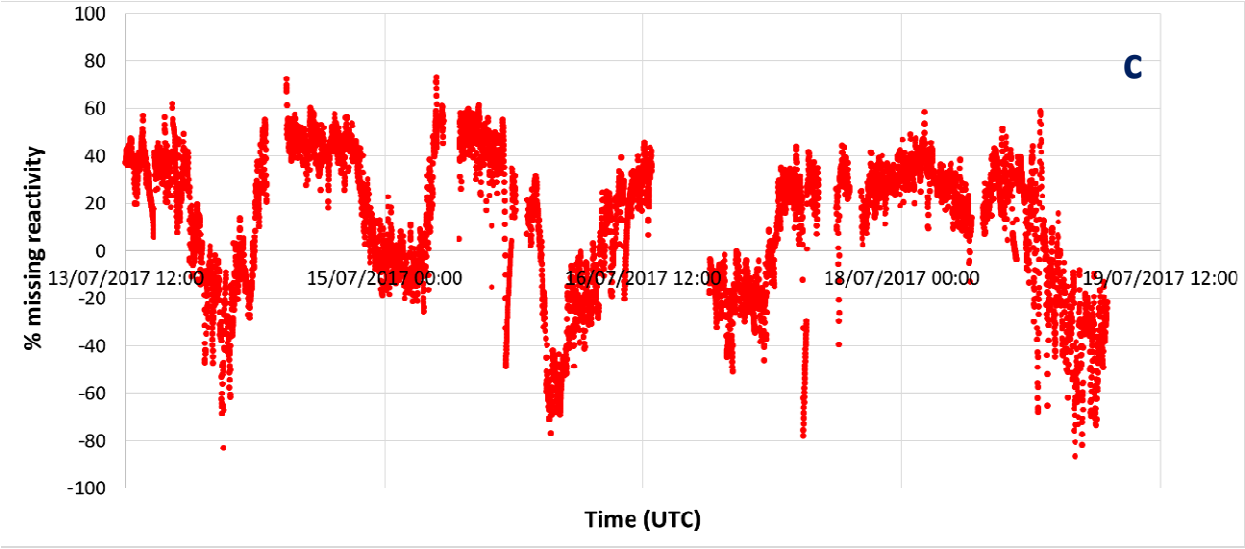

Figure V- 22: graph a, represents the comparison between the measured (orange points) and calculated (blue points) reactivity from PTR data in the canopy (L4), graph b, represents the difference between the measured and calculated reactivity, graph c, represent the percentage of the missing reactivity from 13 to 19 of July 2017.

During most of the nights, no missing reactivity was observed (the monoterpenes are dominant), and sometimes the calculated reactivity is even higher than the measured one as in the night of 17th of July. This behavior can be explained by an overestimation of the monoterpene concentrations by the analytical instruments. At the end of the campaign, a missing reactivity in the range of about 40 % has been observed the night. During the day, a missing reactivity in the order of 40 % is also observed most of the time but it corresponds to weak reactivities and it can be in the range of uncertainty of the measurements (reactivity and VOCs concentrations).

Correlating the reactivity to the species present in the field during daytime and nighttime, we can say that isoprene is the dominant species during the day and monoterpenes during the night as shown in Figure V- 23. Therefore, the oxidation species of these emitted species could be responsible of the missing reactivity during the day.

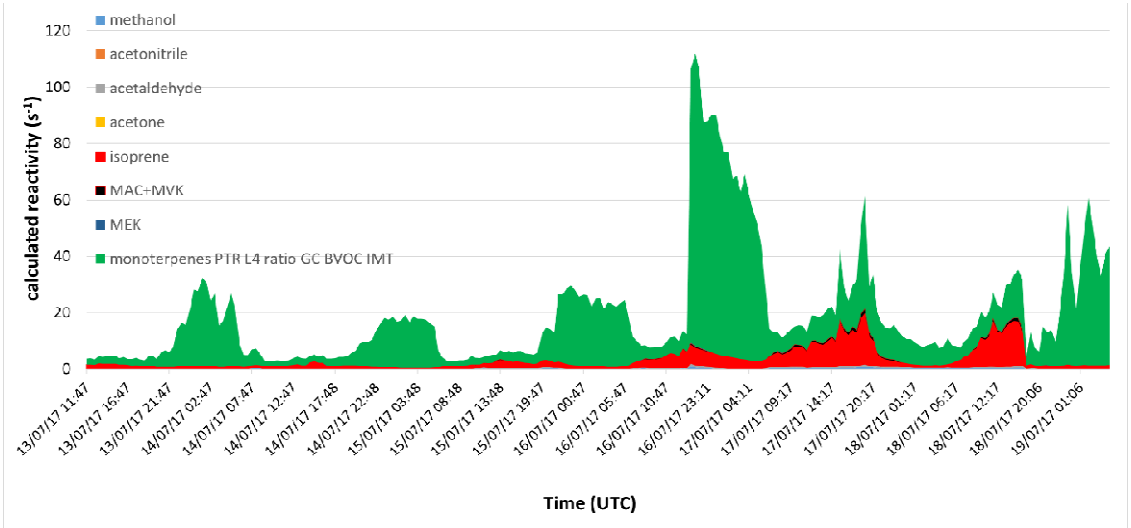

Figure V- 23: contribution of the species present in the field during LANDEX campaign from 13 to 19 of July 2017, the species were measured by PTR-MS in the canopy (L4).

V.5.5.2.2 Level 1 measurements at 12m

For L1 measurements, the comparison between measured and calculated reactivity is presented in theFigure V- 24. The reactivity measured by the LSCE-CRM instrument, and the missing data in the graph corresponds to duration where the CRM was measuring at L4. The comparison between the measured and calculated reactivity shows bigger differences compared to L4 measurements. These results indicate that the missing reactivity at level 1 is more important than at level 4 as shown in the lower graph of Figure V- 24. In contrast to observations at L4, the missing reactivity in L1 reaches more than 60%. The difference in the magnitude of the missing reactivity between the two levels can be explained by the difference in oxidation processes contribution as at L1 they had more time to transform the primary species in secondary species at high level.

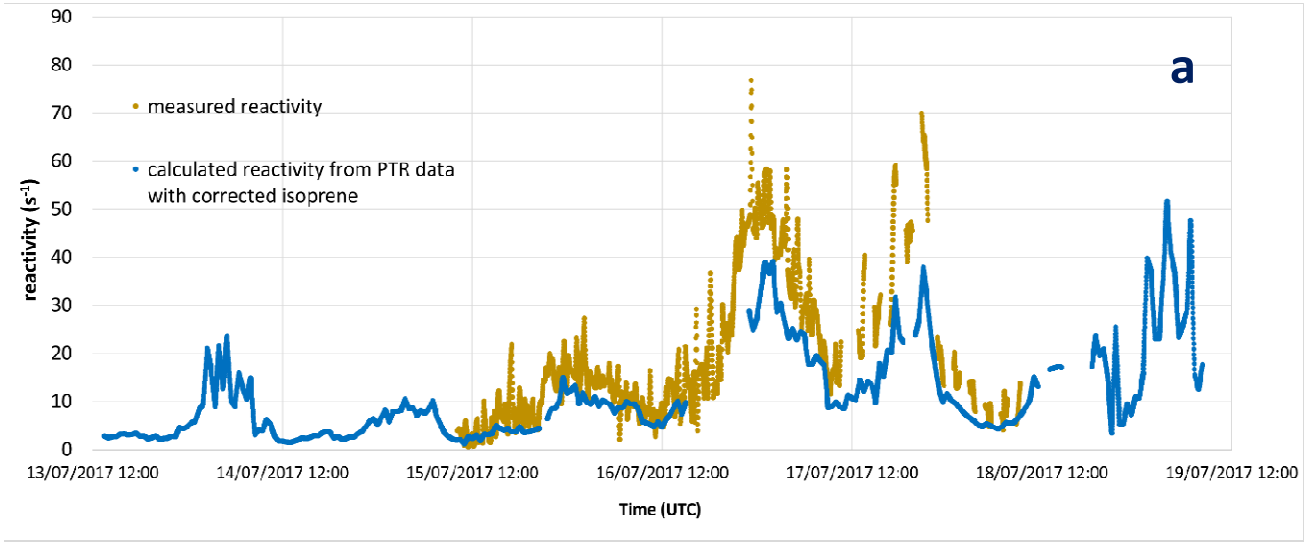

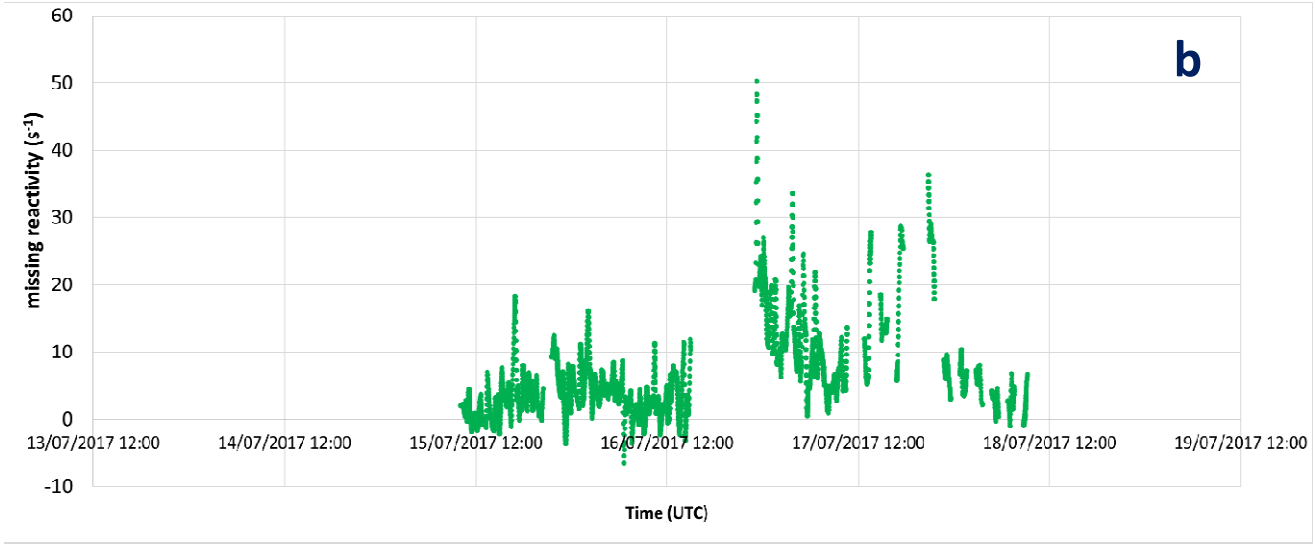

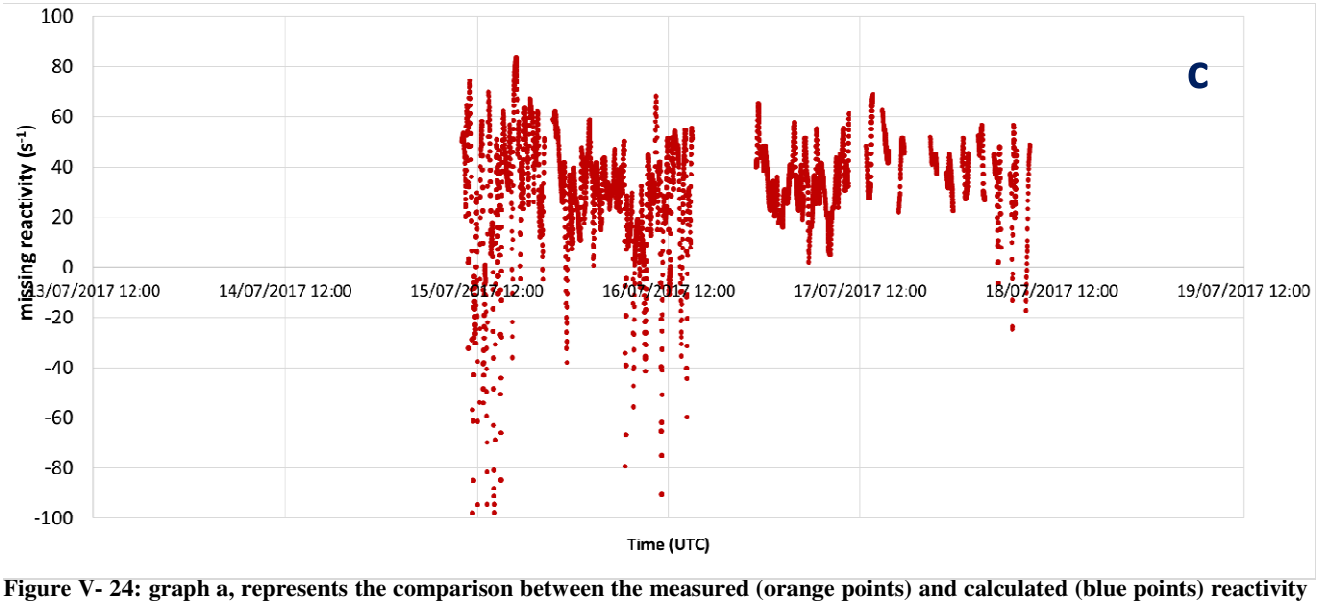

Figure V- 24: graph a, represents the comparison between the measured (orange points) and calculated (blue points) reactivity from PTR data above the canopy (L1), graph b, represents the difference between the measured and calculated reactivity, graph c, represent the percentage of the missing reactivity from 13 to 19 of July 2017.

V.6 Conclusion

In this chapter, we presented the results of the LANDEX campaign in which the UL-FAGE instrument was deployed for quantification of OH, HO_2 and RO_2 radicals and OH reactivity measurements. Together with more than 10 laboratories from France, a comprehensive set of measurements was collected in July 2017 to characterize the photochemistry at the Landes forest consisting mainly of pine trees.

The UL-FAGE was deployed for the first time to measure peroxy radicals by modulating the NO concentration injected in the second cell of the instrument. In order to test if OH measurement included artifacts from OH production inside the measurement cell, chemical modulation tests were performed in the last two days of the campaign. These tests identified unexplained OH signals reaching 50 % of the OH signal.

Daily maximum concentrations of OH, HO_2, and RO_2 radicals ranged from 1 to 30 × 10^6 cm^{-3}, 1 to 15 × 10^7 cm^{-3}, 1 to 10 × $10^7 cm^{-3}$, respectively. Compared to previous filed campaigns, the measured radical concentrations were in the same range for HO_2 and RO_2 while higher in case of OH radical. Model calculations were not performed yet and need to be done when all the data sets from all the groups are finalized.

In addition to the quantification measurements of HO_x radicals, total OH reactivity was measured in the same site of the forest by UL-FAGE. The UL- FAGE was intercompared for a second time during the LANDEX campaign with the CRM from LSCE, after the intercomparison to other pump-probe and

CRM instruments in the SAPHIR chamber. This time, the intercomparison was done in ambient air, the results obtained showed a good correlation between the two instruments sampling from the same place or even different horizontal locations.

During stratification events, with high differences in BVOC concentrations at different heights, strong differences are also observed in the reactivity measurements. The measured reactivity was low during the day, ranging from 5 to 25 s^{-1} at the maximum, while higher reactivity was seen during the night, especially for the second part of the campaign (OH reactivity at night reached 100 s^{-1} at the maximum).

Comparison of the measured and calculated OH reactivity derived from the analysis of trace species show that the magnitude of missing reactivity varies as function of the conditions and height. The candidates of the missing OH sink, particularly observed above the canopy, are thought to be some oxidation products of the biogenic volatile organic compounds.

Bibliography

Abraham, N.L., Archibald, A.T., Bellouin, N., Boucher, O., Braesicke, P., Bushell, A., Carslaw, K., Collins, B., Dalvi, M., and Emmerson, K. (2012). Unified model documentation paper no. 84: United Kingdom Chemistry and Aerosol (UKCA) technical description MetUM version 8.2. UK Met Off. Exeter UK.

Adame, J.A., Martínez, M., Sorribas, M., Hidalgo, P.J., Harder, H., Diesch, J.-M., Drewnick, F., Song, W., Williams, J., Sinha, V., et al. (2014). Meteorology during the DOMINO campaign and its connection with trace gases and aerosols. Atmospheric Chem. Phys. *14*, 2325–2342.

Amédro, D. (2012a). Atmospheric measurements of OH and HO2 radicals using FAGE: Development and deployment on the field. Lille 1.

Amédro, D. (2012b). Atmospheric measurements of OH and HO2 radicals using FAGE: Development and deployment on the field. Lille 1.

Amedro, D., Miyazaki, K., Parker, A., Schoemaecker, C., and Fittschen, C. (2012). Atmospheric and kinetic studies of OH and HO 2 by the FAGE technique. J. Environ. Sci. *24*, 78–86.

Archibald, A.T., Cooke, M.C., Utembe, S.R., Shallcross, D.E., Derwent, R.G., and Jenkin, M.E. (2010). Impacts of mechanistic changes on HO x formation and recycling in the oxidation of isoprene. Atmospheric Chem. Phys. *10*, 8097–8118.

Armerding, W., Spiekermann, M., and Comes, F.J. (1994). OH multipass absorption: Absolute and in situ method for local monitoring of tropospheric hydroxyl radicals. J. Geophys. Res. Atmospheres *99*, 1225–1239.

Aschmutat, U., Hessling, M., Holland, F., and Hofzumahaus, A. (1994). A tunable source of hydroxyl (OH) and hydroperoxy (HO2) radicals: in the range between 106 and 109 cm- 3. Phys.-Chem. Behav. Atmospheric Pollut. *2*, 811–816.

Assaf, E. (2017). Kinetic study of reactions with interest to atmospheric chemistry by simultaneous detection of OH and RO2 radicals coupled to laser photolysis. PhD Thesis. Lille 1.

Assaf, E., Song, B., Tomas, A., Schoemaecker, C., and Fittschen, C. (2016). Rate Constant of the Reaction between CH3O2 Radicals and OH Radicals revisited. J. Phys. Chem. A *120*, 8923–8932.

Assaf, E., Sheps, L., Whalley, L., Heard, D., Tomas, A., Schoemaecker, C., and Fittschen, C. (2017a). The reaction between CH3O2 and OH radicals: Product yields and atmospheric implications. Environ. Sci. Technol. *51*, 2170–2177.

Assaf, E., Tanaka, S., Kajii, Y., Schoemaecker, C., and Fittschen, C. (2017b). Rate constants of the reaction of C2–C4 peroxy radicals with OH radicals. Chem. Phys. Lett. *684*, 245–249.

Assaf, E., Schoemaecker, C., Vereecken, L., and Fittschen, C. (2018a). The reaction of fluorine atoms with methanol: yield of CH 3 O/CH 2 OH and rate constant of the reactions CH 3 O+ CH 3 O and CH 3 O+ HO 2. Phys. Chem. Chem. Phys.

Assaf, E., Schoemaecker, C., Vereecken, L., and Fittschen, C. (2018b). Experimental and theoretical investigation of the reaction of RO2 radicals with OH radicals: Dependence of the HO2 yield on the size of the alkyl group. Int. J. Chem. Kinet. *50*, 670–680.

Atkinson, R., Baulch, D.L., Cox, R.A., Hampson Jr, R.F., Kerr, J.A., Rossi, M.J., and Troe, J. (1997). Evaluated kinetic, photochemical and heterogeneous data for atmospheric chemistry: Supplement V. IUPAC Subcommittee on Gas Kinetic Data Evaluation for Atmospheric Chemistry. J. Phys. Chem. Ref. Data *26*, 521–1011.

Atkinson, R., Baulch, D.L., Cox, R.A., Crowley, J.N., Hampson, R.F., Hynes, R.G., Jenkin, M.E., Rossi, M.J., and Troe, J. (2005). Evaluated kinetic and photochemical data for atmospheric chemistry: Volume II? reactions of organic species. Atmospheric Chem. Phys. Discuss. *5*, 6295–7168.

Atkinson, R., Baulch, D.L., Cox, R.A., Crowley, J.N., Hampson, R.F., Hynes, R.G., Jenkin, M.E., Rossi, M.J., Troe, J., and Subcommittee, I. (2006). Evaluated kinetic and photochemical data for atmospheric chemistry: Volume II–gas phase reactions of organic species. Atmospheric Chem. Phys. *6*, 3625–4055.

Baardsen, E.L., and Terhune, R.W. (1972). Detection of OH in the atmosphere using a dye laser. Appl. Phys. Lett. *21*, 209–211.

Barker, J.R. (1995). Progress and problems in atmospheric chemistry (World Scientific).

Berresheim, H., Elste, T., Plass-Dülmer, C., Eiseleb, F.L., and Tannerb, D.J. (2000). Chemical ionization mass spectrometer for long-term measurements of atmospheric OH and H 2 SO 4. Int. J. Mass Spectrom. *202*, 91–109.

Berresheim, H., Plass-Dülmer, C., Elste, T., Mihalopoulos, N., and Rohrer, F. (2003). OH in the coastal boundary layer of Crete during MINOS: Measurements and relationship with ozone photolysis. Atmospheric Chem. Phys. *3*, 639–649.

Bey, I., Aumont, B., and Toupance, G. (2001). A modeling study of the nighttime radical chemistry in the lower continental troposphere. J Geophys Res-Atmos *106*, 9991–10001.

Blocquet, M., Schoemaecker, C., Amedro, D., Herbinet, O., Battin-Leclerc, F., and Fittschen, C. (2013). Quantification of OH and HO2 radicals during the low-temperature oxidation of hydrocarbons by Fluorescence Assay by Gas Expansion technique. Proc. Natl. Acad. Sci. *110*, 20014–20017.

Blocquet, M., Ward, M., Verriele, M., Dusanter, S., Calvé, S.L., Hanoune, B., Pillier, L., Locoge, N., Fittschen, C., and Schoemaecker, C. (2016). Oxidants behaviour in a low energy consumption building with mechanical ventilation. In 14th International Conference of Indoor Air Quality and Climate, p.

Branche, S.L. (2016). Étude sociologique sur la pollution due au chauffage au bois dans l'agglomération grenobloise: synthèse des principaux résultats. 2268-3798.

Brune, W.H., Stevens, P.S., and Mather, J.H. (1995). Measuring OH and HO2 in the troposphere by laser-induced fluorescence at low pressure. J. Atmospheric Sci. *52*, 3328–3336.

Buenker, R.J., Olbrich, G., Schuchmann, H.P., Schuermann, B.L., and Von Sonntag, C. (1984). Photolysis of methanol at 185 nm. Quantum-mechanical calculations and product study. J. Am. Chem. Soc. *106*, 4362–4368.

Cantrell, C.A., and Stedman, D.H. (1982). A possible technique for the measurement of atmospheric peroxy radicals. Geophys. Res. Lett. *9*, 846–849.

Cantrell, C.A., Zimmer, A., and Tyndall, G.S. (1997). Absorption cross sections for water vapor from 183 to 193 nm. Geophys. Res. Lett. *24*, 2195–2198.

Carr, S.A., Baeza-Romero, M.T., Blitz, M.A., Pilling, M.J., Heard, D.E., and Seakins, P.W. (2007). OH yields from the CH3CO+ O2 reaction using an internal standard. Chem. Phys. Lett. *445*, 108–112.

Carslaw, N., Creasey, D.J., Heard, D.E., Lewis, A.C., McQuaid, J.B., Pilling, M.J., Monks, P.S., Bandy, B.J., and Penkett, S.A. (1999). Modeling OH, HO2, and RO2 radicals in the marine boundary layer: 1. Model construction and comparison with field measurements. J. Geophys. Res. Atmospheres *104*, 30241–30255.

Chatani, S., Shimo, N., Matsunaga, S., Kajii, Y., Kato, S., Nakashima, Y., Miyazaki, K., Ishii, K., and Ueno, H. (2009). Sensitivity analyses of OH missing sinks over Tokyo metropolitan area in the summer of 2007. Atmospheric Chem. Phys. *9*, 8975–8986.

Chew, A.A., and Atkinson, R. (1996). OH radical formation yields from the gas-phase reactions of O3 with alkenes and monoterpenes. J. Geophys. Res. Atmospheres *101*, 28649–28653.

Creasey, D.J., Halford-Maw, P.A., Heard, D.E., Pilling, M.J., and Whitaker, B.J. (1997). Implementation and initial deployment of a field instrument for measurement of OH and HO 2 in the troposphere by laser-induced fluorescence. J. Chem. Soc. Faraday Trans. *93*, 2907–2913.

Crounse, J.D., Paulot, F., Kjaergaard, H.G., and Wennberg, P.O. (2011). Peroxy radical isomerization in the oxidation of isoprene. Phys. Chem. Chem. Phys. *13*, 13607–13613.

Dewick, P.M. (2002). The biosynthesis of C 5–C 25 terpenoid compounds. Nat. Prod. Rep. *19*, 181–222.

Di Carlo, P., Brune, W.H., Martinez, M., Harder, H., Lesher, R., Ren, X., Thornberry, T., Carroll, M.A., Young, V., Shepson, P.B., et al. (2004). Missing OH reactivity in a forest: Evidence for unknown reactive biogenic VOCs. Science *304*, 722–725.

Dilecce, G., Ambrico, P.F., and De Benedictis, S. (2004). An ambient air RF low-pressure pulsed discharge as an OH source for LIF calibration. Plasma Sources Sci. Technol. *13*, 237.

Dillon, T.J., and Crowley, J.N. (2008). Direct detection of OH formation in the reactions of HO 2 with CH 3 C (O) O 2 and other substituted peroxy radicals. Atmospheric Chem. Phys. *8*, 4877–4889.

Dillon, T.J., Tucceri, M.E., Dulitz, K., Horowitz, A., Vereecken, L., and Crowley, J.N. (2012). Reaction of hydroxyl radicals with C4H5N (pyrrole): temperature and pressure dependent rate coefficients. J. Phys. Chem. A *116*, 6051–6058.

Dlugi, R., Berger, M., Zelger, M., Hofzumahaus, A., Siese, M., Holland, F., Wisthaler, A., Grabmer, W., Hansel, A., Koppmann, R., et al. (2010). Turbulent exchange and segregation of HO x radicals and volatile organic compounds above a deciduous forest. Atmospheric Chem. Phys. *10*, 6215–6235.

Dolgorouky, C., Gros, V., Sarda-Esteve, R., Sinha, V., Williams, J., Marchand, N., Sauvage, S., Poulain, L., Sciare, J., and Bonsang, B. (2012). Total OH reactivity measurements in Paris during the 2010 MEGAPOLI winter campaign. Atmospheric Chem. Phys. *12*, 9593–9612.

Dorn, H.-P., Brandenburger, U., Brauers, T., and Hausmann, M. (1995). A new in situ laser long-path absorption instrument for the measurement of tropospheric OH radicals. J. Atmospheric Sci. *52*, 3373–3380.

Dusanter, S., Vimal, D., and Stevens, P.S. (2008). Measuring tropospheric OH and HO 2 by laser-induced fluorescence at low pressure. A comparison of calibration techniques. Atmospheric Chem. Phys. *8*, 321–340.

Dusanter, S., Vimal, D., Stevens, P.S., Volkamer, R., Molina, L.T., Baker, A., Meinardi, S., Blake, D., Sheehy, P., Merten, A., et al. (2009). Measurements of OH and HO 2 concentrations during the MCMA-2006 field campaign–Part 2: Model comparison and radical budget. Atmospheric Chem. Phys. *9*, 6655–6675.

Edwards, G.D., Cantrell, C.A., Stephens, S., Hill, B., Goyea, O., Shetter, R.E., Mauldin, R.L., Kosciuch, E., Tanner, D.J., and Eisele, F.L. (2003). Chemical ionization mass spectrometer instrument for the measurement of tropospheric HO2 and RO2. Anal. Chem. *75*, 5317–5327.

Edwards, P.M., Evans, M.J., Furneaux, K.L., Hopkins, J., Ingham, T., Jones, C., Lee, J.D., Lewis, A.C., Moller, S.J., Stone, D., et al. (2013). OH reactivity in a South East Asian tropical rainforest during the Oxidant and Particle Photochemical Processes (OP3) project. Atmospheric Chem. Phys. *13*, 9497–9514.

Eisele, F.L., and Tanner, D.J. (1991). Ion-assisted tropospheric OH measurements. J. Geophys. Res. Atmospheres *96*, 9295–9308.

Eisele, F.L., Tanner, D.J., Cantrell, C.A., and Calvert, J.G. (1996). Measurements and steady state calculations of OH concentrations at Mauna Loa Observatory. J. Geophys. Res. Atmospheres *101*, 14665–14679.

Faloona, I., Tan, D., Brune, W., Hurst, J., Barket, D., Couch, T.L., Shepson, P., Apel, E., Riemer, D., and Thornberry, T. (2001). Nighttime observations of anomalously high levels of hydroxyl radicals above a deciduous forest canopy. J. Geophys. Res. Atmospheres *106*, 24315–24333.

Faloona, I.C., Tan, D., Lesher, R.L., Hazen, N.L., Frame, C.L., Simpas, J.B., Harder, H., Martinez, M., Di Carlo, P., and Ren, X. (2004). A laser-induced fluorescence instrument for detecting tropospheric OH and HO2: Characteristics and calibration. J. Atmospheric Chem. *47*, 139–167.

Feiner, P.A., Brune, W.H., Miller, D.O., Zhang, L., Cohen, R.C., Romer, P.S., Goldstein, A.H., Keutsch, F.N., Skog, K.M., and Wennberg, P.O. (2016a). Testing atmospheric oxidation in an alabama forest. J. Atmospheric Sci. *73*, 4699–4710.

Feiner, P.A., Brune, W.H., Miller, D.O., Zhang, L., Cohen, R.C., Romer, P.S., Goldstein, A.H., Keutsch, F.N., Skog, K.M., and Wennberg, P.O. (2016b). Testing atmospheric oxidation in an alabama forest. J. Atmospheric Sci. *73*, 4699–4710.

Felton, C.C., Sheppard, J.C., and Campbell, M.J. (1988). Measurements of the diurnal OH cycle by a 14C-tracer method. Nature *335*, 53.

Ferracci, V., Heimann, I., Abraham, N.L., Pyle, J.A., and Archibald, A.T. Global modelling of the total OH reactivity: investigations on the “missing” OH sink and its atmospheric implications.

Finlayson-Pitts, B.J., and Jr, J.N.P. (1999). Chemistry of the Upper and Lower Atmosphere: Theory, Experiments, and Applications (San Diego: Academic Press).

Finlayson-Pitts, B.J., and Pitts, J.N. (2000). Chemistry of the upper and lower troposphere (Academic Press: New York).

Finlayson-Pitts, B.J., and Pitts Jr, J.N. (1999). Chemistry of the upper and lower atmosphere: theory, experiments, and applications (Academic press).

Fuchs, H. (2006). Measurement of Peroxy Radicals using Laser-Induced Fluorescence.

Fuchs, Dorn, H.-P., Bachner, M., Bohn, B., Brauers, T., Gomm, S., Hofzumahaus, A., Holland, F., Nehr, S., Rohrer, F., et al. (2012). Comparison of OH concentration measurements by DOAS and LIF during SAPHIR chamber experiments at high OH reactivity and low NO concentration. Atmospheric Meas. Tech. *5*, 1611–1626.

Fuchs, Tan, Z., Hofzumahaus, A., Broch, S., Dorn, H.-P., Holland, F., Künstler, C., Gomm, S., Rohrer, F., Schrade, S., et al. (2016). Investigation of potential interferences in the detection of atmospheric RO x radicals by laser-induced fluorescence under dark conditions. Atmospheric Meas. Tech. *9*, 1431–1447.

Fuchs, H., Holland, F., and Hofzumahaus, A. (2008). Measurement of tropospheric RO2 and HO2 radicals by a laser-induced fluorescence instrument. Rev. Sci. Instrum. *79*, 084104–084104.

Fuchs, H., Brauers, T., Dorn, H.-P., Harder, H., Haseler, R., Hofzumahaus, A., Holland, F., Kanaya, Y., Kajii, Y., Kubistin, D., et al. (2010a). Technical Note: Formal blind intercomparison of HO2 measurements in the atmosphere simulation chamber SAPHIR during the HOxComp campaign.

Fuchs, H., Brauers, T., Dorn, H.-P., Harder, H., Haseler, R., Hofzumahaus, A., Holland, F., Kanaya, Y., Kajii, Y., and Kubistin, D. (2010b). Formal blind intercomparison of HO2 measurements in the atmosphere simulation chamber SAPHIR during the HOxComp campaign.

Fuchs, H., Bohn, B., Hofzumahaus, A., Holland, F., Lu, K.D., Nehr, S., Rohrer, F., and Wahner, A. (2011). Detection of HO 2 by laser-induced fluorescence: calibration and interferences from RO 2 radicals. Atmospheric Meas. Tech. *4*, 1209–1225.

Fuchs, H., Hofzumahaus, A., Rohrer, F., Bohn, B., Brauers, T., Dorn, H.P., Häseler, R., Holland, F., Kaminski, M., and Li, X. (2013). Experimental evidence for efficient hydroxyl radical regeneration in isoprene oxidation. Nat. Geosci. *6*, 1023.

Fuchs, H., Tan, Z., Lu, K., Bohn, B., Broch, S., Brown, S.S., Dong, H., Gomm, S., Häseler, R., He, L., et al. (2017a). OH reactivity at a rural site (Wangdu) in the North China Plain: contributions from OH reactants and experimental OH budget. Atmospheric Chem. Phys. *17*, 645–661.

Fuchs, H., Li, X., Elste, T., Kiendler-Scharr, A., Brumby, C.A., Novelli, A., Gros, V., Kubistin, D., Muller, J.B.A., Cryer, D.R., et al. (2017b). Comparison of OH reactivity measurements in the atmospheric simulation chamber SAPHIR (Troposphäre).

George, L.A., Hard, T.M., and O'Brien, R.J. (1999). Measurement of free radicals OH and HO2 in Los Angeles smog. J. Geophys. Res. Atmospheres *104*, 11643–11655.

Goldstein, A.H., and Galbally, I.E. (2007). Known and unexplored organic constituents in the earth's atmosphere. Environ. Sci. Technol. *41*, 1514–1521.

Griffith, S.M., Hansen, R.F., Dusanter, S., Stevens, P.S., Alaghmand, M., Bertman, S.B., Carroll, M.A., Erickson, M., Galloway, M., Grossberg, N., et al. (2013). OH and HO 2 radical chemistry during PROPHET 2008 and CABINEX 2009–Part 1: Measurements and model comparison. Atmospheric Chem. Phys. *13*, 5403–5423.

Griffith, S.M., Hansen, R.F., Dusanter, S., Michoud, V., Gilman, J.B., Kuster, W.C., Veres, P.R., Graus, M., Gouw, J.A., Roberts, J., et al. (2016). Measurements of hydroxyl and hydroperoxy radicals during CalNex-LA: Model comparisons and radical budgets. J. Geophys. Res. Atmospheres *121*, 4211–4232.

Hanke, M., Uecker, J., Reiner, T., and Arnold, F. (2002). Atmospheric peroxy radicals: ROXMAS, a new mass-spectrometric methodology for speciated measurements of HO2 and∑ RO2 and first results. Int. J. Mass Spectrom. *213*, 91–99.

Hansen, R.F., Griffith, S.M., Dusanter, S., Rickly, P.S., Stevens, P.S., Bertman, S.B., Carroll, M.A., Erickson, M.H., Flynn, J.H., Grossberg, N., et al. (2014). Measurements of total hydroxyl radical reactivity during CABINEX 2009–Part 1: field measurements. Atmospheric Chem. Phys. *14*, 2923–2937.

Hansen, R.F., Blocquet, M., Schoemaecker, C., Léonardis, T., Locoge, N., Fittschen, C., Hanoune, B., Stevens, P.S., Sinha, V., and Dusanter, S. (2015). Intercomparison of the comparative reactivity method (CRM) and pump–probe technique for measuring total OH reactivity in an urban environment. Atmospheric Meas. Tech. *8*, 4243–4264.

Hard, T.M., O'Brien, R.J., Cook, T.B., and Tsongas, G.A. (1979). Interference suppression in HO fluorescence detection.

Hard, T.M., O'Brien, R.J., Chan, C.Y., and Mehrabzadeh, A.A. (1984). Tropospheric free radical determination by fluorescence assay with gas expansion. Environ. Sci. Technol. *18*, 768–777.

Hard, T.M., George, L.A., and O'Brien, R.J. (1995). FAGE Determination of Tropospheric HO and H02. J. Atmospheric Sci. *52*, 3354–3372.

Hard, T.M., George, L.A., and O'Brien, R.J. (2002). An absolute calibration for gas-phase hydroxyl measurements. Environ. Sci. Technol. *36*, 1783–1790.

Hausmann, M., Brandenburger, U., Brauers, T., and Dorn, H.-P. (1997). Detection of tropospheric OH radicals by long-path differential-optical-absorption spectroscopy: Experimental setup, accuracy, and precision. J. Geophys. Res. Atmospheres *102*, 16011–16022.

Heard, D.E. (2006). Atmospheric field measurements of the hydroxyl radical using laser-induced fluorescence spectroscopy. Annu Rev Phys Chem *57*, 191–216.

Heard, D.E., and Pilling, M.J. (2003). Measurement of OH and HO2 in the troposphere. Chem. Rev. *103*, 5163–5198.

Heimann, M., and Reichstein, M. (2008). Terrestrial ecosystem carbon dynamics and climate feedbacks. Nature *451*, 289.

Hofzumahaus, A., Brauers, T., Aschmutat, U., Brandenburger, U., Dorn, H.-P., Hausmann, M., He\s sling, M., Holland, F., Plass-Dülmer, C., Sedlacek, M., et al. (1997). Reply [to "Comment on 'The measurement of tropospheric OH radicals by laser-induced fluorescence spectroscopy during the POPCORN field campaign'by Hofzumahaus et al. and 'Intercomparison of tropospheric OH radical measurements by multiple folded long-path laser absorption and laser induced fluorescence'by Brauers et al."]. Geophys. Res. Lett. *24*, 3039–3040.

Hofzumahaus, A., Rohrer, F., Lu, K., Bohn, B., Brauers, T., Chang, C.-C., Fuchs, H., Holland, F., Kita, K., and Kondo, Y. (2009). Amplified trace gas removal in the troposphere. Science *324*, 1702–1704.

Holland, F., Hessling, M., and Hofzumahaus, A. (1995). In situ measurement of tropospheric OH radicals by laser-induced fluorescence—a description of the KFA instrument. J. Atmospheric Sci. *52*, 3393–3401.

Holland, F., Hofzumahaus, A., Sedlacek, M., and Weber, M. (1999). Measurements of OH and HO2 radicals in clean marine air during the ALBATROSS field campaign. Eos Trans AGU *80*, 46.

Holland, F., Hofzumahaus, A., Schäfer, J., Kraus, A., and Pätz, H.-W. (2003). Measurements of OH and HO2 radical concentrations and photolysis frequencies during BERLIOZ. J. Geophys. Res. Atmospheres *108*.

Hornbrook, R.S., Crawford, J.H., Edwards, G.D., Goyea, O., Mauldin III, R.L., Olson, J.S., and Cantrell, C.A. (2011). Measurements of tropospheric HO 2 and RO 2 by oxygen dilution modulation and chemical ionization mass spectrometry. Atmospheric Meas. Tech. *4*, 735–756.

Ingham, T., Goddard, A., Whalley, L.K., Furneaux, K.L., Edwards, P.M., Seal, C.P., Self, D.E., Johnson, G.P., Read, K.A., Lee, J.D., et al. (2009). A flow-tube based laser-induced fluorescence instrument to measure OH reactivity in the troposphere. Atmospheric Meas. Tech. *2*, 465–477.

Jenkin, M.E., Saunders, S.M., Wagner, V., and Pilling, M.J. (2003). Protocol for the development of the Master Chemical Mechanism, MCM v3 (Part B): tropospheric degradation of aromatic volatile organic compounds. Atmospheric Chem. Phys. *3*, 181–193.

Johnson, D., and Marston, G. (2008). The gas-phase ozonolysis of unsaturated volatile organic compounds in the troposphere. Chem. Soc. Rev. *37*, 699–716.

Kaiser, J., Skog, K.M., Baumann, K., Bertman, S.B., Brown, S.B., Brune, W.H., Crounse, J.D., De Gouw, J.A., Edgerton, E.S., and Feiner, P.A. (2016). Speciation of OH reactivity above the canopy of an isoprene-dominated forest. Atmospheric Chem. Phys. *16*, 9349–9359.

Kammer, J. (2016). LANDEX: étude des aérosols organiques secondaires (AOS) générés par la forêt des Landes. PhD Thesis. Université de Bordeaux.

Kanaya, Y., Sadanaga, Y., Hirokawa, J., Kajii, Y., and Akimoto, H. (2001). Development of a ground-based LIF instrument for measuring HOx radicals: Instrumentation and calibrations. J. Atmospheric Chem. *38*, 73–110.

Kanaya, Y., Cao, R., Kato, S., Miyakawa, Y., Kajii, Y., Tanimoto, H., Yokouchi, Y., Mochida, M., Kawamura, K., and Akimoto, H. (2007). Chemistry of OH and HO2 radicals observed at Rishiri Island, Japan, in September 2003: Missing daytime sink of HO2 and positive nighttime correlations with monoterpenes. J. Geophys. Res. Atmospheres *112*.

Kesselmeier, J., and Staudt, M. (1999). Biogenic volatile organic compounds (VOC): an overview on emission, physiology and ecology. J. Atmospheric Chem. *33*, 23–88.

Kim, S., Guenther, A., Karl, T., and Greenberg, J. (2011). Contributions of primary and secondary biogenic VOC tototal OH reactivity during the CABINEX (Community Atmosphere-Biosphere INteractions Experiments)-09 field campaign. Atmospheric Chem. Phys. *11*, 8613–8623.

Kim, S., Sanchez, D., Wang, M., Seco, R., Jeong, D., Hughes, S., Barletta, B., Blake, D.R., Jung, J., and Kim, D. (2016). OH reactivity in urban and suburban regions in Seoul, South Korea–an East Asian megacity in a rapid transition. Faraday Discuss. *189*, 231–251.

Kovacs, T.A., and Brune, W.H. (2001). Total OH loss rate measurement. J. Atmospheric Chem. *39*, 105–122.

Kovacs, T.A., Brune, W.H., Harder, H., Martinez, M., Simpas, J.B., Frost, G.J., Williams, E., Jobson, T., Stroud, C., Young, V., et al. (2003). Direct measurements of urban OH reactivity during Nashville SOS in summer 1999. J. Environ. Monit. *5*, 68–74.

Kubistin, D., Harder, H., Martinez, M., Rudolf, M., Sander, R., Bozem, H., Eerdekens, G., Fischer, H., Gurk, C., Klüpfel, T., et al. (2010). Hydroxyl radicals in the tropical troposphere over the Suriname rainforest: comparison of measurements with the box model MECCA. Atmospheric Chem. Phys. *10*, 9705–9728.

Kukui, A., Ancellet, G., and Le Bras, G. (2008). Chemical ionisation mass spectrometer for measurements of OH and Peroxy radical concentrations in moderately polluted atmospheres. J. Atmospheric Chem. *61*, 133–154.

Kumar, V., and Sinha, V. (2014). VOC–OHM: A new technique for rapid measurements of ambient total OH reactivity and volatile organic compounds using a single proton transfer reaction mass spectrometer. Int. J. Mass Spectrom. *374*, 55–63.

Kumar, V., Garg, S., Chandra, P., and Sinha, V. (2013). A large OH sink in summertime surface air of the northern Indo-Gangetic plain revealed through in-situ total OH Reactivity measurements. In AGU Fall Meeting Abstracts, p.

Laothawornkitkul, J., Taylor, J.E., Paul, N.D., and Hewitt, C.N. (2009). Biogenic volatile organic compounds in the Earth system. New Phytol. *183*, 27–51.

Lee, J.D., Young, J.C., Read, K.A., Hamilton, J.F., Hopkins, J.R., Lewis, A.C., Bandy, B.J., Davey, J., Edwards, P., Ingham, T., et al. (2009). Measurement and calculation of OH reactivity at a United Kingdom coastal site. J. Atmospheric Chem. *64*, 53–76.

Lelieveld, J., Butler, T.M., Crowley, J.N., Dillon, T.J., Fischer, H., Ganzeveld, L., Harder, H., Lawrence, M.G., Martinez, M., Taraborrelli, D., et al. (2008). Atmospheric oxidation capacity sustained by a tropical forest. Nature *452*, 737–740.

Levy, H. (1971). Normal atmosphere: Large radical and formaldehyde concentrations predicted. Science *173*, 141–143.

Liu, Y., Morales-Cueto, R., Hargrove, J., Medina, D., and Zhang, J. (2009). Measurements of Peroxy Radicals Using Chemical Amplification- Cavity Ringdown Spectroscopy. Environ. Sci. Technol. *43*, 7791–7796.

Liu, Y., Chen, L., Chen, D., Wang, W., Liu, F., and Wang, W. (2017). Computational study on mechanisms of C2H5O2+ OH reaction and properties of C2H5O3H complex. Chem. Res. Chin. Univ. *33*, 623–630.

Lou, S., Holland, F., Rohrer, F., Lu, K., Bohn, B., Brauers, T., Chang, C.C., Fuchs, H., Häseler, R., Kita, K., et al. (2010). Atmospheric OH reactivities in the Pearl River Delta–China in summer 2006: measurement and model results. Atmospheric Chem. Phys. *10*, 11243–11260.

Lu, K.D., Rohrer, F., Holland, F., Fuchs, H., Bohn, B., Brauers, T., Chang, C.C., Häseler, R., Hu, M., and Kita, K. (2012). Observation and modelling of OH and HO 2 concentrations in the Pearl River Delta 2006: a missing OH source in a VOC rich atmosphere. Atmospheric Chem. Phys. *12*, 1541–1569.

Mao, J., Ren, X., Brune, W.H., Olson, J.R., Crawford, J.H., Fried, A., Huey, L.G., Cohen, R.C., Heikes, B., Singh, H.B., et al. (2009). Airborne measurement of OH reactivity during INTEX-B. Atmospheric Chem. Phys. *9*, 163–173.

Mao, J., Ren, X., Chen, S., Brune, W.H., Chen, Z., Martinez, M., Harder, H., Lefer, B., Rappenglück, B., Flynn, J., et al. (2010). Atmospheric oxidation capacity in the summer of Houston 2006: Comparison with summer measurements in other metropolitan studies. Atmos. Environ. *44*, 4107–4115.

Mao, J., Ren, X., Zhang, L., Van Duin, D.M., Cohen, R.C., Park, J.-H., Goldstein, A.H., Paulot, F., Beaver, M.R., Crounse, J.D., et al. (2012). Insights into hydroxyl measurements and atmospheric oxidation in a California forest. Atmospheric Chem. Phys. *12*, 8009–8020.

Matsumi, Y., Kono, M., Ichikawa, T., Takahashi, K., and Kondo, Y. (2002). Laser-induced fluorescence instrument for the detection of tropospheric OH radicals. Bull. Chem. Soc. Jpn. *75*, 711–717.

Mauldin, R.L., Frost, G.J., Chen, G., Tanner, D.J., Prevot, A.S.H., Davis, D.D., and Eisele, F.L. (1998). OH measurements during the First Aerosol Characterization Experiment (ACE 1): Observations and model comparisons. J. Geophys. Res. Atmospheres *103*, 16713–16729.

Michoud, V., Hansen, R.F., Locoge, N., Stevens, P.S., and Dusanter, S. (2015). Detailed characterizations of a Comparative Reactivity Method (CRM) instrument: experiments vs. modelling. Atmospheric Meas. Tech. Discuss. *8*, 3803–3850.

Mihelcic, D., Heitlinger, M., Kley, D., Müsgen, P., and Volz-Thomas, A. (1999). Formation of hydroxyl and hydroperoxy radicals in the gas-phase ozonolysis of ethene. Chem. Phys. Lett. *301*, 559–564.

Miyazaki, K., Parker, A.E., Fittschen, C., Monks, P.S., and Kajii, Y. (2010). A new technique for the selective measurement of atmospheric peroxy radical concentrations of HO 2 and RO 2 using a denuding method. Atmospheric Meas. Tech. *3*, 1547–1554.

Mogensen, D., Smolander, S., Sogachev, A., Zhou, L., Sinha, V., Guenther, A., Williams, J., Nieminen, T., Kajos, M.K., and Rinne, J. (2011). Modelling atmospheric OH-reactivity in a boreal forest ecosystem. Atmospheric Chem. Phys. *11*, 9709–9719.

Monks, P.S. (2005). Gas-phase radical chemistry in the troposphere. Chem. Soc. Rev. *34*, 376–395.

Mount, G.H., and Eisele, F.L. (1992). An intercomparison of tropospheric OH measurements at Fritz Peak Observatory, Colorado. Science *256*, 1187–1190.

Müller, J.-F., Liu, Z., Nguyen, V.S., Stavrakou, T., Harvey, J.N., and Peeters, J. (2016). The reaction of methyl peroxy and hydroxyl radicals as a major source of atmospheric methanol. Nat. Commun. *7*, 13213.

Nakashima, Y., Kato, S., Greenberg, J., Harley, P., Karl, T., Turnipseed, A., Apel, E., Guenther, A., Smith, J., and Kajii, Y. (2014). Total OH reactivity measurements in ambient air in a southern Rocky mountain ponderosa pine forest during BEACHON-SRM08 summer campaign. Atmos. Environ. *85*, 1–8.

Nölscher, A.C., Williams, J., Sinha, V., Custer, T., Song, W., Johnson, A.M., Axinte, R., Bozem, H., Fischer, H., Pouvesle, N., et al. (2012a). Summertime total OH reactivity measurements from boreal forest during HUMPPA-COPEC 2010. Atmospheric Chem. Phys. *12*, 8257–8270.

Nölscher, A.C., Sinha, V., Bockisch, S., Klüpfel, T., and Williams, J. (2012b). Total OH reactivity measurements using a new fast Gas Chromatographic Photo-Ionization Detector (GC-PID). Atmospheric Meas. Tech. *5*, 2981–2992.

Nölscher, A.C., Yanez-Serrano, A.M., Wolff, S., De Araujo, A.C., Lavrič, J.V., Kesselmeier, J., and Williams, J. (2016). Unexpected seasonality in quantity and composition of Amazon rainforest air reactivity. Nat. Commun. *7*, 10383.

Novelli, A., and Harder, H. (2012). Assessment of the role of stabilized Criegee Intermediates in OH radical measurements by LIF. In EGU General Assembly Conference Abstracts, p. 9491.

Novelli, A., Vereecken, L., Lelieveld, J., and Harder, H. (2014a). Direct observation of OH formation from stabilised Criegee intermediates. Phys. Chem. Chem. Phys. *16*, 19941–19951.

Novelli, A., Hens, K., Ernest, C.T., Kubistin, D., Regelin, E., Elste, T., Plass-Dulmer, C., Martinez, M., Lelieveld, J., and Harder, H. (2014b). Characterisation of an inlet pre-injector laser-induced fluorescence instrument for the measurement of atmospheric hydroxyl radicals.

Novelli, A., Hens, K., Tatum Ernest, C., Martinez, M., Nölscher, A.C., Sinha, V., Paasonen, P., Petäjä, T., Sipilä, M., and Elste, T. (2017). Estimating the atmospheric concentration of Criegee intermediates and their possible interference in a FAGE-LIF instrument. Atmospheric Chem. Phys. *17*, 7807–7826.

Parker, A.E., Monks, P.S., Wyche, K.P., Balzani-Lööv, J.M., Staehelin, J., Reimann, S., Legreid, G., Vollmer, M.K., and Steinbacher, M. (2009). Peroxy radicals in the summer free troposphere: seasonality and potential for heterogeneous loss. Atmospheric Chem. Phys. *9*, 1989–2006.

Parker, A.E., Amédro, D., Schoemaecker, C., and Fittschen, C. (2011). OH RADICAL REACTIVITY MEASUREMENTS BY FAGE. Environ. Eng. Manag. J. EEMJ *10*.

Paulot, F., Crounse, J.D., Kjaergaard, H.G., Kürten, A., Clair, J.M.S., Seinfeld, J.H., and Wennberg, P.O. (2009). Unexpected epoxide formation in the gas-phase photooxidation of isoprene. Science *325*, 730–733.

Peeters, J., and Müller, J.-F. (2010). HOx radical regeneration in isoprene oxidation via peroxy radical isomerisations. II: experimental evidence and global impact. Phys. Chem. Chem. Phys. *12*, 14227–14235.

Peeters, J., Nguyen, T.L., and Vereecken, L. (2009). HO x radical regeneration in the oxidation of isoprene. Phys. Chem. Chem. Phys. *11*, 5935–5939.

Perner, D., Platt, U., Trainer, M., Hübler, G., Drummond, J., Junkermann, W., Rudolph, J., Schubert, B., Volz, A., and Ehhalt, D.H. (1987). Measurements of tropospheric OH concentrations: A comparison of field data with model predictions. J. Atmospheric Chem. *5*, 185–216.

Petäjä, T., Mauldin Iii, R.L., Kosciuch, E., McGrath, J., Nieminen, T., Paasonen, P., Boy, M., Adamov, A., Kotiaho, T., and Kulmala, M. (2009). Sulfuric acid and OH concentrations in a boreal forest site. Atmospheric Chem. Phys. *9*, 7435–7448.

Pugh, T.A.M., MacKenzie, A.R., Hewitt, C.N., Langford, B., Edwards, P.M., Furneaux, K.L., Heard, D.E., Hopkins, J.R., Jones, C.E., Karunaharan, A., et al. (2010). Simulating atmospheric composition over a South-East Asian tropical rainforest: performance of a chemistry box model. Atmospheric Chem. Phys. *10*, 279–298.

Pusede, S.E., Gentner, D.R., Wooldridge, P.J., Browne, E.C., Rollins, A.W., Min, K.-E., Russell, A.R., Thomas, J., Zhang, L., Brune, W.H., et al. (2014). On the temperature dependence of organic reactivity, nitrogen oxides, ozone production, and the impact of emission controls in San Joaquin Valley, California. Atmospheric Chem. Phys. *14*, 3373–3395.

Ren, X., Harder, H., Martinez, M., Lesher, R.L., Oliger, A., Shirley, T., Adams, J., Simpas, J.B., and Brune, W.H. (2003). HO x concentrations and OH reactivity observations in New York City during PMTACS-NY2001. Atmos. Environ. *37*, 3627–3637.

Ren, X., Harder, H., Martinez, M., Faloona, I.C., Tan, D., Lesher, R.L., Di Carlo, P., Simpas, J.B., and Brune, W.H. (2004). Interference testing for atmospheric HOx measurements by laser-induced fluorescence. J. Atmospheric Chem. *47*, 169–190.

Ren, X., Brune, W.H., Cantrell, C.A., Edwards, G.D., Shirley, T., Metcalf, A.R., and Lesher, R.L. (2005). Hydroxyl and peroxy radical chemistry in a rural area of Central Pennsylvania: Observations and model comparisons. J. Atmospheric Chem. *52*, 231–257.

Ren, X., Brune, W.H., Oliger, A., Metcalf, A.R., Simpas, J.B., Shirley, T., Schwab, J.J., Bai, C., Roychowdhury, U., Li, Y., et al. (2006). OH, HO2, and OH reactivity during the PMTACS–NY Whiteface Mountain 2002 campaign: Observations and model comparison. J. Geophys. Res. Atmospheres *111*.

Rickly, P., and Stevens, P.S. (2018). Measurements of a potential interference with laser-induced fluorescence measurements of ambient OH from the ozonolysis of biogenic alkenes. Atmospheric Meas. Tech. *11*, 1.

Rohrer, F., Lu, K., Hofzumahaus, A., Bohn, B., Brauers, T., Chang, C.-C., Fuchs, H., Häseler, R., Holland, F., and Hu, M. (2014). Maximum efficiency in the hydroxyl-radical-based self-cleansing of the troposphere. Nat. Geosci. *7*, 559–563.

Ruzicka, L. (1953). The isoprene rule and the biogenesis of terpenic compounds. Experientia *9*, 357–367.

Sadanaga, Y., Matsumoto, J., Sakurai, K., Isozaki, R., Kato, S., Nomaguchi, T., Bandow, H., and Kajii, Y. (2004a). Development of a measurement system of peroxy radicals using a chemical amplification/laser-induced fluorescence technique. Rev. Sci. Instrum. *75*, 864–872.

Sadanaga, Y., Yoshino, A., Watanabe, K., Yoshioka, A., Wakazono, Y., Kanaya, Y., and Kajii, Y. (2004b). Development of a measurement system of OH reactivity in the atmosphere by using a laser-induced pump and probe technique. Rev. Sci. Instrum. *75*, 2648–2655.

Sadanaga, Y., Yoshino, A., Kato, S., and Kajii, Y. (2005). Measurements of OH reactivity and photochemical ozone production in the urban atmosphere. Environ. Sci. Technol. *39*, 8847–8852.

Schlosser, E., Brauers, T., Dorn, H.-P., Fuchs, H., Häseler, R., Hofzumahaus, A., Holland, F., Wahner, A., Kanaya, Y., Kajii, Y., et al. (2009). Technical Note: Formal blind intercomparison of OH measurements: results from the international campaign HOxComp. Atmospheric Chem. Phys. *9*, 7923–7948.

Seinfeld, J.H., and Pandis, S.N. (2016). Atmospheric chemistry and physics: from air pollution to climate change (John Wiley & Sons).

Shirley, T.R., Brune, W.H., Ren, X., Mao, J., Lesher, R., Cardenas, B., Volkamer, R., Molina, L.T., Molina, M.J., Lamb, B., et al. (2006). Atmospheric oxidation in the Mexico City metropolitan area (MCMA) during April 2003. Atmospheric Chem. Phys. *6*, 2753–2765.

Sindelarova, K., Granier, C., Bouarar, I., Guenther, A., Tilmes, S., Stavrakou, T., Müller, J.-F., Kuhn, U., Stefani, P., and Knorr, W. (2014). Global data set of biogenic VOC emissions calculated by the MEGAN model over the last 30 years. Atmospheric Chem. Phys. *14*, 9317–9341.

Sinha, V., Williams, J., Crowley, J.N., and Lelieveld, J. (2008). The Comparative Reactivity Method–a new tool to measure total OH Reactivity in ambient air. Atmospheric Chem. Phys. *8*, 2213–2227.

Sinha, V., Williams, J., Lelieveld, J., Ruuskanen, T.M., Kajos, M.K., Patokoski, J., Hellen, H., Hakola, H., Mogensen, D., Boy, M., et al. (2010). OH reactivity measurements within a boreal forest: evidence for unknown reactive emissions. Environ. Sci. Technol. *44*, 6614–6620.

Stavrakou, T., Peeters, J., and Müller, J.-F. (2010). Improved global modelling of HO x recycling in isoprene oxidation: evaluation against the GABRIEL and INTEX-A aircraft campaign measurements. Atmospheric Chem. Phys. *10*, 9863–9878.

Stevens, P.S., Mather, J.H., and Brune, Wh. (1994). Measurement of tropospheric OH and HO2 by laser-induced fluorescence at low pressure. J. Geophys. Res. Atmospheres *99*, 3543–3557.

Stone, D., K. Whalley, L., and E. Heard, D. (2012). Tropospheric OH and HO 2 radicals: field measurements and model comparisons. Chem. Soc. Rev. *41*, 6348–6404.

Tan, D., Faloona, I., Simpas, J.B., Brune, W., Shepson, P.B., Couch, T.L., Sumner, A.L., Carroll, M.A., Thornberry, T., Apel, E., et al. (2001). HO x budgets in a deciduous forest: Results from the PROPHET summer 1998 campaign. J. Geophys. Res. Atmospheres *106*, 24407–24427.

Tan, Z., Fuchs, H., Lu, K., Bohn, B., Broch, S., Dong, H., Gomm, S., Häseler, R., He, L., Hofzumahaus, A., et al. (2016). Radical chemistry at a rural site (Wangdu) in the North China Plain: Observation and model calculations of OH, HO2 and RO2 radicals.

Tanner, D.J., and Eisele, F.L. (1995). Present OH measurement limits and associated uncertainties. J. Geophys. Res. Atmospheres *100*, 2883–2892.

Vogelezang, D.H.P., and Holtslag, A. a. M. (1996). Evaluation and model impacts of alternative boundary-layer height formulations. Bound.-Layer Meteorol. *81*, 245–269.

Wallace, J.M., and Hobbs, P.V. (2006). Atmospheric science: an introductory survey (Academic press).

Watanabe, T., Yoshida, M., Fujiwara, S., Abe, K., Onoe, A., Hirota, M., and Igarashi, S. (1982). Spin trapping of hydroxyl radical in the troposphere for determination by electron spin resonance and gas chromatography/mass spectrometry. Anal. Chem. *54*, 2470–2474.

Wayne, R.P. (2000). Chemistry of Atmospheres: an Introduction to the Chemistry of the Atmospheres of Earth, the Plants and their Satellites (Oxford University Press Oxford).

Weinstock, B. (1969). Carbon monoxide: Residence time in the atmosphere. Science *166*, 224–225.

Wennberg, P.O., Bates, K.H., Crounse, J.D., Dodson, L.G., McVay, R.C., Mertens, L.A., Nguyen, T.B., Praske, E., Schwantes, R.H., and Smarte, M.D. (2018). Gas-Phase Reactions of Isoprene and Its Major Oxidation Products. Chem. Rev.

Whalley, L., Stone, D., Bandy, B., Dunmore, R., Hamilton, J.F., Hopkins, J., Lee, J.D., Lewis, A.C., and Heard, D.E. (2016). Atmospheric OH reactivity in central London: observations, model predictions and estimates of in situ ozone production. Atmospheric Chem. Phys. *16*, 2109–2122.

Whalley, L.K., Edwards, P.M., Furneaux, K.L., Goddard, A., Ingham, T., Evans, M.J., Stone, D., Hopkins, J.R., Jones, C.E., Karunaharan, A., et al. (2011). Quantifying the magnitude of a missing hydroxyl radical source in a tropical rainforest. Atmospheric Chem. Phys. *11*, 7223–7233.

Whalley, L.K., Blitz, M.A., Desservettaz, M., Seakins, P.W., and Heard, D.E. (2013). Reporting the sensitivity of laser-induced fluorescence instruments used for HO2 detection to an interference from RO2 radicals and introducing a novel approach that enables HO2 and certain RO2 types to be selectively measured. Atmospheric Meas. Tech. *6*, 3425–3440.

Winiberg, F.A.F., Smith, S.C., Bejan, I., Brumby, C.A., Ingham, T., Malkin, T.L., Orr, S.C., Heard, D.E., and Seakins, P.W. (2015). Pressure-dependent calibration of the OH and HO2 channels of a FAGE HOx instrument using the Highly Instrumented Reactor for Atmospheric Chemistry (HIRAC). Atmospheric Meas. Tech. *8*, 523.

Wood, E.C., and Charest, J.R. (2014). Chemical amplification-cavity attenuated phase shift spectroscopy measurements of atmospheric peroxy radicals. Anal. Chem. *86*, 10266–10273.

Yang, Y., Shao, M., Wang, X., Nölscher, A.C., Kessel, S., Guenther, A., and Williams, J. (2016). Towards a quantitative understanding of total OH reactivity: A review. Atmos. Environ. *134*, 147–161.

Yang, Y., Shao, M., Ke\s sel, S., Li, Y., Lu, K., Lu, S., Williams, J., Zhang, Y., Zeng, L., and Nölscher, A.C. (2017). How the OH reactivity affects the ozone production efficiency: case studies in Beijing and Heshan, China. Atmospheric Chem. Phys. *17*, 7127–7142.

Yoshino, A., Sadanaga, Y., Watanabe, K., Kato, S., Miyakawa, Y., Matsumoto, J., and Kajii, Y. (2006). Measurement of total OH reactivity by laser-induced pump and probe technique—comprehensive observations in the urban atmosphere of Tokyo. Atmos. Environ. *40*, 7869–7881.

Yoshino, A., Nakashima, Y., Miyazaki, K., Kato, S., Suthawaree, J., Shimo, N., Matsunaga, S., Chatani, S., Apel, E., Greenberg, J., et al. (2012). Air quality diagnosis from comprehensive observations of total OH reactivity and reactive trace species in urban central Tokyo. Atmos. Environ. *49*, 51–59.

Zannoni, N. (2015). OH reactivity measurements in the Mediterranean region. PhD Thesis. Université Paris-Saclay.

Zannoni, N., Gros, V., Lanza, M., Sarda, R., Bonsang, B., Kalogridis, C., Preunkert, S., Legrand, M., Jambert, C., and Boissard, C. (2016). OH reactivity and concentrations of biogenic volatile organic compounds in a Mediterranean forest of downy oak trees. Atmospheric Chem. Phys. *16*, 1619–1636.

Zannoni, N., Gros, V., Sarda Esteve, R., Kalogridis, C., Michoud, V., Dusanter, S., Sauvage, S., Locoge, N., Colomb, A., and Bonsang, B. (2017). Summertime OH reactivity from a receptor coastal site in the Mediterranean Basin. Atmospheric Chem. Phys. *17*, 12645–12658.

Zeng, G., Heard, D.E., Pilling, M.J., and Robertson, S.H. (1998). A master equation study of laser-generated interference in the detection of hydroxyl radicals using laser-induced fluorescence. Geophys. Res. Lett. *25*, 4497–4500.

General conclusion

The OH radical is the most important oxidizing species in the troposphere, involved in the removal of greenhouse gases such as methane, oxidation of VOCs, and ozone formation. Comprehensive knowledge of its distribution and its sources and sinks throughout the atmosphere is necessary. Similarly, characterization of HO_2 and RO_2 radicals, involvedin these oxidation cycles are needed to better understand the atmospheric chemistry in the boundary layer.

HO_x and RO_x radicals exist in very low concentrations (10^6 cm^{-3} for OH and 1 to 10 × 10^8 cm^{-3} for HO_2 and RO_2 radicals)which are highly variable with time and location. For this reason, different types of instruments have been developed and deployed to measure these radicals in the field. In chapter 1, we reviewed the different reactions involving these species in the atmosphere as well as the different techniques used to quantify $HO_x$and RO_xradicals but also to measure the OH reactivity, representative of the sum of OH losses. Fluorescence Assay by Gas Expansion (FAGE) is the most widely-used technique for OH and HO_2 detection, having good sensitivity, good spatial and temporal resolution, and sufficiently low detection limits to enable the detection of these radicals in the atmosphere, but need calibration. Comparisons between measurements in different environments and modelled profiles allow to identify discrepancies between the chemical mechanisms used in the model and the reality. However, bias in the calibration or interferences in the instruments may affect the results. Recent studies, in biogenic environments have highlighted strong differences between measurements and modelling which cannot be explained by chemical mechanisms improvements.It has then been shown that some FAGE instruments suffer from unknown interferenceproducing OH internally within the FAGE cells. For HO_2, it has also been demonstrated that in all FAGE instruments certain RO_2 species were interfering to the HO_2 measurement increasingly with the NO level (used to convert HO_2 in OH within the FAGE cell). These potential biases due to calibration or interferences affecting the measurements of OH and HO_2have been extensively studied during this thesis with the objective of a deployment of the instrument in the field, in a biogenic environment.

In chapter II, the UL-FAGE instrument usedduring my thesis for quantifying OH, HO_2 and RO_2 radical and to measure the OH reactivity in the atmosphere is explained as well as the improvements of the instrument and its calibration system. A preinjectorsystem, allowing the quantification of the level of interference on OH measurement, has been developed and characterized.

In Chapter III, we have shown that the product of the reaction of RO_2 radicals with OH radicals (ROOOH) leads to an OH interference signal in the UL-FAGE instrument. If occurring also in other

FAGE instruments, it can explain several observations obtained with FAGE instruments from other laboratories such as the disagreement observed between model and measurements in remote, biogenic environments.

In chapter IV, attention was given to the interferencesin HO_2 measurement as well asto the calibration system. UL-FAGE has been successfully calibrated for different nozzles and different RO_2 radicals coming from the reaction of OH with methane, butane, isoprene and toluene hydrocarbons. The obtained results showed that the interference of HO_2 measurements from RO_2 produced by the reaction of OH with alkanes (methane and butane) is within the range of uncertaintyand considered negligible while the interference from RO_2 radicals produced by the reaction of OH with alkenes and aromatic hydrocarbons found to be significant to the HO_2 measurement in UL-FAGE, similarly to what has been observed in other FAGE instruments. This characterization has shown that it is possible to discriminate HO_2 and RO_2 radicals using variable NO levels in the FAGE. The calibration system has also been intercompared with two other calibrators (IMT-Douai and LPC2E calibration cells).The intercomparison between PC2A and LPC2E calibration cells for HO_x and RO_2 measurements showed a very good agreement over a wide range of concentrations and conditions.Similar agreement was seen for the RO_2 measurement between PC2A and IMT-Douai calibrators. The intercomparison for HO_x measurements showed a good agreement for HO_x if the generationtook place near the exit of the calibrator, but disagreements for $HO_2$was found when radicals are generated higher in the calibrator. Complementary tests will be done during another intercomparison in the HELIOS chamber (Orléans) in the near future.

In the last chapter, we presented the results of the LANDEX campaign in July 2017. The aim of this campaign was to better understand the oxidation processes taking place in this environment dominated by terpene emissions and where nocturnal particle formations have been observed during previous campaigns carried out by the EPOC laboratory but have not clearly been understood. The extensive campaign which took place in 2017 involved more laboratories to better characterize the air composition (VOCs, oxidants, particles, …). The UL-FAGE instrument was deployed for OH, HO_2, RO_2 radicals and OH reactivity measurements in the canopy. UL-FAGE instrument was deployed for the first time to measure peroxy radicals by modulating the NO concentration injected in the second cell of the instrument. In order to test if the OH measurement included artifacts from OH production inside the measurement cell, chemical modulation tests were performed in the last two days of the campaign and significant interferences have been observed. Interference test identified unexplained OH signals reaching 50 % of the OH signal. Daily maximum concentrations of OH, HO_2, and RO_2 radicals ranged from 1 to 30 × 10^6 cm^{-3}, 1 to 15 × 10^7 cm^{-3}, 1 to 10 × $10^7 cm^{-3}$,

respectively.Compared to previous field campaigns, the measured radical concentrations were in the same range for HO_2 and RO_2 while much higher in case of OH radical.

Total OH reactivity was measured in the same site and compared to results obtained with the CRM instrument of the LSCE at the same level or above the canopy. The measured reactivity profiles showed low reactivity during the day and higher one during the night reaching 100 s^{-1}. During the campaign, the pump-probe FAGE was intercompared with LSCE-CRM instrument. The obtained results showed a good correlation between the two instruments sampling from same place or even different locations at the same height. The comparison between the measurements at 2 levels highlighted conditions of strong stratification in VOCs concentrations and OH reactivity. The OH reactivity was mainly dominated by terpenes during the night and isoprene during the day. The analysis of the missing reactivity (comparison between the measured and calculated OH reactivity derived from the analysis of trace species)highlighted a good understanding of the OH losses in the canopy whereas the missing reactivity was more important above the canopy. The candidates of the missing OH sink are thought to be some oxidation products of the biogenic volatile organic compounds present at the site. A more detailed analysis of the different species behavior and the calculation of the production of OH will be done in the near future to better understand the oxidation processes involved in this environment.

The FAGE instrument will be used in the future to quantify also the sum of RO_2 (RO_x measurements) with the development of a new cell and deployed in other campaigns. Laboratory measurements to better understand the radical reactions will be performed in various conditions (from atmospheric to low temperature combustion conditions).